THE IMPACT OF NDRG1 OVEREXPRESSION ON THE IMMUNOLOGICAL AND METABOLIC REPROGRAMMING OF THE PANCREATIC CANCER TUMOUR MICROENVIRONMENT

SHAFI ALENIZI
B.Sc, M.Sc

THE UNIVERSITY OF SYDNEY

A thesis submitted in accordance with the rules for the Degree of Doctor of Philosophy in the Faculty of Medicine and Health at the University of Sydney

2024

ACKNOWLEDGEMENTS

I am deeply grateful to Dr. Zaklina Kovacevic for her invaluable guidance, unwavering support, and insightful feedback throughout my PhD studies. Her expertise, encouragement, and dedication have been instrumental in shaping my research journey and academic growth. I am truly fortunate to have had her as my supervisor. I am deeply grateful to Dr. Zaky for her exceptional commitment and invaluable feedback while reading my thesis. Her dedicated time, extensive insights, and meticulous attention have significantly enriched the quality of my research. I sincerely appreciate her unwavering support and guidance, which have shaped this work.

I am immensely grateful to my mother, father, daughter and wife for their unwavering love, understanding, and encouragement throughout my PhD journey. Their patience, support, and sacrifices have been the cornerstone of my success. I sincerely appreciate their constant belief in me and willingness to stand by me during challenging times. This achievement would not have been possible without their boundless support and affection.

DECLARATION

This thesis is submitted to the University of Sydney in the fulfilment of the requirements for the Degree of Doctor of Philosophy.

I declare that, to the best of my knowledge, this thesis does not contain any material previously published except as acknowledged in the text. It has not been submitted, in whole or in part, for a degree at this or any other university.

SHAFI MEAID R ALENIZI

June 2024

AUTHORSHIP CONTRIBUTION STATEMENT

The publications that I co-authored during my PhD candidature are not included in this thesis, as they were collaborative projects I contributed to, which were separate from my main research project.

During my PhD candidature, I was the primary contributor responsible for planning, conducting experiments, data analysis, statistical analysis, preparing all figures, and writing up the data presented in this thesis.

The contributions of co-authors are listed below:

Task	**Co-author(s) involved**
Extracellular vesicle (EVs) isolation	Jiawei Chang

SHAFI MEAID R ALENIZI

July 2024

As supervisor for the candidature upon which this thesis is based, I confirm that the authorship attribution statements above are correct.

Dr. Zaklina Kovacevic

4/7/2024

ABSTRACT

Pancreatic ductal adenocarcinoma (PDAC) is highly aggressive, with no effective treatments for the 80% of patients that are diagnosed at an advanced stage. A major hurdle in treating PDAC is the extensive tumour microenvironment (TME) which facilitates resistance to all current therapies. N-myc downstream regulated 1 (NDRG1) is a metastasis suppressor that was found to inhibit tumour progression and metastasis in PDAC. Recent studies also suggest that NDRG1 reduced PDAC-mediated activation of pancreatic stellate cells (PSCs), although the mechanisms behind this remain to be established. Our studies investigated the effect of NDRG1 on PDAC metabolism and how this influences key TME elements including tumour-associated macrophages (TAMs) and PSCs. We generated PDAC cells (MIAPaCa-2 and PANC-1) that stably overexpress NDRG1 and performed extensive metabolomic, proteomic and secretome analysis under normoxia and hypoxia. Using conditioned media or direct 3D spheroid co-cultures, we assessed the effect of PDAC cells on THP-1 and U937 monocytes and primary PSCs using flow cytometry, Seahorse metabolic analysis, western blot and immunofluorescence analysis. The findings indicated that NDRG1 expression profoundly affected the metabolism of cancer cells, which led to significant changes in both the immune and fibroblast components of the TME. In cancer cells, NDRG1 reduced the uptake of branched-chain amino acids (BCAA) leading to inhibition of the mTOR pathway. The secretome of PDAC cells, including exosomes, cytokines and chemokines was also altered by NDRG1. Specifically, NDRG1 increased secretion of TNF-α, while reducing CCL2 and TGF-β production by PDAC cells. This led to re-programming of TAMs from an anti-inflammatory M2 phenotype to a pro-inflammatory M1 phenotype and altered TAM metabolism. NDRG1 expression in PDAC cells also markedly influenced the metabolic cross-talk with PSCs, leading to increased infiltration of M1 polarized TAMs into PDAC/PSC co-culture spheroids.

We demonstrate that NDRG1 is highly involved in regulating PDAC metabolism, significantly altering metabolic cross-talk with PSCs and leading to extensive "re-programming" of TAMs into the M1 phenotype. Hence, NDRG1 has the potential to disrupt the oncogenic interactions between PDAC cells and the TME, and promoting the expression of this protein may enhance PDAC vulnerability to current chemo/immunotherapies.

This dissertation comprises seven chapters: Chapter 1 is a literature review; Chapter 2 is a general materials and methods chapter; Chapters 3, 4, and 5 are results chapters; Chapter 6 is a general discussion and future directions chapter; and Chapter 7 is a reference section.

Publications during my PhD candidature (publications that are separate to the thesis)

1- Chang, Jiawei, Zoe H. Y. Lo, **Shafi Alenizi**, and Zaklina Kovacevic. 2023. "**Re-Shaping the Pancreatic Cancer Tumor Microenvironment: A New Role for the Metastasis Suppressor NDRG1**" *Cancers* 15, no. 10: 2779. https://doi.org/10.3390/cancers15102779

2- Jawaher Alharthi, Ali Bayoumi, Khaled Thabet, Ziyan Pan, Brian S. Gloss, Olivier Latchoumanin, Mischa Lundberg, Natalie A. Twine, Duncan McLeod, **Shafi Alenizi**, Leon A. Adams, Martin Weltman, Thomas Berg, Christopher Liddle, Jacob George, and Mohammed Eslam. **metabolic associated fatty liver disease risk variant in MBOAT7 regulates toll like receptor induced outcomes**. Nat Commun. 2022 Dec 6;13(1):7430. doi: https://doi.org/10.1038%2Fs41467-022-35158-9 . PMID: 36473860; PMCID: PMC9726889.

3- Mayada Metwally, Ali Bayoumi, Anis Khan, Leon A. Adams, Rocio Aller, Carmelo García-Monzón, María Teresa Arias-Loste, Elisabetta Bugianesi, Luca Miele, Alisi Anna, Olivier Latchoumanin, Shuanglin Han, **Shafi Alenizi**, Rasha EL Sharkawy, Afaf Elattar, Rocio Gallego-Durán, Janett Fischer, Thomas Berg, Christopher Liddle, Manuel Romero-Gomez, Jacob George, Mohammed Eslam. (2021) **Copy number variation and expression of exportin-4 associates with severity of fibrosis in metabolic associated fatty liver disease.** EBioMedicine, Volume 70, 103521. DOI: https://doi.org/10.1016/j.ebiom.2021.103521

4- Ali Bayoumi, Asmaa Elsayed, Shuanglin Han, Salvatore Petta, Leon A. Adams, Rocio Aller, Anis Khan, Carmelo García-Monzón, María Teresa Arias-Loste, Luca Miele, Olivier Latchoumanin, **Shafi Alenizi**, Rocio Gallego-Durán, Janett Fischer, Thomas Berg, Antonio Craxì, Mayada Metwally, Liang Qiao, Christopher Liddle, Hannele Yki-Järvinen, Elisabetta Bugianesi, Manuel Romero-Gomez, Jacob George and Mohammed Eslam. (2021). **Mistranslation Drives Alterations in Protein Levels and the Effects of a Synonymous Variant at the Fibroblast Growth Factor 21 Locus**. Advanced science (Weinheim, Baden-Wurttemberg, Germany), 8(11), 2004168.

DOI: https://doi.org/10.1002/advs.202004168.

List of abbreviations

abbreviation	Definition
AA	arachidonic acid
ADM	Acinar-to-ductal metaplasia
apCAFs	antigen-presenting CAFs
APCs	antigen-presenting cells
aPSCs	activated pancreatic stellate cells
Arg1	arginase-1
ASCT2	cysteine-preferring transporter 2
ATP	adenosine triphosphate
BAFF	B cell-activating factor
BCA	Bicinchoninic Acid
BCAAs	Branched-chain amino acids
BCAT	BCAA aminotransferase
BCAT1	branched-chain amino acid transaminase 1
BCAT2	branched-chain amino acid transaminase 2
BCKAs	branched-chain α-keto acids
BCKDHA	branched-chain α-keto acid dehydrogenase A
BMSCs	bone marrow-derived mesenchymal stem cells
BP	biological processes
BSA	Bovine serum albumin BSA
CAF	cancer associated fibroblasts
CC	cellular components
CCM	central carbon metabolism
CCR5	chemokine receptor type 5

CDK	cyclin-dependent kinase
CDKN2A	cyclin-dependent kinase inhibitor 2A
CER	cytoplasmic extraction reagent
CM	Conditioned media
CPTI	Carnitine palmitoyltransferase I
CSF2	colony stimulating factor 2
CTLA-4	cytotoxic T-lymphocyte-associated protein 4
CXCL1	C-X-C motif chemokine ligand 1
CXCL12	CXC chemokine ligand 12
CXCL2	C-X-C motif chemokine ligand 2
DC	Dendritic cells
DLST	dihydrolipoamide S-succinyltransferase
DMEM	Dulbecco′s Modified Eagle′s Medium
DMSO	Dimethyl sulfoxide
DpC	di-2-pyridylketone-4-cyclohexyl-4-methyl-3-thiosemicarbazone
ECAR	extracellular acidification rate
ECM	extracellular matrix
ELISA	Enzyme-Linked Immunosorbent Assay
EMT	epithelial-to-mesenchymal transition
EndMT	endothelial-to-mesenchymal transition
ESCC	esophageal squamous cell carcinoma
EVs	extracellular vesicles
FAO	fatty acid oxidation
FBS	Fetal Bovine Serum
G6P	glucose-6-phosphate

GFAP	glial fibrillary acidic protein
GLS	glutaminase
GLUL	glutamate ammonia ligase
GLUT1	Glucose transporter type 1
GO	Gene Ontology
HDI	Human Development Index
HGF	hepatocyte growth factor
HIF-1α	inducible factor 1 alpha
HIF-2α	hypoxia-inducible factor-2α
HK2	Hexokinase 2
HSCs	hepatic stellate cells
iCAFs	Inflammatory CAFs
IDH1	isocitrate dehydrogenase 1
IF	Immunofluorescence staining
IFNγ	interferon gamma
IGF-1	insulin-like growth factor
IL-10	Interleukin-10
IL-11	Interleukin 11
IL-1β	interleukin-1β
IL-6	Interleukin 6
IL-6	Interleukin-6
IL-8	Interleukin-8
iNOS	inducible nitric oxide synthase
IP-10	interferon-γ inducible protein 10
IPMN	intraductal papillary mucinous neoplasms

KRAS	Kirsten rat sarcoma
LAT1	L-type amino acid transporter 1
LDHA	lactate dehydrogenase A
LIF	Leukemia inhibitory factor
MAPK	MAP-kinase
MCN	mucinous cystic neoplasms
MCP-1	Human Monocyte Chemoattractant Protein-1
MCPIP1	Monocyte Chemotactic Protein-Induced Protein 1
MCT 4	monocarboxylate transporter 4
MDSCs	myeloid-derived suppressor cells
MF	molecular function
MHC	Major Histocompatibility Complex
MIF	Macrophage Migration Inhibitory Factor
mTORC1	mammalian target of rapamycin complex 1
myCAFs	myofibroblastic CAFs
NADPH	nicotinamide adenine nucleotide phosphate
NCAM	neural cell adhesion molecule
NDRG1	N-myc downstream regulated gene 1
NEAA	non-essential amino acid
NER	nuclear extraction reagent
NGF	nerve growth factor
NK	Natural Killer
NO	nitric oxide
OCR	oxygen consumption rate
OXPHOS	oxidative phosphorylation

PanIN	pancreatic intraepithelial neoplasias
PanIN	pancreatic intraepithelial neoplasia
PBS	Phosphate Buffered saline
PD-1	programmed cell death protein 1
PD-L1	programmed death-ligand 1
PDAC	pancreatic ductal adenocarcinoma
PDK1	Pyruvate dehydrogenase kinase 1
PFA	paraformaldehyde
PGE2	prostaglandin E2
PMA	Phorbol 12-myristate 13-acetate
PSCs	Pancreatic stellate cells
qPSCs	Quiescent PSCs
RIPA	Radioimmunoprecipitation
ROS	reactive oxygen species
RT	room temperature
SHH	sonic hedgehog
si-Control	silencing control cells (si-Control)
si-NDRG1	silenced cells (si-NDRG1)
SMAD4	*SMAD* family member 4
TAMs	Tumour-associated macrophages
TCA	tricarboxylic acid
TGF-β	transforming growth β
Th1	T helper 1
Th2	T helper 2
TLRs	Toll-like receptors

TME	tumour microenvironment
TNF	tumour necrosis factor
TNF-α	tumor necrosis factor alpha
TP53	tumour suppressor protein 53
T_{regs}	Regulatory T cells
TSP-1	Thrombospondin-1
VC	vector control
VEGFs	vascular epithelial growth factors
α SMA	α smooth muscle actin
αKG	alpha-ketoglutarate

TABLE OF CONTENTS

LIST OF FIGURES

Chapter 1: introduction

Chapter 2: MATERIALS & METHODS

Chapter 3: Effect Of NDRG1 On Metabolism of PDAC Cells

LIST OF TABLES

Chapter 1: introduction

1.1 General Introduction

The pancreas is a yellow, tube-shaped, spongy organ between 12 and 15 cm long in adults divided into a head, neck, body, and tail **(Figure 1.1)** [1]. It is located in the retroperitoneal region of the upper of the abdomen [2]. The healthy pancreas consists of acinar cells, ductal cells, endocrine islets secreting digestive enzymes, bicarbonate and hormone, respectively, centro-acinar cells, and relatively inactive stellate cells [3]. Endocrine and exocrine functions performed by the pancreas play a vital role in digestion and glucose metabolism [4].

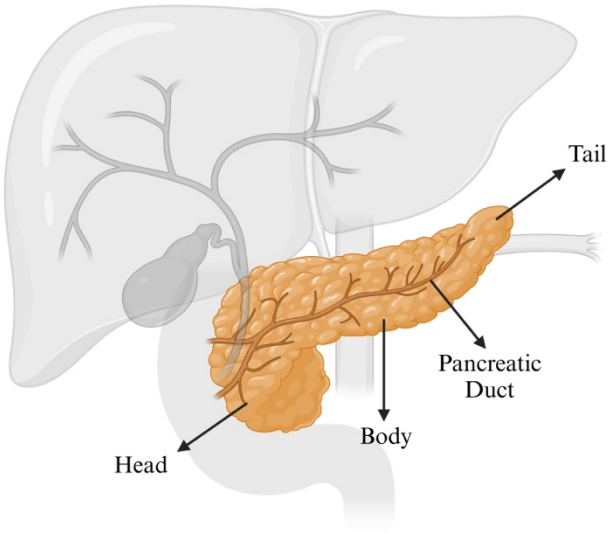

Figure1.1.: Anatomy of The Pancreas.

Pancreatic cancer is a fatal gastrointestinal cancer. Regardless of the significant advances in cancer research, the worldwide burden of pancreatic cancer has more than doubled over the last 25 years, with a dismal 10-12% 5-year survival rate. This is due to the often-late presentation of this disease, with majority of cases being diagnosed at an advanced stage with metastasis [5-7]. More than 90% of cases of pancreatic cancer are pancreatic ductal adenocarcinoma (PDAC) [8], Approximately 65% of PDAC occur in the head of the pancreas. However, approximately 15% are found in the body, 10% in the tail, and 2% in multiple locations. Tumours located in the body and tail are usually detected at a later stage and are linked to poorer prognosis [9]

1.2. Epidemiology of Pancreatic Cancer

Globally, the incidence and death rates of pancreatic cancer are rising. In 2017, the incidence of pancreatic cancer globally was 448,000 (439,000–456,000) cases. The age-standardised incidence rate increased from 5.0 (4.9–5.1) in 1990 to 5.7 (5.6–5.8) in 2017 per 100,000 people. The number of deaths in 2017 were 441,000 (433,000–449,000) compared to 196,000 (193,000–200,000) in 1990, 2.3 times increase for both males and females [10]. In 2020, the mortality of pancreatic cancer globally was 466,000 deaths, with number of cases being 496,000. In high Human Development Index (HDI) countries, these rates are 4 to 5-fold higher.

1.3. Risk Factors

1.3.1. Smoking

Cigarette smoking is considered one of the key risk factors for pancreatic cancer. Cigarette smoking increases the risk of pancreatic cancer by 2-fold, and that increases further with the duration of smoking and the number of cigarettes [11].

1.3.2. Obesity

There is a positive association between the risk of pancreatic cancer and obesity, likely *via* several mechanisms such as altered intestinal microbiota, inflammation, and insulin resistance [12]. Furthermore, particularly in women, the centralised fat distribution increases the risk of pancreatic cancer [13].

1.3.3. Diabetes mellitus

People recently diagnosed with diabetes have around a 7-fold increase in the risk of pancreatic cancer compared with people without diabetes [14]. Notably, the risks of pancreatic cancer were estimated to decrease with increasing years with diabetes [15].

1.3.4. Family History

A family history of pancreatic cancer has been associated with an increased risk of this disease. Approximately 10% of pancreatic cancer cases are correlated with familial pancreatic cancer or hereditary syndromes, including Lynch syndrome, familial atypical multiple mole melanoma, familial adenomatous polyposis, Peutz-Jeghers syndrome, hereditary breast and ovarian cancer syndrome and hereditary pancreatitis. Familial pancreatic cancer patients carry mutations in susceptibility genes like PALB2 and ATM [16].

1.3.5. Pancreatitis

Pancreatitis is considered a risk factor of pancreatic cancer. There is a correlation between acute pancreatitis diagnosis and the long-term risk of pancreatic cancer [17]. Acute pancreatitis patients have only a 0.4% risk of pancreatic cancer if they do not progress to chronic

pancreatitis. However, the risk increases to 9-fold with patients who progress to chronic pancreatitis [18].

1.4. Disease Progression Model of Pancreatic Cancer

The pancreas consists of independent functional units that control two major physiological processes. The exocrine pancreas contains acinar cells and duct cells. The acinar cells (grape-like clusters) generate the digestive enzymes [19]. The mucous and bicarbonate are added to the enzyme mixture by the ducts to carry into the duodenum. The endocrine pancreas comprises four cell types, including: α-cells which secrete the hormone glucagon; β-cells which secrete insulin; δ-cells that secrete the hormone somatostatin; and PP cells which secrete pancreatic polypeptide [19]. Pancreatic cancer can arise from either exocrine or endocrine cells. The most common type of pancreatic cancer originates from exocrine cells, known explicitly as PDAC. PDAC occurs due to the abnormal growth of exocrine cells and makes up over 90% of all pancreatic malignancies [3, 20]. Acinar cell carcinomas are a distinct subtype of exocrine pancreatic cancer known for their abnormal enzyme secretion. Less prevalent types of exocrine pancreatic cancer include Mucinous cyst adenocarcinoma, Intraductal papillary mucinous carcinoma, Adenosquamous, and Undifferentiated/anaplastic carcinoma. However, these subtypes collectively represent a small proportion of pancreatic cancer cases [20, 21].

1.4.1 Precursor Lesions

The development of pancreatic cancer happens due to the accumulation of genetic modifications in genes causing cancer, for instance, tumour suppressor genes and oncogenes [22]. The precursor lesion types that can develop into invasive adenocarcinoma of the pancreas include intraductal papillary mucinous neoplasms (IPMN), mucinous cystic neoplasms (MCN) and pancreatic intraepithelial neoplasias (PanIN) [23]. The process of differentiating the pancreatic acinar cells into ductal-like cells with ducal cell traits is called Acinar-to-ductal metaplasia (ADM). This process might lead to pancreatic intraepithelial neoplasia (PanIN), which is considered the most common precursor of pancreatic cancer [22]. PanIN lesions are microscopic, being < 5 mm in diameter [24].

In pancreatic cancer, the four crucial driver genes are the oncogene Kirsten rat sarcoma (*KRAS*) and the tumour suppressors cyclin-dependent kinase inhibitor 2A (*CDKN2A*), the tumour suppressor protein 53 (*TP53*) and *SMAD* family member 4 (*SMAD4*) [25]. In the early stages of PanIN-1 and PanIN-2 lesions, genetic alterations in *KRAS* and *CDKN2A* genes are observed. However, mutations in *TP53* and *SMAD4* genes are observed in the higher-grade PanIN3 lesions [26, 27] **(Figure 1.2)**.

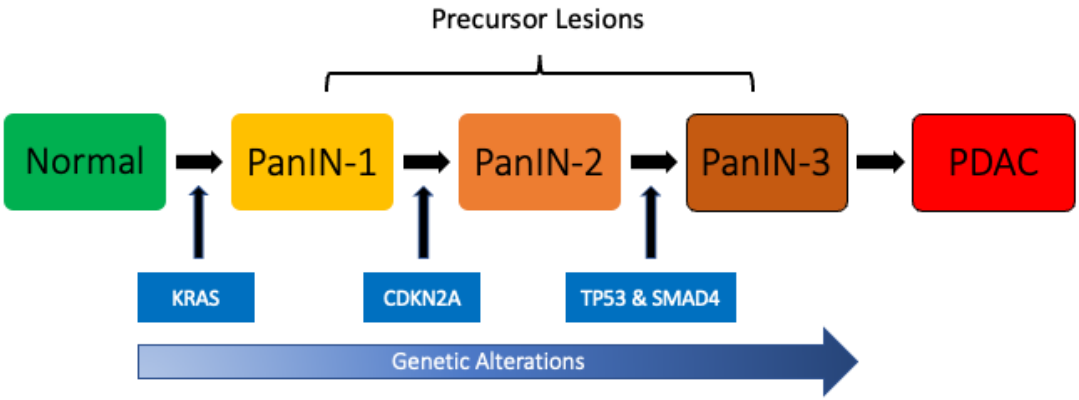

Figure1.2.: Genetic Progression Model of Pancreatic Ductal Adenocarcinoma.

The development is linked to the gradual accumulation of particular genetic alterations.

1.5. The Genetic Landscape of Pancreatic Cancer

The RNA-seq analysis of PDAC identified four subcategories: squamous, pancreatic progenitor, immunogenic, and aberrantly differentiated endocrine exocrine (ADEX), which are associated with histopathological features [28]. However, an integrated analysis of the genome revealed 32 genes that are frequently mutated and can be grouped into 10 pathways: *KRAS*, *TGF-β*, *WNT*, *NOTCH*, *ROBO/SLIT* signalling, *G1/S* transition, *SWI-SNF*, chromatin modification, DNA repair, and RNA processing [28]. The four most frequently genetically mutated genes in pancreatic cancer are *KRAS*, *CDKN2A*, *TP53*, and *SMAD4* [29].

1.5.1 *KRAS*

KRAS is a major oncogene engaged in cellular proliferation and survival and one of the Ras proteins [30, 31]. In pancreatic ductal adenocarcinoma, more than 90% of cases have activating *KRAS* mutations [31]. *KRAS* is involved in tumour initiation and progression; therefore, it is an important therapeutic target [30, 31]. RAS proteins that release from cell surface receptors are fundamental components of signalling pathways. Oncogenic alteration of these proteins due to missense mutations is discovered repeatedly in many types of cancers [32]. The main reason for this is that Ras signals to several effector pathways whose activation promotes oncogenic transformation, including the small GTPases Rho, PI 3-kinase (PI3K)/AKT/mTOR pathway and MAP-kinase (MAPK) pathway [32]. Recently, selective inhibitors targeting the $KRAS^{G12C}$ oncoprotein in patients that harbor *this* mutation have shown promising activity in early clinical trials [33, 34]. Continuing clinical trials experimenting with new drug combinations could enhance patient survival *via* development of new therapeutic strategies [35].

1.5.2. *CDKN2A*

Cyclin-dependent kinase inhibitor 2A *(CDKN2A)* is a tumour-suppressor gene that exists on chromosome 9 and encodes for the $P16^{INK4A}$ and $P14^{ARF}$ proteins [36, 37]. Pathogenic germline CDKN2A variants have been found in up to 3.3% of PDAC patients, depending on their family history. Carriers of this variant face a risk of developing PDAC up to 12.3 times higher [38]. The $P16^{INK4A}$ protein belongs to the cyclin-dependent kinase (CDK) inhibitor family and regulates the cell cycle through the p16/Rb (retinoblastoma) pathway [39]. By inhibiting the phosphorylation of Rb, $P16^{INK4A}$ inhibits cell cycle progression and prevents cells from entry into the S phase of the cell cycle *via* the G1/S transition by CDK4/6 [40-42]. The $p14^{ARF}$ protein inhibits abnormal cell growth by activating the p53 transcription factor, leading to the expression of genes that promote apoptosis and inhibit the cell cycle in response to oncogene insults [43]. The $p14^{ARF}$ binds with mouse double minute 2 (MDM2) in the nucleolus, Which prevents the degradation of p53 [44].The inactivation of *CDKN2A* can occur through three different mechanisms: intragenic mutation with loss of the second allele (40%), homozygous deletion (40%) and epigenetic silencing by promoter methylation (10%–15%) [40, 41]. Mutations affecting *CDKN2A* appear in PanIN-2 during the progression of pancreatic cancer [45].

1.5.3. *TP53*

TP53 is a tumour-suppressor gene located on chromosome 17 and is mutated in 50 - 70 % of pancreatic cancer cases [46-49]. *TP53* encodes P53, which is a critical protein that responds to several stress signals *via* specific cellular responses such as apoptosis, cell cycle and cellular senescence [46]. P53 is controlled by interacting with human double minute 2 (HDM2). A mutated $p14^{ARF}$ causes the degradation of p53 via HDM2 and the simultaneous loss of p21-

mediated suppression of cyclin E-CDK2 [50, 51]. Inactivation mutations affecting *TP53* appear in PaIN-3 during the progression of pancreatic cancer [45].

1.5.4. *SMAD4*

SMAD4 (also called *DPC4*) is a tumour-suppressor gene located on chromosome 18 and is affected in 40-60 % of all pancreatic adenocarcinomas [52-54]. *SMAD4* is inactivated by two mechanisms including homozygous deletion (loss of both copies of the gene) or loss of heterozygosity (loss of one allele) [52]. The *SMAD4* gene encodes an effector that constitutes a significant component in the transforming growth β (TGF-β) signalling pathway [55]. This pathway promotes several physiological processes such as cell growth, proliferation, fibrosis, scar formation and differentiation [56]. The TGF-β-SMAD4 signalling pathway has a dual role in pancreatic ductal adenocarcinoma tumorigenesis and contributes to mediating crosstalk between stroma and tumour and modulating the tumour microenvironment (TME) [57]. Mutations affecting *SMAD4* appear in PanIN-3 during pancreatic cancer progression and have a direct role in facilitating metastasis [45, 58].

1.6. Tumour Microenvironment (TME)

Pancreatic cancer is composed of malignant cells within a complex environment composed of cellular and acellular components called the tumour microenvironment (TME). Cellular components include the stromal cells (including activated pancreatic stellate cells (aPSCs), cancer associated fibroblasts (CAF) and endothelial cells), and the immune cells (innate immune cells (dendritic cells, NK cells, macrophages, and myeloid-derived suppressor cells (MDSCs)) and adaptive immune cells (T cells, CD4, CD8, regulatory T cells and B cells)). Acellular components include the extracellular matrix (ECM) and cytokines (i.e. IL-1β, IL-6,

IL-8, IL-10, MIF, TGF-β and TNF-α) [25, 59]. The tumour microenvironment of pancreatic cancer contributes to controlling tumour growth, invasion, and metastasis via its close interaction and communication with cancer cells [60].

1.6.1. Cellular Components

1.6.1.1. Stromal Cells

1.6.1.1.1 Pancreatic Stellate Cells (PSCs)

Pancreatic stellate cells (PSCs) are myofibroblast-like cells found in the exocrine part of the pancreas and controlled *via* paracrine and autocrine stimulation. PSCs have several similar biological characteristics to hepatic stellate cells (HSCs) [61]. PSCs constitute around 4% of all pancreatic cells and are divided into quiescent and activated phenotypes [61, 62]. In the normal pancreas, PSCs stay in a quiescent state (qPSCs). Quiescent PSCs express abundant levels of vitamin A containing lipid droplets in their cytoplasm and express markers such as vimentin, glial fibrillary acidic protein (GFAP), nestin, desmin, neural cell adhesion molecule (NCAM) and nerve growth factor (NGF) [63]. qPSCs are activated in response to pancreatic injury or inflammation and transformed into myofibroblast-like cells. This activation is associated with loss of vitamin A (retinol) stores in the cytoplasm and leads to express of α smooth muscle actin (*α SMA*), increased production of chemokines and cytokines as well as increased proliferation, migration, and production of ECM such as collagen I [64, 65]. Recent studies have shown a correlation between immunosuppression and pancreatic stellate cells (PSCs). It has been observed that PSC-secreted CXC chemokine ligand 12 (CXCL12) can inhibit the infiltration of CD8+ T cells into the peritumoral stroma of pancreatic cancer [66]. In PDAC, Tregs cells expressing the CXCR3 receptor can be attracted by interferon-γ inducible

protein 10 (IP-10/CXCL10) produced by PSCs in the TME. This recruitment leads to immune suppression and the promotion of tumour growth [67].

1.6.1.1.2 Cancer-Associated Fibroblasts (CAFs)

Cancer-associated fibroblasts (CAFs) are a crucial component of the TME [68]. There are four major sources of CAFs including activation of normal fibroblasts and qPSCs, epithelial-to-mesenchymal transition (EMT), recruitment of bone marrow-derived mesenchymal stem cells (BMSCs) and endothelial-to-mesenchymal transition (EndMT) [68, 69]. CAFs have recently been found to be a heterogenous population, with 3 major sub-types [70]. These include myofibroblastic CAFs (myCAFs), Inflammatory CAFs (iCAFs) and antigen-presenting CAFs (apCAFs) [70]. MyCAFs surround neoplastic cells and express increased *αSMA* levels and need juxtracrine interactions with cancer cells for their development. iCAFs reside further away from neoplastic cells within the dense stroma and have low *αSMA* expression with elevated production of inflammatory mediators and chemokines such as Interleukin 6 (IL-6), Interleukin 11 (IL-11), Leukemia inhibitory factor (LIF) and C-X-C motif chemokine ligand 1(*CXCL1*), C-X-C motif chemokine ligand 2 (*CXCL2*), respectively [71]. Tumour-secreted ligands (TGF-β and IL-1) stimulate CAF heterogeneity in both myCAF and iCAF phenotypes. However, apCAFs are derived from mesothelial cells [72].

1.6.1.1.3 Endothelial Cells

Another cellular component in tissue from pancreatic tumour patients is endothelial cells [73, 74]. Endothelial cells in pancreatic cancer stroma express the surface marker CD31 [75]. In tumours with high expression of CD31, there is significantly upregulated vascular stability and immune response [75]. The stable vessels enable the entry of anti-cancer immune cells such as CD4+T cells, CD8+ T cells, gamma-delta T cells and naïve B cells into the TME. Hence, the

high expression of CD31 in PDACs was correlated with better overall survival in pancreatic cancer patients [75].

1.6.1.2. Immune Cells

1.6.1.2.1. Innate Immune Cells

1.6.1.2.1.1. Macrophages

Macrophages are resident and recruited cells (heterogeneous populations) located in all organs and protect the host and tissue homeostasis [76]. There are two distinct sub-types of macrophages known as M1 and M2. M1 macrophages exhibit pro-inflammatory characteristics and are activated by T helper 1 (Th1) cytokines to stimulate the response of inflammatory and tumoricidal activity [77]. However, M2 macrophages express CD163, CD204, CD206 and are activated by T helper 2 (Th2) cytokines, which play a crucial role in the pro-tumour activities, including tumour proliferation, anti-inflammatory and tissue remodelling [78] **(Figure 1.3)**. Tumour-associated macrophages (TAMs) represent a highly abundant immune cell population within the pancreatic tumour stroma. TAMs tend to undergo M2 polarization, which promotes and sustains various tumour behaviours, including tumorigenesis, metastasis, immune escape and resistance to chemotherapy [79]. Macrophages have an active role in transforming pancreatic cancer from primary to more aggressive phenotype *via* TGF-β regulation [80]. In the PDAC TME, TAMs secrete TGF-β, binding to PDAC cells and triggering Smad2/3 phosphorylation. This leads to the formation of the active phosphor-Smad2/3/4 complex and promotes Snail transcription, which decreases E-cadherin expression and enhances PDAC metastasis [81].

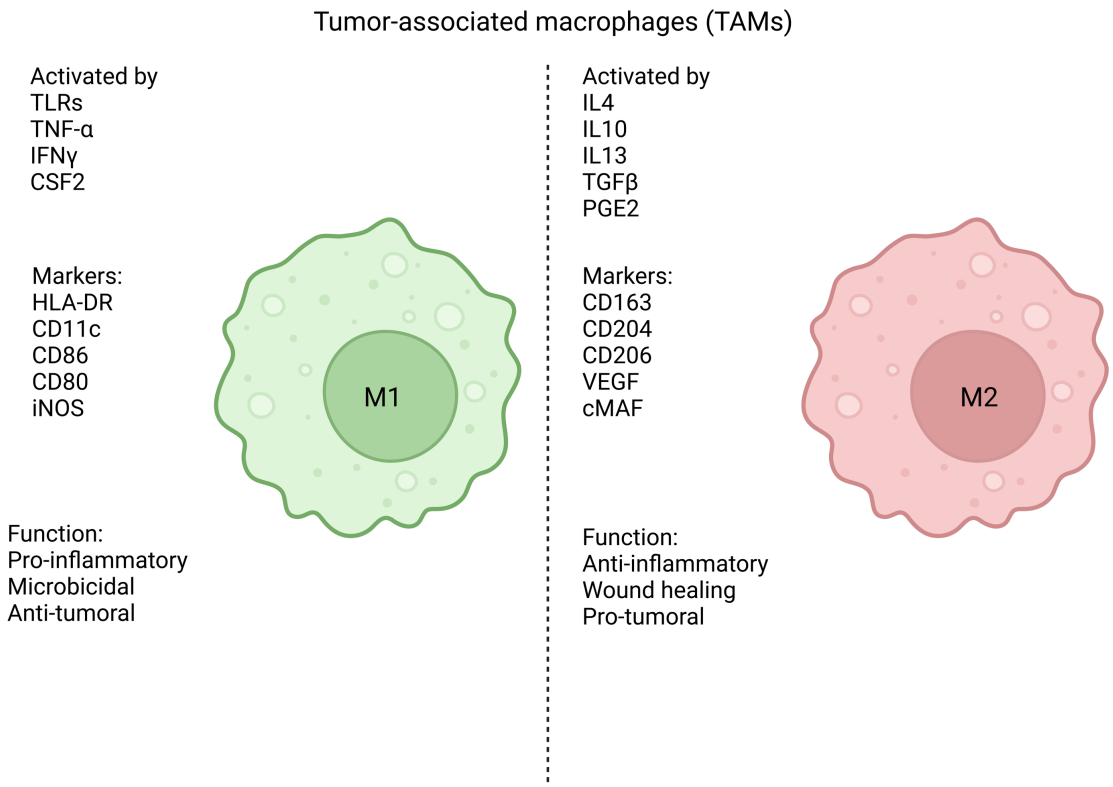

Figure 1.3: Illustration of the activation process and functions of M1 and M2 TAMs. Toll-like receptors (TLRs), tumor necrosis factor alpha (TNF-α), interferon gamma (IFNγ), colony stimulating factor 2 (CSF2), inducible nitric oxide synthase (iNOS), transforming growth factor beta (TGFβ), prostaglandin E2 (PGE2) and vascular epithelial growth factors (VEGFs).

1.6.1.2.1.2. Dendritic Cells (DC)

Dendritic cells (DC) are a heterogeneous population of antigen-presenting cells critical in commencing and forming an immune response. Dendritic cells are responsible for T-cell activation [82]. In pancreatic cancer, the number of functional DCs is decreased compared to normal tissue, which affects antigen presentation and participates in immune tolerance [83]. DCs vaccination strategies have recently been implemented because they have promoted the innate and adaptive immune responses [84]. The aim of the vaccination is to promote tumour-specific effector T cells that can decrease the tumour mass and control tumour relapse via encouraging immunological memory [84].

1.6.1.2.1.3. Natural Killer (NK)

Natural Killer (NK) cells are a group of large granular lymphocytes (about 15% of all circulating lymphocytes), and they are a member of the innate immune system [85, 86]. Cytotoxic functions of NK cells can be triggered through several receptors. These receptors enable NK cells to recognize different kinds of target cells. These receptors signal *via* ITAM-dependent pathways, such as FcRc, CD3f and DAP12, and ITAM-independent pathways [87]. Furthermore, NK cells express several MHC-I-specific inhibitory receptors, and the signals from these receptors control the cytotoxicity of NK cells [87]. According to the density of CD56 on their cell surface, the NK cells are divided into two subsets; those that express low levels of CD56 ($CD56^{dim}$), which constitutes about 90 % of human NK cells, and those with high levels of FCγ receptor III ($CD56^{bright}$), which makes up about 10% of NK cells [86]. In PDAC patients, NK cells are present in average quantity in the peripheral blood while showing the $CD16^{hi}CD57^{hi}$ phenotype, with remarkable downregulation of NK group 2D (NKG2D). Notably, these cells exhibit reduced cytotoxic activity and low levels of IFN-γ expression

instead of producing high intracellular levels of IL-10 (an immunoregulatory cytokine), which is found at increased levels in the blood of PDAC patients [88]. In pancreatic cancer patients, the activity of NK cells was found to decrease as cancer progressed, and this reduced activity correlated with poor clinical outcomes [89].

1.6.1.2.1.4. Myeloid-derived suppressor cells (MDSCs)

Myeloid-derived suppressor cells (MDSCs) are a heterogeneous group of immunosuppressive myeloid cells, including myeloid progenitors and immature cells (macrophages, granulocytes and dendritic cells) found to be high in cancer patients [90-92]. MDSCs have a marked ability to suppress the T-cell response [92]. MDSC constitute two main subsets of granulocytic ($Ly6G^{+}Ly6C^{low}$) and monocytic cells ($Ly6G^{-}Ly6C^{high}$). The granulocytic subset exhibited a high level of reactive oxygen species (ROS) and relatively little nitric oxide (NO). However, the monocytic subset had a relatively little ROS and a high level of NO [93]. MDSCs perform their immune-suppressive functions *via* several mechanisms, including directly *via* cell-to-cell contacts such as programmed death-ligand 1 (PD-L1)/ programmed cell death protein 1 (PD-1) ligation. They also have indirect effects *via* the release of ROS, arginase-1 (Arg1) and iNOS or differentiating into M2 macrophages, which also participate in the release of factors such as IL-10 and TGF-β [94].

1.6.1.2.2. Adaptive immune cells

1.6.1.2.2.1. T cells

T lymphocytes are the main population of immune cells in pancreatic cancer patients [95]. $CD3^+$ T lymphocytes are classified according to the expression of specific surface markers in $CD8^+$ cytotoxic/effector T cell, $CD4^+$ helper T (Th) cell and $CD4^+CD25^+$Forkhead box P3 $(Foxp3)^+$ Treg [96].

1.6.1.2.2.2 CD4+ T cells

CD4+ T cells play a crucial role in the regulation of the immune response against cancer. $CD4^+$ T cells modulate the function of $CD8^+$ T cells by enhancing their priming through activation of antigen-presenting cells (APCs) and maintaining their function and proliferation *via* secretion of cytokines [97]. B cells also require $CD4^+$ T cells for activation [97]. $CD4^+$ T cells differentiate into two subsets of T-helper cell populations, including Th1 and Th2. T helper type 1 (Th1) cells induce cell-mediated immune responses *via* producing interferon-γ (IFN-γ) and interleukin 2 (IL-2). However, T helper type 2 (Th2) cells help humoral immune responses through secreting IL-4, IL-10, and IL-13 [98, 99]. In pancreatic cancer, Th2 ($GATA3^+$) sub-populations are the predominant sub-type of T-helper cells, and their levels are considered to be negative survival markers in pancreatic cancer [100]. Furthermore, pancreatic cancer cells modify the function of $CD4^+$ T-cell *via* inhibiting $CD4^+$ T-cell proliferation and migration [101].

1.6.1.2.2.3. $CD8^+$ T cells

$CD8^+$ T cells are cytotoxic T cells with the capacity to lyse their target cells and are crucial constituents of tumour-specific cellular adaptive immunity [23, 102]. Exhausted $CD8^+$ T (T_{ex}) cells are dysfunctional states in CTLs characterized by loss of effector functions, decreased survival, and high and sustained expression of inhibitory receptors [103]. In pancreatic cancer, the infiltration of $CD8^+$ T cells is marked in low-grade pancreatic lesions, while being decreased during the progression of both PanINs and IPMNs [104]. Pancreatic cancer cells express PD-L1 that binds to PD1 (checkpoint inhibitor) expressed in CD8+ T cells, with this binding leading to impaired $CD8^+$ T cell function [105]. Hence, inhibiting PD-1 leads to increases in effector $CD8^+$ T cells and the production of tumour-specific interferon-γ (IFN-γ) from $CD8^+$ T cells in the tumour microenvironment [106]. In pancreatic carcinoma, the expression of Major Histocompatibility Complex (MHC) class I is frequently lost, which stops the cytotoxic effect of $CD8^+$ T cells [107]. Pancreatic cancer cells also release TGF-β that acts on cytotoxic T cells to inhibit the expression of five cytolytic genes (perforin, granzyme A, granzyme B, Fas ligand, and IFN-γ), which are responsible for cytotoxic T lymphocytes mediated tumour cytotoxicity [108]. Furthermore, increased infiltration of $CD8^+$ T cells in the tumour correlates with prolonged survival [109, 110].

1.6.1.2.2.4. Regulatory T cells (T_{regs})

Regulatory T cells (T_{regs}), defined as $CD4^+$ $CD25^+$ $Foxp3^+$ cells, inhibit the adaptive immune response and are related to poor prognosis in cancer [111]. In pancreatic cancer, T_{regs} control the immune response and appear from premalignant lesion to cancer [104]. T_{regs} suppress the activity of antitumor immune cells such as $CD4^+$ and $CD8^+$ T cells, macrophages, natural killer cells, and dendritic cells in the tumour microenvironment via expression of cytotoxic T-lymphocyte-associated protein 4 (CTLA-4) and production of IL-10 and TGF-β [96]. In

pancreatic cancer patients, the prevalence of T_{regs} in the peripheral blood and the tumour microenvironment are increased, and this may reduce the immune response against cancer [112]. Pancreatic cancer cells release high levels of ligands for chemokine receptor type 5 (CCR5), such as CCL5, while T_{regs} express CCR5. When CCR5/CCL5 signalling is disturbed or obstructed via decreasing the production of CCL5 via tumour cells or via administration of a CCR5 inhibitor, the migration of T_{regs} to tumours decreases and tumours become smaller in size [113].

1.6.1.2.2.5. B cells

The understanding of B cell functions in modulating the immune response to pancreatic cancer has not been widely researched, and their roles remain controversial. In pancreatic cancer, the presence of $CD20^+$ lymphocyte cells are correlated with improved survival (CD20 is a marker for B lymphocytes) [114]. B cell-activating factor (BAFF), a cytokine belonging to the tumour necrosis factor (TNF) superfamily, is extraordinarily expressed in infiltrating B lymphocytes around the pancreatic tissues [115]. BAFF is increased in patients with advanced metastatic PDAC, and it may have a role *via* modulation of epithelial-mesenchymal transition genes (EMT-associated genes) in the progression of tumours [115]. Furthermore, the pro-tumorigenic effect of B cells is mediated by the expression of IL-35 *via* a mechanism including IL-35-mediated stimulation of the proliferation of pancreatic cancer cells [116].

1.6.2. Acellular components

The acellular components consist of structural extracellular matrix (ECM) proteins and soluble signalling molecules, essential for communication with cellular compartments [117].

1.6.2.1 Extracellular matrix (ECM)

The ECM consists of non-cellular components such as polysaccharides, proteins, proteoglycans and glycoproteins with characteristic biochemical and physical properties [25, 118]. In pancreatic cancer, the ECM plays a crucial role in tumour biology by serving as a physical barrier that shields the tumour from host responses and systemic chemotherapy, preserving the tumour microenvironment biomechanical and biochemical properties, and controlling the growth of the tumour [119]. An imbalance in ECM synthesis, production and altered expression of matrix remodelling enzymes leads to abnormal ECM dynamics in PDAC [120, 121]. The mechanisms of ECM-related chemoresistance can be classified into two main types: physical barriers (such as abnormal vascularization and matrix stiffness) and cell adhesion-related factors (including ECM composition, mechanical signalling pathways, and pro-survival signalling pathways) [120, 122].

The physical characteristics of the ECM generally relate to its stiffness, porosity, and insolubility, along with other essential properties that are vital for providing structural support. These traits play a key role in maintaining tissue integrity and facilitating cell migration and anchorage [123, 124]. ECMs offer various anchor points for cells to attach and move, acting as a physical barrier that manages cell mobility by isolating or linking different tissues via variations in hydration [125]. In TME, the ECM often becomes stiffer, primarily because of increased collagen crosslinking. The accumulation of ECM components, such as collagen, shapes the ECM's topography and determines the accessibility of various ligands to cells.

Additionally, interstitial pressure increases as a result of dysfunctional lymphatics and disorganized microvasculature stemming from heightened angiogenesis [122].

The ECM comprises a diverse range of biochemically and structurally varied components. Biochemically, these components can be classified into proteins, proteoglycans, and glycoproteins, each with distinct subcategories and varying physical and biochemical characteristics [123]. The biochemical characteristics of the ECM enable cells to detect and engage with their surroundings through various signalling pathways. ECM components, particularly adhesive proteins like fibronectin, integrins, and non-integrin receptors, along with growth factors and related signalling molecules, provide these chemical signals. Interactions with various matrices through specific receptor sets can elicit unique cellular reactions [126, 127]. Chemical modifications change the biochemical traits and structural features of the ECM [128]. The primary proteins included are lysyl oxidase (LOX), LOX-like proteins (LOXLs) and tissue transglutaminase 2 (TG2) [128]. Increased expression of LOX and LOXLs leads to enhanced fibrosis and stiffness of the ECM and facilitates tumour development and metastasis [128, 129]. Tissue transglutaminase 2 (TG2), which is overexpressed in cancer cells, enhances the cross-linking of the ECM, influencing mechanical characteristics and cell-matrix signalling [128, 130].

The pathological ECM supports cancer growth, survival, and invasion and affects the activity of fibroblasts and immune cells; this leads to the formation of metastases and resistance to chemotherapy. These factors contribute to the high lethality of PDAC [117, 120].
In the process of tumour transformation, CAFs increase the deposition of ECM with the help of molecular messengers such as TGF-ß and sonic hedgehog (SHH). This results in the formation of a dense and stiff matrix around early PDAC cells, which promotes the growth and

invasiveness of PDAC by activating pro-tumorigenic programs [121]. Pancreatic stellate cells (PSCs) play a crucial role in conserving the normal ECM via controlling ECM synthesis and degradation and can induce pancreatic fibrogenesis by heightening the synthesis of ECM proteins [131].

The dense ECM causes blood vessels to collapse, which limits the delivery and diffusion of oxygen (hypoxia) and nutrients, and promotes a more aggressive phenotype [132].A list of the key ECM components and their function in PDAC is shown in **Table 1.1**.

Table 1.1: ECM components in Pancreatic Cancer

ECM components	Function	Ref
Type 1 collagen	As a barrier to invasion. Increasing tumour migration and invasion.	[133]
Laminin	Formation of metastasis via the formation of hemidesmosomes or stimulation motility of epithelial cells by the cleaved form of laminin.	[134]
Fibronectin	Promotes tumour cell proliferation via increased reactive oxygen species (ROS) production. Increases metastatic spread, chemoresistance and angiogenesis.	[135]
Hyaluronan	Play a crucial role in pancreatic cancer progression and survival via its CD44 receptor.	[136]

Osteopontin	Promotes immune escape in pancreatic cancer by compensating for Programmed death receptor ligand-1 (PD-L1) function.	[137]
Thrombospondin-1 (TSP-1)	Increase metastasis and angiogenesis	[138]

1.6.2.2.Cytokines

The PDAC TME comprises various cell types surrounded by dense fibrous stroma. These cells communicate through cytokines, which play a key role in reshaping the PDAC TME by influencing the functions and phenotypes of the neighbouring cells. [139]. Pancreatic cancer is generally considered an immunologically cold cancer, and both tumour and inflammatory cells produce a variety of cytokines or chemokines. These include pro-inflammatory IL-1, IL-6, IL-8, IL-17, and TNFα, the anti-inflammatory IL-10, and the dual-function cytokine TGF-β [139]. In the progression of PDAC, cytokines control the activity of various oncogenic regulators, including NF-κB, c-Myc, growth factor receptors, and mucins. This regulation results in high-grade PanIN lesions, transforming epithelial cells into mesenchymal cells and triggering metastasis [140]. Combined with the oncogenic Kras mutation, these signalling factors released by TAMs and CAFs trigger acinar-ductal metaplasia (ADM), leading to early preneoplastic lesions [139, 140]. A study discovered that patients with pancreatic cancer had elevated levels of IL-6, IL-8, IL-10, and TNFα compared to the healthy control group [141].

A list of the key cytokines involved in PDAC, and their functional effects are summarized in **Table 1.2**.

Table 1.2: Cytokines in Pancreatic Cancer

Cytokines	Function	Ref
Interleukin-1β (IL-1β)	Formation of the pro-tumorigenic tumour microenvironment and promotes immune suppression in pancreatic cancer.	[142]
Interleukin-6 (IL-6)	Promotes epithelial-mesenchymal transition (EMT) in tumour cells through Stat3/Nrf2 pathway. Involved in angiogenesis and metastasis	[143, 144]
Interleukin-8 (IL-8)	Enhance angiogenesis and metastasis via the MAPK pathway.	[145]
Interleukin-10 (IL-10)	Help tumour cells to escape immune identification and elimination.	[102]
Macrophage Migration Inhibitory Factor (MIF)	Promotes tumour growth, invasiveness, aggressiveness, and therapeutic resistance	[146]
Transforming Growth Factor-β (TGF-β)	Tumour formation and metastases	[147]
Tumor Necrosis Factor (TNF-α)	Enhance tumour proliferation and metastasis	[148]

1.7. Metabolic re-programming of the TME

PDAC exhibits a distinct metabolic phenotype, with calorie restriction in *in vivo* models of PDAC reduces tumour growth, supporting the vital role of metabolism in this cancer type [149]. PDAC cells adjust their metabolism based on the surrounding environment, often depending on various nutrient sources [150]. The signature event in PDAC is the oncogenic KRAS mutation. KRAS signalling is critical in controlling the transcription of glucose transporters (GLUTs) and essential glycolysis genes [151, 152]. However, the alteration of glycolysis in PDAC cells involves multiple pathways, such as the UHRF1/SIRT4 axis, PRMT5/FBW7/cMyc axis, JWA/AMPK/FOXO3a/FAK axis, and KRAS/TP53/TIGAR axis. These signalling pathways are crucial for glycolysis and could be potential targets for treating PDAC [153]. Hence, PDAC cells primarily rely on glycolysis for energy production, even under normoxic conditions, a phenomena called the Warburg effect [154].

Non-neoplastic cells convert glucose into pyruvate *via* glycolysis, and the majority of pyruvate is then utilized in mitochondrial oxidative phosphorylation (OXPHOS) to efficiently produce adenosine triphosphate (ATP) energy. The primary usage of glucose is for energy production, and elevated ATP levels inhibit glycolysis through feedback inhibition (**Figures 1.4A**) [155]. The Warburg Effect refers to an elevation in the rate of glucose uptake, with the resulting pyruvate being converted into lactate instead of being used for OXPHOS. The selective production of lactate, even when oxygen is present leads to acidification of the TME and contributes to immunosuppression (**Figures 1.4B**) [156]. The Warburg effect enables PDAC cells to generate ATP even in aerobic conditions. This metabolic process also helps PDAC cells avoid producing reactive oxygen species (ROS) and efficiently fulfils their biosynthesis requirements during proliferation, invasion, migration, and metastasis [154, 157]. HIF-1α overexpression stimulates the expression and function of glucose transporters

(GLUTs), hexokinase (HK), phosphofructokinase (PFK-L), aldolase (ALD-A), glyceraldehyde 3-phosphate dehydrogenase (GAPDH), phosphoglycerate mutase (PGAM-B), Enolase (ENO-α), and Pyruvate kinase pyruvate kinase (PKM-2), leading to enhanced glycolysis and glucose uptake in PDAC [158, 159]. Although pyruvate is diverted away from the mitochondria during the Warburg effect, PDAC cells can also enhance mitochondrial OXPHOS by enhancing uptake of the amino-acid glutamine. Glutamine is metabolized into glutamate, which is then used to fuel a network of enzymes and intermediates [149]. For instance, PDAC cells use glutamate to activate the tricarboxylic acid (TCA) cycle and the electron transport chain by converting it into alpha-ketoglutarate (αKG) within the mitochondria [149, 160]. PDAC cells can meet their higher metabolic demands by boosting glutamine production or enhancing environmental glutamine uptake. This reduces glutamine levels in the bloodstream, even in the presence of many fibrotic cells in the pancreas [149, 161].

Recent studies have identified that the Warburg effect also extends to the stroma – with PDAC cells promoting glycolysis in neighbouring CAFs. This phenomena is known as the reverse Warburg effect, with PSCs and CAFs engaging in glycolysis and subsequently transfer of metabolites to PDAC cells to support mitochondrial respiration and energy production (**Figures 1.4A**) [162]. Activated PSCs were found to release non-essential amino acids (NEAA) including alanine and glutamine, which are then taken up by PDAC cells and vital for PDAC survival and progression [163]. The metabolism of TAMs can also be affected by PDAC cells, with TAMs exhibiting reduced glycolytic activity due to nutrition and immune circuit changes, ultimately promoting tumour progression [153].

Hypoxia occurs when the tissue's oxygen supply is reduced, leading to insufficient oxygen levels for the body's local needs. Hypoxia is a prominent feature in 50–60% of solid tumours, including PDAC [164]. In a hypoxic TME, mutant KRAS helps maintain the stability of HIF1A and HIF2A, leading to increased production of carbonic anhydrase 9 (CA9), which regulates pH and glycolysis in PDAC [165]. The hypoxic microenvironment of PDAC mainly results from desmoplastic fibrotic stroma, rapid proliferation of cancer cells, and poor vascularization, which increased oxygen consumption and compromised oxygen supply [166-168]. Oxygen is associated with the expression of GLUT-1 *via* HIF-1α [149]. PDAC hypoxic cells have a higher glycolytic potential than cells exhibiting aerobic glycolysis, leading to a more robust activation of all enzymes and transporters involved in glucose uptake and the formation of lactic acid [169].

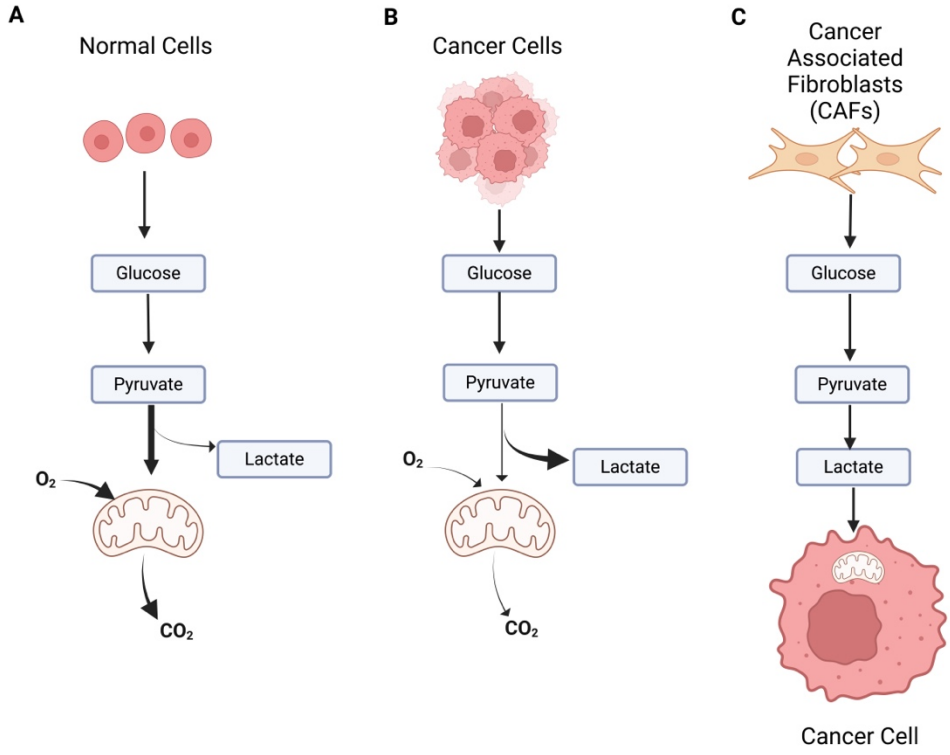

Figure1.4.: The Warburg effect and the reverse Warburg effect: (A) Normal cells, (B) Warburg effect in cancer cells and (C) Reverse Warburg effect in CAFs.

1.8. Limited treatment

The PDAC is considered one of the leading causes of cancer-related mortality worldwide [170]. This is a result of delayed diagnosis and traditional chemotherapy resistance. The delay in diagnosis is caused by the wide range of non-specific symptoms related to the disease. Genetic mutations develop resistance to chemotherapy, such as gemcitabine [171]. PDAC patients are classified into four stages based on the tumour's location within the pancreas and the involvement of the arterial or venous systems. The stages include resectable, borderline

resectable and unresectable according to National Comprehensive Cancer Network (NCCN) guidelines [172-174]. In pancreatic cancer, surgical resection is the only curative treatment. However, after careful evaluation, only 15-20% of patients are eligible for the surgery [172, 175]. For patients with resectable or borderline resectable pancreatic cancer, the recommended treatment is surgical resection followed by six months of postoperative chemotherapy or preoperative chemotherapy with or without chemoradiotherapy [176]. Patients in the locally advanced unresectable stage are treated with systemic chemotherapy, and surgical resection may be considered for down-staged patients. For patients in the metastatic stage, the recommended treatment is systemic chemotherapy [176]. Most patients at the time of diagnosis are considered unresectable due to the disease remaining symptomatically silent in the early stages and the unavailability of effective screening tests [177]. Adjuvant therapy, such as chemoradiotherapy (to decrease the risk of locoregional failure) and systemic treatment (to reduce the risk of distant metastases), has been extensively studied due to the poor outcomes of surgery alone [173]. The first FDA-approved treatment for patients with pancreatic cancer is gemcitabine [177]. The mechanism of gemcitabine is to inhibit DNA synthesis during the S phase of the cell cycle [178]. However, the efficacy of gemcitabine in PDAC is low, increasing the survival of patients for an average of just 3 months [179]. More recently, the combination of gemcitabine with nab-paclitaxel (Abraxane) has been found to prolong overall survival compared to gemcitabine alone [173]. A more effective strategy for PDAC was introduced in 2010 and consist of a combination of 4 drugs including oxilaplatin, leucovorin, irinotecan and 5-fluorouracyl (FOLFIRINOX). FOLFIRINOX significantly improved survival compared with monotherapy with gemcitabine alone, resulting in an increased average survival of 4.3 months, although it also comes with greater side effects than the gemcitabine/nab-paclitaxel regime and is given to younger, more fit patients as it has greater efficacy [180]. FOLFIRINOX and gemcitabine-nab-paclitaxel regimens are the two most effective chemotherapy regimens

for patients with metastatic PDAC at present [180]. Previously, survival for two years among metastatic pancreatic cancer patients was rare but is now observed in approximately 10% of patients who have undergone one of these treatment regimens [173]. However, despite these advances, low vessel density and the formation of fibrotic barriers in pancreatic cancer tissue areas reduce drug penetration, leading to drug resistance [173, 181]. Hence, despite initial efficacy, many patients ultimately develop resistance to current treatments for advanced pancreatic cancer. However, there have been significant advancements in the research and application of immunotherapy and stromal-targeting therpies for various types of cancer, including a recent breakthrough in treating pancreatic cancer [182].

1.9. *N-myc downregulated gene-1* (*NDRG1*)

In humans, n-myc downstream-regulated gene-1 (NDRG1) is located on chromosome 8q24.3 and encodes a 3.0 kb mRNA, translating to a 43 kD protein. It belongs to the NDRG family, which is classified within the alpha/beta hydrolase superfamily [183, 184]. NDRG1 shows a sequence identity of 53–65% with other NDRG proteins (NDRG2, NDRG3, and NDRG4), with the highest similarity found in the α/β hydrolase motif. Notably, none of the NDRG isoforms display any hydrolase activity [183, 185]. NDRG1 has a unique structure compared to other NDRG proteins because it contains three tandem repeats of 10 amino acids (GTRSRSHTSE) in its C terminus and a helix-turn-helix (HTH) motif at the N-terminus of the protein sequence (**Figure 1.5**) [183, 186].

NDRG1 is a cytoplasmic protein contributing to stress responses, hormone responses, cell growth, and differentiation [187]. NDRG1 has been reported to suppress metastasis, act as a biomarker for negative outcomes, and even promote disease progression. Thus, the function of NDRG1 in cancer is complex and not fully comprehended due to its pleiotropic and context-

dependent functions [184]. NDRG1 has reported to have anti-metastatic functions in several pancreatic [188], breast [189], colon [190] and prostate [191] cancers. However, NDRG1 has a pro-oncogenic role in other cancers, including of the skin [192], uterine cervix [193], liver [194], lung [195] and stomach [196]. The progression to metastasis is influenced by oncogenic pathways, including TGF-β and Wnt, which exert both direct and indirect effects. The expression of NDRG1 is linked to these pathways [184]. The reduced expression of NDRG1 is associated with accelerated tumour growth in pancreatic tissues, while elevated levels of NDRG1 inhibit multiple oncogenic pathways in PDAC cells [188, 197]. Recent research indicates that NDRG1 plays a critical role in controlling the metabolism of PDAC cells. Specifically, NDRG1 has been shown to decrease the expression of GLUT1 and necessary glycolysis enzymes such as Hexokinase 2 (HK2), lactate dehydrogenase A (LDHA), and Pyruvate dehydrogenase kinase 1 (PDK1), resulting in reduced glycolysis and increased mitochondrial respiration in PANC-1 and MIAPaCa-2 PDAC cells [198]. Furthermore, there is evidence to suggest that NDRG1 suppresses glycolysis enzymes by diminishing the function of hypoxia-inducible factor 1 (HIF1), potentially playing a role in this regulatory process [198, 199].

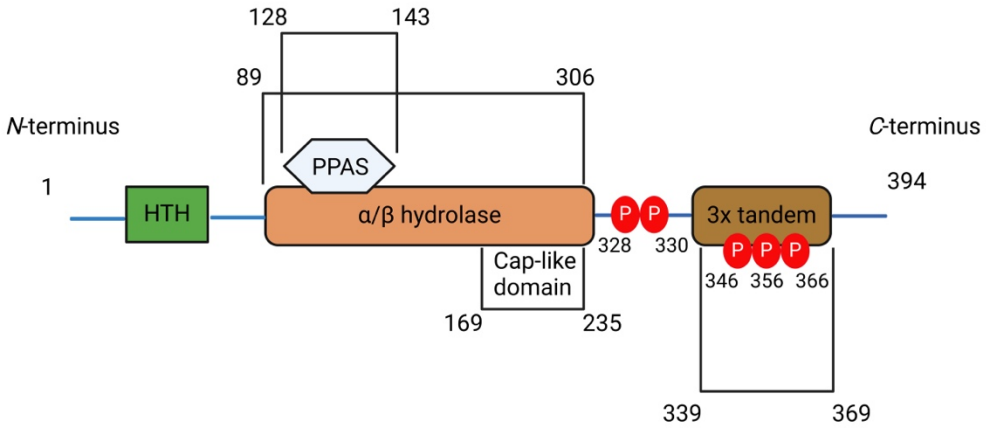

Figure 1.5: General structure of NDRG1 protein.

1.10. MIA PaCa-2 and PANC-1 cell lines

The human cells PANC-1 and MIAPaCa-2 were both derived from PDAC patients [200]. MIAPaCa-2 cells were derived from the pancreas adenocarcinoma of a 65-year-old man. The tumour involved the pancreas's body and tail and infiltrated the periaortic area [200, 201]. PANC-1 cells were derived from a 56-year-old male with PDAC located in the head of the pancreas, which had invaded the duodenal wall [200, 202]. MIAPaCa-2 and PANC-1 cells were genotyped, and it was confirmed that a homozygous missense mutation was present in codon 12 of KRAS in MIAPaCa-2 cells. A heterozygous missense mutation was also identified in the same codon in PANC-1 cells [203]. The MIAPaCa-2 cells have a homozygous deletion that includes exons 1, 2, and 3 of the CDKN2A/p16INK4A gene. They also have a homozygous missense mutation in exon 7 of the TP53 gene [203, 204]. However, the CDKN2A/p16INK4A gene has a homozygous deletion of exons 1, 2, and 3, and there are two missense variants in the TP53 gene, one missense variant is in exon 4, and the other is in exon 8 in PANC-1 cells

[203, 204]. Through sequencing, no SMAD4/DPC4 mutation was identified in either the PANC-1 or MIA PaCa-2 cell lines [203, 204]. These two cell lines were chosen for this study as they are very well characterized and widely used to investigate PDAC biology. Further, earlier work from our group has used these two cell lines to demonstrate the potent anti-cancer effects of NDRG1 and its ability to influence the cross-talk between these cell lines and the stroma [205, 206]

1.11. Conclusion

Pancreatic cancer has the lowest 5-year survival rate at around 11% compared to other types of cancer, making it the deadliest type. Currently, surgery is the most effective treatment option, but only a small percentage of pancreatic cancer cases, about 10–20%, are operable at the time of diagnosis [170, 207]. PDAC is an extremely aggressive and often fatal malignancy characterized by late diagnosis and poor response to available treatments [208]. PDAC is the most common form of pancreatic neoplasm, predominantly found in the exocrine component of the pancreas and represents over 90% of pancreatic cancer cases [208]. A key hallmark of cancer is the metabolic reprogramming of cancer cells, which favours glycolysis over mitochondrial oxidative phosphorylation (TCA cycle) despite the latter being more energy efficient (known as the "Warburg Effect") [209]. However, recent studies have revealed that cancer cells are metabolically coupled to CAFs (Reverse Warburg Effect) [162, 209, 210]. In this model, cancer cells induce surrounding CAFs to undergo a metabolic switch to glycolysis, producing energy-rich metabolites, such as lactate, that are then taken up by cancer cells [210]. This metabolic reprogramming of CAFs creates a supportive environment for tumour cells, enabling their survival in low-nutrient conditions and contributing to resistance to chemotherapy [209, 210].

1.12. Hypothesis and Aims of the study

There is evidence that the reverse Warburg effect also occurs in PDAC [211]. However, the effect of CAF heterogeneity on CAF-PDAC metabolic coupling has yet to be examined and may lead to exciting new avenues for treatment. The metastasis suppressor, N-myc downstream regulated gene 1 (NDRG1), was discovered to be an inhibitor of the PDAC-CAF cross-talk [206]. The overall goal of this project was to determine the impact of NDRG1 overexpression on the immunological and metabolic reprogramming of the pancreatic tumour microenvironment.

The aims of this study were as follows:

1. Analysis of PDAC metabolic parameters in PANC-1 and MIAPaCa-2 cells following over-expression of NDRG1.
2. Characterize the effect of NDRG1 expression in PANC-1 and MIAPaCa-2 cells on macrophage polarization using THP-1 and U937 monocytes.
3. Understanding the mechanism by which NDRG1 expression in PDAC influences macrophage polarisation.
4. Investigate how NDRG1 expression in MIAPaCa-2 and PANC-1 PDAC cells influences the metabolism of surrounding pancreatic stellate cells (PSCs) and their activation into cancer associated fibroblasts (CAFs).
5. Assess mechanism by which NDRG1 influences metabolic cross-talk between PDAC cells and PSCs

Chapter 2: MATERIALS & METHODS

2.1. Cell culture

The human cells PANC-1 and MIAPaCa-2 were purchased from the American Type Culture Collection (Rockville, MD). Both cells were maintained in Dulbecco′s Modified Eagle′s Medium ((DMEM; Life Technologies, VIC, Australia) supplemented with 10% Fetal Bovine Serum (FBS) (Sigma), 1% (v/v) MEM Non-essential Amino Acid Solution (100x) (Sigma), 1% (v/v) Sodium pyruvate solution (100mM) (gibco) and 1% (v/v) Penicillin-Streptomycin (10,000 units penicillin and 10 mg Streptomycin/ml) (Sigma).

The MRC-5 cells were maintained in Eagle's Minimum Essential Medium (Gibco) supplemented with 10% fetal bovine serum (FBS) (Sigma), 1% (v/v) MEM non-essential amino acid solution (100x) (Sigma), 1% (v/v) sodium pyruvate solution (100mM) (gibco) and 1% (v/v) penicillin-streptomycin (10,000 units penicillin and 10 mg streptomycin/ml) (Sigma).

Human monocytic leukaemia cell line, THP-1, was purchased from (ATCC), was grown in RPMI-1640 Medium (gibco) supplemented with 10% Fetal Bovine Serum (FBS) (Sigma), 1% (v/v) MEM Non-essential Amino Acid Solution (100x) (Sigma), 1% (v/v) Sodium pyruvate solution (100mM) (gibco), 1% (v/v) Penicillin-Streptomycin (10,000 units penicillin and 10 mg Streptomycin/ml) (Sigma) and 0.05 mM 2-Mercaptoethanol (Sigma).

The human myeloid leukaemia cell line, U937, was a generous gift from Dr Justin Wong (Faculty of Health and Medicine, the University of Sydney). The cell line was grown in RPMI-1640 Medium (gibco) supplemented with 10% Fetal Bovine Serum (FBS) (Sigma), 1% (v/v) MEM Non-essential Amino Acid Solution (100x) (Sigma), 1% (v/v) Sodium pyruvate solution (100mM) (gibco) and 1% (v/v) Penicillin-Streptomycin (10,000 units penicillin and 10 mg Streptomycin/ml) (Sigma).

Human Pancreatic Stellate Cells (HPaSteC) from ScienCell Research Laboratories (San Diego, CA, USA) were culture in Iscove's Modified Dulbecco's Medium (IMDM) (Gibco Laboratories, NY). The cells supplemented with 10% fetal bovine serum (FBS; Sigma), 1% MEM non-essential amino acid solution (100x; Sigma), 1% sodium pyruvate solution (100mM; Gibco), and 1% penicillin-streptomycin (10,000 units penicillin and 10 mg streptomycin/ml; Sigma).

All cells were grown in the incubator at 37^{o}C in a humidified atmosphere of 5 %CO_2 and 95% air. Adherent cells were sub-cultured by incubating with 4-6 ml 1mM PBS/EDTA and incubated for 5-10 minutes in the incubator at 37^{o}C to detach from the culture flask. All cells suspension and adherent (after dissociation) were transferred to a conical centrifuge tube and then centrifuged for 5 minutes at room temperature (RT) at 300 g. The supernatant was removed, the cell pellet was suspended with new media and added the culture flask. Cells growth and morphology were assessed by phase contrast microscopy, and cells viability was evaluated by The Countess® II FL Automated Cell Counter (Thermo Fisher Scientific, AU) after mixing cells with Trypan Blue (Sigma). All cells were cultured for no longer than three months.

2.2 Stable transfection

PANC-1 and MIAPaCa-2 cells were stably transfected to over-express NDRG1 (WT-NDRG1), empty vector-transfected control (VC) and NDRG1 construct (ΔCAP) has the CAP region of the NDRG1 protein deleted (**Figure 4.1)** [212]. In brief, Kill Curve Assay using G418 (Gentamicin) (Enzo Life Science, USA) was performed for both cells, and then plasmids were prepared using GeneJET Plasmid Miniprep Kit (Thermo Fisher Scientific, AU). The

concentration of extracted DNA was measured by a Nanodrop ND-1000 spectrophotometer (Thermo Fisher Scientific, MA, USA). Following the manufacturer's protocol, the cells were transfected using Lipofectamine™ 3000 Transfection Reagent (Invitrogen). After 48 h of transfection, the culture media was replaced with fresh supplemented DMEM medium. After 72 h of transfection, the growth media was supplemented with G418 (0.5 mg/ml). The media containing G418 was replenished every three days. The transfected cell lines were maintained in media containing G418 for 10-12 days. Then, single colonies were transferred to a T25 flask for subsequent sub-culture as described in Section 2.1. The media permanently being supplemented with 0.3 mg/ml of G418 to maintain selective pressure. The expression of NDRG1 was assessed *via* Western Blot to check the success of stable transfection (**Figure 2.1**).

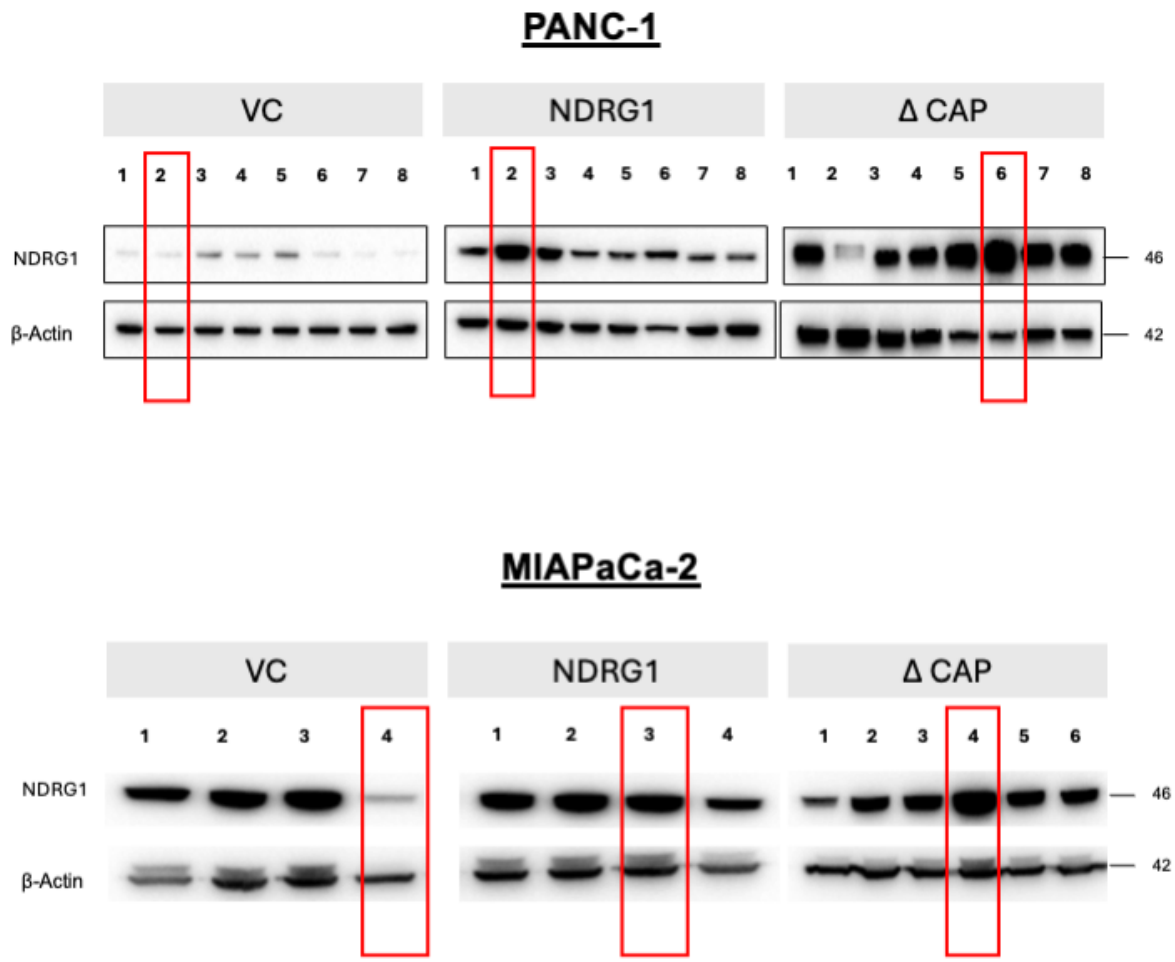

Figure 2.1: Western Blot analysis for PDAC cells stably expression NDRG1. Cell lysates from stable cell lines (A) PANC-1 and (B) MIAPaCa-2 cells stably transfected with empty vector-transfected control (VC), over-express NDRG1 (WT-NDRG1), and NDRG1 construct (ΔCAP). Red boxes indicate that the clones were selected for further studies in this thesis.

2.3 3D Spheroids Culture

A 10% methylcellulose (Sigma) stock solution was made using 10 g methylcellulose + 100 ml Milli-Q water and 100µl from the stock solution was added into PDAC cells suspended in 10 ml culture medium. The cells (2500 cells per well) were then seeded into ultra-low attachment 96-well plates to form 3D spheroids. The media was changed every 3-4 days.

2.4 Polarization of macrophage cell lines

Phorbol 12-myristate 13-acetate (PMA) was purchased from Sigma (Australia). The THP-1 or U937 monocytes were seeded at a concentration of 500,000 cells/ml and incubated in media containing 160 nM PMA for 24 hours to differentiate them into M0 macrophages. This was followed by a 24-hour incubation in fresh medium (10% FBS). For M2 polarization, the M0 macrophages were then incubated with media containing 20 ng/mL IL-4 and 20 ng/mL IL-13 (R&D Minneapolis, MN) for 72 hours. Conversely, for M1 polarization, M0 macrophages were incubated with media containing 100 ng/mL IFN-gamma and 100 ng/mL LPS (Ultrapure; InvivoGen, San Diego, CA) for 24 hours.

2.5 Protein extraction (Whole Protein)

Cells were harvested and suspended in 1X Radioimmunoprecipitation assay buffer (RIPA buffer) (cat.#: ab156034; Abcam), protease inhibitor cocktail (Roche) and phosSTOP (Roche). Before adding RIPA buffer, the cell media was removed, and the cells were washed in ice-cold PBS. On ice, RIPA buffer was added directly to the culture plates, and the cells were detached via a cell scraper. The cell suspensions were transferred to ice-cold Eppendorf tubes. The lysates were sonicated 10 x 2 s (BRANSON Sonifier 150) and then centrifugated at 13 200 g

for 40 minutes. The supernatants were collected without disturbing the cell pellet. The protein concentration was measured by BCA Protein Assay (Thermo Fisher Scientific, USA) and a UV spectrophotometer ((UV-1800; Shimadzu, Japan).

2.6 Western Blot Analysis

Equal amounts of protein 40 - 100 µg were mixed with 5% loading dye (20% Sodium dodecyl sulfate (SDS) (Sigma), 1M Tris buffer at pH 6.8 (Formedium Ltd, England), 0.06% Bromophenol blue (ICN Biomedicals Inc, Cleveland, Ohio) and 30% Glycerol (Sigma)) containing 10% 2-Mercaptoethanol (Sigma Aldrich), then boiled at 95^{o}C for 5 minutes using Block Heaters (Thermo Scientific).. The protein lysates and Kaleidoscope Precision Plus^{TM} protein molecular weight standard (Bio-Rad Laboratories, Inc., CA, USA) were used as a protein ladder. The lysates and the ladder were separated on 8-12% SDS-PAGE gel with resolving gel (1.5 M Tris-HCl pH 8.8) and stacking gel (1 M Tris-HCl pH 6.8). The running was for 2 h at 120 V in a running buffer (0.1% SDS (Sigma), 25 mM Tris (Formedium Ltd, England), 192 mM glycine (Sigma Aldrich), pH 8.3) then transferred by useing transfer buffer ((20% methanol (Sigma Aldrich), 25 mM Tris (Formedium Ltd, England), 192 mM glycine (Sigma), pH 8.3) overnight to polyvinylidene difluoride (PVDF) with 0.45 µm pore size (Immobilon®) at 4^{o} C at 30V. The PVDF membrane was activated by soaking it in methanol prior to being used. Post transfer, the membrane was blocked in 5% Blocking Reagent (Bovine Serum Albumin (BSA) (Sigma Aldrich) or non-fat dried milk) in TBS-T (tris-buffered saline with Tween 20) (150 mM NaCl, 20 mM Tris base (Formedium Ltd, England), 0.1% (v/v) Tween 20 (Sigma), pH 7.6) for 1h at RT. The membrane was incubated with primary antibody overnight at 4^{o}C. The membrane was washed with TBS-T thrice (15 minutes each) before adding the secondary antibody for one hour at RT. After applying the secondary antibody, the

membrane was washed with TBS-T three times (15 minutes each). Both antibodies (primary and secondary) were diluted in a 5% solution of either BSA or non-fat dried milk in TBS-T according to the manufacturer's protocol. The antigen-antibody complex was detected using Immobilon® ECL Ultra Western HRP Substrate (Merck Millipore, MA, USA), and then the membrane was exposed to ChemiDoc™ (Bio-Rad, CA, USA). The quantification of Western blot bands was performed using Bio-Rad's ImageLab software. The densitometry data was analyzed using GraphPad Prism 10 (GraphPad, U.S.A.) and Microsoft Excel (Microsoft, U.S.A.). The data was normalised using the loading control β-actin.

2.7 XFe96 seahorse assay

Stably transfected MIAPaCa-2 and PANC-1 cells (2 x 10^4 in 80 µl of media per well) were plated in Seahorse XF 96-well plate from Agilent Seahorse XFe96/XF Pro Extracellular Flux Assay Kits (Agilent Technologies, Santa Clara, CA). The plate was kept for one hour at room temperature inside the biosafety cabinet, followed by incubation at 37 °C with 5% CO_2 overnight. On the same day, 20 ml of Agilent Seahorse XF Calibrant was placed in a non-CO_2 37°C incubator overnight (water bath) and filled the utility plate with 200 µl of Milli-Q water. Next, the sensor cartridge was lowered onto a utility plate and incubated overnight at 37°C in a non-CO_2 incubator using XF Prep Station (Agilent Technologies, Santa Clara, CA). The next day, the Milli-Q water in the utility plate was replaced with 200 µl of the pre-warmed XF Calibrant then the plate was placed in a non-CO_2 incubator using XF Prep Station (Agilent Technologies, Santa Clara, CA) for one hour. XF assay medium (97 ml Seahorse XF DMEM Medium, pH 7.4, 1 ml Seahorse XF Glucose (1.0 M solution), 1 ml Seahorse XF Pyruvate (100 mM solution) and 1 ml Seahorse XF L-Glutamine (200 mM solution) was warm at 37°C. First, the cells were washed by removing 60 µl then washed 2X with 200 µl and then added 160 µl

(final volume 180 µl). Next, the plate was incubated in a non-CO_2 incubator using XF Prep Station (Agilent Technologies, Santa Clara, CA) for one hour. Both plates were loaded into Seahorse XF96 Analyzer (Agilent Technologies, Santa Clara, CA) and started with calibrate cartridge (assembled sensor cartridge with utility) then Seahorse XF96 Cell Culture Microplates. The oxygen consumption rate (OCR) and extracellular acidification rate (ECAR) for the cells were assayed using this protocol (loop start 8x, mix 3 min, wait 2 min and measure 5 min). IncuCyte was used to check the confluency of the cells for normalization.

2.8 Cell Cycle Analysis

The cell cycle was analyzed using the Cell Cycle Analysis Kit (ab287852, Abcam) according to the manufacturer's protocol. The cells were harvested and centrifuged at 400x g for 5 minutes. The supernatant was removed, and the cells were resuspended in 2 ml of ice-cold 1X Cell Cycle Assay Buffer. Then, the cells were centrifuged at 400x g for 5 minutes to remove the supernatant, and the cell pellet was fixed by adding 2 ml ice-cold 70% ethanol (drop by drop while vortexing) to the cell pellet and putting it on ice for at least 30 minutes. The cells were centrifuged at 400 x g for 5 minutes, and the supernatant was carefully removed. The cells were washed in 2 ml of 1X Cell Cycle Assay Buffer and centrifuged at 400 x g for 5 minutes, and the supernatant was carefully removed. The cells were entirely resuspended with 500 µl of Staining Solution to protect them from light exposure. The analysis was performed using the Attune NxT flow cytometer (Thermo Fisher Scientific), and the data was further analyzed using FlowJo software (TreeStar, Ashland, OR).

2.9 MitoPlate S-1

The mitochondrial metabolic activity of the cells was analyzed using MitoPlate S-1 (Biolog Cat. #14105, Hayward, CA, U.S.A.) according to the manufacturer's instructions. First, 30ul per well of the Assay Mix was added into all wells and incubated at 37 °C for 1 hour to allow substrates to dissolve fully. The cells were harvested and resuspended cells in 1x Biolog MAS. Then, the cells were filtered through a 70-micron nylon filter (cell strainer, Falcon 352350) to remove clumps. The cells were counted, and their viability was determined with trypan blue. The cells should have viability >95%. The cell suspension was dispensed to all wells by adding 30ul per well of the 2x cell suspension in 1x Biolog MAS. The cells were incubated at 37°C for 6 hours, and the absorbance at 590 nm was measured at 30-minute intervals using the SpectraMax M3 reader (Molecular Devices, San Jose, CA, U.S.A.). The data were normalized by subtracting the "No substrate" control from all other substrates to account for the background signal. Wells containing substrates requiring L-malate transport and metabolism were adjusted by subtracting the 100 μM L-malate well. Data was analyzed using Microsoft Excel (Microsoft, U.S.A.) and GraphPad Prism 10 (GraphPad, U.S.A.).

2.10 Preparation of Conditioned media (CM)

Stable NDRG1 over-expressing cells or the relevant VC cells (PANC-1 and MIAPaCa 2) were seeded into 75 cm^2 flasks at a 4×10^6 cells/flask density for 72 hours. After incubation, the conditioned media were collected, centrifuged at 500 g for 5 minutes to remove cell debris and filtered through a 0.2 μm filter ((Sigma)). The conditioned media was either used fresh or stored at -80^o C. The conditioned media was mixed 50:50 with fresh media (10% FBS).

2.11 Statistics and densitometry

The experimental data were compared using a student t-test and presented as mean ± standard deviation (SD). All experiments were conducted in triplicate, and statistical significance was considered when the p-value was < 0.05. The results are shown as mean ± SD ($n = 3$). Statistical significance levels are denoted as follows: *$p<0.05$, **$p<0.01$, ***$p<0.001$, ****$p<0.0001$. The densitometry data was analyzed using GraphPad Prism 10 (GraphPad, U.S.A.) and Microsoft Excel (Microsoft, U.S.A.).

Chapter 3: Effect of NDRG1 on Metabolism of PDAC Cells

3.1 Introduction

Pancreatic cancer is characterized by its high aggressiveness, limited response to existing therapies, and low 5-year survival rates, which typically range from 10% to 15% [213]. The development of pancreatic cancer is influenced by lifestyle factors such as smoking and alcohol consumption, as well as genetic and environmental factors [6]. Most exocrine pancreatic cancer is classified as pancreatic ductal adenocarcinoma (PDAC), which accounts for about 90% of cases [214]. In PDAC, the tumour microenvironment (TME) represents most of the tumour mass. It comprises a complex mix of extracellular matrix components and non-neoplastic cells, such as fibroblasts and vascular and immune cells [215].

The development of tumours relies on the reprogramming of cellular metabolism, which occurs as a direct or indirect result of oncogenic mutations [216]. A key characteristic of cancer cell metabolism is their capability to obtain essential nutrients from an often nutrient-deficient environment and use them to sustain viability and generate new biomass. The changes in intracellular and extracellular metabolites that can occur due to cancer-associated metabolic reprogramming significantly impact gene expression, cellular differentiation, and the tumour microenvironment [216]. Increasing evidence indicates that PDAC cells modify metabolic processes, such as glucose, amino acids, and lipid metabolism, and depend on continuous nutrition for survival, proliferation, and invasion [217]. The Warburg effect, also known as aerobic glycolysis, refers to the high rate of glycolysis observed in cancer cells, even in the presence of oxygen, which produces a significant amount of lactate [160].

Aerobic glycolysis is the process of converting glucose into lactate and providing the carbon skeleton necessary for synthesizing macromolecular compounds such as nicotinamide adenine

nucleotide phosphate (NADPH) and adenosine triphosphate (ATP), which are essential for the proliferation of PDAC cells [217, 218]. This process involves the overexpression of glucose transporters, activation of key glycolytic enzymes, an increase in glycolytic flux, and the accumulation and transfer of glycolytic metabolic intermediates [217, 218]. Glucose transporter type 1 (GLUT1) is the main transporter responsible for cellular glucose uptake in several tissues [219]. Several studies have shown that high expression of GLUT1 is associated with shorter overall survival in pancreatic cancer patients [220-222].

Branched-chain amino acids (BCAAs), including leucine, isoleucine, and valine, are essential amino acids obtained from the diet. Cancer cells require higher levels of nutrients, such as amino acids, to support sustained growth. Consequently, cancer cells demonstrate increased uptake of BCAAs [223, 224]. L-type amino acid transporter 1 (LAT1), also known as SLC7A5, facilitates the transport of BCAAs to support the growth of cancer cells through mTOR-induced translations. Meanwhile, Alanine, serine, cysteine-preferring transporter 2 (ASCT2), also known as SLC1A5, maintains the cytoplasmic amino acid pool to support LAT1 function. Together, ASCT2 and LAT1 work to decrease apoptosis, boost energy production, and promote cell growth [225]. PDAC cells showed a significant increase in BCAA uptake *via* solute carrier transporters, which were significantly upregulated in pancreatic tumour tissues compared to normal tissues [223]. A study revealed that increased levels of BCAAs in the plasma are linked to more than a 2–fold higher risk of being diagnosed with PDAC in the future [226]. Overexpression of LAT1 is associated with a poor prognosis and correlated with chemotherapy resistance in PDAC patients [227, 228].

New findings indicate that the protein N-myc downstream regulated 1 (NDRG1) is significantly involved in tumorigenesis and acts as a metastasis suppressor in PDAC and other

cancers [229]. The downregulation of NDRG1 is associated with enhanced tumour growth in pancreatic tissues, with NDRG1 over-expression inhibiting numerous oncogenic pathways in PDAC cells [188, 197]. A recent study has also revealed that NDRG1 plays a crucial role in regulating the metabolism of PDAC cells. In fact, NDRG1 was found to downregulate GLUT1 and key glycolysis enzymes such as, Hexokinase 2 (HK2), lactate dehydrogenase A (LDHA), and Pyruvate dehydrogenase kinase 1 (PDK1) leading to reduced glycolysis and enhanced mitochondrial respiration in PANC-1 and MIAPaCa-2 PDAC cells [198]. Additionally, it has been observed that NDRG1 inhibits glycolysis enzymes by reducing the activity of hypoxia-inducible factor 1 (HIF1), potentially contributing to this regulatory effect [198, 199].

In this study, we performed untargeted metabolomic analysis to gain a more comprehensive insight into the effect of NDRG1 on PDAC cell metabolism. These experiments were conducted under both normoxia and hypoxia to gain a deeper understanding of how NDRG1 influences metabolic re-programming and the Warburg effect in PDAC cells under physiological conditions. This was of particular importance as the PDAC TME is often highly hypoxic due to the extensive desmoplasia [230]. Our findings indicate that as well as reducing glycolysis in PDAC cells, NDRG1 also significantly changed how PDAC cells respond to hypoxia. Further, NDRG1 also reduced the uptake of BCAAs by downregulating the expression of membrane transporters LAT1 and ASCT2.

3.2. MATERIALS & METHODS

3.2.1. Cell Culture

The human pancreatic cancer cells PANC-1 and MIAPaCa-2 were cultured as described above (***Section 2.1***).

3.2.2 Stable transfection

PANC-1 and MIAPaCa-2 cell lines were transfected as described above (***Section 2.2***).

3.2.3. Gene silencing by small interfering RNA (siRNA)

The PANC-1 and MIAPaCa-2 cells were transiently transfected using Lipofectamine™ RNAiMAX (Invitrogen) following the manufacturer's instructions. The siRNA used was specific for NDRG1 (siNDRG1, Cat. #4392422), as well as a negative control siRNA (siControl; Invitrogen).

3.2.4. Protein Extraction

3.2.4.1. Whole Protein

The protein extraction for whole cells was extracted as described above (***Section 2.5***).

3.2.4.2. Cytoplasmic and Nuclear Fractionation

MIAPaCa-2 VC and NDRG1 cells were incubated for 24 h in normoxia (20% O_2) and hypoxia (0.5% O_2). The cells were kept on ice, and then the media was removed and washed with PBS. The cytoplasmic extraction reagent (CER) (10 mM HEPES pH 7.5 (Sigma Aldrich), 10mM KCL (Sigma Aldrich), 0.1 mM EDTA (Sigma), 0.5% NP40 (Thermo Fisher Scientific), 1 mM 2-Mercaptoethanol (Sigma Aldrich), 1X protease inhibitor cocktail (Roche) and 1X phosSTOP (Roche)) was added to the cells, and the cells were detached using a cell scraper. The cell

suspensions were transferred to ice-cold Eppendorf tubes, vortexed for 15 seconds, and then incubated on ice for 10 minutes. After that, the cells were vortexed for 5 seconds and centrifuged at 13,200 g for 5 minutes. The supernatant (cytoplasmic extract) was collected without disturbing the cell pellet. Finally, the pellet fraction (containing nuclei) was resuspended in an ice-cold nuclear extraction reagent (NER) (20 mM HEPES (Sigma Aldrich), 400mM NaCl (Sigma Aldrich), 1 mM EDTA (Sigma), 1 mM 2-Mercaptoethanol (Sigma Aldrich), 1X protease inhibitor cocktail (Roche) and 1X phosSTOP (Roche)) . The solution was vortexed on the highest setting for 15 seconds, then incubated on ice for 40 minutes, and then centrifuged at 13,200 g for 10 minutes. The supernatant was transferred to an ice-cold Eppendorf tube. The ratio of CER to NER was 3:1. The protein concentration was measured using a BCA Protein Assay (Thermo Fisher Scientific, USA) and a UV spectrophotometer (UV-1800; Shimadzu, Japan).

3.2.5. Western Blot Analysis

Western blot was performed *via* standard methods (see ***Section 2.6***) using antibodies listed in **Table 3.1**.

Table 3.1: The list of primary and secondary antibodies used for western blot studies.

No	Name of antibody	Catalogue #	Company	Dilution
1	Fumarase	4567	Cell Signalling	1:1000
2	DLST	11954	Cell Signalling	1:1000
3	IDH1	3997	Cell Signalling	1:1000
4	Glut1	73015	Cell Signalling	1:1000
5	Hexokinase II	2867	Cell Signalling	1:1000
6	HIF-1α	36169	Cell Signalling	1:1000

7	Hexokinase I	2024	Cell Signalling	1:1000
8	LDHA	3582	Cell Signalling	1:1000
9	PKM1/2	3190	Cell Signalling	1:1000
10	Pyruvate Dehydrogenase	3205	Cell Signalling	1:1000
11	PKM2	4053	Cell Signalling	1:1000
12	IDH2	56439	Cell Signalling	1:1000
13	ACO2	6571	Cell Signalling	1:1000
14	MPC1	14462	Cell Signalling	1:1000
15	LAT1/SLC7A5	32683	Cell Signalling	1:1000
16	ASCT2	5345	Cell Signalling	1:1000
17	Phospho-mTOR (Ser2481)	2974	Cell Signalling	1:1000
18	mTOR	2983	Cell Signalling	1:1000
19	Raptor	2280	Cell Signalling	1:1000
20	NDRG1	9485	Cell Signalling	1:1000
21	β-Actin	A5316	Sigma-Aldrich	1:10,000
22	Mouse IgG secondary	A4416	Sigma-Aldrich	1:10,000
23	Rabbit IgG secondary	A6154	Sigma-Aldrich	1:10,000

3.2.6. Cell Cycle Analysis

The cell cycle of PANC-1 and MIAPaCa-2 cells was analyzed as described above ***(Section 2.8)***.

3.2.7. MitoPlate S-1

The mitochondrial metabolic activity of MIAPaCa-2 cells was analyzed using MitoPlate S-1 as described above ***(Section 2.9)***.

3.2.8. XFe96 seahorse assay

The Baseline Oxygen Consumption Rate (OCR) and Extracellular Acidification Rate (ECAR) were measured for PANC-1 and MIAPaCa-2 cells as described above ***(Section 2.7)***.

3.2.9. LC-MS metabolomic analysis

An optimized sample preparation protocol was utilized to extract metabolites from MIAPaCa-2 cells **(Figure 4)**. The cells were seeded on two 6-well plates and incubated overnight at 37°C in a humidified atmosphere with 5% CO_2 and 95% air. The following day, the media in both plates was changed to 1% FBS media. One plate was then incubated at 20% O_2, while the other was incubated at 0.5% O_2 for 24 hours. Subsequently, the media from both plates were collected for plasma metabolite analysis. The plates were washed with 1 ml of ice-cold 0.9% NaCl and then snap-frozen by adding 1 ml of liquid N2. The central carbon and plasma metabolites were measured using liquid chromatography/mass spectrometry (LC-MS), a service performed by Sydney Mass Spectrometry (University of Sydney). The data was analyzed using MetaboAnalyst 5.0 (https://www.metaboanalyst.ca) and GraphPad Prism 10 (GraphPad, U.S.A.).

3.2.10. Statistics and densitometry

The experimental data were compared using a student t-test and presented as mean ± standard deviation (SD). All experiments were conducted in triplicate, and statistical significance was considered when the p-value was < 0.05. The results are shown as mean ± SD ($n = 3$). Statistical significance levels are denoted as follows: *$p<0.05$, **$p<0.01$, ***$p<0.001$, ****$p<0.0001$. The densitometry data was analyzed using GraphPad Prism 10 (GraphPad, U.S.A.) and Microsoft Excel (Microsoft, U.S.A.).

3.3. RESULTS

3.3.1. Upregulation of NDRG1 in PANC-1 and MIAPaCa-2 cells impacts the cellular oxygen consumption rate (OCR) and extracellular acidification rate (ECAR) in PDAC cells.

To investigate how NDRG1 expression in PDAC cells affects metabolism, we first established stably-transfected PANC-1 and MIAPaCa-2 cells expressing either the vector control (VC) or wild-type NDRG1 (NDRG1). As expected, the western blot results showed that PANC-1 and MIAPaCa-2 cells overexpressing NDRG1 had significantly higher NDRG1 expression when compared to the VC cells (**Figures 3.1A and 3.1B**).

The metabolic shift in pancreatic cancer is primarily characterized by changes in glycolysis. This altered glycolytic flux is carefully regulated to support cancer cells' rapid growth and supply the necessary components for synthetic processes [231]. To investigate whether NDRG1 modifies the glycolytic metabolism of PDAC cells, we used the Seahorse analyzer to measure the oxygen consumption rate (OCR) and extracellular acidification rate (ECAR) in the overlying media.

The results indicated that NDRG1 significantly reduced the ECAR, while significantly increasing the OCR in PANC-1 NDRG1 cells compared to PANC-1 VC cells **(Figure 3.1C)**. Similar results were observed in MIAPaCa-2 cells, where NDRG1 again significantly reduced the ECAR while increasing the OCR compared to MIAPaCa-2 VC cells (**Figure 3.1D**). These findings are in agreement with previous studies [198] and suggest that NDRG1 decreased glycolysis and increased oxidative phosphorylation (OXPHOS) in PANC-1 and MIAPaCa-2 cells.

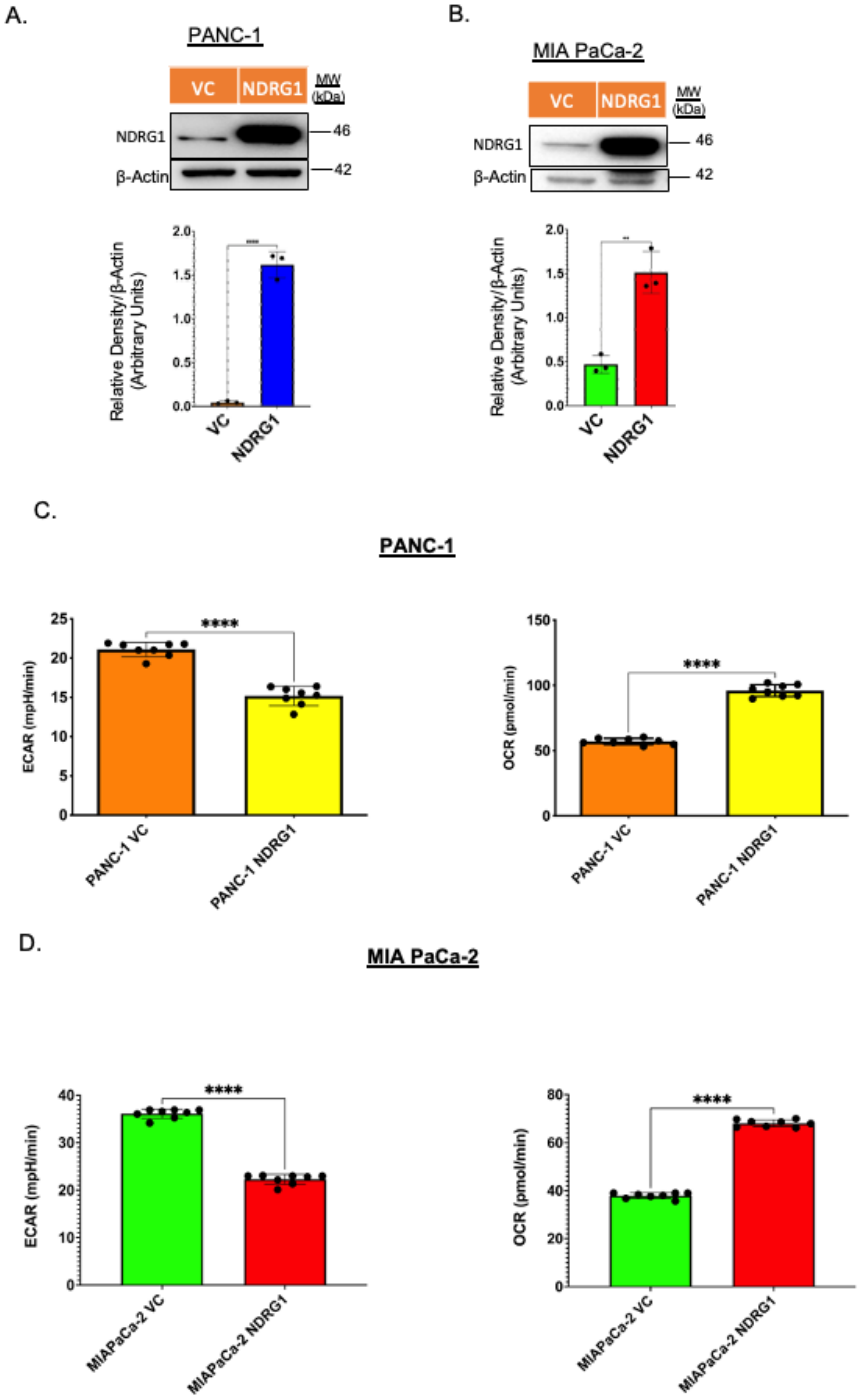

Figure 3.1: NDRG1 decreased ECAR and increased OCR in the PDAC cells Western blot and densitometry analysis of (**A**) PANC-1 and (**B**) MIAPaCa-2 cells stably transfected with VC or NDRG1. β-actin was used as a loading control. The Seahorse analyser was used to measure the oxygen consumption rate (OCR) and extracellular acidification rate (ECAR) in (**C**) PANC-1 or **(D)** MIAPaCa-2 cells. The data presented is a representative analysis of the average of three independent experiments. *p<0.05, **p<0.01 ***p<0.001 ****p<0.0001 denote statistical significance comparing each condition to the relevant VC control.

3.3.2. NDRG1 expression altered the cell cycle of PDAC cells.

Based on our findings above, NDRG1 can influence glycolysis in PDAC cells. Elevated glucose levels facilitate cell progression from the G1 to the S phase, whereas low glucose levels lead to cell cycle arrest in the G0/G1 phase [232]. To further investigate whether NDRG1 could influence glycolysis *via* the glucose transporter GLUT1, we next examined the expression of this protein in both PANC-1 and MIAPaCa-2 cells.

As expected, the Western blot results revealed a significant decrease in GLUT1 expression in PANC-1 NDRG1 cells compared to PANC-1 VC cells (**Figure 3.2A**). Similar results were observed in the MIAPaCa-2 cells, where the GLUT1 expression was markedly reduced in MIAPaCa-2 NDRG1 cells compared to MIAPaCa-2 VC cells (**Figure 3.2B**).

We next conducted a cell cycle analysis using flow cytometry to explore the potential impact of NDRG1 expression on the cell cycle of PDAC cells. The cell cycle analysis demonstrated a significantly higher proportion of cells in the G1 phase in PANC-1 NDRG1 cells and a notably lower proportion of cells in the S phase when compared to PANC-1 VC cells (**Figure 3.2C**). The proportion of cells in the G2 phase was not significantly affected by NDRG1. Similar results were also observed with the MIAPaCa-2 cells, where a significant increase in G1 and a decrease in S phase was also evident in the NDRG1 cells (**Figure 3.2D**).

Overall, these results suggest that NDRG1 expression in PDAC cells might modify the cell cycle, resulting in an increased proportion of cells in the G0/G1 phase. This further indicates that NDRG1 reduces the metabolic capacity of PDAC cells, potentially by reducing the expression of GLUT1 and subsequent glycolysis pathways.

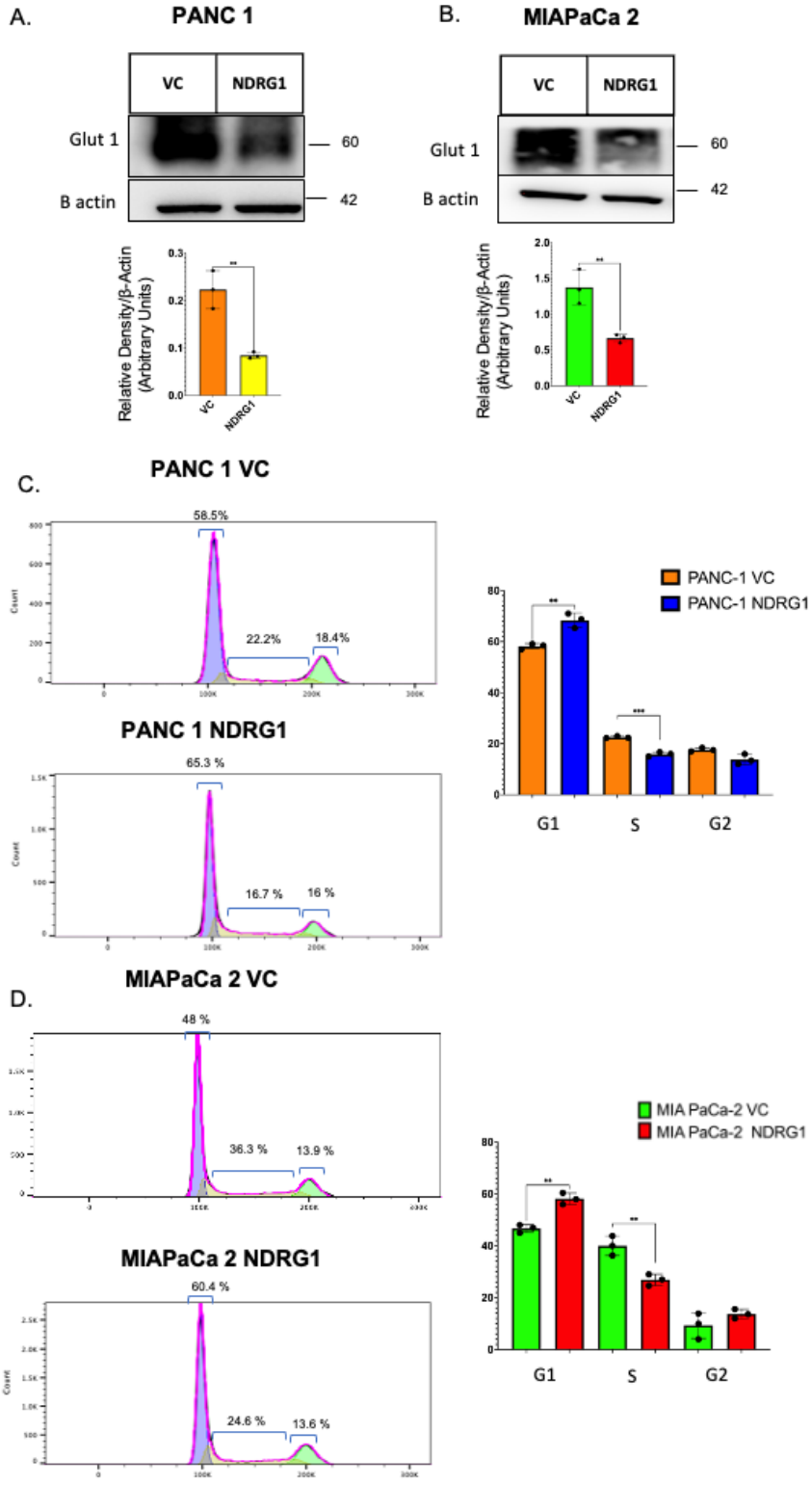

Figure 3.2: NDRG1 increases the proportion of PDAC in the G0/G1 phase. Western blots and densitometric analysis of GLUT1 in **(A)** PANC-1 and **(B)** MIAPaCa-2 cells.
Flow cytometry analysis was used to assess for the cell cycle distribution of PANC-1 (**C**) or MIAPaCa-2 (**D**) VC and NDRG1 cells. Results are mean ± SD (n = 3). **p<0.01 ***p<0.001 denote statistical significance comparing each condition to the VC control.

3.3.3. Western blot analysis of the effect of NDRG1 on metabolic enzymes in PDAC cells

Following our findings above that NDRG1 can impact the metabolism in PDAC cells, we conducted further studies to examine the expression of essential metabolic enzymes in PANC-1 and MIAPaCa-2 cell under normoxia or hypoxia. PANC-1 or MIAPaCa-2 cells were seeded on 6-well plates and incubated overnight at 37°C in a humidified atmosphere with 5% CO_2 and 95% air. The following day, the media was changed to 1% FBS for both plates, and one plate was incubated at 20% O_2, while the other was incubated at 0.5% O_2 for 24 hours.

We initially examined the expression of NDRG1 and the hypoxia marker HIF-1α. The results show that the levels of NDRG1 were potently up-regulated under hypoxia, with a further significant increase in the MIAPaCa-2 NDRG1 cells compared to MIAPaCa-2 VC under hypoxic conditions (**Figure 3.3A**). As expected, HIF-1α was also potently upregulated in the cells exposed to hypoxia. However, the increase in NDRG1 expression under hypoxia significantly reduced the expression of HIF-1α in MIAPaCa-2 NDRG1 cells compared to MIAPaCa-2 VC cells (**Figure 3.3A**).

Western blotting was then performed on these lysates to assess the expression of key metabolic enzymes including HK2, fumarase, dihydrolipoamide S-succinyltransferase (DLST) and isocitrate dehydrogenase 1 (IDH1). HK2 is a key enzyme in glycolysis, catalysing the first step of glucose metabolism [233]. Fumarase is a crucial intermediate metabolite in the citric acid cycle where it catalyses the conversion of fumerate to malate, and its levels often rise in cancer cells [234-236]. The mitochondrial protein DLST governs the entry of glutamine into the TCA cycle [237]. The cytoplasmic enzyme IDH1 catalyzes the decarboxylation of isocitrate to α-ketoglutarate (α-KG), as part of the TCA cycle, although this reaction is reversed under hypoxia [238].

Our results indicate that the expression of HK2 in MIAPaCa-2 NDRG1 cells was significantly decreased under both normoxia and hypoxia when compared to relevant MIAPaCa-2 VC cells under each condition (**Figure 3.3B**). NDRG1 also significantly decreased the expression of fumarase and DLST in both normoxic and hypoxic conditions when compared to MIAPaCa-2 VC cells (**Figure 3.3B**). However, the opposite results were observed in the expression of IDH1. The results indicate that NDRG1 increased the expression of IDH1 under both normoxia and particularly under hypoxia compared to MIAPaCa-2 VC cells (**Figure 3.3B**). Notably, the levels of Fumerase, DLST and IDH1 were significantly increased under hypoxic conditions in both NDRG1 and VC cells when compared to normoxia, which is consistent with the cells enhancing glycolysis and scavenging more TCA intermediates to fuel their proliferation under low oxygen conditions [239].

Furthermore, we examined the expression of several additional glycolysis-related proteins in MIAPaCa-2 cells, including HK1, LDHA, PKM1/2, Pyruvate Dehydrogenase, and PKM2 (**Figure 3.4**). We also investigated IDH2, ACO2, and MPC1, which play a role in the TCA cycle (**Figure 3.4**). While most of these proteins were up-regulated under hypoxic conditions, their levels were not affected by NDRG1 expression under either normoxia or hypoxia. One exception was MPC1, a TCA cycle enzyme that was reduced by NDRG1 under normoxia and hypoxia. However, this result was observed in only one set of lysates and thus its significance was not able to be deduced.

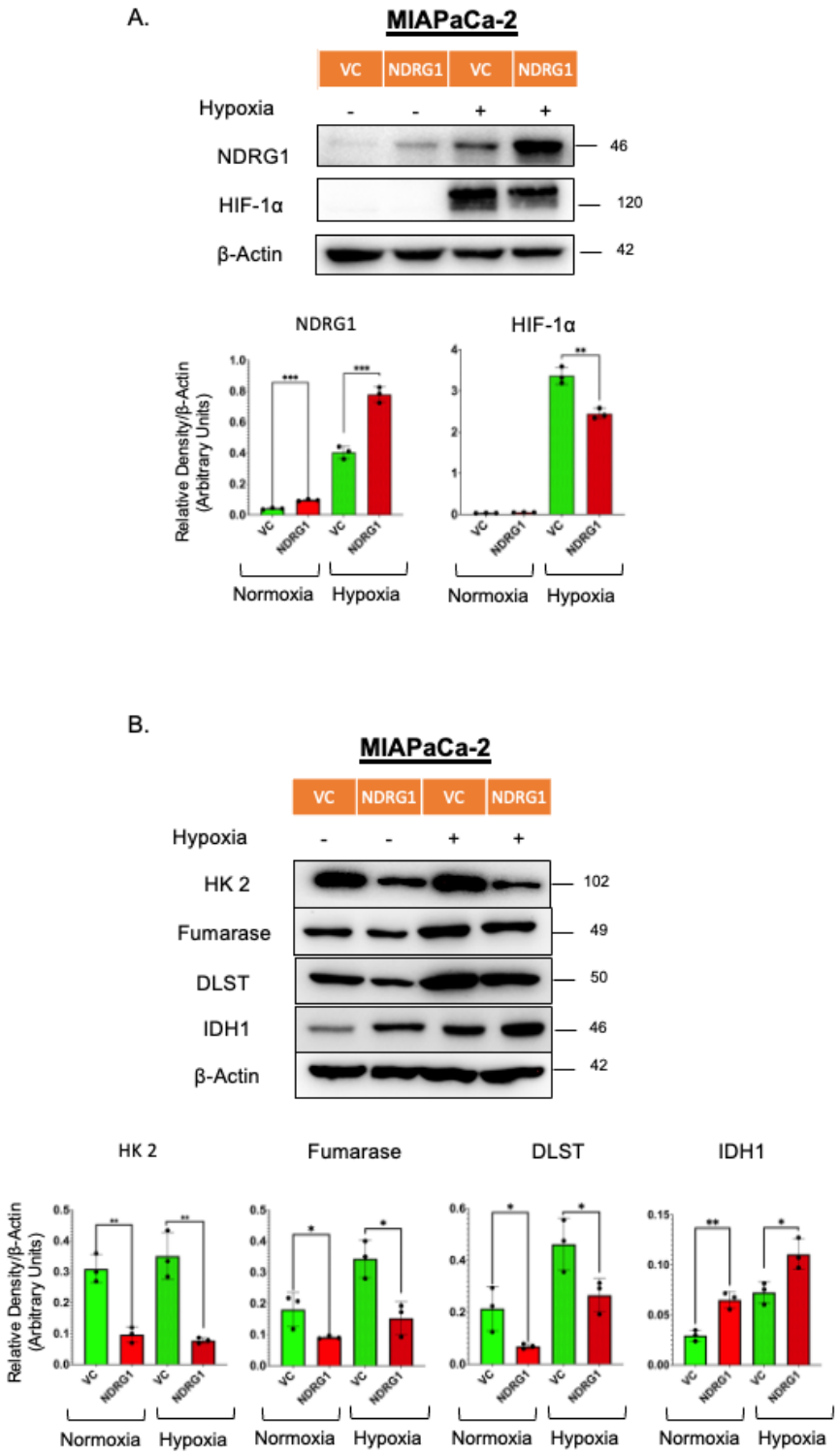

Figure 3.3: NDRG1 impacts the metabolism of MIAPaCa-2 cells. (**A**) Western blots and densitometric analysis of NDRG1 and HIF-1α in MIAPaCa-2 cells under normoxia or hypoxia. (**B**) Western blots and densitometric analysis of HK2, Fumarase, DLST and IDH1 in MIAPaCa-2 cells under normoxia or hypoxia. Results are mean ± SD (n = 3). *p<0.05, **p<0.01 ***p<0.001 denote statistical significance comparing each condition to the relevant VC control.

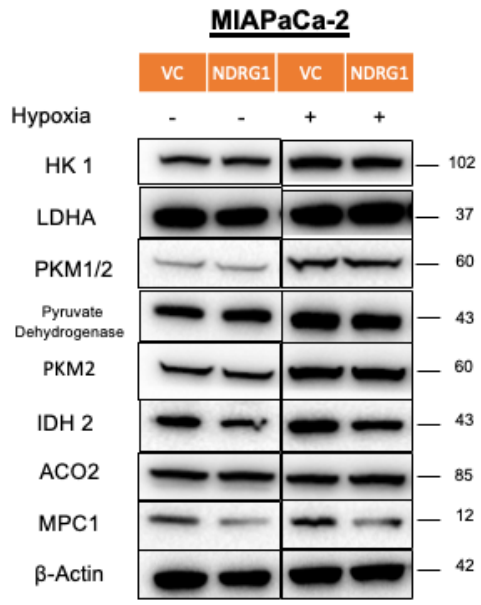

Figure 3.4: NDRG1 effect on various additional metabolic enzymes in MIAPaCa-2 cells. Western blots analysis of HK1, LDHA, PKM1/2, Pyruvate Dehydrogenase, PKM2, IDH2, ACO2 and MPC1 in MIAPaCa-2 cells under normoxia or hypoxia (n = 1). Samples were run on the same blot at the same exposure but had to be cropped to display the normoxia VC and NDRG1 next to the hypoxia VC and NDRG1 (as depicted by the line in the middle).

Examining the metabolic enzymes HK2, Fumerase, DLST and IDH1 in the PANC-1 cells, similar results were also observed. The results again showed that NDRG1 reduced the expression of HK2, Fumarase, and DLST while increasing the expression of IDH1 in PANC-1 cells compared to the VC cells under both normoxia and hypoxia (**Figure 3.5**).

Overall, the findings indicate that NDRG1 potentially reduces glycolysis under both normoxic and hypoxic conditions in PDAC cells and is in line with our Seahorse analysis and earlier studies [198]. These findings also demonstrate that NDRG1 expression can influence different enzymes in the TCA cycle, potentially reducing the ability of PDAC cells to metabolize amino acids and other metabolic intermediates that are scavenged from the TME and fed into the TCA cycle.

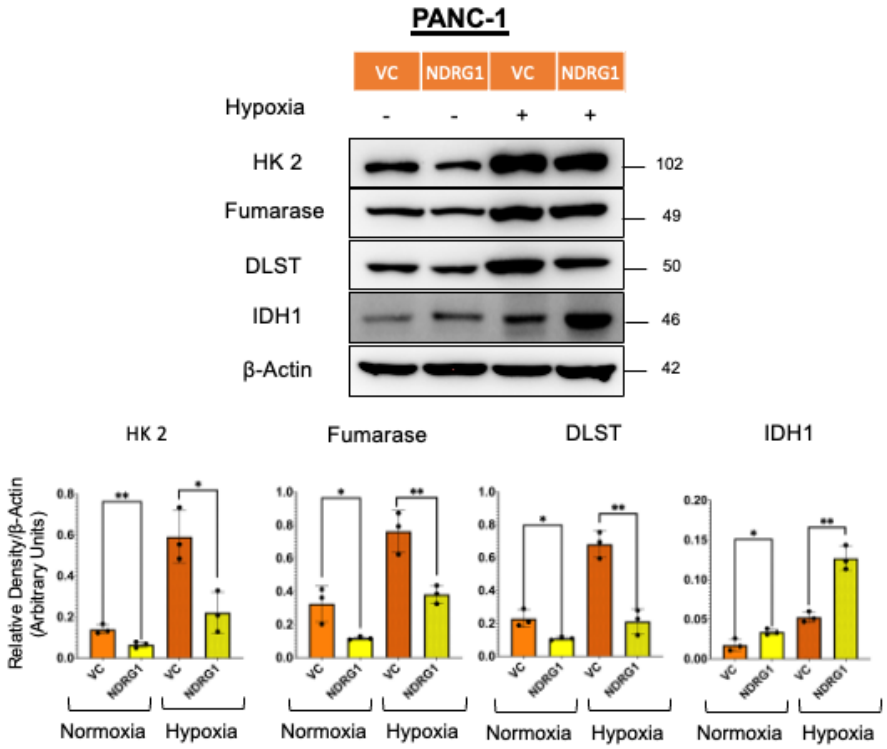

Figure 3.5: NDRG1 impacts the metabolism of PANC-1 cells. Western blots and densitometric analysis of HK2, Fumarase, DLST and IDH1 in PANC-1 cells under normoxia or hypoxia. Results are mean ± SD (n = 3). *p<0.05, **p<0.01 denote statistical significance comparing each condition to the relevant VC control.

3.3.4 The expression of NDRG1 in PDAC cells impacts their mitochondrial metabolism.

To further investigate PDAC metabolism, we performed a Mitoplate S-1 assay. MitoPlate S-1 is a 96-well microplate used to analyze the electron flow rate in live cells and assess mitochondrial functionality. It is pre-coated with different substrates (31) used as probes to examine the activity of mitochondrial metabolic pathways based on a colorimetric assay. The plate measures the rates of electron flow into and through the electron transport chain using different NADH and FADH2-producing metabolic substrates [240].

The MIAPaCa-2 cells were seeded onto MitoPlate S-1 and incubated for 6 hours at 37°C. Substrate metabolism was assessed by monitoring a colorimetric change, and the optical density was recorded at 590 nm at 15-minute intervals for 13 cycles using a kinetic plate reader (**Figure 3.6A**).

The results indicated that NDRG1 reduced the metabolism of α-D-Glucose, L-Lactic Acid, and D-Glucose-1-PO4 in MIAPaCa-2 cells compared to MIAPaCa-2 VC cells **(Figure 3.6B, C, and D)**. These findings are consistent with the western blot results mentioned earlier, which suggested that NDRG1 decreased glycolysis in PDAC cells. The results also indicate that NDRG1 influenced the metabolism of TCA substrates, reducing the metabolism of Fumaric Acid, while slightly increasing α-Keto-Glutaric Acid, in MIAPaCa-2 cells compared to MIAPaCa-2 VC cells **(Figure 3.6E and F)**.

The Mitoplate also contained metabolic intermediates namely acetyl-L-carnitine, octanoyl-L-carnitine and palmitoyl-D, L-carnitine, which facilitate the mitochondrial β-oxidation of short, medium and long chain fatty acids. L-Carnitine plays a key role in lipid metabolism,

transporting fatty acids into the mitochondria, where they are subsequently oxidised for energy generation [241]. The results showed that NDRG1 potently decreased the ability of MIAPaCa-2 cells to metabolise acetyl-L-carnitine + L-malic acid, octanoyl-L-carnitine + L-malic acid, and palmitoyl-D, L-carnitine + L-malic acid compared to MIAPaCa-2 VC cells **(Figure 3.6G, H and I)**. This suggests that NDRG1 expression reduces the capacity of MIAPaCa-2 cells to metabolise fatty acids.

The de novo synthesis pathway of serine metabolism creates an intricate metabolic network with glycolysis, the folate cycle, and one-carbon metabolism, which is crucial for the growth of rapidly proliferating cells [242]. The MitoPlate S-1 results showed that NDRG1 reduced L-serine metabolism in MIAPaCa-2 NDRG1 cells compared to MIAPaCa-2 VC cells **(Figure 3.6J)**.

The results indicate that MIAPaCa-2 NDRG1 cells have higher L-Glutamine metabolism than MIAPaCa-2 VC cells **(Figure 3.6K)**. However, the results in MIAPaCa-2 NDRG1 cells indicated that L-Glutamic Acid was reduced after 4 hours of the experiment **(Figure 3.6L)**.

Additionally, NDRG1 reduced the metabolism of substrates such as cis-aconitic acid, D,L-α-glycerol-PO_4, pyruvic acid, and D, L-isocitric acid, tryptamine and γ-amino-butyric acid in MIAPaCa-2 NDRG1 cells compared to MIAPaCa-2 VC cells **(Figure 3.7)**. These findings align with the earlier western blot results, indicating that NDRG1 reduced several metabolic enzymes which may be responsible for the general reduction in mitochondrial metabolism in PDAC cells.

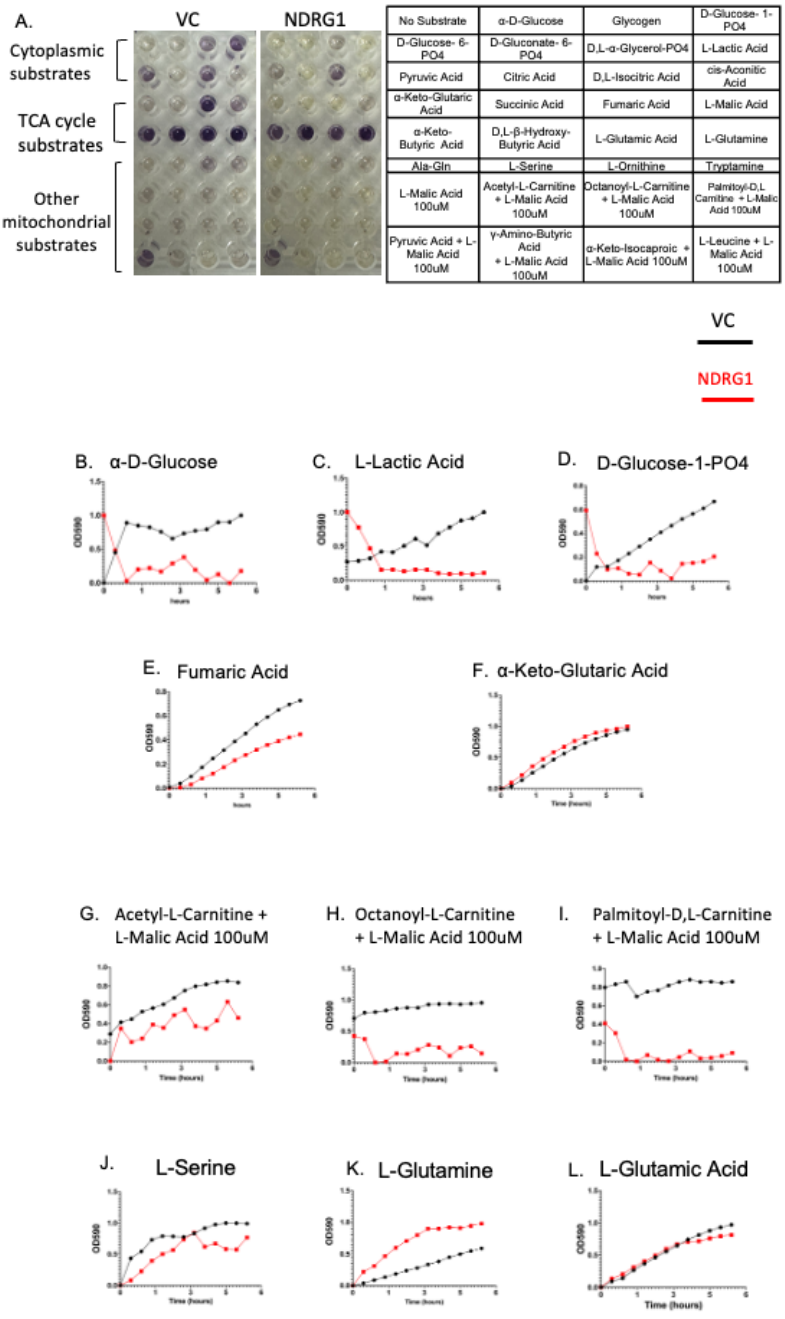

Figure 3.6: NDRG1 influences the mitochondrial metabolism of MIAPaCa-2 cells. MIAPaCa-2 cells were seeded into Mitoplate S-1 to be assessed by monitoring a colorimetric change at 590 nm at an interval of 30 minutes for 12 cycles using a kinetic plate reader. **(A)** Image of the plate layout after dye reduction, indicated by the purple colour formation in MIAPaCa-2 cells. Kinetic graphs of D-Glucose **(B)**, L-Lactic Acid **(C)**, D-Glucose-1-PO4 **(D)**, Fumaric Acid **(E)**, α-Keto-Glutaric Acid **(F)**, Acetyl-L-Carnitine + L-Malic Acid 100uM**(G),** Octanoyl-L-Carnitine + L-Malic Acid 100uM **(H),** Palmitoyl-D,L-Carnitine + L-Malic Acid 100uM **(I)**, L-Serine **(J)**, L-Glutamine **(K)**, and L-Glutamic Acid **(L)** comparing the MIAPaCa-2 cells VC (black) and NDRG1 (red). The substrates were normalized to the no-substrate control or L-malic acid 100uM. The data presented is a representative analysis of the average of three independent experiments.

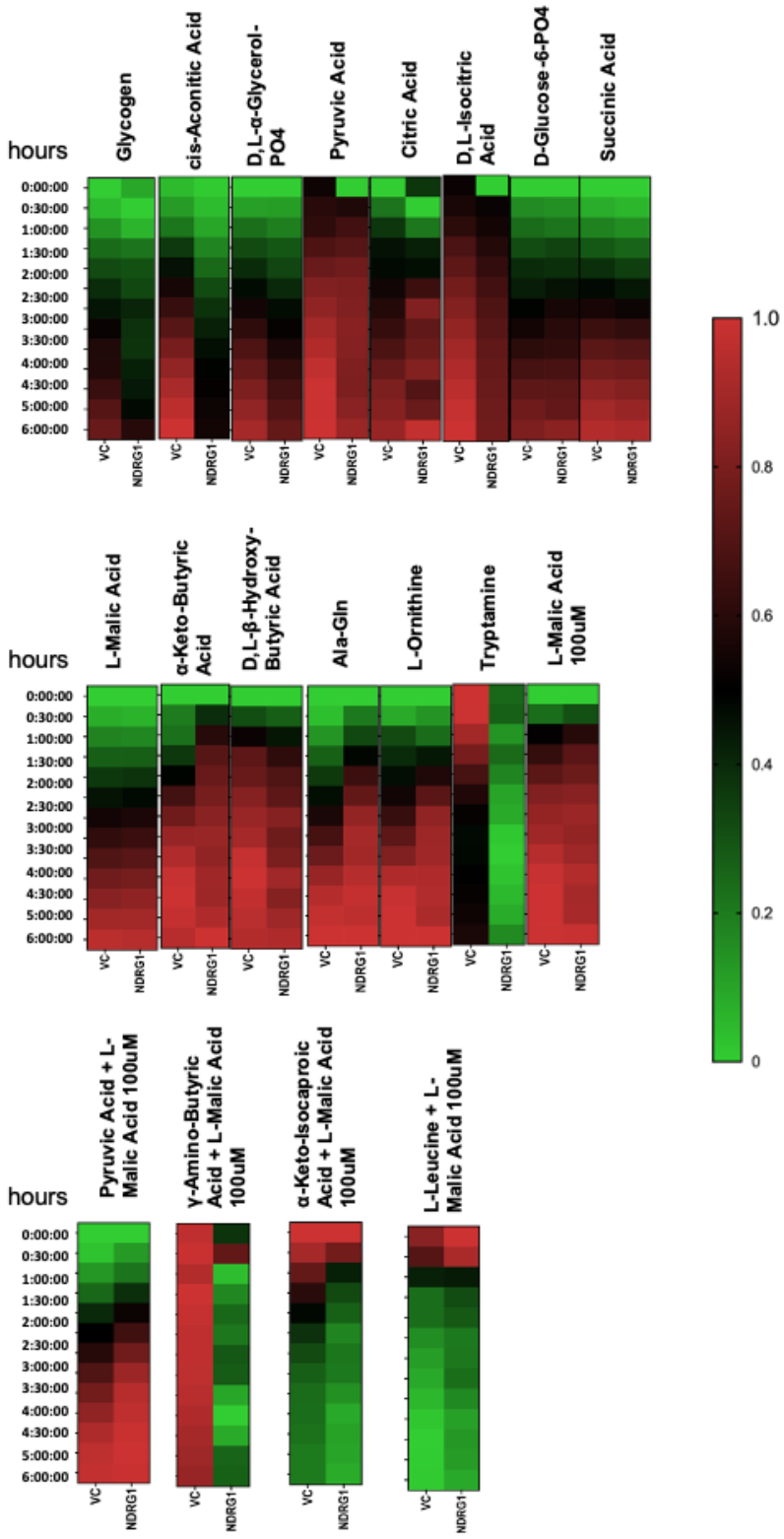

Figure 3.7: NDRG1 influences the mitochondrial metabolism of MIAPaCa-2 cells. Heat maps for all remaining Mitoplate S-1 substrates comparing the MIAPaCa-2 VC and NDRG1 cells. The substrates were normalized to the no-substrate control or L-malic acid 100uM. The data presented is a representative analysis of the average of three independent experiments.

3.3.5. Impact of NDRG1 on metabolic variations in response to normoxia and hypoxia in PDAC cells.

Considering the results above demonstrating that NDRG1 can significantly influence the expression of various metabolic enzymes and influence the processing of numerous metabolic substrates, we conducted a more comprehensive untargeted metabolomic analysis in MIAPaCa-2 PDAC cells. For this analysis, MIAPaCa-2 VC and NDRG1 cells were incubated under normoxia (20% O_2) or hypoxia (0.5% O_2) for 24 h, and both the overlying media as well as the cells were collected and snap frozen (**Figure 3.8**). The intracellular (cell lysates) and extracellular (media) samples were then examined for both central carbon and plasma metabolites *via* LC-MS.

Examining the intracellular metabolites, it was evident that NDRG1 expression altered the expression of numerous metabolites, particularly under hypoxia when compared to the VC cells (**Figure 3.9A**). Pathway impact analysis involves using enrichment analysis methods to identify the metabolic pathways with the most significance, utilizing pathway impact and adjusted p-values [243]. The pathway analysis from the normoxia samples indicated that NDRG1 significantly influenced metabolites involved in ammonia recycling, beta-alanine metabolism, pterine biosynthesis, estrone metabolism, and androstenedione metabolism pathways (**Figure 3.9B**). In the hypoxic samples, NDRG1 significantly altered metabolites involved in ammonia recycling, glucose-alanine cycle, alanine metabolism, malate-aspartate shuttle and aspartate metabolism (**Figure 3.9C**).

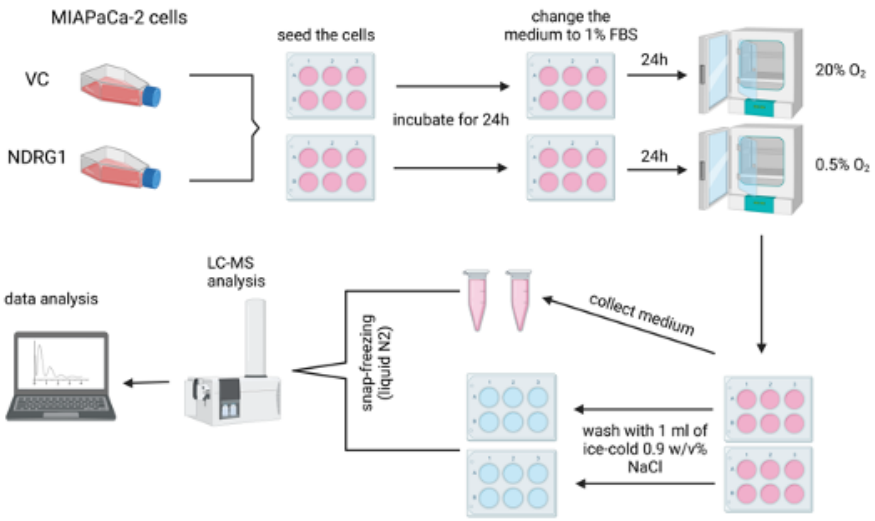

Figure 3.8: A schematic diagram illustrating the procedure used to perform extracellular and intracellular metabolomics with MIAPaCa-2 cells.

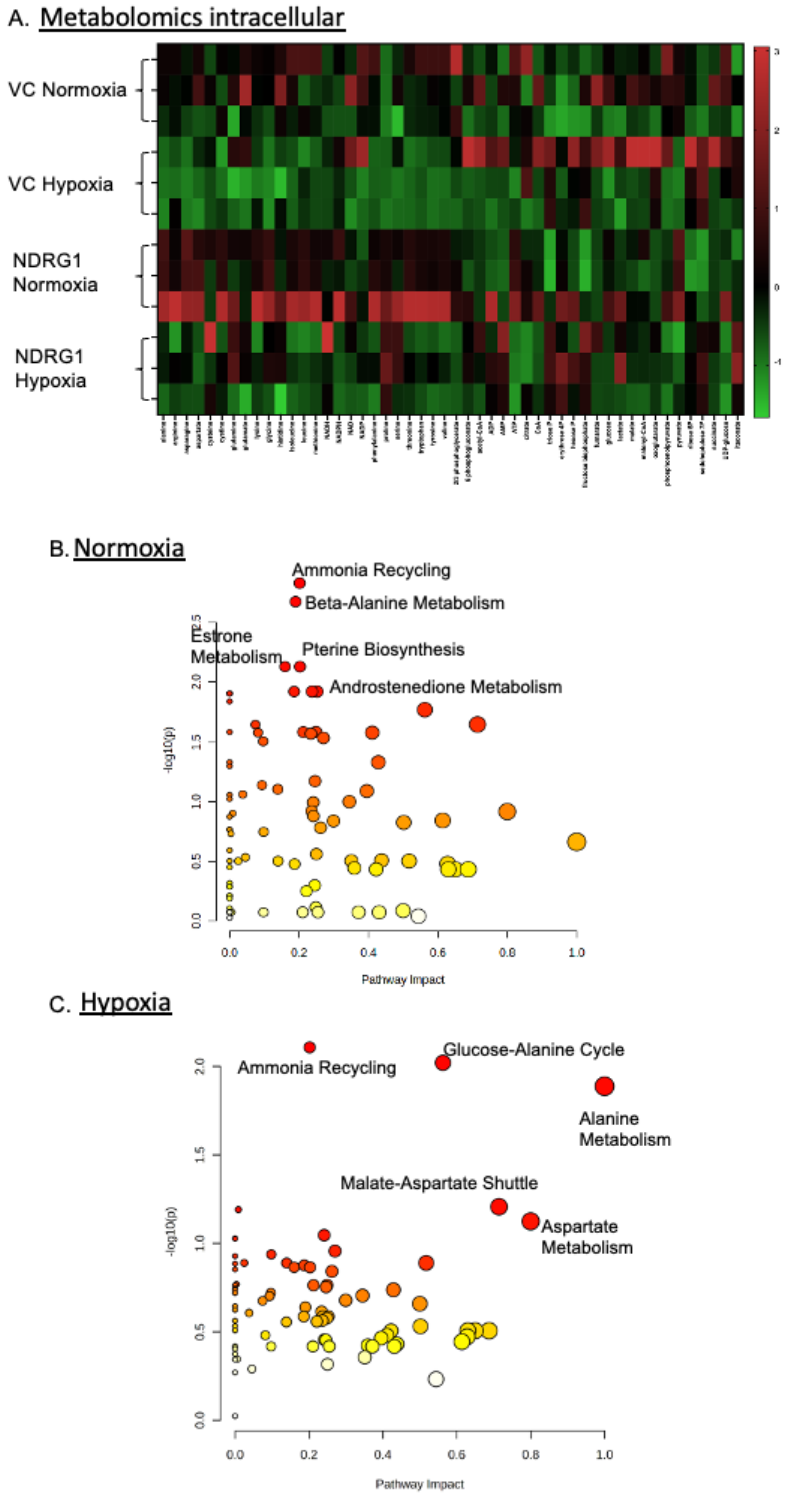

Figure 3.9: Heat map and pathway enrichment analysis of MIAPaCa-2 cell intracellular metabolites. (A) Heat map of intracellular metabolites from VC and NDRG1 cells under normoxia and hypoxia. Pathway impact graph demonstrating the altered metabolic pathways in NDRG1versus VC cells in **(B)** Normoxia and **(C)** Hypoxia. The data MIAPaCa-2 cells were analyzed using MetaboAnalyst 5.0. The red indicates the most significant effects based on the *p*-value, and the pathway impact value determines the node's size. Results are mean ± SD (n = 3).

Metabolite Pathway Enrichment Analysis takes a ranked list of metabolites and determines whether a particular known metabolic pathway tends to appear more towards the top or bottom of that list. The output is metabolic pathways with p-values indicating whether the pathway was significantly enriched [244]. The enrichment analysis showed that NDRG1 influences multiple pathways under normoxic conditions, including Glucose-Alanine Cycle, Pterine Biosynthesis, Androgen and Estrogen Metabolism, Steroidogenesis and Androstenedione Metabolism (**Figure 3.10A**). The findings indicated that NDRG1 impacted multiple pathways in hypoxic conditions, including Alanine Metabolism, Ammonia Recycling, Aspartate Metabolism, Glutathione Metabolism, and Arginine and Proline Metabolism (**Figure 3.10B**).

Most notable intracellular amino acids altered by NDRG1 included asparagine, proline and glycine, which were all significantly increased in the MIAPaCa-2 NDRG1 cells compared to VC cells under both normoxic and hypoxic conditions (**Figure 3.11A**) and (**Figure 3.12A**). Threonine was also significantly up-regulated by NDRG1 under hypoxia (**Figure 3.11A**).

Notably, NDRG1decreased several TCA cycle metabolites, including citrate, fumarate, malate, oxoglutarate, and succinate in MIAPaCa-2 cells under both normoxic and hypoxic conditions, although these effects were not found to be statistically significant (**Figure 3.12B**).

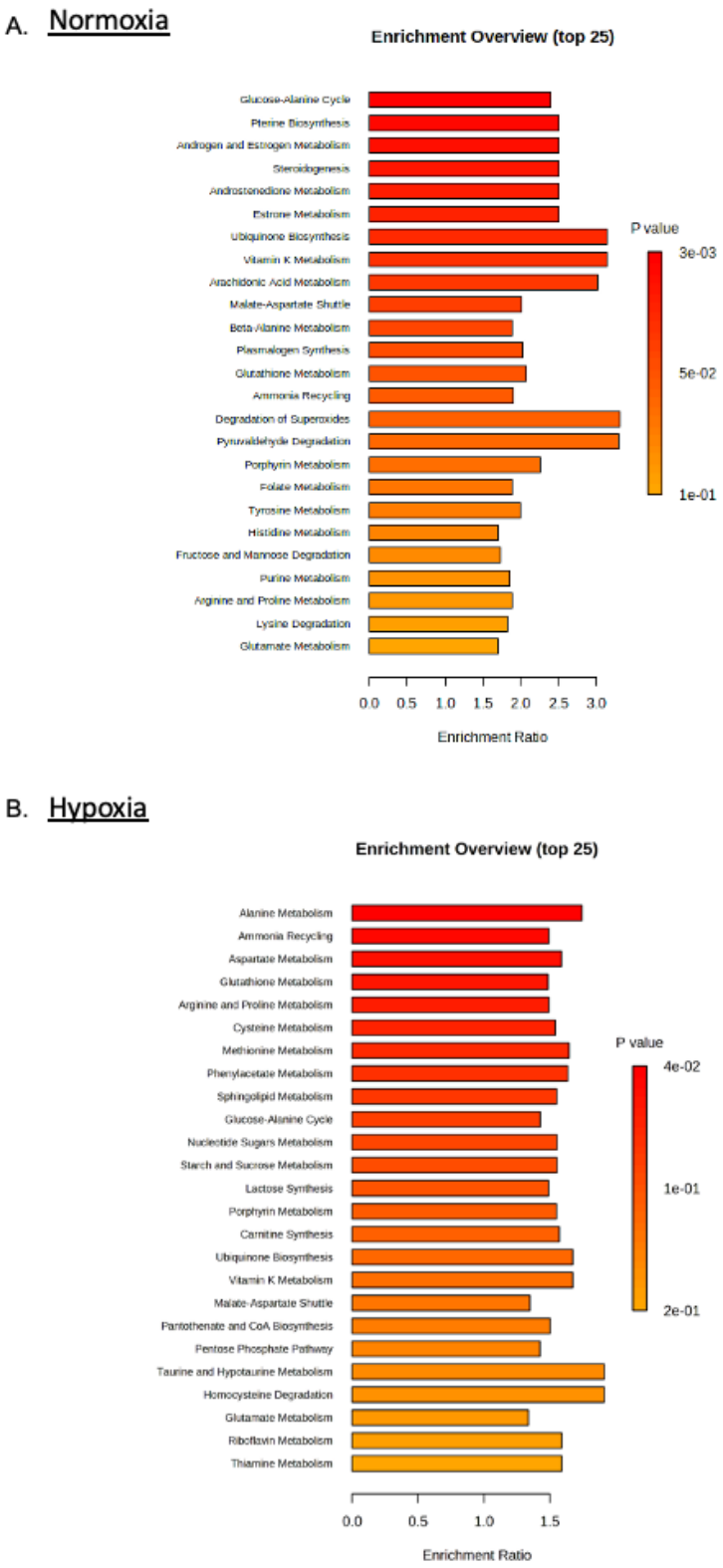

Figure 3.10: Pathway enrichment analysis of intracellular metabolites of MIAPaCa-2 cells. Pathway enrichment analysis to assess the differential intracellular metabolites in VC versus NDRG1 cells as ranked by *p*-value in **(A)** Normoxia and **(B)** Hypoxia. The data was analyzed using MetaboAnalyst 5.0. Results are mean ± SD (n = 3).

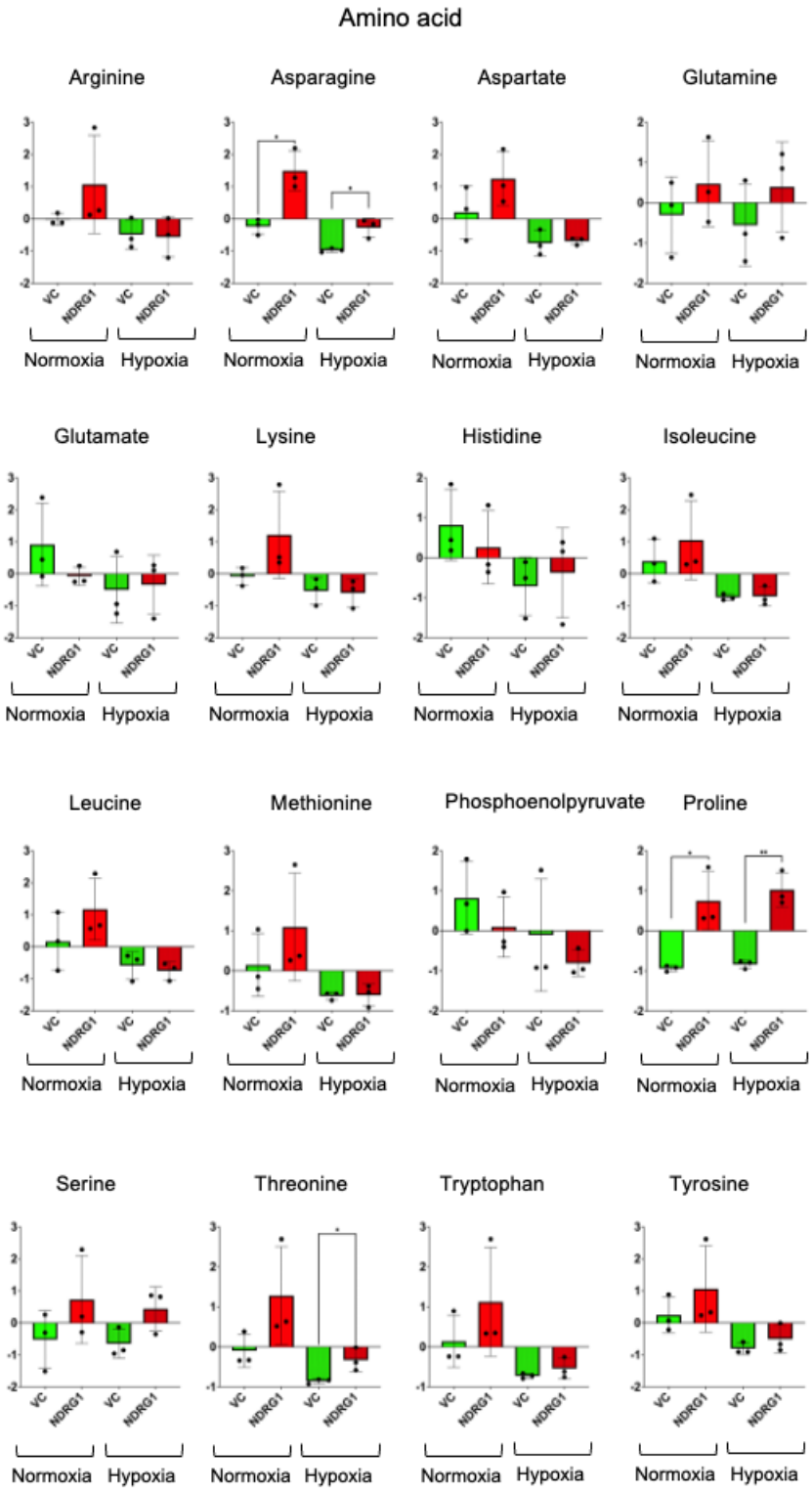

Figure 3.11: NDRG1 impacts the amino acid intracellular metabolites of MIAPaCa-2 cells. Graphs for all examined intracellular amino acids in MIAPaCa-2 cells under normoxia and hypoxia. The data were analyzed using MetaboAnalyst 5.0. Results are mean ± SD (n = 3). *p<0.05, **p<0.01 denote statistical significance comparing each condition to the relevant VC control.

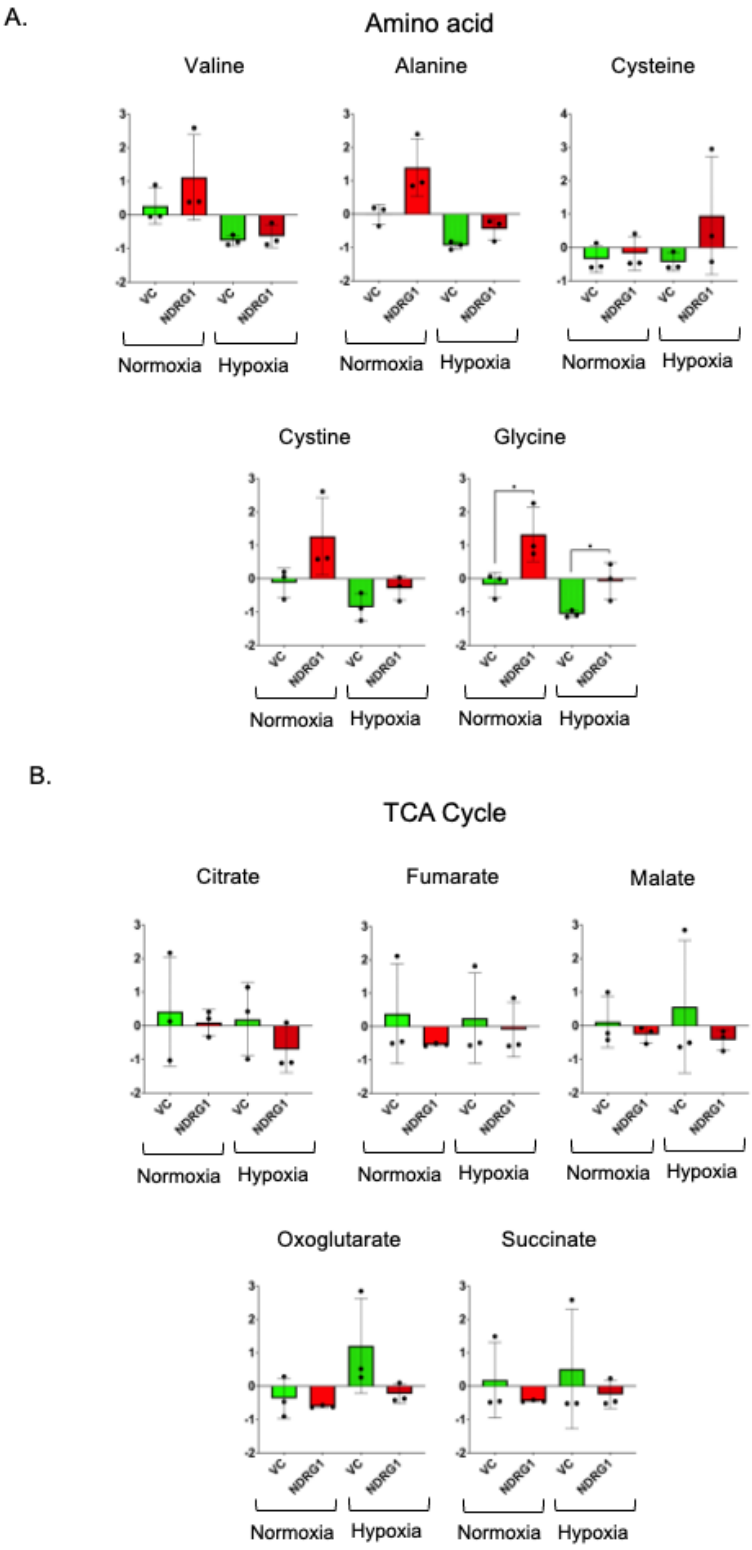

Figure 3.12: NDRG1 impacts the amino acid and TCA cycle intracellular metabolites of MIAPaCa-2 cells. Graphs for intracellular **(A)** amino acids and **(B)** TCA cycle metabolites of MIAPaCa-2 cells under normoxia and hypoxia. The data were analyzed using MetaboAnalyst 5.0. Results are mean ± SD (n = 3). *p<0.05 denote statistical significance comparing each condition to the relevant VC control.

The central carbon metabolism (CCM) converts carbon sources into biomass precursors through enzymatic reactions. It includes both anabolic reactions for building biomass and catabolic reactions for breaking down macromolecules to produce energy. Cell metabolism relies on biochemical oscillators like NAD+/NADH, NADP+/NADPH, and ATP/ADP, and changes in CCM are linked to these bio-oscillators. The NAD+/NADH ratio measures the glycolytic flux. A high NADP+/NADPH ratio causes a shift from glucose oxidation to the pentose phosphate pathway, while a lower ratio leads to lipogenesis. The ATP/ (ADP + Pi) ratio monitors the cell's metabolic state and can prompt metabolic changes in the CCM [245]. Our results indicate that NDRG1 leads to NAD (low)/NADH (high) ratio in normoxia and hypoxia (**Figure 3.13A**). Additionally, NDRG1 results in NADP (low)/NADPH (high) ratio in normoxia, while causing NADP (low)/NADPH (low) ratio in hypoxia (**Figure 3.13A**).

The intracellular levels of sugars were not markedly affected by NDRG1 (**Figure 3.13B**), while the levels of pyruvate were significantly increased by NDRG1 under normoxia (**Figure 3.14**).

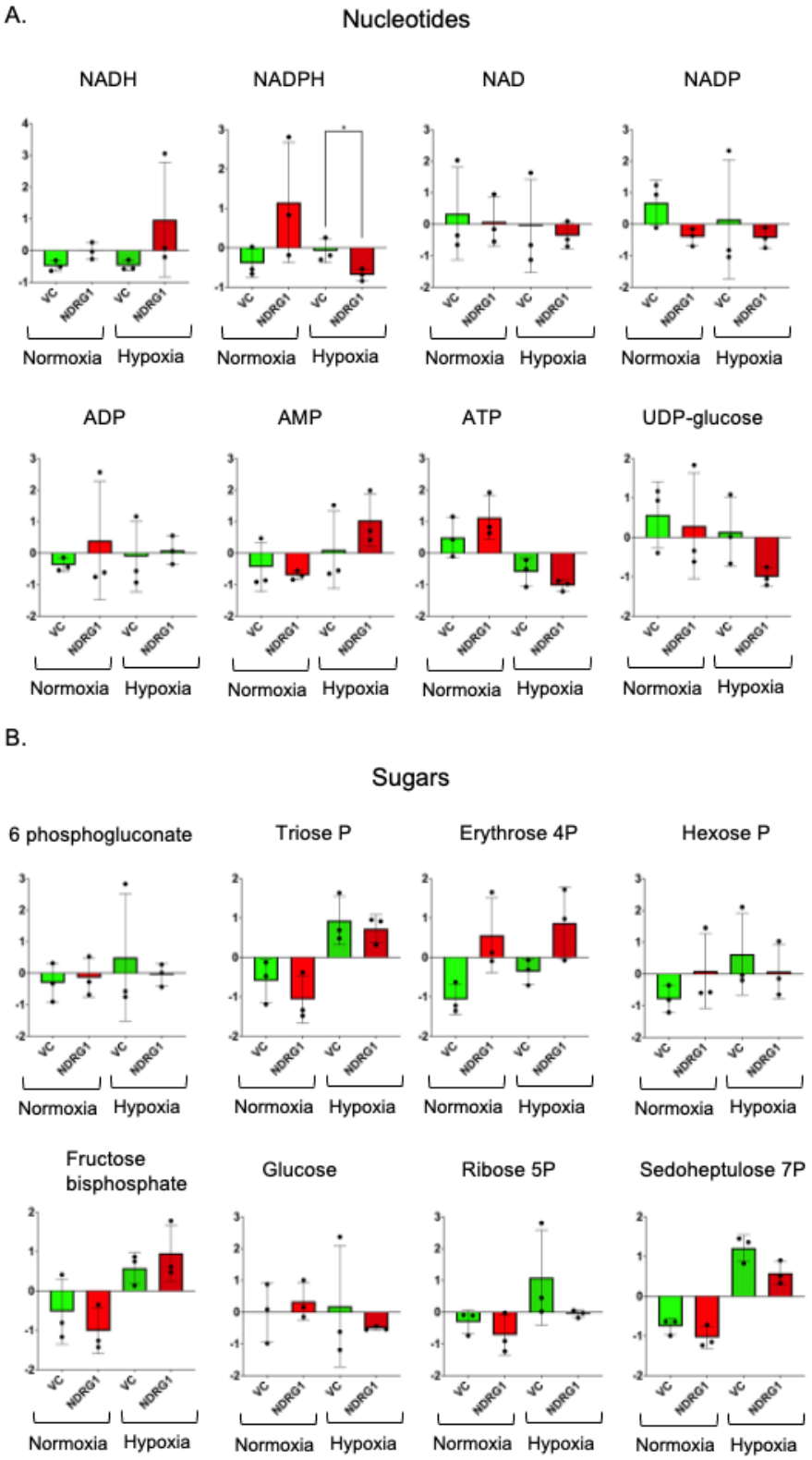

Figure 3.13: NDRG1 impacts the intracellular nucleotides and sugars in MIAPaCa-2 cells. Graphs for all intracellular nucleotides and sugars in MIAPaCa-2 cells under normoxia and hypoxia. The data were analyzed using MetaboAnalyst 5.0. Results are mean ± SD (n = 3). *p<0.05 denote statistical significance comparing each condition to the relevant VC control.

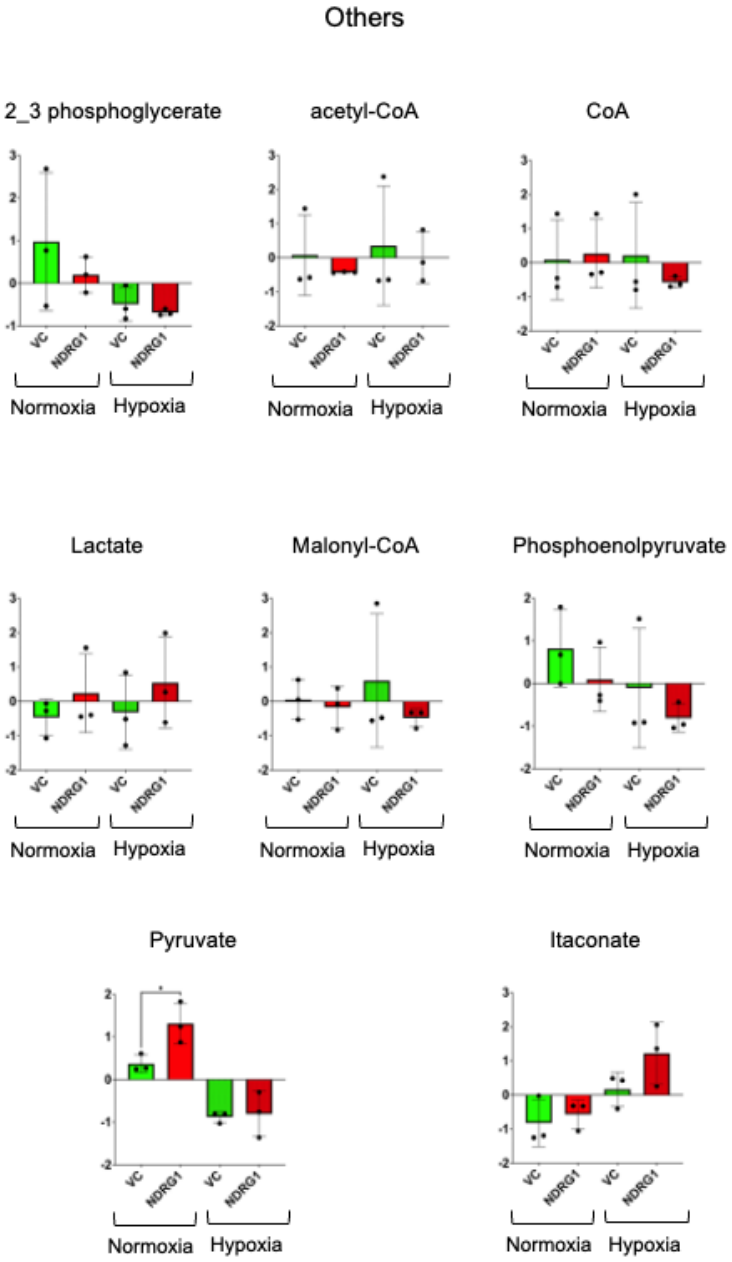

Figure 3.14: NDRG1 impacts the intracellular metabolites of MIAPaCa-2 cells. Graphs for all remaining intracellular metabolites in MIAPaCa-2 cells under normoxia and hypoxia. The data were analyzed using MetaboAnalyst 5.0. Results are mean ± SD (n = 3). *p<0.05 denote statistical significance comparing each condition to the relevant VC control.

Examining the extracellular metabolites further revealed some notable differences between the VC and NDRG1 cells **(Figure 3.15A)**. The pathway analysis of the normoxic samples indicates that NDRG1 is significantly associated with cysteine metabolism, urea cycle, aspartate metabolism, arginine and proline metabolism and the glucose-alanine cycle (**Figure 3.15B**). However, in the hypoxic samples, NDRG1 was found to be related to histidine metabolism, tryptophan metabolism, beta-alanine metabolism, oxidation of branched chain fatty acids and glycine and serine metabolism (**Figure 3.15C**).

The enrichment analysis revealed that NDRG1 has a potent impact on several pathways under normoxic conditions, including amino sugar metabolism, nicotinate and nicotinamide metabolism, folate metabolism and arachidonic acid metabolism (**Figure 3.16A**). Under hypoxia, the most enriched pathways in the NDRG1 samples included methylhistidine metabolism, betaine metabolism, spermidine and spermine biosynthesis and histidine metabolism (**Figure 3.16B**).

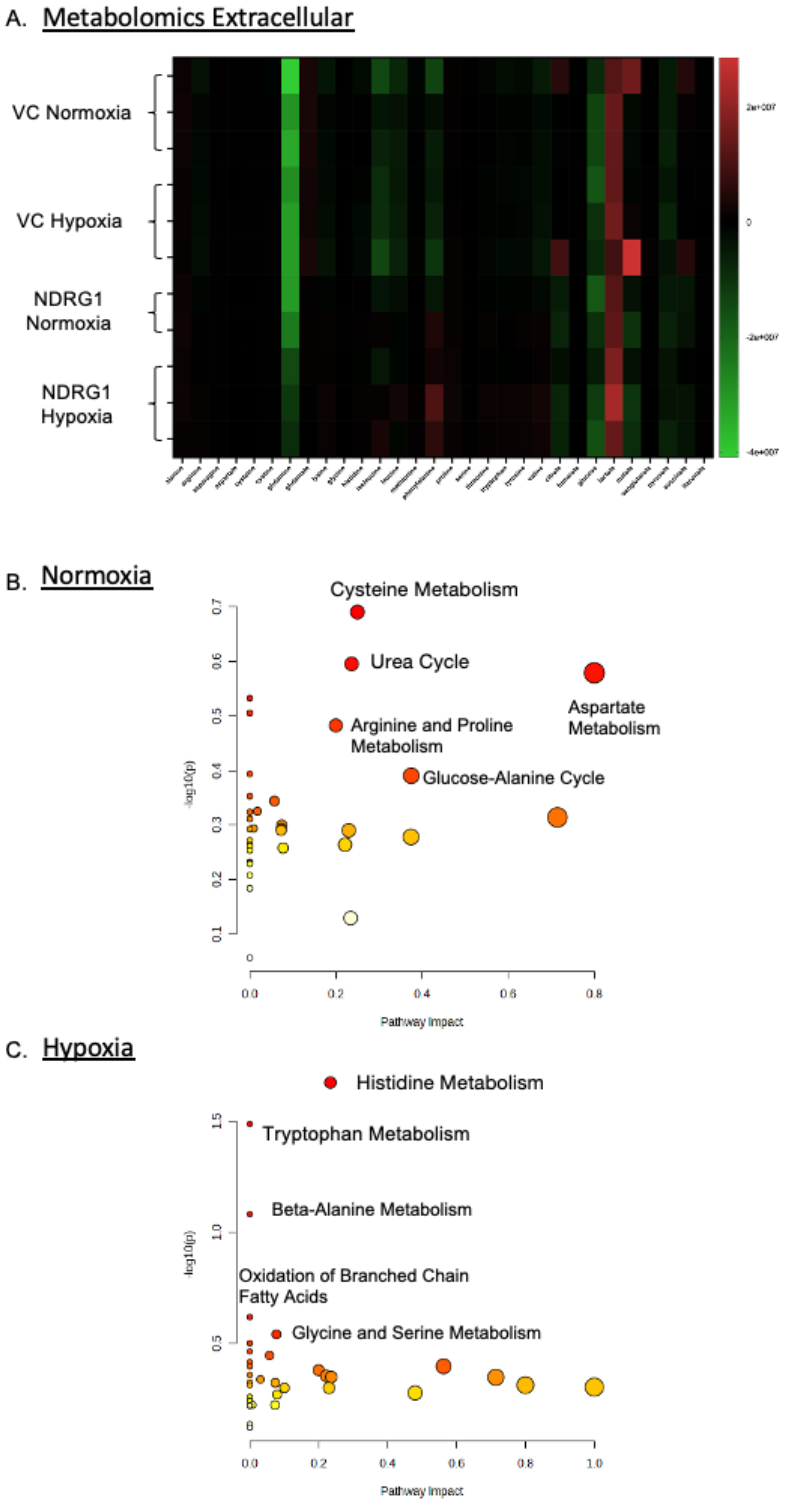

Figure 3.15: Heat map and pathway enrichment analysis of MIAPaCa-2 cell extracellular metabolites. (A) Heat map of extracellular metabolites from VC and NDRG1 cells under normoxia and hypoxia. Pathway impact graph demonstrating the altered metabolic pathways in **(B)** Normoxia and **(C)** Hypoxia. The data MIAPaCa-2 cells were analyzed using MetaboAnalyst 5.0. The red indicates the most significant effects based on the p-value, and the pathway impact value determines the node's size. Results are mean ± SD (n = 3).

A. Normoxia

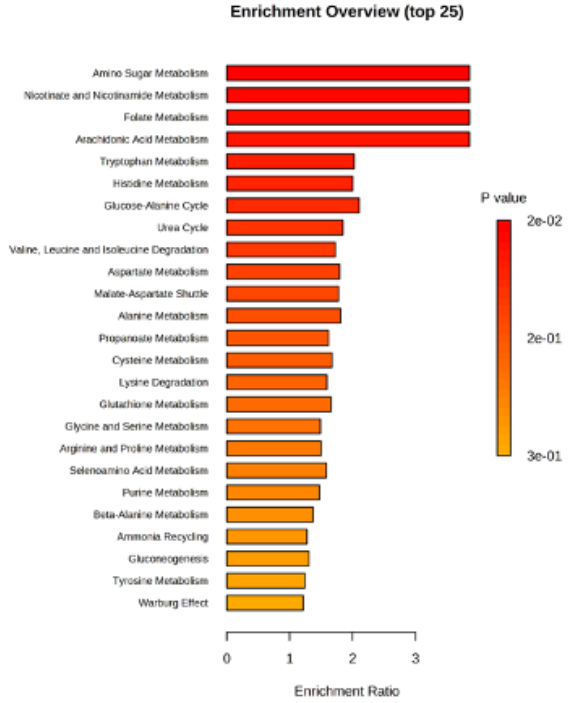

B. Hypoxia

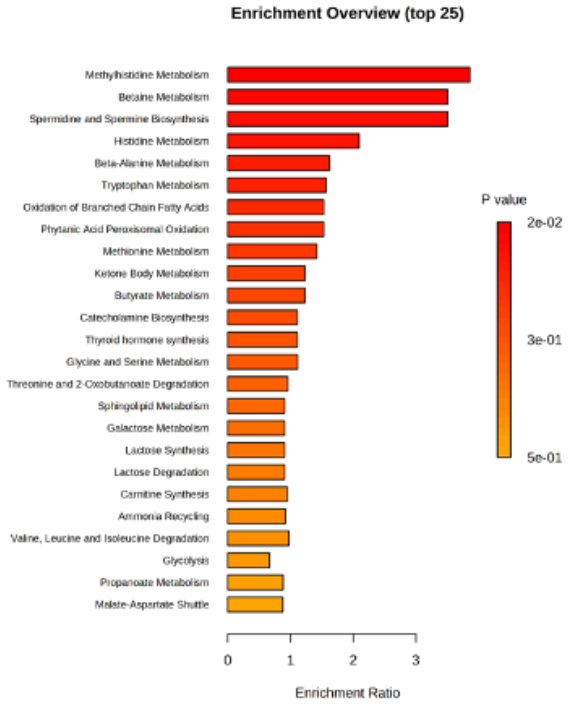

Figure 3.16: Pathway enrichment analysis of extracellular metabolites of MIAPaCa-2 cells. Pathway enrichment analysis to assess the differential extracellular metabolites in VC versus NDRG1 cells as ranked by p-value in **(A)** Normoxia and **(B)** Hypoxia. The data was analyzed using MetaboAnalyst 5.0. Results are mean ± SD (n = 3).

Examining the extracellular amino acid levels, NDRG1 expression in MIAPaCa-2 cells significantly increased the extracellular levels of aspargine and proline, while reducing aspartate, cysteine and glutamate when compared to the VC cells under normoxic conditions (**Figure 3.17**). However, under hypoxia, NDRG1 significantly increased the extracellular levels of arginine, glutamine, cystine, lysine, isoleucine, leucine, methionine, phenylalanine, proline, serine, threonine, tryptophan, valine and tyrosine when compared to the VC cells (**Figure 3.17, Figure 3.18**). Notable exceptions were cysteine and glutamate, both of which were significantly reduced by NDRG1 under hypoxia (**Figure 3.17**). This suggests that NDRG1 broadly reduces the uptake of most amino acids under hypoxic conditions and may even promote the secretion of amino acids by PDAC cells into the media (as demonstrated for arginine, lysine, methionine, phenylalanine, proline, threonine, tryptophan, valine and tyrosine) in response to hypoxia.

Examining the TCA cycle metabolites in the extracellular media, NDRG1 generally reduced citrate, fumarate, malate, oxoglutarate, and succinate levels under both normoxic and hypoxic conditions, although with the exception of succinate under normoxia, these effects were not statistically significant (**Figure 3.18B**). Another notable extracellular metabolite that was consistently and significantly reduced under normoxia and hypoxia by NDRG1 was itaconate, which is a byproduct of the TCA cycle (**Figure 3.18C**).

The findings indicate that the expression of NDRG1 significantly impacts the metabolic profile of PDAC cells, changing their response to hypoxia and altering the ability of PDAC cells to take up numerous amino acids.

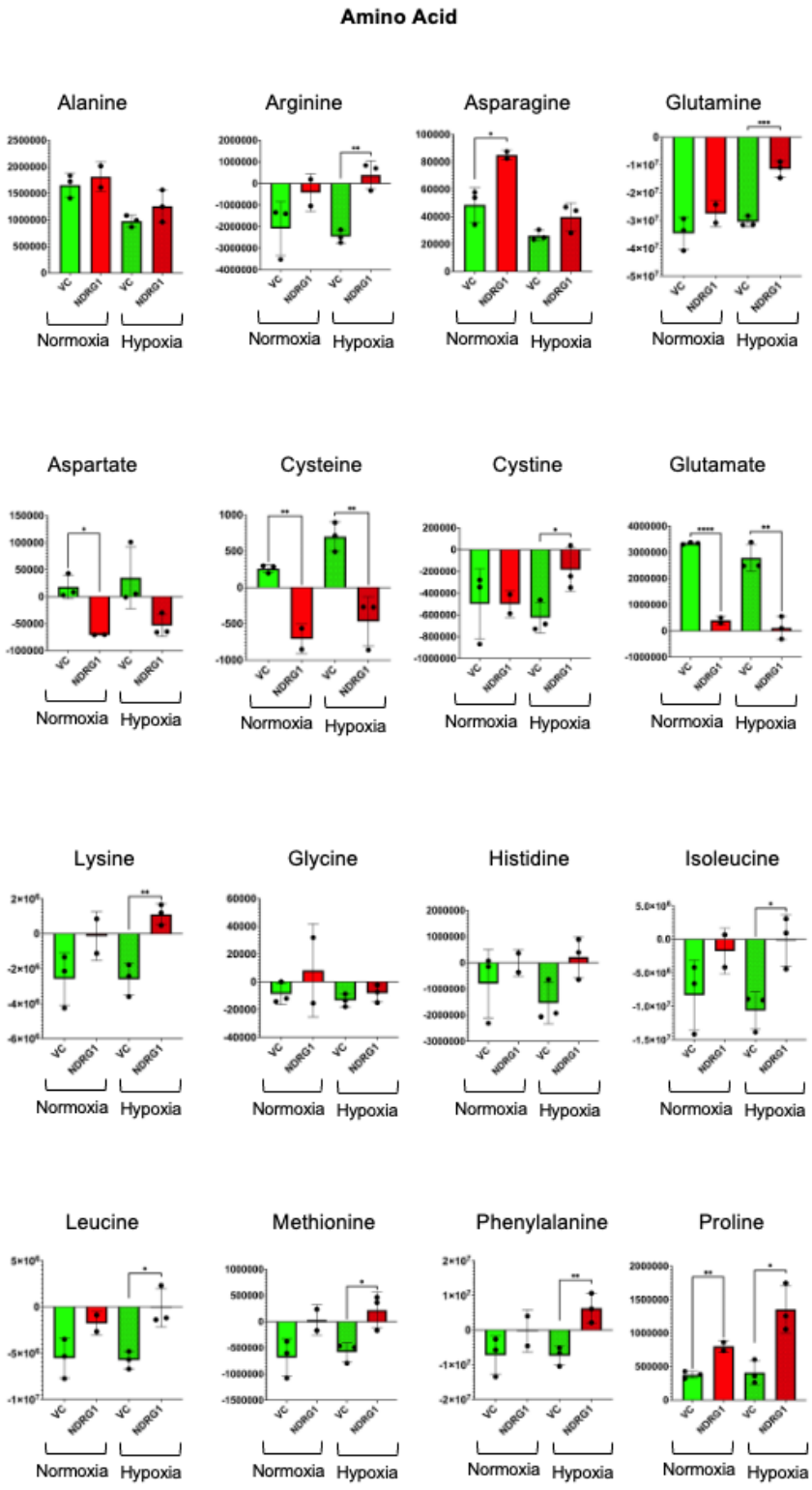

Figure 3.17: NDRG1 impacts the amino acid extracellular metabolites of MIAPaCa-2 cells. Graphs for all examined extracellular amino acids in MIAPaCa-2 cells under normoxia and hypoxia. The data were analyzed using MetaboAnalyst 5.0. Results are mean ± SD (n = 3). *p<0.05, **p<0.01 denote statistical significance comparing each condition to the relevant VC control.

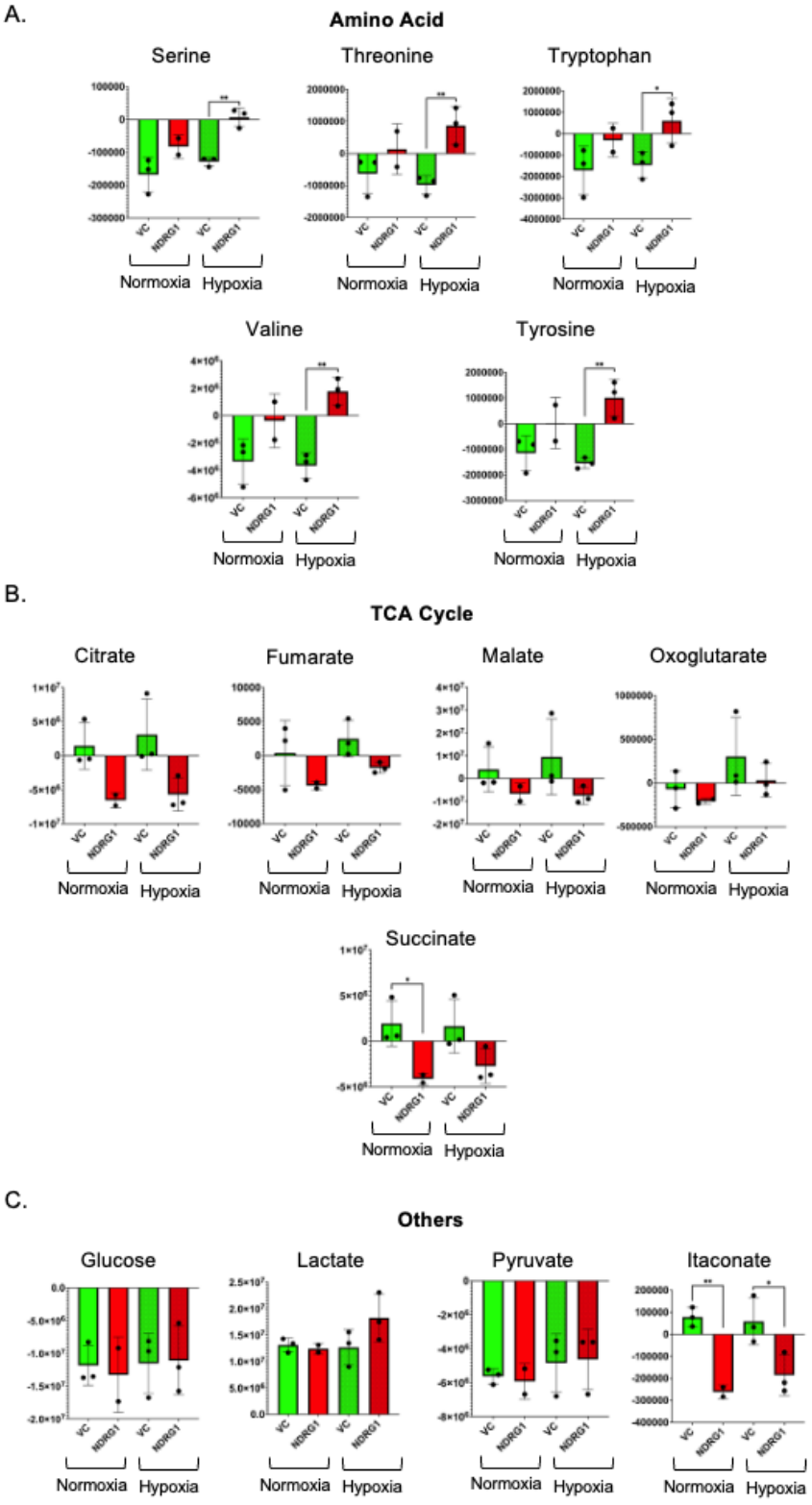

Figure 3.18: NDRG1 impacts the amino acid and TCA cycle extracellular metabolites of MIAPaCa-2 cells. Graphs for extracellular **(A)** amino acids, **(B)**TCA cycle and **(C)** Others metabolites of MIAPaCa-2 cells under normoxia and hypoxia. The data were analyzed using MetaboAnalyst 5.0. Results are mean ± SD (n = 3). *p<0.05 denote statistical significance comparing each condition to the relevant VC control.

3.3.6. NDRG1 inhibits LAT-1, ASCT2 and the mTOR pathway in PDAC Cells

Considering the extracellular metabolite results above demonstrate that NDRG1 expression in PDAC cells can significantly decrease the uptake of branched chain amino acids (BCAAs), including isoleucine, leucine, and valine (**Figures 3.17 and 3.18A**), we conducted further studies to delineate the mechanisms behind this effect. This was of particular importance as BCAA metabolism is essential in regulating lipogenesis in PDAC growth, and PDAC cells demonstrate increased BCAA uptake [223].

We performed both over-expression and siRNA mediated knock-down of NDRG1 in the PANC-1 cells. As shown in **Figure 3.19A and B**, NDRG1 levels were significantly higher in the NDRG1 over-expressing cells when compared to the VC cells, while being significantly lower in the silenced cells (si-NDRG1) when compared to the silencing control cells (si-Control).

We first examined whether NDRG1 was able to affect the expression of the key BCAA membrane transporter, L-Type Amino Acid Transporter 1 (LAT1; also known as SLC7A5) in the PANC-1 cells. LAT1 facilitates the transportation of BCAAs into the cell through a bi-transport system that also exports glutamine simultaneously [246, 247].

Examining the expression of LAT1, we observed a significant reduction in the levels of this transporter in the NDRG1 over-expressing cells, while a significant increase in LAT1 was observed in the si-NDRG1 cells compared to the relevant controls (**Figure 3.19A)**. This suggests that NDRG1 reduces the ability of PANC-1 cells to take up BCAAs *via* its inhibitory effect on LAT1.

Another important transporter that facilitates BCAA uptake is ASCT2/SLC1A5, with this transporter being coupled with LAT1 function [248]. ASCT2 drives glutamine uptake, which serves as an exchange substrate for LAT1 uptake of BCAAs [248]. As demonstrated in **Figure 3.12A**, ASCT2 was also significantly reduced in the PANC1 NDRG1 cells when compared to the VC control, while being significantly increased in the si-NDRG1 cells compared to the si-Control.

A key down-stream effect of BCAAs in cancer cells is the activation of the mTOR pathway and subsequent cellular proliferation [248]. The mTOR complex (mTORC) is critical for cell growth and is activated by amino acids, particularly leucine [249]. Hence, we further investigated whether NDRG1 expression in PANC-1 cells was able to influence mTOR expression and activation. Over-expression of NDRG1 did not affect total mTOR levels, although the activating mTOR phosphorylation (on Ser 2481) was significantly reduced (**Figure 3.19A**). Further, the regulatory associated protein of mTOR (Raptor), which is an adaptor that brings substrates to the mTOR kinase domain [250] was also significantly reduced in PANC-1 NDRG1 cells compared to the VC cells (**Figure 3.19A**). These effects were reversed when NDRG1 was knocked-down, with p-mTOR (Ser 2481) and Raptor being significantly increased when compared to the si-Control cells (**Figure 3.19A**).

Similar findings were observed in the MIAPaCa-2 cells, where NDRG1 reduced the expression of LAT1/SLC7A5, ASCT2/SLC1A5, p-mTOR Ser2481, and Raptor in MIAPaCa-2 NDRG1 cells while increasing their expression in the MIAPaCa-2 si-NDRG1 cells (**Figure 3.19B**).

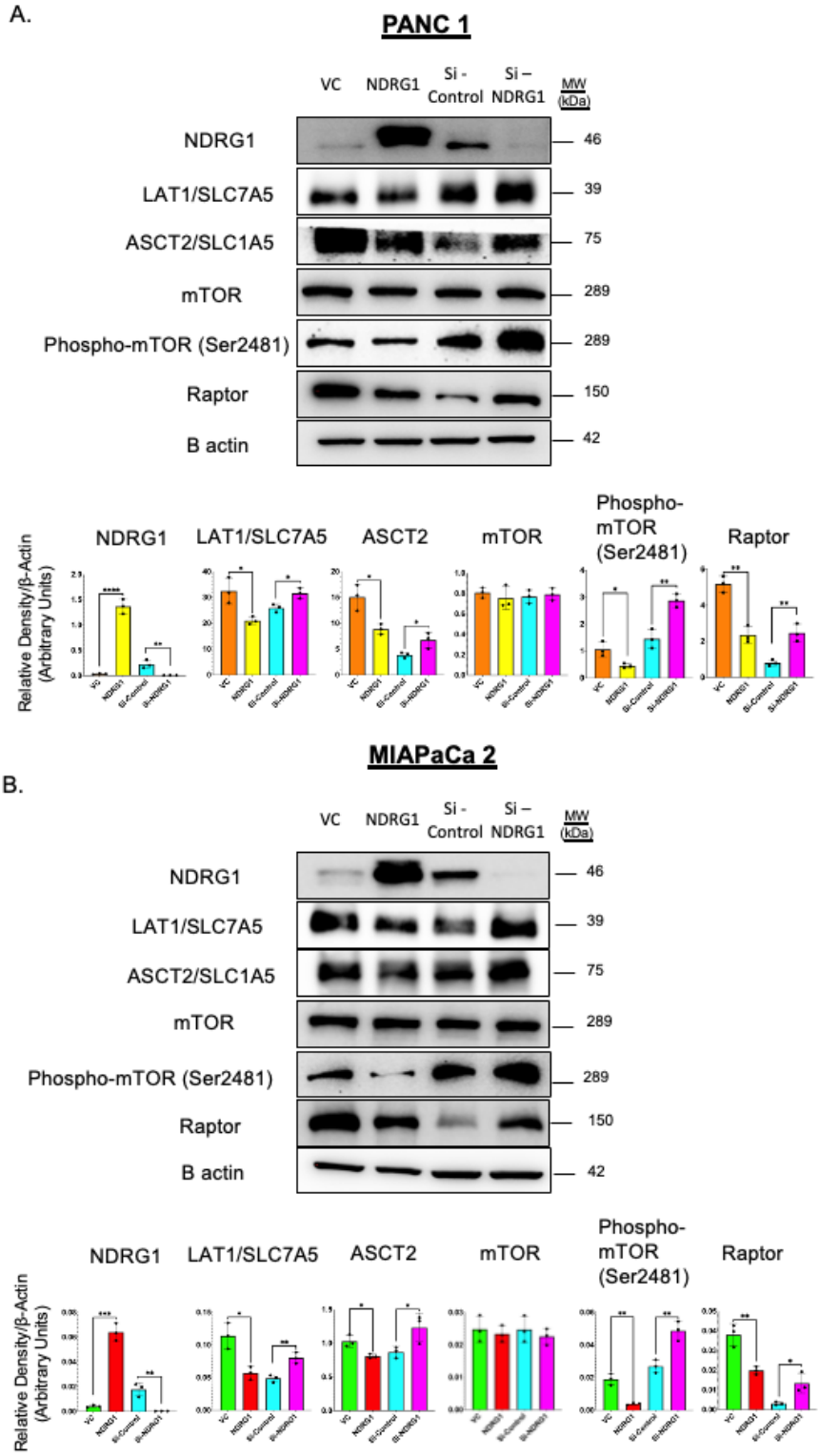

Figure 3.19: NDRG1 inhibits LAT-1, ASCT2 and the mTOR pathway in PDAC Cells Western blots and densitometric analysis of NDRG1, LAT1/SLC7A5, ASCT2/SLC1A5, mTOR, Phospho-mTOR (Ser2481) and raptor in (**A**) PANC-1 and (**B**) MIAPaCa-2 VC, NDRG1, Si-Control and Si-NDRG1 cells. Results are mean ± SD (n = 3). *p<0.05, **p<0.01 ***p<0.001 denote statistical significance comparing each condition to the relevant VC or si-control.

Overall, these findings indicate that increasing the expression of NDRG1 in PANC-1 and MIAPaCa-2 cells reduced the uptake of glutamine and BCAAs by PDAC cells by suppressing both LAT1 and ASCT2 amino acid transporters. This suppression led to inhibition of the mTOR pathway, which is likely responsible for the reduced cell growth and proliferation observed in our cell cycle analysis (**Figure 3.20**).

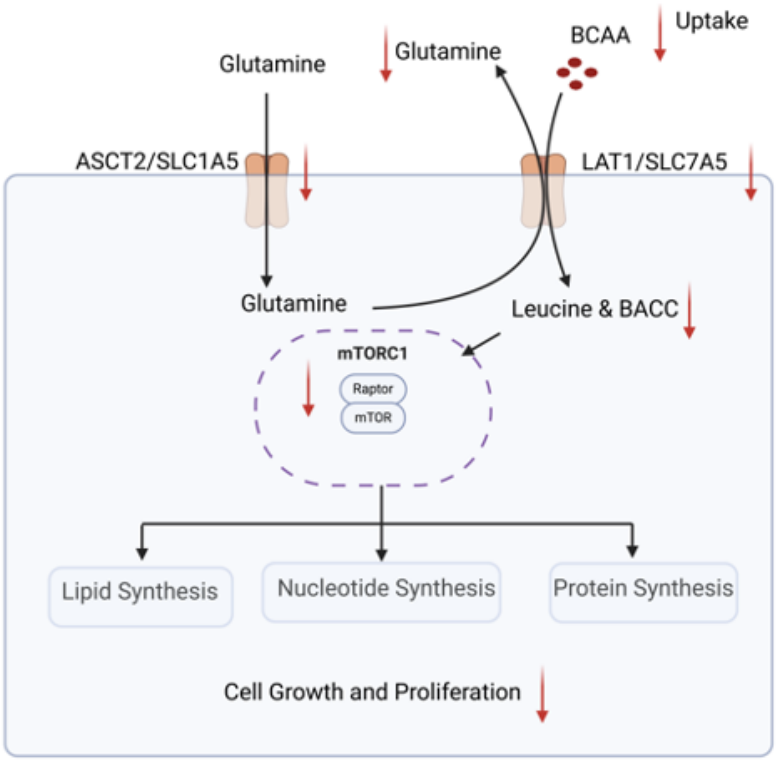

Figure 3.20: Schematic pathway demonstrating the impact of NDRG1 expression in PDAC cells on LAT1 and ASCT2 expression and down-stream mTOR signalling.

3.4. Discussion

Metabolism is essential in human physiology and pathology, affecting PDAC and other tumours. Anabolic and catabolic processes are not only about energy but are also closely linked to various cellular functions, such as DNA replication and redox reactions [149]. Metabolomics is a growing field that systematically measures various metabolites. Its primary objective is to match the metabolites with specific biological phenotypes and then study the underlying mechanisms [251].

In breast cancer cells, the overexpression of NDRG1 was associated with increased expression of genes related to glycolysis and hypoxia [252]. PDAC is known to be highly hypoxic, with a median oxygen concentration of less than 0.7%. In contrast, surrounding tissue has oxygen levels ranging from 1.2% to 12.3% [253, 254].Regarding the impact of NDRG1 on tumour metabolism under normoxia and hypoxia, our research focused on examining the effect of NDRG1 on the metabolism of PDAC cells under both normoxic and hypoxic conditions.

In PDAC, the activation of KRAS leads to increased transcription of GLUT1, which in turn enhances glucose uptake, lactic acid production, and the activation of glycolytic enzymes such as HK2, Phosphofructokinase 1 (PFK1), and lactate dehydrogenase A (LDHA) [153]. In primary PDAC patient tumours, HK2 expression was increased, indicating the potential involvement of glycolysis in driving the progression of the disease. Notably, PDAC metastases exhibited high levels of HK2, indicating a potential association between HK2 and the aggressive nature of the tumours [255]. ATP is produced at a high rate to meet energy demands, while lactic acid buildup promotes tumour development [153]. The current study demonstrates that NDRG1 expression in PDAC cells led to decreased expression of GLUT1, HK2 and lactic acid. This was associated with lower ECAR rates by PDAC cells. Furthermore, this was

accompanied by reduced numbers of TCA cycle intermediates in the NDRG1 over-expressing cells.

Fatty acid oxidation is the process by which long-chain fatty acids are converted into acetyl-CoA, which then enters the TCA cycle, to produce NADH and FADH2. This conversion takes place mainly within the mitochondria [256, 257]. Carnitine palmitoyltransferase I (CPTI) play a crucial role in the initial step of fatty acid oxidation (FAO) and is overexpressed in many types of tumours. Research has shown that inhibiting CPTI can effectively suppress cancer's growth [258]. The inhibition of CPTI has been shown to suppress cancer growth effectively [258]. We observed that NDRG1 reduced the metabolism of acetyl-L-carnitine, octanoyl-L-carnitine, and palmitoyl-D, L-carnitine. This suggests that NDRG1 impairs fatty acid oxidation in PDAC cells. Interestingly, NDRG1 has previously been shown to direct the intracellular fate of fatty acids in breast cancer, potentially dictating how fatty acids are utilized by cells [252].

IDH1 plays a vital role as a metabolic enzyme in cellular respiration during the TCA cycle. Its role involves converting isocitrate into α-ketoglutarate (α-KG) and generating NADPH [259]. IDH1 functions physiologically by regulating the intracellular NADP+/NADPH ratio to protect cells from oxidative stress [260]. Mutations in IDH genes lead to a decrease in the cellular NADPH/NADP+ ratio [261]. NDRG1 is a stress response protein that inhibits multiple oncogenic signalling pathways and links to the endoplasmic reticulum (ER) stress response [262]. The current study demonstrates that NDRG1 expression in PDAC cells leads to increased IDH1 expression in normoxia and hypoxia. This may be related to a stress-response effect, as IDH1 was found to protect PDAC cells from oxidative stress.

The increased levels of BCAA in the bloodstream have been identified as an early sign of potential PDAC development, indicating that BCAA metabolism may play a role in the progression of PDAC or disruptions in the body's metabolism [226]. LAT1 controls the mammalian target of rapamycin complex 1 (mTORC1) activity by regulating the levels of BCAAs in the cytoplasm at the cell's plasma membrane [263]. This study demonstrates that NDRG1 expression in PDAC cells reduces the expression of ASCT2/SLC1A5 and LAT1/SLC7A5, leading to decreased BCAA uptake, which inhibits the mTORC1 pathway in PDAC cells (**Figure 3.20**). The mTOR pathway regulates the communication between the stroma and the tumour, impacting tumour immunity and angiogenesis. Activating mTOR signalling is linked to these cancer-promoting cellular processes, highlighting mTOR as a potential target for new combination therapies [264]. Preclinical research indicates that targeting mTOR in specific KRAS-dependent PDAC subtypes can effectively inhibit tumour growth in vitro and in vivo [265].

The cell membrane contains glutamine transporters such as SLC1A5, SLC38A1/SLC38A2, and SLC6A14, facilitating glutamine transport into the cytosol. Subsequently, the SLC1A5 variant carries glutamine to the mitochondrial matrix, transforming it into glutamate by the glutaminase (GLS), representing the pivotal step of glutaminolysis. The glutamate derived from glutamine is then converted to α-KG [266, 267]. It may suggest that NDRG1 increases the ability of PDAC cells to metabolise glutamine but potentially reduces their ability to undergo de novo glutamine synthesis (from glutamate). This step is mediated by glutamate ammonia ligase (GLUL), an enzyme responsible for de novo glutamine biosynthesis and elevated in cancers [267].

In conclusion, NDRG1 significantly affects the metabolism of PDAC cells and changes how these cells respond to hypoxia. Our findings indicate that, as well as reducing glycolysis in PDAC cells, NDRG1 also reduces the uptake of BCAAs by downregulating the expression of amino-acid transporters LAT1 and ASCT2. Overall, PDAC cells that had over-expression of NDRG1 were less metabolically flexible and had generally lower abilities to metabolize different mitochondrial substrates and to scavenge extracellular amino acids and metabolites (**Figure 3.21**). This suggests that NDRG1 restricts the extensive metabolic re-wiring that cancer cells undergo to survive and thrive in oxygen and nutrient-depleted conditions and may enhance their vulnerability to metabolic inhibitors.

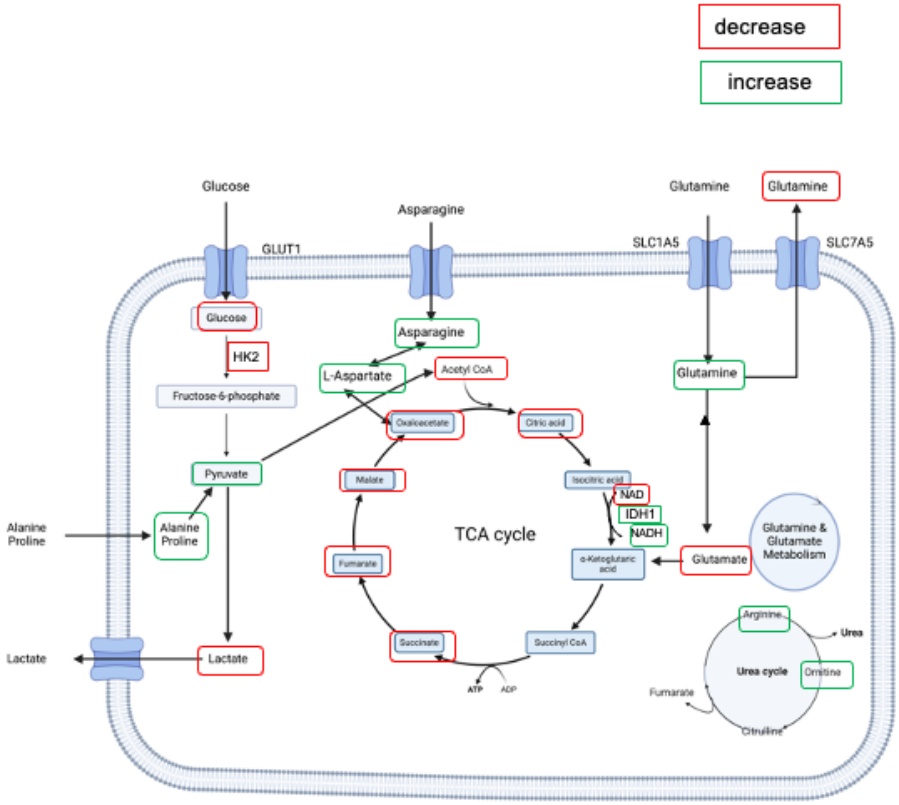

Figure 3.21: The schematic pathway illustrates the impact of NDRG1 expression in PDAC cells on metabolic pathways. Metabolites found to be increased by NDRG1 are shown in green, while those found to be reduced by NDRG1 are shown in red.

Chapter 4: Effect of NDRG1 Expression Levels in PDAC Cells on Macrophage Polarization

4.1. Introduction

Pancreatic ductal adenocarcinoma (PDAC) is the most common type of pancreatic cancer, making up over 90% of all pancreatic tumours. Unfortunately, PDAC is a highly aggressive cancer with a poor outlook for patients [268]. The 5 years survival rate is 10% [269]. There is currently no reliable screening method for PDAC, which means that a majority of patients are diagnosed with advanced stages of the disease. Specifically, around 30-35% of patients have locally advanced PDAC, while 50-55% of patients have metastatic PDAC at the time of diagnosis [270].

PDAC is characterised by a dense, fibrotic stroma called desmoplasia composed of acellular components, primarily the extracellular matrix, and cellular components such as endothelial cells, perivascular cells, immune cells, neurons, pancreatic stellate cells (PSCs) and fibroblasts that plays a pivotal role in its pathogenesis through the restriction of chemotherapy agents, impeding the infiltration of immune cells, and inducing hypoxia [271, 272]. Cancer-associated fibroblasts (CAFs) are the major non-neoplastic component in the PDAC tumour microenvironment (TME) and can be derived from multiple sources including the PSCs [273].

CAFs can control the immunosuppressive TME by interacting with the tumour's immune microenvironment. They do this by releasing chemokines, cytokines, and other molecules such as TGF-β, IL-6, CXCL12, CCL2, SDF-1, VEGF, IDO, and PGE2 [274]. 3D co-culturing of monocytes, pancreatic cancer cells, and fibroblasts caused the formation of immunosuppressive cytokines, known to be connected to the polarization of macrophages into the type M2 immunosuppressive phenotype and myeloid-derived suppressor cells (MDSCs) [275]. CAFs also produce high levels of an extracellular matrix (ECM) protein called βig-h3

(also known as TGFβi) in the stroma, which has a direct suppressive effect on CD8+ T-cell activity while also promoting macrophage M2 polarization [276].

The primary immune cells in the PDAC TME are tumour-associated macrophages (TAMs), which make up 11% of all cellular components [73]. Macrophages are usually the most dominant component among the infiltrating cells in the tumour microenvironment of PDAC. [277]. The functional properties of macrophages can be altered in response to external stimuli such as IL-10, TGF-α, and other cytokines. Consequently, macrophages can be divided into two distinct categories: M1 (pro-inflammatory or 'classically activated' macrophages) and M2 (anti-inflammatory or 'alternatively activated' macrophages) [278]. In the tumour microenvironment, TAMs tend to deviate towards M2 activation, which aids in promoting and supporting various tumour behaviours such as tumour growth, immune system evasion, metastasis, and resistance to chemotherapy [279].

Macrophages play a critical role in tumour development and progression [280]. In a mouse study, the fibroblasts in the hypoxic stroma of PDAC produce the hypoxia-inducible factor-2α (HIF-2α) that promotes M2 macrophage polarization [281]. TAMs that are polarized to the M2 phenotype are linked to a poor prognosis in pancreatic cancer, primarily due to increased lymphatic metastasis. To improve the prognosis, inhibiting the functional interaction between M2-polarized TAMs and tumour cells may be beneficial.[282]. TAMs have the capacity to produce immunosuppressive cellular activity *via* the release of cytokines, chemokines, and proteases, including TGF-*β,* CCL17, Arg-1, CCL22, and IL-10 [283]. Thus, focusing on TAMs is a crucial approach for the immunotherapy of PDAC [284].

N-myc downregulated gene-1 (NDRG1) is a cytoplasmic protein contributing to stress responses, hormone responses, cell growth, and differentiation [187]. The function of NDRG1 in cancer is complex and not fully comprehended due to its pleiotropic and context-dependent functions [184]. Several studies have shown that NDRG1 is a metastasis-suppressor protein in different cancers, such as prostate [285], colon [286] and pancreas [198]. Oncogenic pathways such as TGF-β and Wnt, which affect metastasis progression and the TME, have been found to be inhibited by NDRG1 in PDAC [184]. NDRG1 was shown to inhibit the Wnt signalling pathway by interacting with LRP6, the Wnt receptor, to regulate a cellular network that impairs the metastatic progression of cancer cells [287].

The process of epithelial-to-mesenchymal transition (EMT), which is induced by TGF-β, was also found to be inhibited by NDRG1 in PDAC cells [288, 289]. NDRG1 suppressed oncogenic effects of TGF-β in PDAC, leading to increased E-cadherin and β-catenin expression and co-localization at the cell membrane [288]. This was mediated by inhibition of the oncogenic NF-κB signalling pathway, including suppressing the expression of NEMO, Ικκα, and IκBα and decreasing the activating phosphorylation of Ικκα/β and IκBα in PDAC cells [288]. Moreover, NDRG1 also decreased the levels, nuclear co-localization, and DNA-binding activity of NF-κB p65. Additionally, Ικκα has been identified as a target of NDRG1, which combines NF-κB and TGF-β signalling to upregulate ZEB1, SNAIL, and SLUG [288]. As a result, loss of NDRG1 is associated with more aggressive tumours and metastasis in pancreatic cancer [188].

Recent studies have identified for the first time that NDRG1 expression in PDAC cells can significantly influence the TME, leading to inactivation of PSCs [205, 206]. Upon exposure to cancer cell-secreted ligands such as TGF-β and sonic hedgehog (SHH), PSCs become activated and start producing hepatocyte growth factor (HGF) and insulin-like growth factor (IGF-1),

which in turn support PDAC proliferation, metastasis, and chemotherapy resistance [206]. NDRG1 was found to inhibit this oncogenic cross-talk between PDAC cells and PSCs, by inhibiting HGF and IGF-1 signalling in PDAC cells while also reducing their ability to secrete TGF-β and SHH, leading to de-activation of PSCs [206]. This was validated *in vivo* using the novel anti-cancer drug di-2-pyridylketone-4-cyclohexyl-4-methyl-3-thiosemicarbazone (DpC), which markedly increased NDRG1 expression and inhibited SHH, HGF, and IGF-1 signalling in an orthotopic PDAC xenograft, resulting in significant inhibition of desmoplasia [206].

Although NDRG1 has been shown to inhibit the cross-talk between PDAC and PSC, no studies have investigated how NDRG1 affects the immune cells in PDAC. Given the crucial role of TAMS in immune suppression in PDAC, this study aimed to determine how the levels of NDRG1 in tumour cells affect the polarisation and activity of macrophages in the PDAC TME.

We established 3D multicellular tumour spheroids composed of PDAC, MRC-5 and monocytes cells to assess the effect of NDRG1 on infiltration of monocytes into spheroids and their polarization into M1 or M2 phenotypes. For the first time, we demonstrate that NDRG1 expression in PDAC cells significantly reduces the polarization of monocytes into the M2 macrophage phenotype while promoting the M1 phenotype. This effect is potentially mediated through the increased secretion of TNF-α from cancer cells, which activated the NF-κB signalling pathway in macrophages, promoting their pro-immunogenic functions.

4.2. MATERIALS & METHODS

4.2.1. Cell Culture

The human pancreatic cancer cells PANC-1 and MIAPaCa-2, MRC-5, THP-1 and U937 were cultured as described above ***(Section 2.1)***.

4.2.2 Stable transfection

PANC-1 and MIAPaCa-2 were stably transfected with either the empty vector control (VC), full-length wild-type NDRG1 (NDRG1) or an NDRG1 construct in which the CAP region has been deleted (ΔCAP; **Figure 4.1A**) as described above ***(Section 2.2)*** [212] .

4.2.3. Preparation of Conditioned media (CM)

The Conditioned media (CM) were collected as described above ***(Section 2.10)***.

4.2.4. Polarization of monocytes into M1 and M2 macrophages.

THP-1 or U937 monocytes were differentiated as described above ***(Section 2.4)***.

4.2.5. Spheroid culture and Immunofluorescence staining (IF)

3D spheroid co-cultures containing PDAC cells, MRC-5 fibroblasts and THP-1 monocytes were generated by seeding into Corning® 96-well Clear Round Bottom Ultra-Low Attachment Microplates (Corning Costar, #7007). Eagle's Minimum Essential Medium (EMEM) (gibco) containing 10% methylcellulose (Sigma) medium was used to enhance spheroid formation [290]. Specifically, 1000 PANC-1 or MIAPaCa-2 cells were mixed with 1500 MRC-5 fibroblasts and seeded into the 96-well microplates followed by incubation at 37°C with 5%

CO_2, with media being replaced every 3-4 days. On day 7, 10,000 THP1 monocytes were added to each well and the spheroids incubated for a further 7 days. The spheroids were then imaged using the InCucyte SX5 system (Sartorius, Göttingen, Germany) for 7 days.

To prepare the spheroids for IF imaging, at the end of the incubation period they were washed with filtered PBS 3 times, fixed with 4% paraformaldehyde (PFA) for 20 minutes, and then washed with PBS. Next, the spheroids were permeabilized by treating them with 0.2 % Triton X-100 in PBS for 20 minutes at room temperature. The spheroids were blocked with 5% BSA for 30 minutes at room temperature and then incubated with the primary antibody against CD206/MRC1 (Cell Signalling, 91992) or CD86 (abcam, ab239075) overnight at 4˚C. The following day, the spheroids were washed with filtered PBS 3 times and then incubated with the secondary antibody (Alexa Fluor® 594 Conjugate #8889) at room temperature for 1 hour. Following another 3 washes with PBS, DAPI (NucBlue™ Fixed Cell ReadyProbes™ Reagent (DAPI)) (Invitrogen, cat R37606) was added into each well (one drop of DAPI was added to 1ml PBS and incubated for 15 to 30 minutes). The spheroids were then imaged within the 96-well plates using a Nikon Ti-E Spinning Disk Confocal Live Cell microscope (Nikon). The images were analysed using Fiji-ImageJ software.

4.2.6. Immunofluorescence staining (IF)

Immunofluorescence staining (IF) was used to examine the location and translocation of NF-κB p65. THP-1 and U937 cells (2 x 10^4 in 80 µl of media) were plated in 96-well black/clear bottom plate (Corning #3603) as described above *(Section 2.4)*. The cells were exposed to CM from either VC or NDRG1 expressing PANC-1 or MIAPaCa-2 cells for 24 hours. The cells were then washed with filtered PBS 3 times, fixed with 4% paraformaldehyde (PFA) for 20 minutes at room temperature, and then washed with PBS. The cells were blocked with 5% BSA for 30 minutes at room temperature and then incubated with the primary antibody

against NF-κB p65 (D14E12) (Cell Signalling, 8242) overnight at 4˚C. The following day, the cells were washed with filtered PBS 3 times and then incubated with the secondary antibody (Alexa Fluor® 594 Conjugate #8889) at room temperature for one hour. Following a further 3 washes with PBS, DAPI (NucBlue™ Fixed Cell ReadyProbes™ Reagent (DAPI)) (Invitrogen, cat R37606) was then added to all wells (one drop of DAPI was added to 1m PBS and incubated for 15 to 30 minutes). The cells were imaged using the 3i Marianas LightSheet™ microscope (3i Intelligent Imaging Innovations, Inc., USA). The images were analysed using Fiji-ImageJ software.

4.2.7. Human cytokine array

MIAPaCa-2 VC and NDRG1 cells were cultured in a 100 mm dish at a density of 4×10^6 cells/flask for 24 hours under two conditions: Normoxia (20–21% O_2) and Hypoxia (0.5% O_2). After 24 hours, the medium was changed to a medium containing 1% FBS (Sigma) and cultured for another 24 hours. The conditioned medium was then collected, centrifuged at 500g for 5 minutes, and filtered through a 0.2 μm filter. The conditioned media (mixed 50:50 with fresh media 1% FBS) was either used fresh or stored at -80 ºC. To analyze the levels of secreted cytokines in the supernatant, a human cytokine antibody array (ab133998, Abcam) was used as per the manufacturer's instructions. The ChemiDoc MP (Bio-Rad) was used to capture images of the membranes, while the Fiji-ImageJ software was utilized to analyze and quantify the Dot Blot membrane.

4.2.8. Reactive oxygen species (ROS) Assay

To analyse ROS production by macrophages, THP-1 and U937 cells were seeded at a density of $8x10^4$ in 100μl of media with 160 nM PMA and were placed in a 96-well black/clear bottom plate (Corning #3603) and differentiated into M0, M1, or M2 macrophages as described above

(Section 2.4) or treated M0 cells with conditioned media from NDRG1 or VC cells for 72 hours. To measure cellular ROS levels, the cell permeant reagent 2',7' –dichlorofluorescin diacetate (DCFDA) - Cellular ROS Assay Kit (ab113851; Abcam) was utilized following the provided instructions. The fluorescence intensity of cellular ROS was then assessed in endpoint mode at Ex/Em=485/535 nm using the SpectraMax M3 reader (Molecular Devices, San Jose, CA, USA).

4.2.9. Protein Extraction

The protein extraction for whole cells was extracted as described above ***(Section 2.5)***.

4.2.10. Western Blot Analysis

Western blot was performed *via* standard methods (see ***Section 2.6***) using antibodies listed in **Table 4.1**.

Table 4.1: The list of primary and secondary antibodies used for western blot studies

No	Name of antibody	Catalogue #	Company	Dilution
1	CD206/MRC1	91992	Cell Signalling	1:500
2	CD163	ab182422	abcam	1:1000
3	CD86	ab239075	abcam	1:100
4	Glut1	73015	Cell Signalling	1:1000
5	Hexokinase II	2867	Cell Signalling	1:1000
6	Arginase-1	93668	Cell Signalling	1:1000
7	iNOS	20609	Cell Signalling	1:1000
8	IκBα	4812	Cell Signalling	1:1000
9	NF-κB p65	8242	Cell Signalling	1:1000

10	Phospho-NF-κB p65 (Ser536)	3033	Cell Signalling	1:1000
11	NDRG1	9485	Cell Signalling	1:1000
12	β-Actin	A5316	Sigma-Aldrich	1:10,000
13	Mouse IgG secondary	A4416	Sigma-Aldrich	1:10,000
14	Rabbit IgG secondary	A6154	Sigma-Aldrich	1:10,000

4.2.11. Flow cytometry

Macrophages were detached from the cell plate surface using phosphate buffered saline EDTA (PBS/EDTA) and washed twice with cold PBS. The cells were blocked using Human TruStain FcX™ (BioLegend, San Diego, CA) for 10 min. The cells were washed twice and incubated for 45 minutes at 4˚C with the following anti-human antibodies in the dark: CD163-APC (GHI/61; 1:200) and CD206-BV421 (15–2; 1:20). Compensation beads were used to create artificial populations with positive and negative fluorescence, simulating the heterogeneous cell populations in a sample that are either positive or negative for a specific marker. One drop from each bottle of positive and negative Compensation Beads (Cat. 424602, BioLegend) was added to several tubes. The desired concentration of each antibody was then added to a single tube. The tubes were mixed and incubated at room temperature for 15-20 minutes, avoiding exposure to light. The cells were then washed twice with Cell Staining Buffer (BioLegend, San Diego, CA) and incubated for 5 minutes in the dark with Zombie Red™ Fixable Viability Kit (BioLegend, San Diego, CA) to determine cell viability. All antibodies were purchased from BioLegend (San Diego, CA, USA). The cells were analysed with the BD LSRFortessa™ X-20 (BD Biosciences), and the data were analysed using FlowJo software (TreeStar, Ashland, OR).

4.2.12. Enzyme-Linked Immunosorbent Assay (ELISA)

Supernatant was collected from THP1 and U937 cells differentiated into M0, M1 or M2 macrophages, as well as M0 macrophages incubated with CM from either VC, NDRG1, or ΔCAP-NDRG1 PANC-1 or MIAPaCa-2 cells and centrifuged at 1000 × g for 10 minutes. Using the instructions provided by the manufacturer, IL-12 was measured using a commercial ELISA kit (ab46037, Abcam). The results were normalised using the identical CM for each condition before being added to THP1 and U937 cells.

The levels of MCP-1, TNF-α, IL-8 and RANTES were measured in the CM of VC and NDRG1 over-expressing PANC-1 or MIAPaCa-2 cells cultured under normoxia or hypoxia using commercial ELISA kits for each protein (Abcam, USA). The kits used included human MCP1 (ab179886, Abcam), human TNF alpha (ab181421, Abcam), human IL-8 (ab214030, Abcam) and human RANTES (ab174446, Abcam). The instructions provided by the manufacturer were followed for all assays. Data was analyzed using GraphPad Prism 10 (GraphPad, U.S.A.) and Microsoft Excel (Microsoft, U.S.A.).

4.2.13. Cell Cycle Analysis

THP1 and U937 cells were differentiated into M0, M1 and M2 macrophages as described above (***Section 2.4***). The cells were exposed to CM from either VC or NDRG1 expressing PANC-1 or MIAPaCa-2 cells for 72 hours. The cell cycle was analyzed as described above ***(Section 2.8)***.

4.2.14. MitoPlate S-1

The U937 cells were differentiated into M0 macrophages (***Section 2.4***), followed by incubation with PANC-1 VC or PANC-1 NDRG1 CM for 72 hours. The mitochondrial metabolic activity was analyzed using MitoPlate S-1 as described above ***(Section 2.9)***.

4.2.15. Incucyte® Cytotoxicity Assay

3D spheroid co-cultures containing PDAC cells, MRC-5 and monocytes were generated using Corning® 96-well Clear Round Bottom Ultra-Low Attachment Microplates (Corning Costar, #7007). Specifically, 1000 PANC 1 or MIAPaCa-2 cells mixed with 1500 MRC-5 fibroblasts were seeded into each well in media with (Incucyte® Cytotox Green Dye, Item no. 4633) and incubated at 37°C with 5% CO2. On day 2, the media were replaced with fresh media containing 10,000 THP1 cells or media without THP1 cells. The spheroids were imaged every 12 hours for 5 days using the InCucyte SX5 (Sartorius, Göttingen, Germany).

4.2.16. XFe96 seahorse assay

THP-1 and U937 cells (2 x 10^4 in 80 µl of media) were plated as described above ***(Section 2.4)*** in Seahorse XF 96-well plate from Agilent Seahorse XFe96/XF Pro Extracellular Flux Assay Kits (Agilent Technologies, Santa Clara, CA). The cells were exposed to CM from either VC or NDRG1 expressing PANC-1 or MIAPaCa-2 cells for 72 hours. The Baseline Oxygen Consumption Rate (OCR) and Extracellular Acidification Rate (ECAR) were measured for as described above ***(Section 2.7)***.

4.2.17. EV isolation

MIAPaCa-2 cells were cultured in media without FBS until they reached 75-90% confluency. The media overlaying the cells was then collected and subjected to 3 rounds of centrifugation for 5 minutes each at 4ºC to remove any debris from the cells. After that, a 10-minute centrifugation at 2800 RCF at 4ºC was performed to isolate large oncosomes and apoptotic bodies. The remaining media was then subjected to gradient ultracentrifugation at 10,000 RCF at 4ºC for 45 minutes (Hitachi equipment, Japan). This was done to isolate large EVs or MVs. The remaining media was ultracentrifuged at 100,000 RCF at 4ºC for 65 minutes to collect small EVs or exosomes. The EV pellets were then suspended in 200 uL of PBS and stored at -80 ºC.

4.2.18. Label-free qualitative proteomic and DIANN library free peptide search

The exosome samples were suspended in 1x RIPA (ab156034 - Abcam) containing 12.5% protease and phosphatase inhibitors (Roche, Germany). Quantitative proteomics was performed on cancer cell-derived exosomes by Sydney Mass Spectrometry. To begin with, an ice-cold acetone precipitation was carried out overnight at -30°C. The following day, the samples were spun at 15 g for 10 minutes at 0°C, the supernatant was discarded, and 200 ul ice-cold 80% acetone was added to the pellet. The samples were spun again at 15 g for 10 minutes, and the pellet was air-dried. Further sample preparations were conducted with 50 uL urea/thiourea (6M, 2M), followed by the addition of 5 uL DTT (100 mM) and 10uL of IAA (250 mM) to the samples, which were then incubated at room temperature for 1 h. Finally, 250 uL HEPES and 0.4 ug of trypsin were added to each sample and centrifuged at 37°C for 16 h at 1000 rpm. Exosome peptide samples were desalted and concentrated using an HLB column before loading. The peptides were eluted in 200 uL, 50% acetone, and 0.1% TFA, and dried overnight. Each sample was added with 30 uL of loading buffer, and protein qualification was

done with the Qubit quantitation system. Exosome samples were run on DIA mode on HFX4 for peptide search, and the HFX4 output files were uploaded to DIANN version 1.8.1 for processing in a library-free search against the Human genome for peptide identification.

4.2.19. Statistics and densitometry

The experimental data were compared using a student t-test and presented as mean ± standard deviation (SD). All experiments were conducted in triplicate, and statistical significance was considered when the p-value was < 0.05. The results are shown as mean ± SD ($n = 3$). Statistical significance levels are denoted as follows: *$p<0.05$, **$p<0.01$, ***$p<0.001$, ****$p<0.0001$. The densitometry data was analyzed using GraphPad Prism 10 (GraphPad, U.S.A.) and Microsoft Excel (Microsoft, U.S.A.).

4.3. RESULTS

4.3.1. Upregulation of NDRG1 in PANC-1 and MIAPaCa-2 decreases the activation of macrophages to the M2 phenotype.

To investigate how NDRG1 expression in PDAC cells affects the polarization of THP-1 and U937 monocytes, we first established stably-transfected PANC-1 and MIAPaCa-2 cells expressing either the vector control (VC), wild-type NDRG1 (NDRG1) or NDRG1 in which the CAP region has been deleted (ΔCAP-NDRG1; **Figure 4.1A**). The deletion of the CAP region, which is located within the α/β hydrolase fold of NDRG1 [212], was investigated because earlier studies identified this region to be important for protein-protein interactions or ligand binding [291, 292].

As expected, the western blot results showed that PANC-1 and MIAPaCa-2 cells overexpressing NDRG1 had significantly higher NDRG1 expression in both NDRG1 and ΔCAP-NDRG1 transfected cells when compared to the VC cells (**Figures 4.1B and 4.1C**). Notably, in the PANC1 cells, the ΔCAP-NDRG1 cells had the highest NDRG1 expression (**Figure 4.1B**), while in the MIAPaCa-2 cells, the NDRG1 cells had the highest NDRG1 expression levels (**Figure 4.1C**).

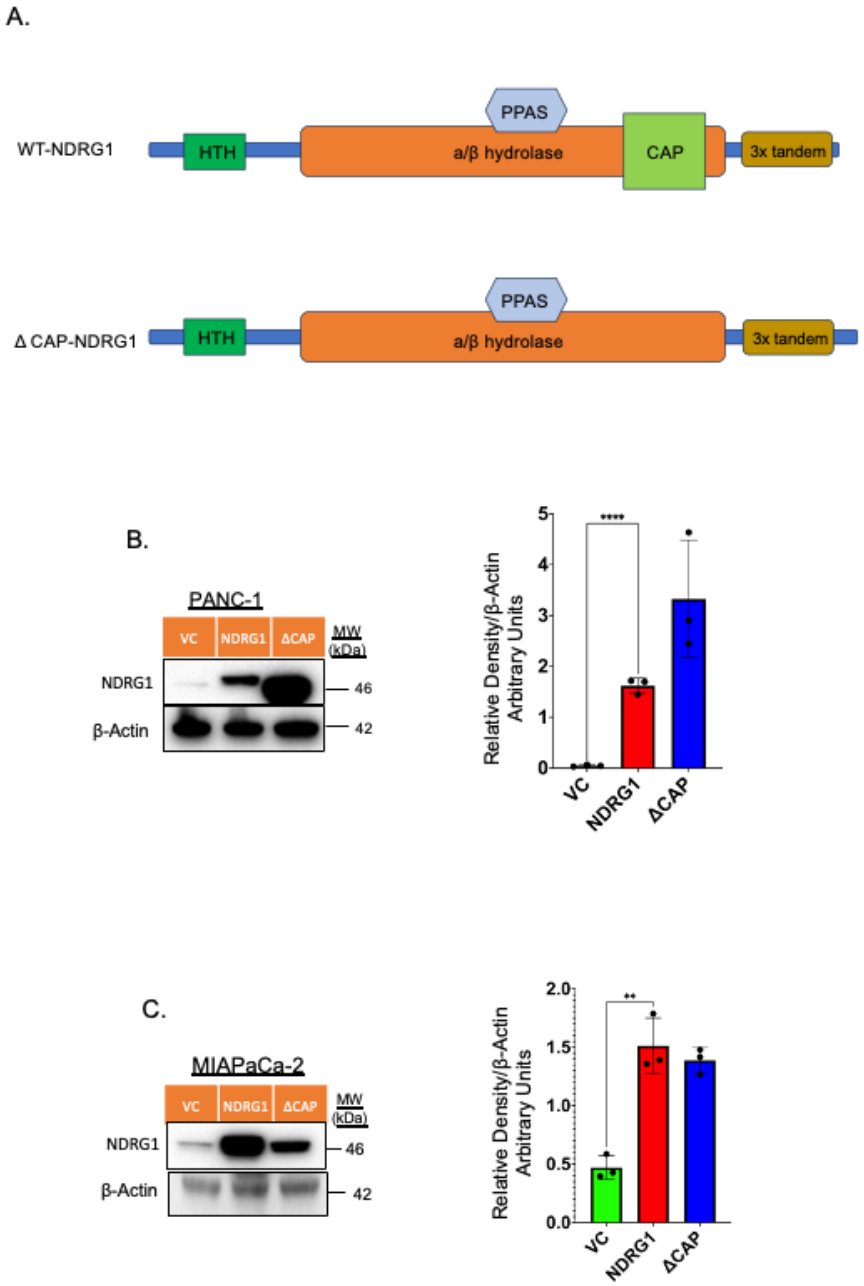

Figure 4.1: Schematic of NDRG1 and ΔCAP-NDRG1 structure and their expression in PDAC cells. (A) Schematic of wild-type NDRG1 (WT-NDRG1) and the NDRG1 deletion mutant that is missing the CAP region (ΔCAP-NDRG1). Western blots and densitometric analysis of (**B**) PANC-1 and (**C**) MIAPaCa-2 cells stably transfected with VC, NDRG1 and ΔCAP. β-actin was used as a loading control. Results are mean ± SD (n = 3). **p<0.01 ****p<0.0001 denote statistical significance comparing NDRG1 cells to the VC control.

Furthermore, to validate our M1 and M2 protein markers, we polarized THP-1 and U937 cells into either the M1 or M2 phenotype using established methods as described above ***(Section 4.2.4)*** [293-295] and examined the expression of M1 marker iNOS [296] and M2 markers CD163 and CD206 [293] *via* western blot (**Figure 4.2A and 4.2B**) [296]. As expected, M2-polarized THP-1 cells had significantly higher expression of CD206 and CD163 when compared to the M1-polarized cells (**Figure 4.2A**). On the other hand, M1-polarized THP-1 cells expressed significantly higher levels of iNOS when compared to the M2 cells (**Figure 4.2A**). Similar results were observed with the U937 cells, where CD206 and CD163 were higher in the M2-polarized cells, while iNOS was significantly higher in the M1 polarized cells (**Figure 4.2B**). This was consistent with the literature [293, 296] and validated the use of these M1 and M2 markers in our studies.

To determine whether NDRG1 expression in the PDAC cells can influence monocyte polarization into the M1 or M2 phenotype, we incubated the THP-1 and U937 cells with conditioned media (CM) derived from either PANC-1 or MIAPaCa-2 VC, NDRG1 or ΔCAP-NDRG1 cells for 72 hours (**Figure 4.2C**). We then analyzed the expression of M1 and M2 markers using Western blot. Examining the THP-1 cells, our findings showed a significant increase in M2 markers CD206 and CD163 when M0 macrophages were incubated with media from PANC-1 VC cells (**Figure 4.3A**). This suggests that the cancer cell CM induces an M2 phenotype in these macrophages. However, this effect was markedly reduced when using CM from NDRG1 or ΔCAP-NDRG1 expressing PANC-1 cells, with both CD206 and CD163 being significantly reduced when compared to the cells incubated with VC CM (**Figure 4.3A**). In contrast, the M1 marker iNOS was significantly increased in the cells incubated with CM from NDRG1 and ΔCAP-NDRG1 compared to VC CM (**Figure 4.3A**). Similar effects were also observed in U937 cells, with a significant decrease in the expression of both M2 markers and

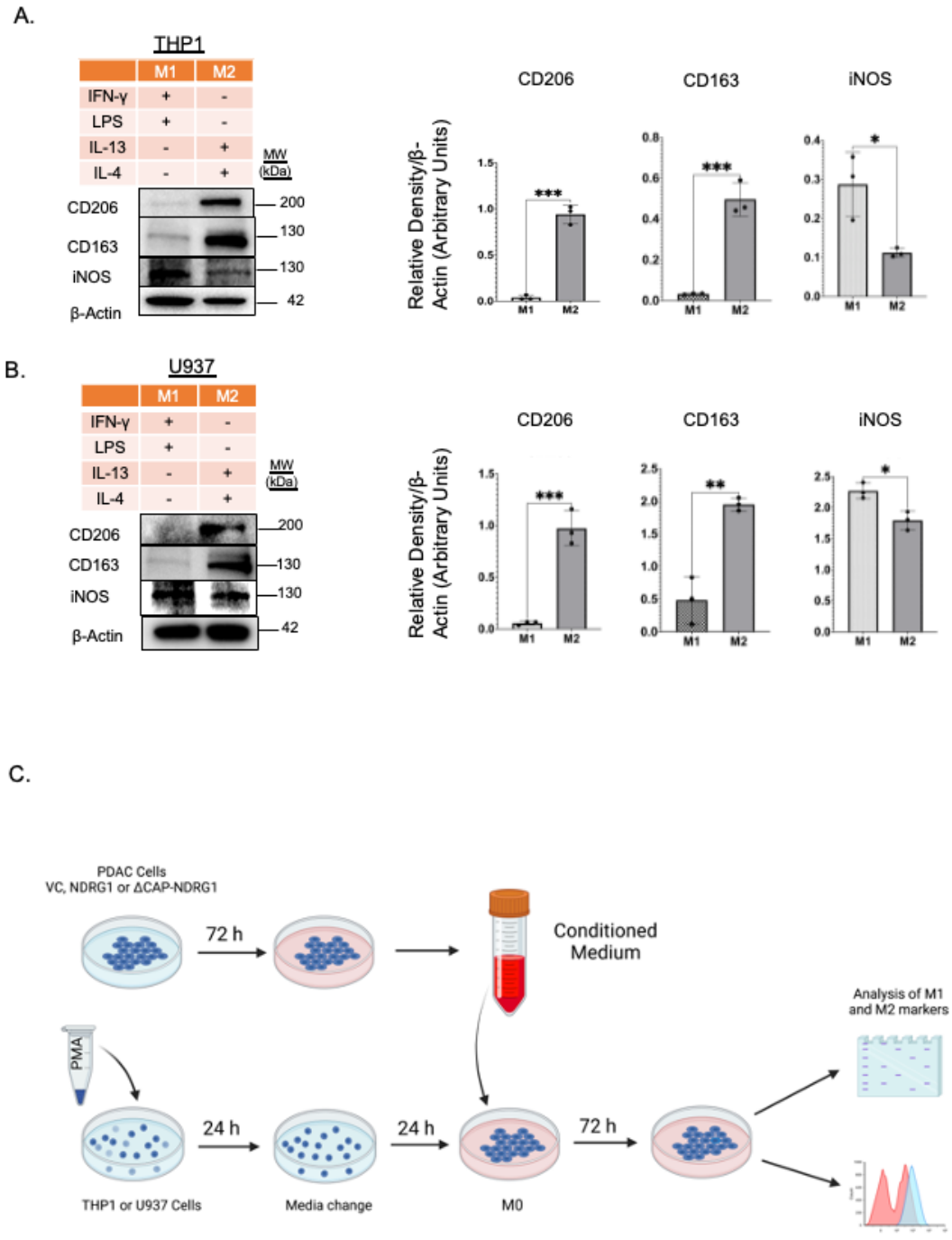

Figure 4.2: Validation of the M1 and M2 protein markers in THP-1 and U937 cells. THP-1 (**A**) and U937 (**B**) cells were incubated with 160 nM PMA for 24 h, followed by an incubation for 24 h with 100 ng/mL IFN-gamma and 100 ng/mL LPS (to generate M1 macrophages) or with 20 ng/mL IL-4 and 20 ng/mL IL-13 for 72 hours (to generate M2 macrophages) and assessed for protein levels of CD206, CD163 and iNOS. β-actin was used as a loading control. Results are mean ± SD (n = 3). *p<0.05, **p<0.01 ***p<0.001 denote statistical significance comparing M1 to M2 cells. **(C)** Schematic diagram of THP1 and U937 cell polarization using conditioned medium (CM) from PANC-1 and MIAPaCa-2 cells.

increase in the M1 marker in cells incubated with PANC-1 CM from NDRG1 and ΔCAP-NDRG1 cells compared to VC CM (**Figure 4.3B**).

To further validate these results, we also incubated THP-1 and U937 monocytes with CM from MIAPaCa-2 cells expressing either the VC, NDRG1 or ΔCAP-NDRG1. Our results were similar to those observed with PANC-1 CM, where the NDRG1 and ΔCAP-NDRG1 CM decreased the expression of both M2 markers, while increasing the M1 marker when compared to VC CM in both THP-1 (**Figure 4.3C**) and U937 (**Figure 4.3D**) cells. Notably, while the addition of VC CM to the M0 macrophages potently induced both CD163 and CD206 expression, the iNOS levels were also slightly induced in response to PANC-1 CM, while being significantly induced in response to MIAPaCa-2 CM. This suggests that the CM from these cancer cells contains factors that can promote the polarization of macrophages into both the M1 and M2 phenotypes, although the M2 phenotype appeared to be more robustly induced.

Overall, the data presented in **Figure 4.3** suggests that NDRG1 expression in PDAC cells can influence the polarization of macrophages, with high NDRG1 promoting the M1 polarization while reducing the M2 polarization of exposed macrophages. Notably, deletion of the CAP region of NDRG1 further enhanced these effects, being generally more potent at reducing the M2 macrophage markers and increasing the M1 macrophage markers when compared to full-length NDRG1.

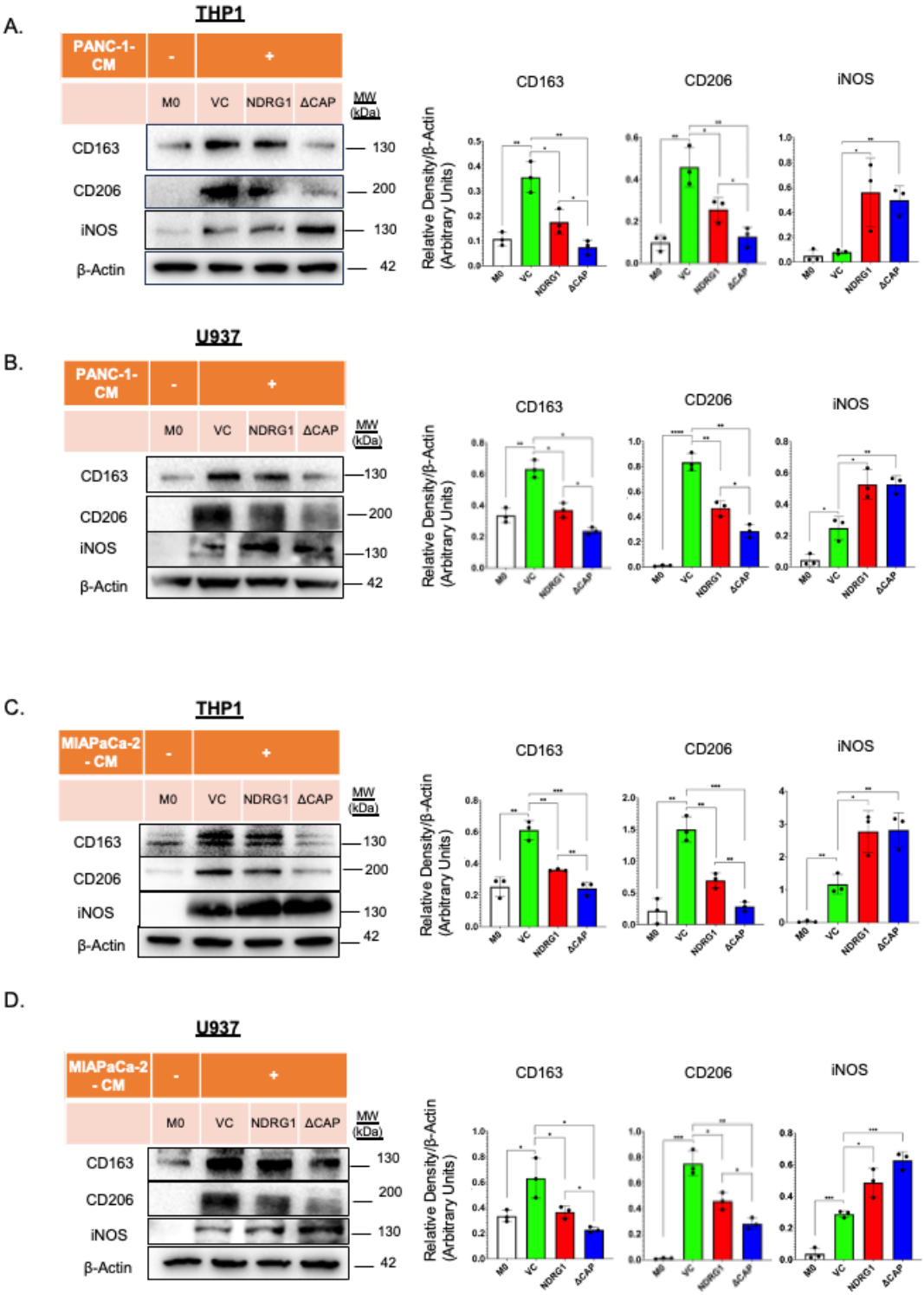

Figure 4.3: Western blot analysis of THP-1 and U937 polarization following exposure to conditioned media from PDAC cells. Western blots and densitometric analysis of CD163, CD206 and iNOS in (**A**) THP-1 and (**B**) U937 cells treated with CM from PANC-1 VC, NDRG1 and ΔCAP cells. Western blots and densitometric analysis of CD163, CD206 and iNOS in (**C**) THP-1 and (**D**) U937 cells treated with CM from MIAPaCa-2 VC, NDRG1 and ΔCAP cells. β-actin was used as a loading control. Results are mean ± SD (n = 3). *p<0.05, **p<0.01 ***p<0.001 ****p<0.0001 denote statistical significance comparing each condition to either the VC CM or the untreated control, as indicated.

These results were then further confirmed using flow cytometry to look for the surface expression of the M2 markers CD163 and CD206 (**Figure 4.4**). The results showed that when THP-1 cells were exposed to PANC-1 NDRG1 and ΔCAP-NDRG1 CM, there was a significant decrease in CD163 and CD206 when compared to VC CM (**Figure 4.4 A and B**). Similar results were observed when THP-1 cells were exposed to MIAPaCa-2 NDRG1 and ΔCAP-NDRG1 CM compared to VC CM (**Figure 4.4 C and D**). The same effects were also shown using the U937 cells, with a significant decrease in the expression of both M2 markers when the cells were incubated with PANC-1 CM from NDRG1 and ΔCAP-NDRG1 cells compared to VC CM (**Figure 4.4 E and F**). U937 cells exposed to MIAPaCa-2 NDRG1 and ΔCAP-NDRG1 CM also exhibited significantly lower CD163 and CD206 expression when compared to VC CM (**Figure 4.4 G and H**).

These findings further validate that the expression of NDRG1 and ΔCAP-NDRG1 in PDAC cells leads to a decrease in the expression of M2 macrophage markers CD163 and CD206 in both THP1 and U937-derived macrophages exposed to these cancer cells.

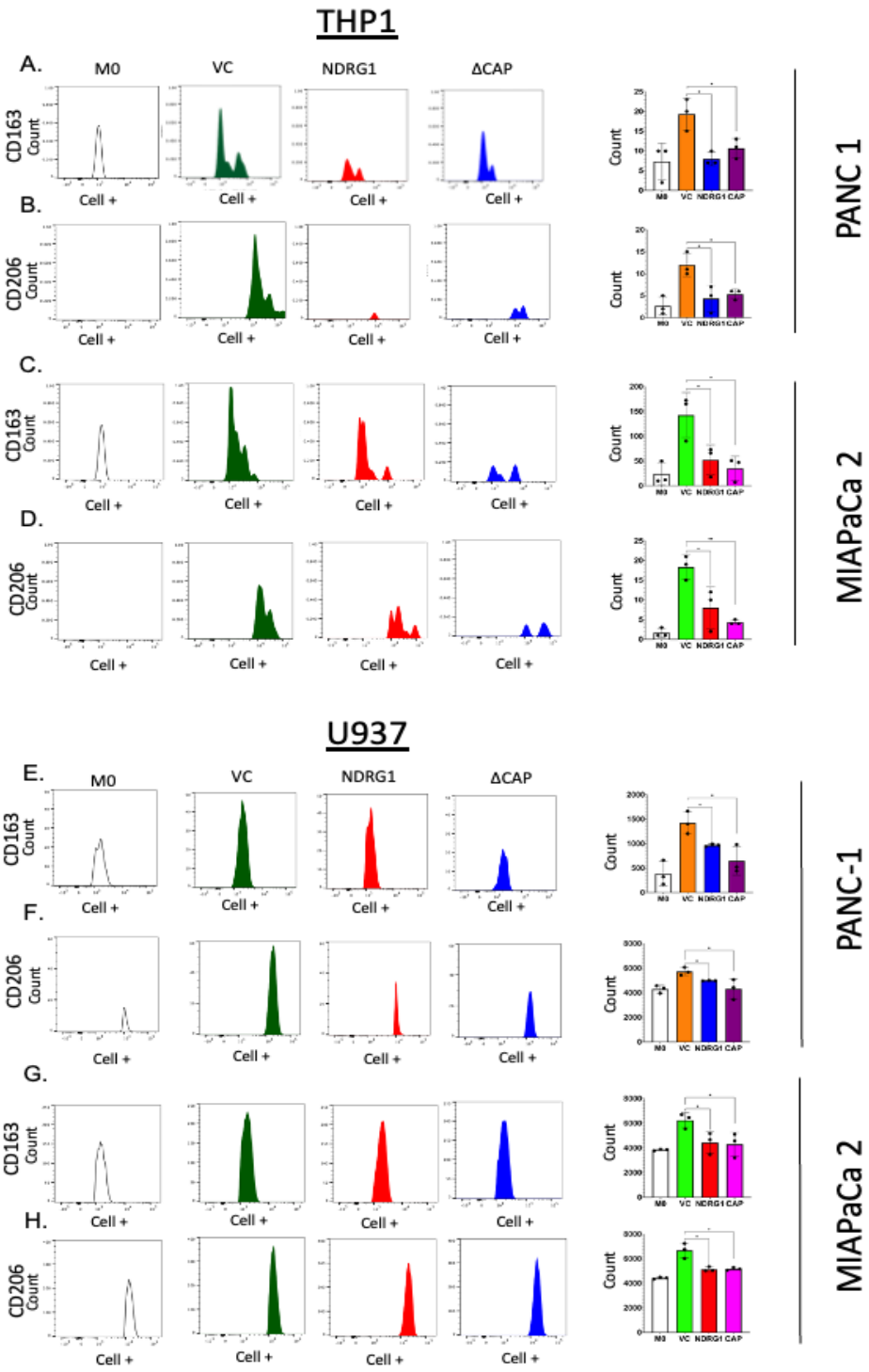

Figure 4.4: Flow cytometry analysis of CD163 and CD206 expression on THP-1 and U937 cells following incubation with PDAC conditioned media. Flow cytometry analysis of THP1 M0 macrophages cells treated with control media (M0) or conditioned media from either PANC-1 (**A, B**) or MIAPaCa-2 (**C, D**) VC, NDRG1 and ΔCAP cells and assessed for CD163 and CD206 expression. Flow cytometry analysis of U937 M0 macrophages treated with control media (M0) or conditioned media from either PANC-1 (**E, F**) or MIAPaCa-2 (**G, H**) VC, NDRG1 and ΔCAP cells and assessed for CD163 and CD206 expression. Results are mean ± SD (n = 3). *p<0.05, **p<0.01 denote statistical significance comparing each condition to the VC control.

4.3.2. NDRG1 expression in PDAC cells altered the cell cycle of exposed macrophages

In a recent RNA-seq study, it was found that the cell cycle impacted 74% of the M2 gene expression program [297]. Similarly, the core M1 polarization program was also sensitive to the cell cycle, affecting 76% of gene expression [297]. It has been reported that M1 macrophages increase the proportion of cells in the G0/G1 phase, while M2 macrophages are more commonly found in the S-G2/M phases of the cell cycle [297, 298].

Therefore, we performed a cell cycle analysis *via* flow cytometry to investigate whether NDRG1 expression in PDAC cells could impact the cell cycle of exposed macrophages. First, the THP1 and U937 cells were polarized into the M0, M1, or M2 macrophage phenotype (2.5) and their cell cycle distribution examined (**Figure 4.5A, B**). As suggested by previous studies, the proportion of M1 macrophages was significantly higher in the G1-phase, while being markedly lower in the S-phase when compared to both M0 and M2 macrophages. This was the case for both THP-1 (**Figure 4.5A**) and U937 (**Figure 4.5B**) macrophages. There were no marked differences between the distribution of these cells in the G2-phase.

We next examined if the cell cycle distribution of the M0, M1 and M2 macrophages could be affected by PANC-1 or MIAPaCa-2 CM derived from VC or NDRG1 over-expressing cells. Examining the differentiated THP-1 macrophages, NDRG1 CM from PANC-1 cells consistently increased the proportion of M0, M1 and M2 macrophages in the G1 phase, while reducing the amount of these cells in the S-phase of the cell cycle (**Figure 4.5C, D and E**). The same result was also observed when incubating the THP-1 macrophages with MIAPaCa-2 media (**Figure 4.5F, H and L**).

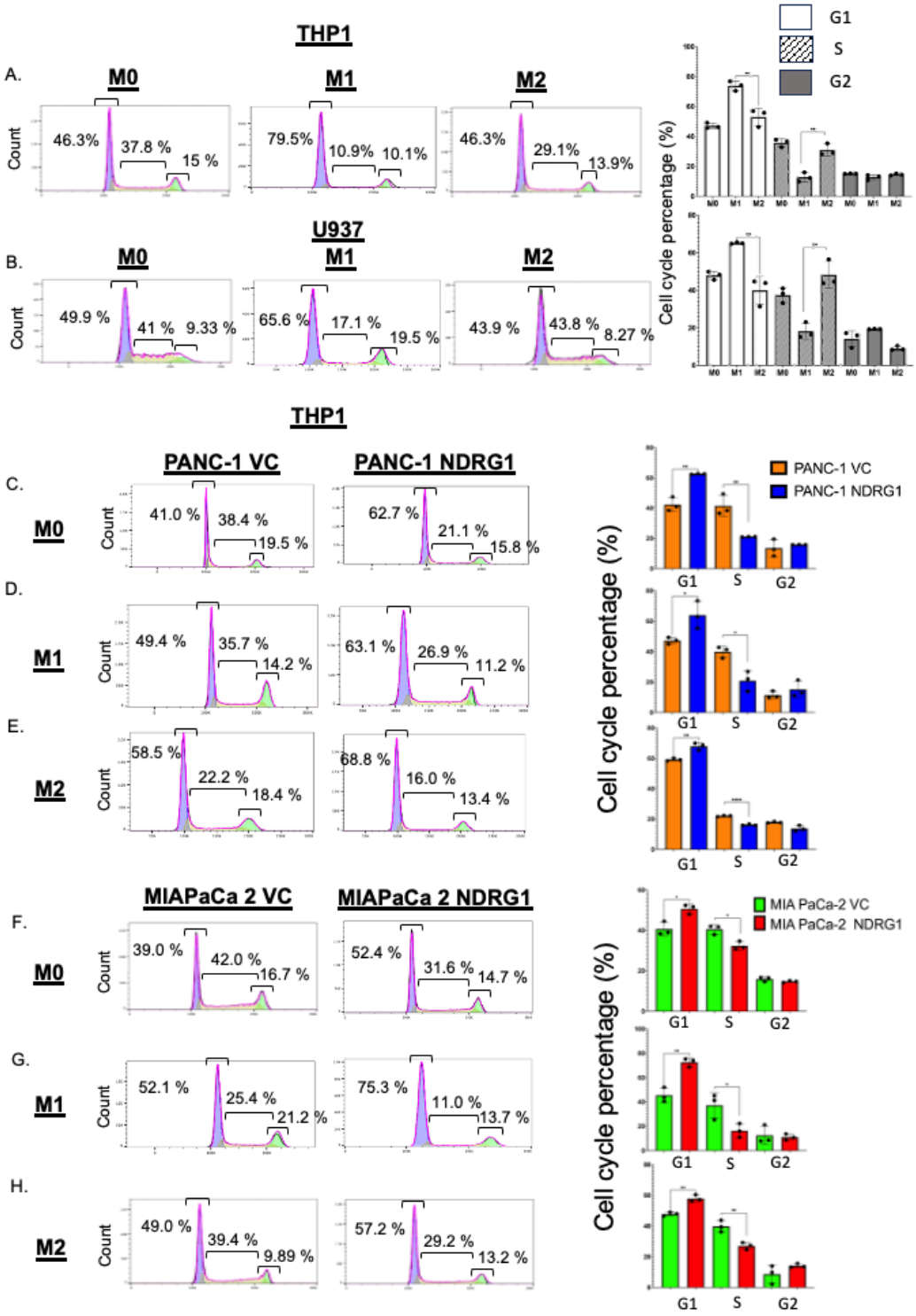

Figure 4.5: NDRG1 increases the proportion of THP1 and U937 macrophages in the G0/G1 phase. Flow cytometry was used to assess the cell cycle distribution of THP-1 (**A**) or U937 (**B**) macrophages polarized into the M0, M1 or M2 phenotype. Results are mean ± SD (n = 3). **p<0.01 denotes statistical significance comparing M1 to M2. Cell cycle analysis of THP-1 M0 (**C**), M1 (**D**) or M2 (**E**) cells after exposure to PANC-1 conditioned media from NDRG1 or VC cells. Cell cycle analysis of THP-1 M0 (**F**), M1 (**G**) or M2 (**H**) cells after exposure to MIAPaCa-2 conditioned media from NDRG1 or VC cells. Results are mean ± SD (n = 3). *p<0.05, **p<0.01 ***p<0.001 ****p<0.0001 denote statistical significance comparing NDRG1 to the VC control.

This was further validated using the U937 macrophages, with NDRG1 CM from both PANC-1 and MIAPaCa-2 cells also increasing the proportion of U937 macrophages in the G1-phase, while decreasing the number of macrophages in the S-phase (**Figure 4.6**).

Overall, these results indicate that NDRG1 expression in PDAC cells can alter the cell cycle of exposed macrophages, leading to an increase in the proportion of cells in the G0/G1-phase, which is again consistent with the M1 macrophage phenotype.

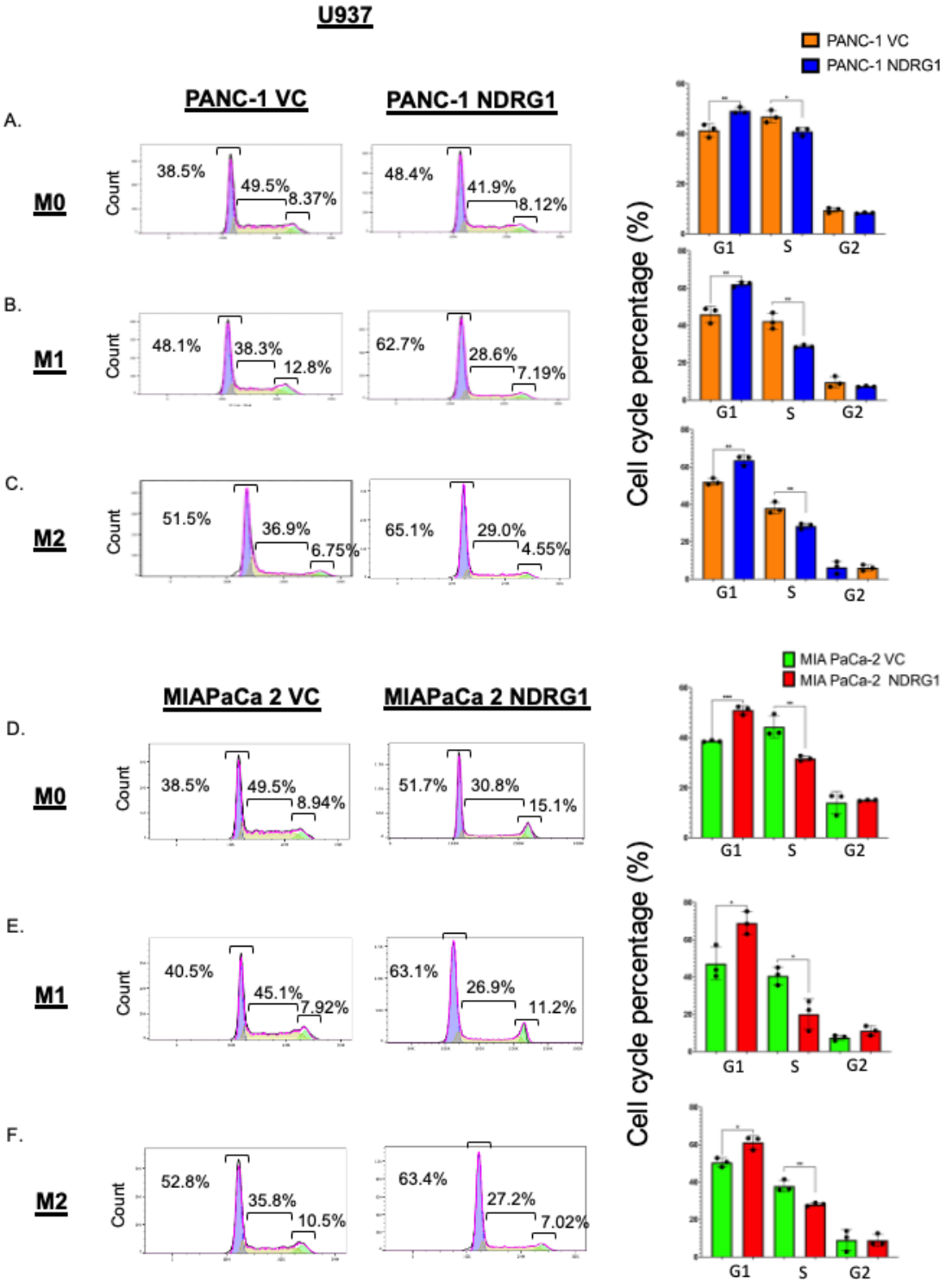

Figure 4.6: NDRG1 increases the proportion of U937 macrophages in the G0/G1 phase. Cell cycle analysis of U937 M0 (**A**), M1 (**B**) or M2 (**C**) cells after exposure to PANC-1 conditioned media from NDRG1 or VC cells. Cell cycle analysis of U937 M0 (**D**), M1 (**E**) or M2 (**F**) cells after exposure to MIAPaCa-2 conditioned media from NDRG1 or VC cells. Results are mean ± SD (n = 3). *p<0.05, **p<0.01 ***p<0.001 denote statistical significance comparing NDRG1 to the VC control.

4.3.3. NDRG1 reduces M2 polarization of monocytes in co-culture spheroids.

We next aimed to investigate the polarization of macrophages into co-culture spheroids consisting of PANC-1 or MIAPaCa-2 cells (VC or NDRG1) and MRC-5 fibroblasts in a 1:1.5 ratio. The fibroblasts were included as they are a major constituent of the PDAC TME and recent studies also suggest that PDAC cells mediate macrophage polarization *via* their effects on neighbouring fibroblasts, which in turn produce immunosuppressive factors [299]. The PDAC cells were initially co-cultured with MRC-5 fibroblasts for 7 days to form spheroids. Then, 10,000 cell/well of THP-1 monocytes were added to the overlying media and the spheroids incubated for an additional 7 days. **Figure 4.7A** shows images of the spheroids taken on day 8 (1 day following the addition of monocytes).

To analyse the polarization of the monocytes into macrophages, we used confocal immunofluorescence (IF) to examine the expression of M2 macrophage marker CD206 and M1 macrophage marker CD86 [300] in these spheroids at the end of the 14 day incubation period. Our findings indicate a significant difference in the polarization of macrophages between PANC-1 VC and NDRG1 spheroids co-cultured with THP-1 monocytes. As expected, no CD206 was detected in spheroids that had no monocytes added (**Figure 4.7B, C**). However, the expression of CD206 was markedly induced in VC + monocyte spheroids with some expression deep inside the spheroid structure, suggesting polarization of M2 macrophages (**Figure 4.7D**). This was significantly reduced in the NDRG1 + monocyte spheroids, where the CD206 staining was minimal (**Figure 4.7E**).

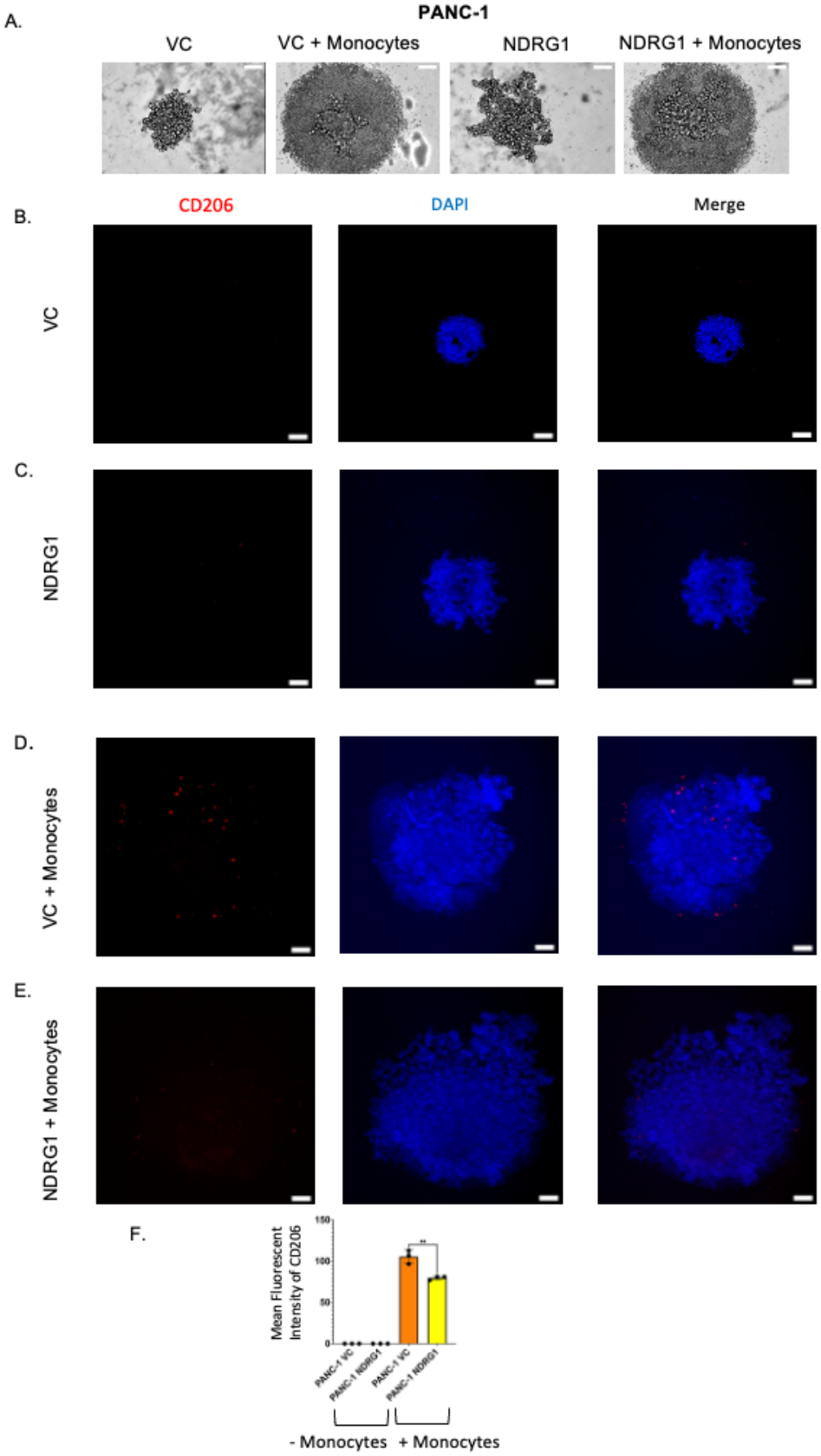
A.
PANC-1
VC
VC + Monocytes
NDRG1
NDRG1 + Monocytes
B.
CD206
DAPI
Merge
VC
C.
NDRG1
D.
VC + Monocytes
E.
NDRG1 + Monocytes
F.
Mean Fluorescent Intensity of CD206
150
100
50
0
**
PANC-1 VC
PANC-1 NDRG1
PANC-1 VC
PANC-1 NDRG1
- Monocytes
+ Monocytes

Figure 4.7: NDRG1 reduces M2 polarization of monocytes in PANC-1 co-culture spheroids. PANC-1 cells were mixed with MRC-5 fibroblasts for 7 days, and then monocytes were added for a further 7 days. **(A)** Brightfield images (from InCucyte SX5 using a 20x objective) at day 8 showing the VC or NDRG1 cells co-cultured with MRC-5 fibroblasts as spheroids with or without the THP-1 monocytes. Confocal immunofluorescence (IF) imaging to examine the expression of M2 macrophage marker CD206 and DAPI at day 14 for **(B)** VC and **(C)** NDRG1 co-culture spheroids without THP-1 monocytes, or **(D)** VC and **(E)** NDRG1 co-culture spheroids with THP-1 monocytes. **(F)** Quantitative analysis of CD206 expression in spheroids from 3 biological repeats. All images were taken with a Nikon Ti-E Spinning Disk Confocal Live Cell microscope using a 4x objective and performed at the same exposure time (scale bar = 200 μm). Results are mean ± SD (n = 3). *$p<0.05$, **$p<0.01$ denotes statistical significance comparing NDRG1 to the VC control.

As shown in **Figure 4.8A**, images of the spheroids taken at day 8 (1 day following addition of monocytes) demonstrate that NDRG1 over-expressing cells formed markedly smaller spheroids compared to the VC control cells when co-cultured with MRC-5 fibroblasts. Further, the monocytes generally formed a halo around the spheroid structures shortly after being added to the overlying media (The development of a hollow (necrotic) core in spheroids depends on various factors, including the spheroid size, culture conditions, or imaging at different planes). The M1 marker CD86 was also detected in VC + monocyte spheroids, although its expression was very low, with very few cells found inside the spheroid structure (**Figure 4.8C**). However, CD86 expression was significantly increased in the NDRG1 + monocyte spheroids, although again these were mostly located on the periphery of the spheroid (**Figure 4.8D**).

We found similar results in MIAPaCa-2 spheroids when co-cultured with MRC-5 cells (**Figure 4.9A**). NDRG1 over-expressing cells again formed smaller spheroids when compared to VC cells after 7 days of co-culture with MRC-5 fibroblasts. In VC + monocytes spheroids, there was an increase in polarization M2 macrophages, and we observed some expression inside the spheroid structure (**Figure 4.9D**). However, this was significantly reduced in the NDRG1 + monocyte spheroids, where only a few distinct cells on the periphery of the spheroid were found to stain for CD206 (**Figure 4.9E**).

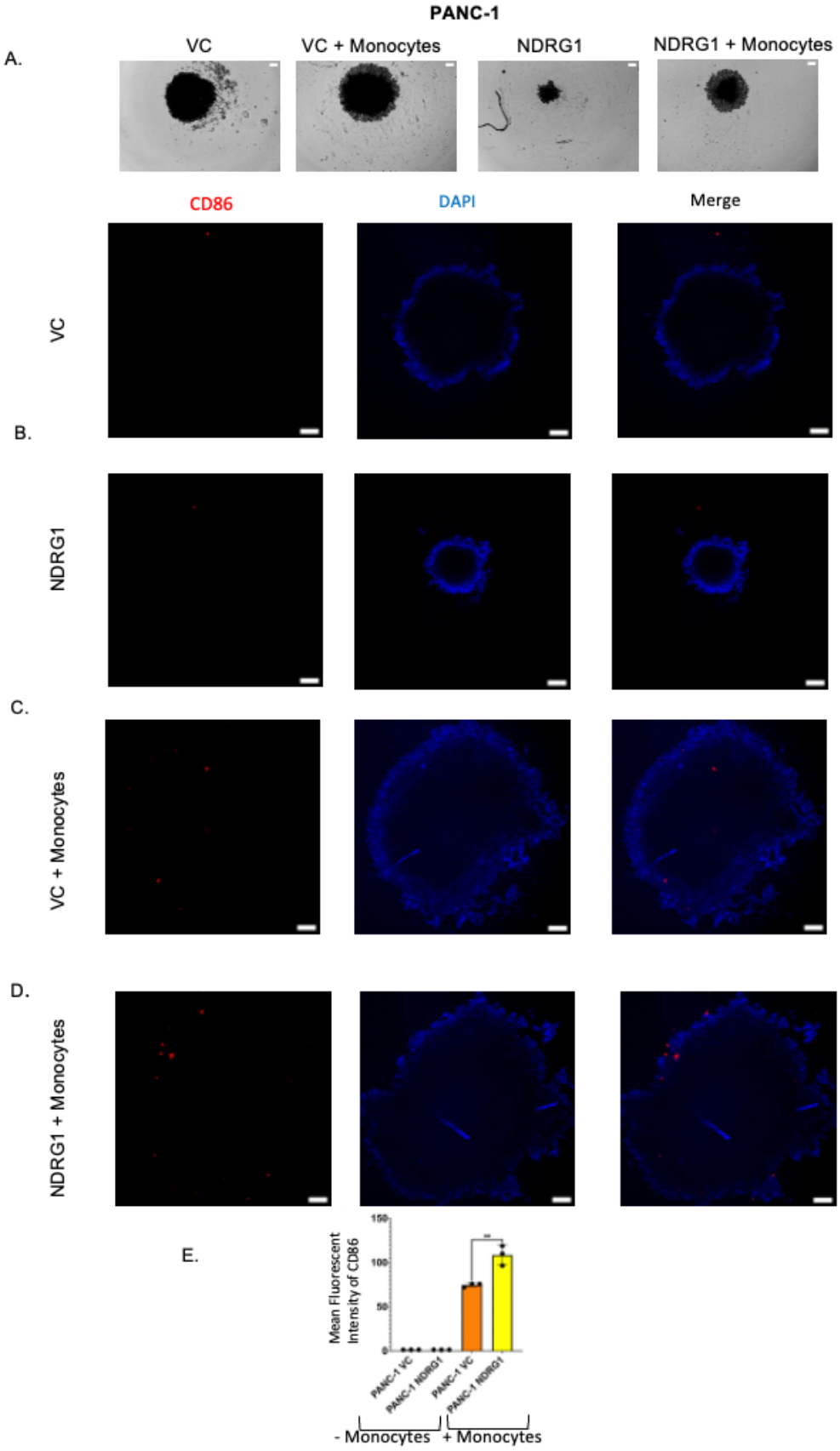
PANC-1
A.
VC
VC + Monocytes
NDRG1
NDRG1 + Monocytes
CD86
DAPI
Merge
VC
B.
NDRG1
C.
VC + Monocytes
D.
NDRG1 + Monocytes
E.
Mean Fluorescent Intensity of CD86
150
100
50
0
PANC-1 VC
PANC-1 NDRG1
PANC-1 VC
PANC-1 NDRG1
- Monocytes
+ Monocytes

Figure 4.8: NDRG1 increases M1 polarization of infiltrated monocytes in co-culture spheroids. PANC-1 cells were mixed with MRC-5 fibroblasts for 7 days, and then monocytes were added for a further 7 days. **(A)** Brightfield images (from InCucyte SX5 using a 10x objective) at day 8 showing the VC or NDRG1 cells co-cultured with MRC-5 fibroblasts as spheroids with or without the THP-1 monocytes. Confocal immunofluorescence (IF) imaging to examine the expression of M1 macrophage marker CD86 and DAPI at day 14 for **(B)** VC and **(C)** NDRG1 co-culture spheroids without THP-1 monocytes, or **(D)** VC and **(E)** NDRG1 co-culture spheroids with THP-1 monocytes. **(F)** Quantitative analysis of CD86 expression in spheroids from 3 biological repeats. All images were taken with a Nikon Ti-E Spinning Disk Confocal Live Cell microscope using a 4x objective and performed at the same exposure time (scale bar = 200 μm). Results are mean ± SD (n = 3). *$p<0.05$, **$p<0.01$ denotes statistical significance comparing NDRG1 to the VC control.

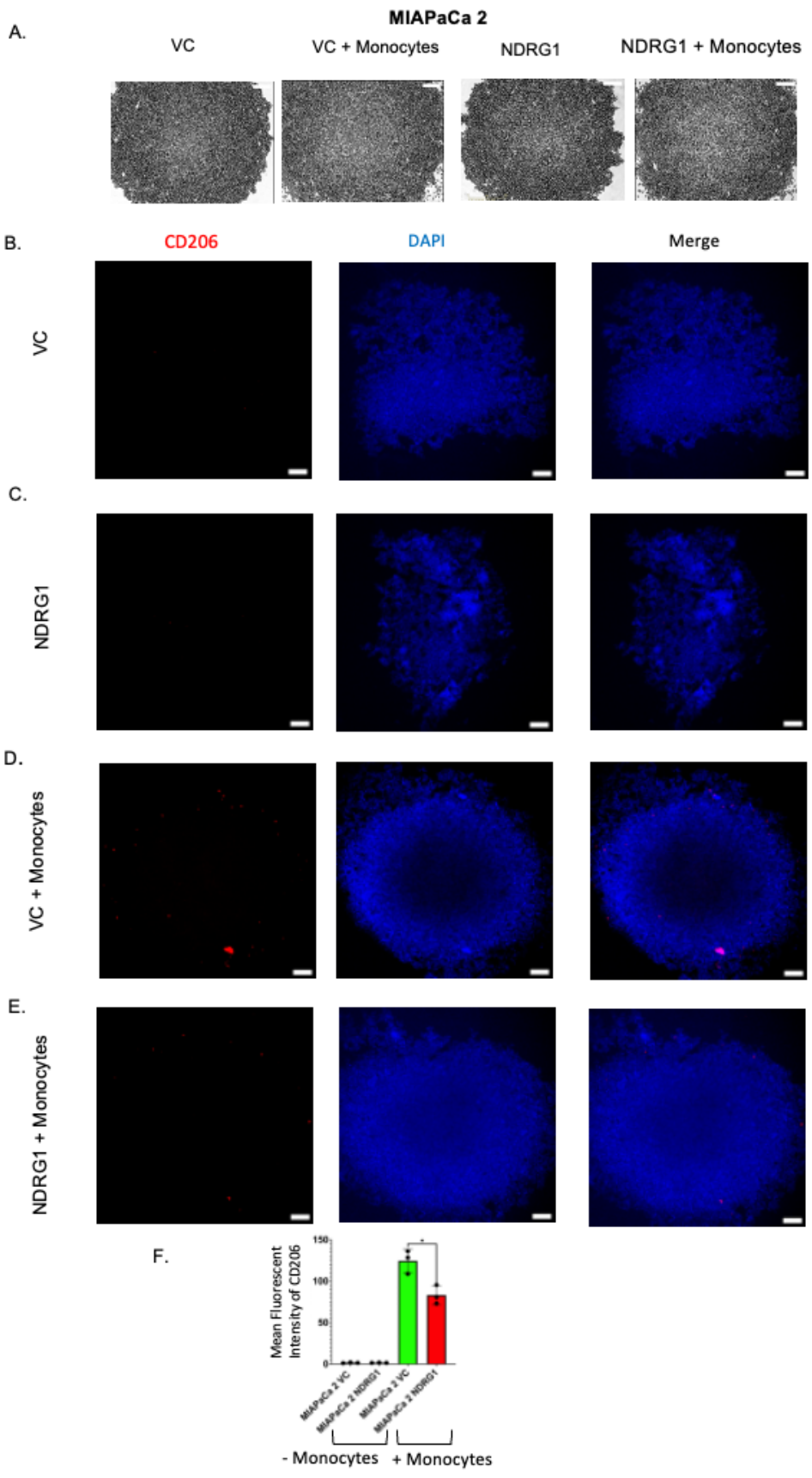
A.
MIAPaCa 2
VC
VC + Monocytes
NDRG1
NDRG1 + Monocytes
B.
CD206
DAPI
Merge
VC
C.
NDRG1
D.
VC + Monocytes
E.
NDRG1 + Monocytes
F.
Mean Fluorescent Intensity of CD206
150
100
50
0
MIAPaCa 2 VC
MIAPaCa 2 NDRG1
MIAPaCa 2 VC
MIAPaCa 2 NDRG1
- Monocytes
+ Monocytes

Figure 4.9: NDRG1 reduces M2 polarization of infiltrated monocytes in co-culture spheroids. MIAPaCa-2 cells were mixed with MRC-5 fibroblasts for 7 days, and then monocytes were added for a further 7 days. **(A)** Brightfield images (from InCucyte SX5 using a 20x objective) at day 8 showing the VC or NDRG1 cells co-cultured with MRC-5 fibroblasts as spheroids with or without the THP-1 monocytes. Confocal immunofluorescence (IF) imaging to examine the expression of M2 macrophage marker CD206 and DAPI at day 14 for **(B)** VC and **(C)** NDRG1 co-culture spheroids without THP-1 monocytes, or **(D)** VC and **(E)** NDRG1 co-culture spheroids with THP-1 monocytes. **(F)** Quantitative analysis of CD206 expression in spheroids from 3 biological repeats. All images were taken with a Nikon Ti-E Spinning Disk Confocal Live Cell microscope using a 4x objective and performed at the same exposure time (scale bar = 200 μm). Results are mean ± SD (n = 3). *$p<0.05$, **$p<0.01$ denotes statistical significance comparing NDRG1 to the VC control.

Figure 4.10A shows images of the spheroids taken on day 8 (1 day following the addition of monocytes). Notably, the expression of CD86 was barely detectable in the VC + monocyte spheroids of MIAPaCa-2 cells, being similar to the VC controls that had no monocytes (**Figure 4.10C**). Conversely, in the NDRG1 + monocyte spheroids, CD86 expression was significantly increased, with many distinct cells on both the periphery and deep inside the spheroid staining for CD86 (**Figure 4.10D**).

These findings suggest that NDRG1 decreases the polarization of macrophages into the M2 phenotype, while increases their polarization into the M1 phenotype when co-cultured in spheroids containing fibroblasts. These results reinforce the data from **Figures 4.3-6**, highlighting NDRG1's ability to reduce the polarization of M2 macrophages and increase the polarization of M1 macrophages in PDAC.

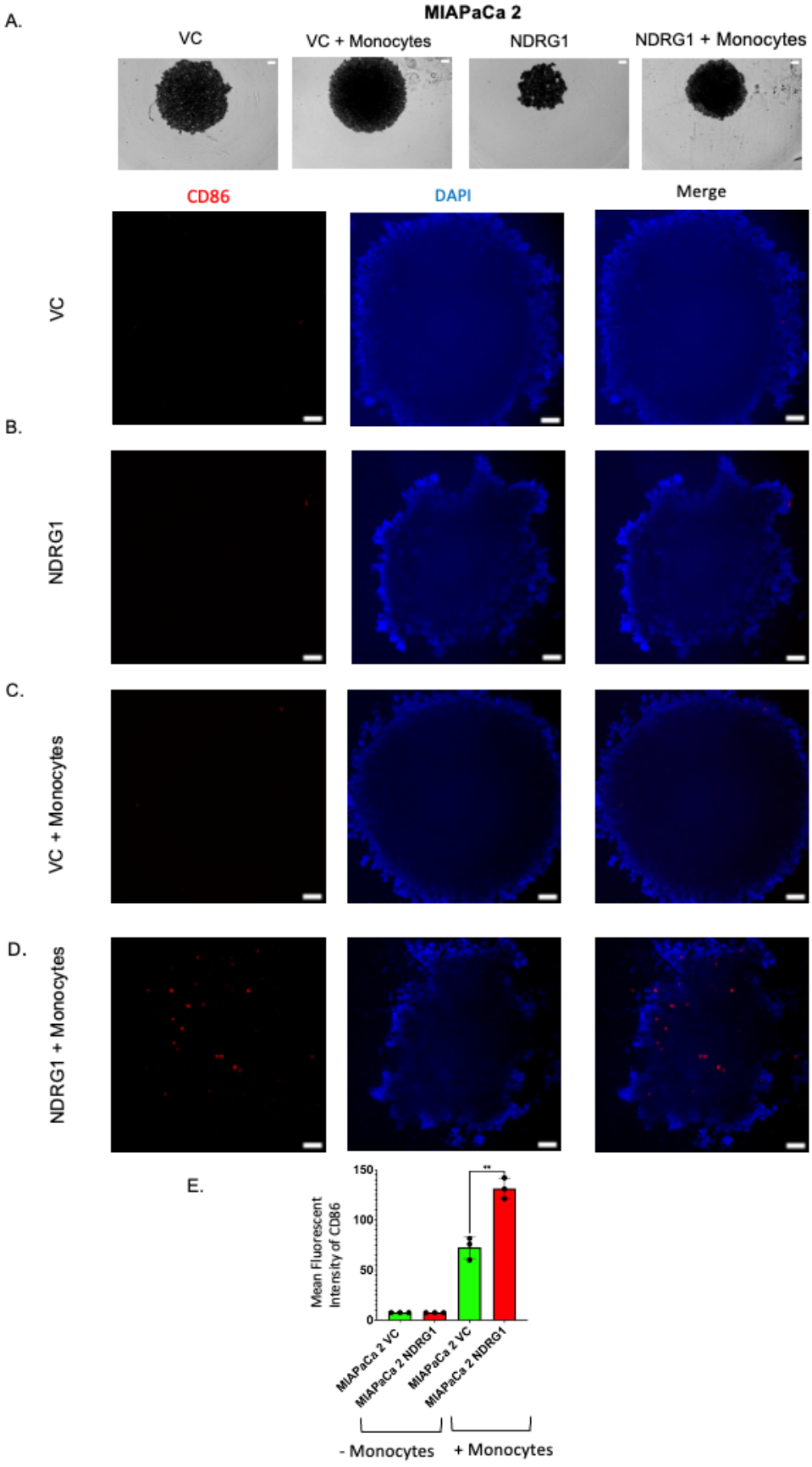
A.
MIAPaCa 2
VC
VC + Monocytes
NDRG1
NDRG1 + Monocytes
CD86
DAPI
Merge
VC
B.
NDRG1
C.
VC + Monocytes
D.
NDRG1 + Monocytes
E.
Mean Fluorescent Intensity of CD86
150
100
50
0
**
MIAPaCa 2 VC
MIAPaCa 2 NDRG1
MIAPaCa 2 VC
MIAPaCa 2 NDRG1
- Monocytes
+ Monocytes

Figure 4.10: NDRG1 increases M1 polarization of infiltrated monocytes in co-culture spheroids. MIAPaCa-2 cells were mixed with MRC-5 fibroblasts for 7 days, and then monocytes were added for a further 7 days. **(A)** Brightfield images (from InCucyte SX5 using a 10x objective) at day 8 showing the VC or NDRG1 cells co-cultured with MRC-5 fibroblasts as spheroids with or without the THP-1 monocytes. Confocal immunofluorescence (IF) imaging to examine the expression of M1 macrophage marker CD86 and DAPI at day 14 for **(B)** VC and **(C)** NDRG1 co-culture spheroids without THP-1 monocytes, or **(D)** VC and **(E)** NDRG1 co-culture spheroids with THP-1 monocytes. **(F)** Quantitative analysis of CD86 expression in spheroids from 3 biological repeats. All images were taken with a Nikon Ti-E Spinning Disk Confocal Live Cell microscope using a 4x objective and performed at the same exposure time (scale bar = 200 μm). Results are mean ± SD (n = 3). *$p<0.05$, **$p<0.01$ denotes statistical significance comparing NDRG1 to the VC control.

4.3.4. Upregulation of NDRG1 in PANC-1 and MIAPaCa-2 increases the secretion of interleukin 12.

M1 macrophages secrete pro-inflammatory cytokines, one of which is interleukin 12 (IL-12; [301, 302]). IL-12 is an effective cytokine that can stimulate anti-tumour immunity. Specifically, IL-12 drives the effector Th1 response, which activates cytotoxic T and NK cells necessary for tumour clearance [303]. This was further confirmed by examining the IL-12 cytokine production by both M1 and M2 polarized THP-1 and U937 macrophages using an ELISA assay. As shown in **Figure 4.11A and B**, M1 polarized THP-1 and U937 macrophages produced significantly more IL-12 when compared to their M2 counterparts.

Considering our results above indicate that NDRG1 expression promotes the M1 pro-inflammatory macrophage phenotype, we next investigated whether NDRG1 expression in PDAC cells can influence the ability of macrophages to produce the pro-inflammatory cytokine IL-12. We performed an ELISA assay on both THP-1 and U937 cell secretions following a 24 h incubation with CM from either VC, NDRG1 or ΔCAP-NDRG1 PANC-1 or MIAPaCa-2 cells. Importantly, these results were normalized to the relative CM that was not incubated with THP-1 or U937 cells, to allow assessment of IL-12 being secreted by the macrophages and not any potential IL-12 that might be contained in the CM itself.

Examining the THP-1 macrophages, the production of IL-12 was significantly higher following incubation with PANC-1 NDRG1 and ΔCAP-NDRG1 CM when compared to the VC control CM (**Figure 4.11C**). Similar results were obtained when MIAPaCa-2 CM was used, with significantly more IL-12 being produced by THP-1 cells exposed to NDRG1 and ΔCAP-NDRG1 CM compared to VC CM (**Figure 4.11D**). This effect was further validated using the U937 macrophages, which also produced significantly more IL-12 when incubated with CM

from NDRG1 and ΔCAP-NDRG1 overexpressing PANC-1 and MIAPaCa-2 cells compared to the VC control CM (**Figure 4.11E and F**).

Overall, these findings indicate that NDRG1 expression in PDAC cells increases the production of IL-12 from both THP1 and U937-derived macrophages, further confirming that NDRG1 promotes a pro-inflammatory macrophage phenotype.

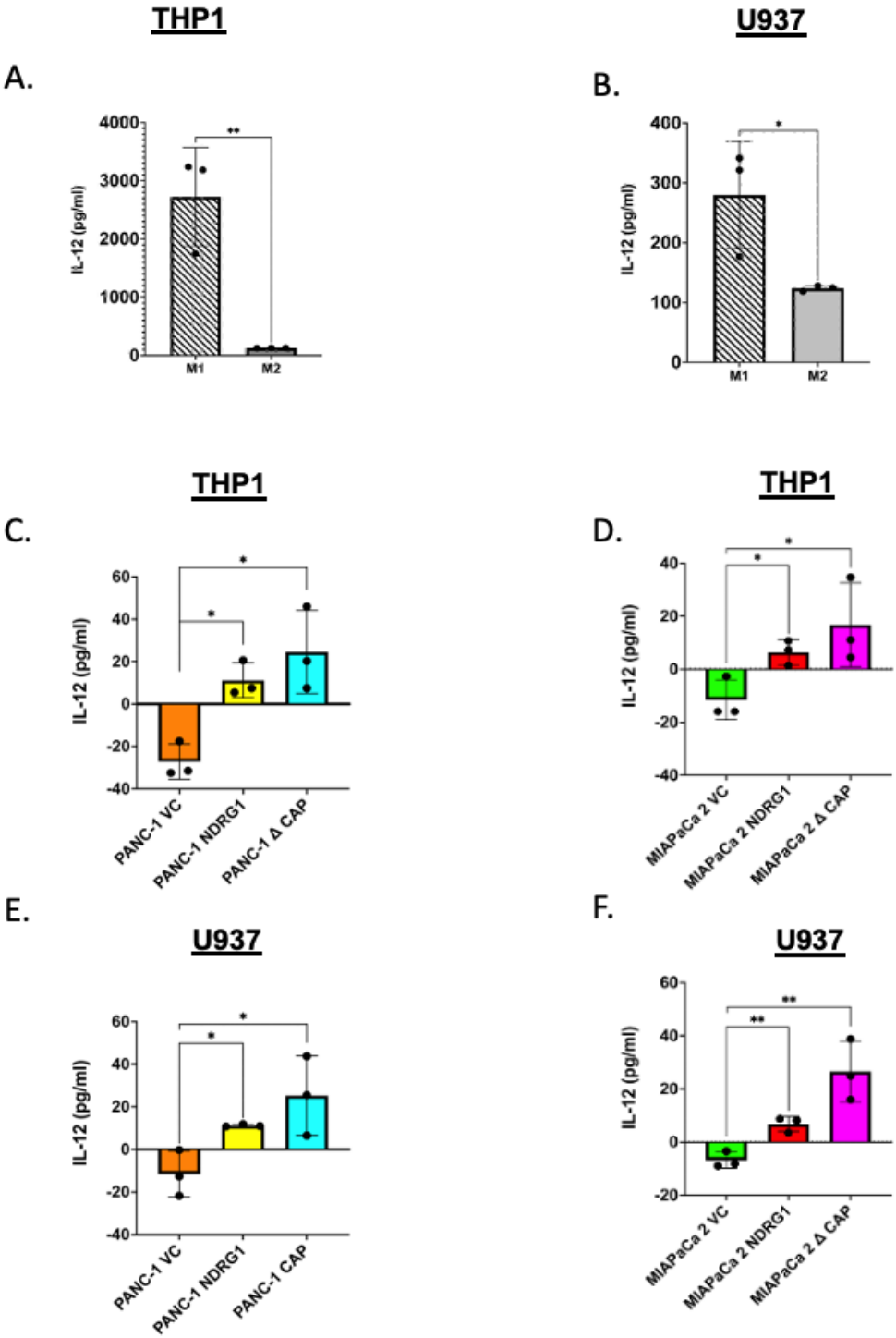

Figure 4.11: NDRG1 increases the secretion of interleukin 12 from THP-1 and U937 macrophages. ELISA assay measuring the IL-12 levels in media from **(A)** THP-1 and (**B**) U937 M1 and M2 polarized macrophages. THP-1 macrophages were incubated with conditioned media derived from PANC-1 (**C**) or MIAPaCa-2 (**D**) VC, NDRG1 or ΔCAP-NDRG1 for 72h and assessed for IL-12 production *via* ELISA. U937 macrophages were incubated with conditioned media derived from PANC-1 (**E**) or MIAPaCa-2 (**F**) VC, NDRG1 or ΔCAP-NDRG1 for 72h and assessed for IL-12 production *via* ELISA. Results are mean ± SD (n = 3). *p<0.05, **p<0.01 denote statistical significance comparing each condition to the VC control. Data in C-F were normalized to the conditioned media derived from the respective VC, NDRG1 or ΔCAP-NDRG1 cells.

4.3.5. NDRG1 increased the levels of reactive oxygen species production by macrophages.

M1 macrophages produce higher levels of reactive oxygen species (ROS) when compared to M2 macrophages, which plays a crucial role in their anti-cancer effects [304, 305]. To investigate whether NDRG1 influences the ability of macrophages to produce ROS, we next performed a reactive oxygen species (ROS) assay. We initially differentiated both THP-1 and U937 monocytes into M1 or M2 macrophages following a standard protocol (***Section 2.4***) and examined their abilities to generate ROS using a DCFDA ROS assay kit. As shown in **Figures 4.12A and B**, M1 macrophages produced significantly higher levels of ROS when compared to M0 and M2 macrophages for both THP1 and U937 cells **(Figure 4.12A and B)**.

We then conducted an experiment to measure the levels of ROS in THP1 M0 macrophages following their exposure to the CM of PANC1 VC, NDRG1 or Δ CAP-NDRG1 cells. The results showed that THP-1 cells exposed to NDRG1 and ΔCAP-NDRG1 CM produced significantly higher levels of ROS when compared to those cultured with VC CM (**Figure 4.12C**). Similar results were obtained when incubating THP-1 cells with CM from MIAPaCa-2 cells over-expressing NDRG1 or ΔCAP-NDRG1 (**Figure 4.12D**).

To further validate these findings, we also exposed U937 M0 macrophages to CM derived from both PANC-1 and MIAPaCa-2 cells. We again observed that CM from NDRG1 or ΔCAP-NDRG1 over-expressing PDAC cells induced significantly more ROS production by the macrophages when compared to CM from VC cells (**Figure 4.12E and F**). These findings suggest that NDRG1 expression in both PANC-1 and MIAPaCa-2 PDAC cells is capable of increasing the production of ROS by both THP1 and U937 derived macrophages when they are exposed to the cancer CM. Notably, the deletion of the CAP region of NDRG1 did not influence this effect, with the ΔCAP variant producing similar results to the wild-type NDRG1.

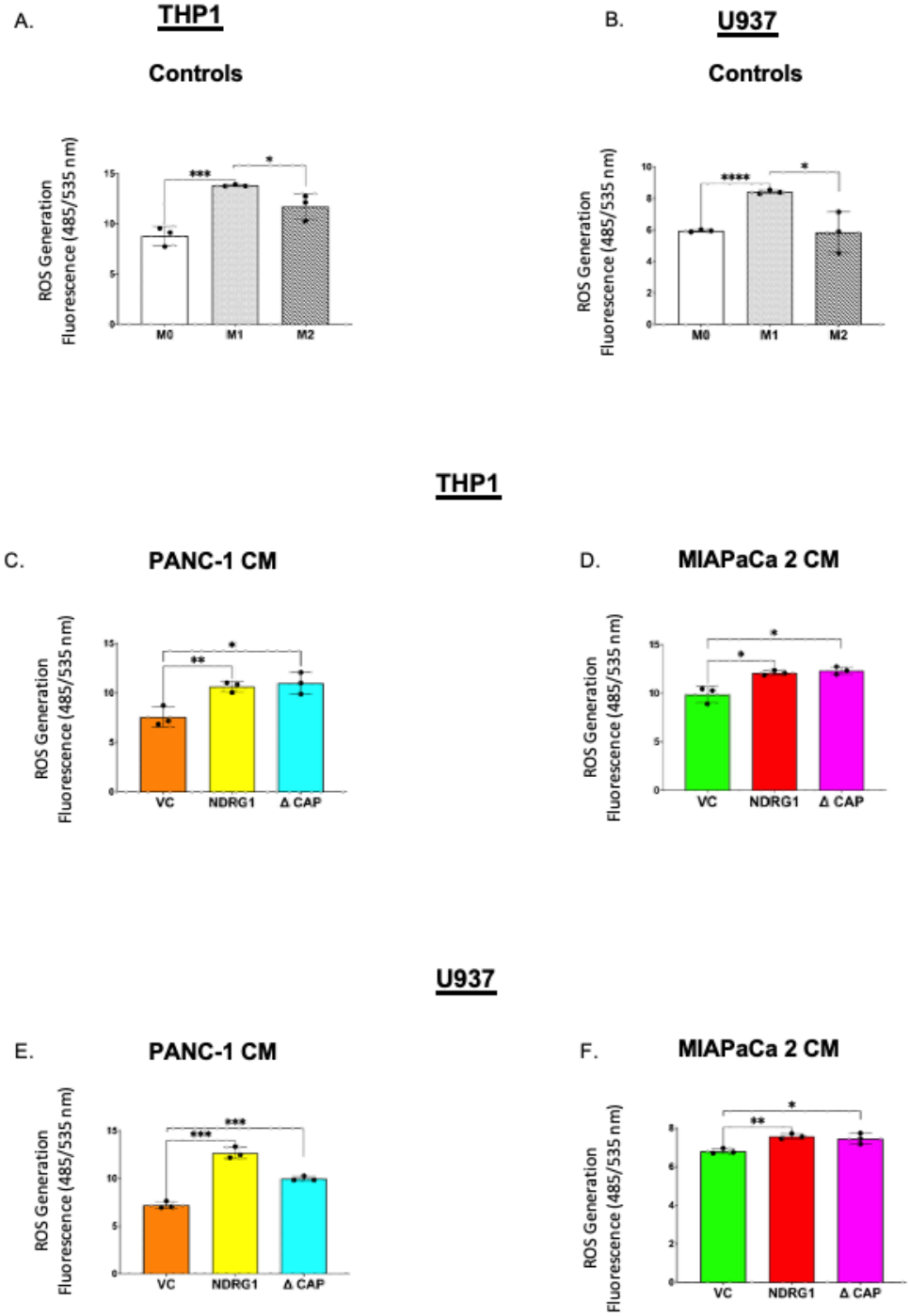

Figure 4.12: NDRG1 increased the production of ROS by THP-1 and U937 macrophages following exposure to PDAC conditioned media. THP-1 (**A**) and U937 (**B**) macrophages were incubated for 72 h and assessed for ROS production *via* a DCFDA ROS assay. THP-1 macrophages were incubated for 72 h in either PANC-1 (**C**) or MIAPaCa-2 (**D**) conditioned media derived from VC, NDRG1 or ΔCAP NDRG1 cells and assessed for ROS production. U937 macrophages were incubated for 72 h in either PANC-1 (**E**) or MIAPaCa-2 (**F**) conditioned media derived from VC, NDRG1 or ΔCAP NDRG1 cells and assessed for ROS production. Results are mean ± SD (n = 3). *p<0.05, **p<0.01 ***p<0.001 denote statistical significance comparing each condition to the VC control.

4.3.6. NDRG1 increased the cytotoxicity of PDAC cells.

M1 macrophages directly kill tumour cells by mediating cytotoxicity and antibody-dependent cell-mediated cytotoxicity (ADCC), exerting anti-tumour functions [306]. To investigate the impact of NDRG1 expression in PDAC cells on the cytotoxic function of macrophages *in vitro*, we established multi-cellular co-culture spheroids consisting of PDAC cells (VC or NDRG1) and MRC-5 fibroblasts, followed by the addition of THP-1 monocytes. The spheroids were cultured for 5 days, and viability monitored every 12 hours using a cytotoxicity dye.

Examining the PANC-1 VC spheroids without any monocytes, significant cytotoxicity was observed going from day 3 to day 5, as shown by the increasing intensity of the green cytotox dye (**Figure 4.13A**). Notably, this toxicity was more pronounced in the centre of the spheroid, suggesting the formation of a necrotic core, as is typically observed with spheroids as they get larger [307]. However, the cytotoxicity in the PANC-1 NDRG1 spheroids was significantly higher compared to the PANC-1 VC spheroids, and this was apparent at days 3, 4 and 5 (**Figure 4.13A**). This suggests that NDRG1 expression is increasing the necrotic core in these spheroids and may be related to its ability to inhibit oncogenic cross-talk between PDAC cells and fibroblasts [206].

When THP-1 monocytes were added to these spheroids, the hypoxic core was no longer prominent in the PANC-1 VC spheroids (**Figure 4.13B**). This was unexpected and may suggest that the monocytes are supporting the spheroid growth, potentially *via* metabolic cross-talk, as has been observed with M2 macrophages [308]. Notably, in the PANC-1 NDRG1 spheroids, the hypoxic core was again apparent, with cytotoxicity being significantly higher compared to the VC spheroids at days 4 and 5 (**Figure 4.13B**).

A.

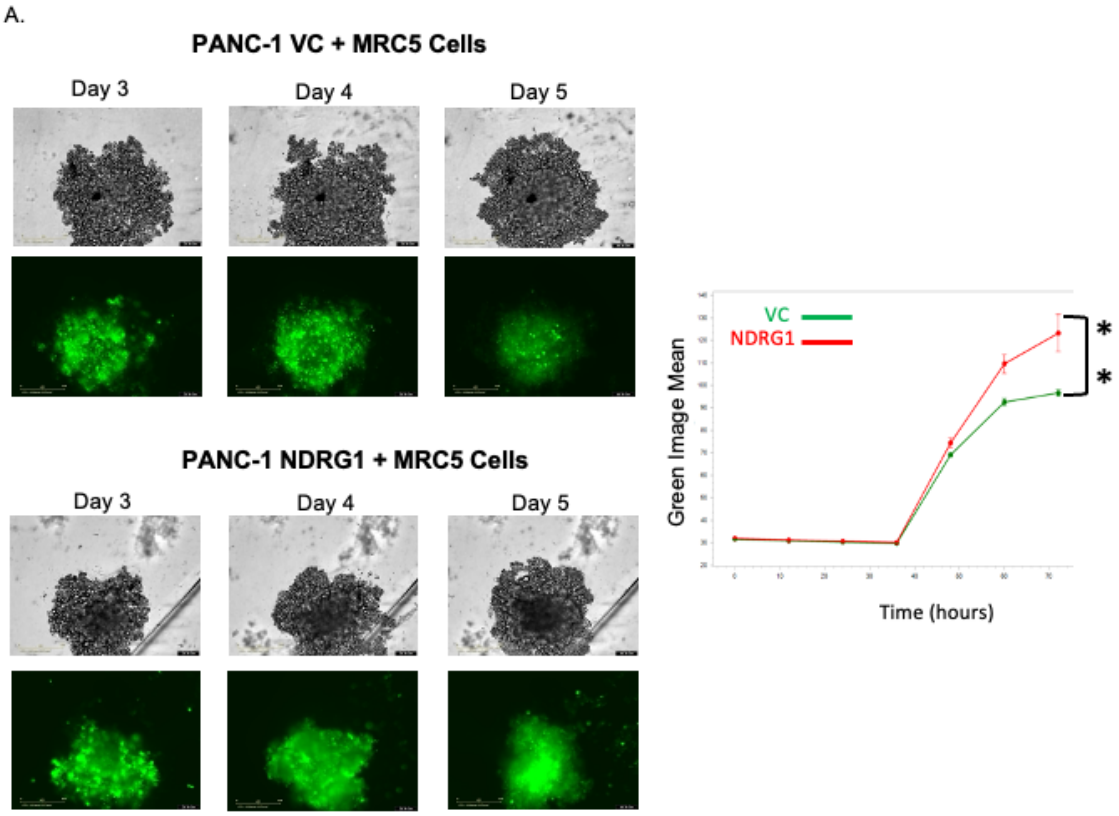
PANC-1 VC + MRC5 Cells
Day 3
Day 4
Day 5
PANC-1 NDRG1 + MRC5 Cells
Day 3
Day 4
Day 5
VC
NDRG1
Green Image Mean
Time (hours)
*
*

B.

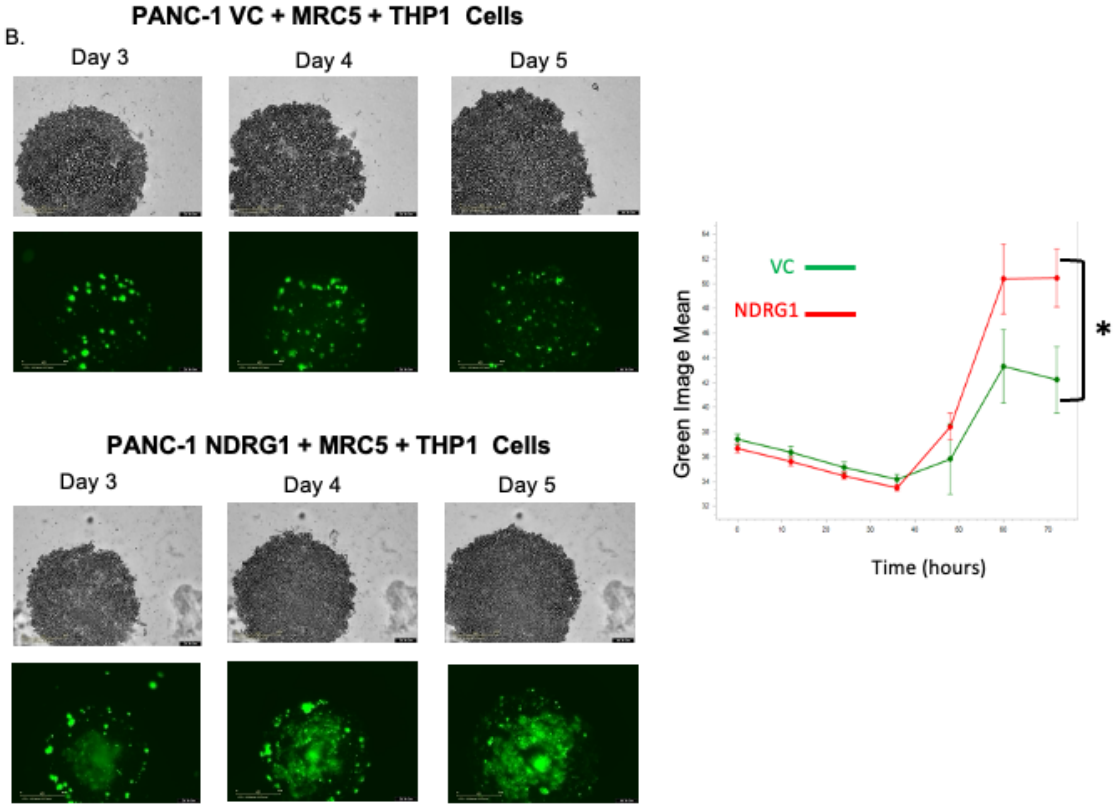
PANC-1 VC + MRC5 + THP1 Cells
Day 3
Day 4
Day 5
PANC-1 NDRG1 + MRC5 + THP1 Cells
Day 3
Day 4
Day 5
VC
NDRG1
Green Image Mean
Time (hours)
*

Figure 4.13: NDRG1 increased the cytotoxicity in PANC-1 co-culture spheroids.
PANC-1 cells (1000 cells) were mixed with MRC-5 fibroblasts (1500 cells) and incubated for 5 days alone (**A**) or with THP-1 monocytes added (**B**). Viability was monitored every 12 h using Cytotox Green Dye and spheroids imaged using the InCucyte SX5 (scale bar = 400 μm). Results are mean ± SD (n = 3). *p<0.05, **p<0.01 denote statistical significance comparing NDRG1 to the VC control.

Further validation was obtained when the MIAPaCa-2 cells were used. The cytotoxicity results again showed that NDRG1 significantly increased the cytotoxicity in the spheroids both in the absence and presence of monocytes (**Figure 4.14A and B**).

These findings suggest that NDRG1 expression in both PANC-1 and MIAPaCa-2 PDAC cells increases the cytotoxicity in 3D co-culture spheroids. However, whether these effects were due to NDRG1 enhancing macrophage-mediated cytotoxicity or due to its ability to reduce oncogenic cross-talk between PDAC cells and fibroblasts and thus reduce cell viability, could not be concluded based on these results.

A.

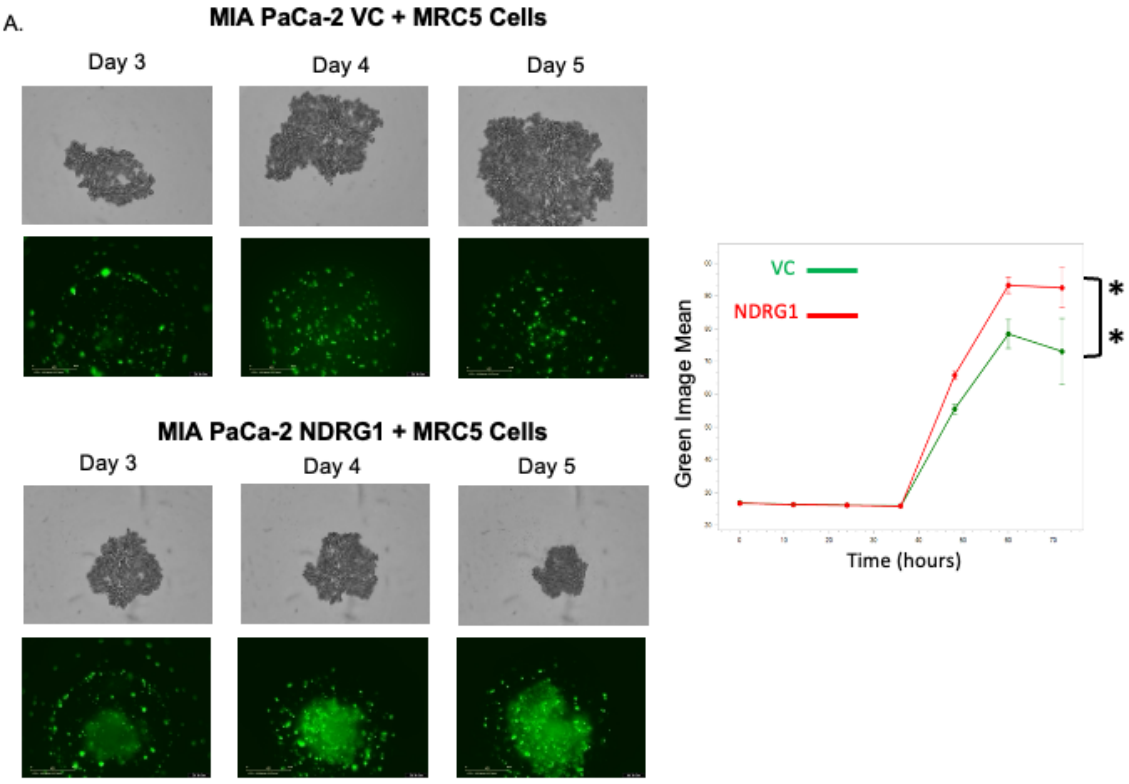
MIA PaCa-2 VC + MRC5 Cells
Day 3
Day 4
Day 5
MIA PaCa-2 NDRG1 + MRC5 Cells
Day 3
Day 4
Day 5
VC
NDRG1
Green Image Mean
Time (hours)
*
*

B.

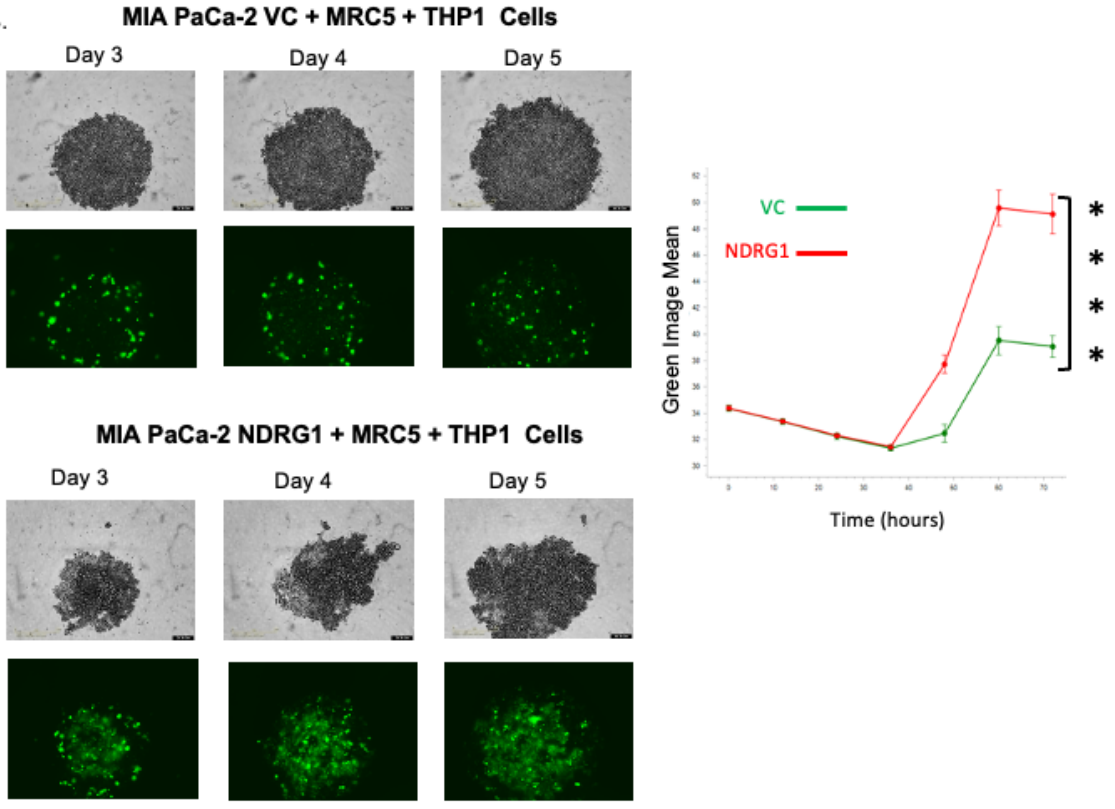
MIA PaCa-2 VC + MRC5 + THP1 Cells
Day 3
Day 4
Day 5
MIA PaCa-2 NDRG1 + MRC5 + THP1 Cells
Day 3
Day 4
Day 5
VC
NDRG1
Green Image Mean
Time (hours)
*
*
*
*

Figure 4.14: NDRG1 increased the cytotoxicity of MIAPaCa-2 co-culture spheroids. MIAPaCa-2 cells (1000 cells) were mixed with MRC-5 fibroblasts (1500 cells) and incubated for 5 days alone (**A**) or with THP-1 monocytes added (**B**). Viability was monitored every 12 h using Cytotox Green Dye and spheroids imaged using the InCucyte SX5 (scale bar = 400 μm). Results are mean ± SD (n = 3). *$p<0.05$, **$p<0.01$ denote statistical significance comparing NDRG1 to the VC control.

4.3.7. NDRG1 expression in PDAC cells impacts the metabolism of exposed macrophages.

Pro-inflammatory M1 macrophages primarily utilize glycolysis and have reduced functionality of the tricarboxylic acid (TCA) cycle and mitochondrial oxidative phosphorylation (OXPHOS) [308, 309]. In contrast, anti-inflammatory M2 macrophages were found to rely more on mitochondrial OXPHOS [309] and have been shown to express high levels of arginase-1 (Arg-1) which promotes cell proliferation and has an anti-inflammatory effect [310]. This was further validated in the current study by comparing the metabolic flux of M0, M1 and M2 polarized U937 macrophages using the Seahorse analyser, which measures the oxygen consumption rate (OCR) and extracellular acidification rate (ECAR) in the overlying media. Indeed, as shown in **Figure 4.15A**, M2 macrophages had significantly higher OCR when compared to M1 macrophages, suggesting their increased rates of OXPHOS. Conversely, M1 macrophages had significantly higher ECAR when compared to M2 macrophages (**Figure 4.15A**), suggesting increased glycolysis, as lactic acid is a major bi-product of glycolysis [308].

We next assessed the metabolism of THP-1 M0 macrophages exposed to PDAC CM. Examining THP1 macrophages exposed to the PANC-1 CM, NDRG1 CM slightly but significantly reduced the OCR, while potently increasing the ECAR of these macrophages when compared to the VC CM (**Figure 4.15B**). Similar results were observed when the THP 1 macrophages were exposed to MIAPaCa-2 NDRG1 CM, with the OCR being significantly reduced, while the ECAR levels were significantly higher compared to the VC CM (**Figure 4.15C**).

We also exposed U937 M0 macrophages to CM derived from PANC-1 (**Figure 4.15D**) or MIAPaCa-2 (**Figure 4.15E**) cells to validate these findings further. Similar results were

obtained, with U937 macrophages exposed to NDRG1 CM again having lower OCR and higher ECAR rates (**Figure 4.15D and E**).

These results are consistent with reduced OXPHOS and increased glycolysis in the macrophages exposed to NDRG1 CM, which resembles the metabolic profile of M1 macrophages (**Figure 4.15A**; [308]).

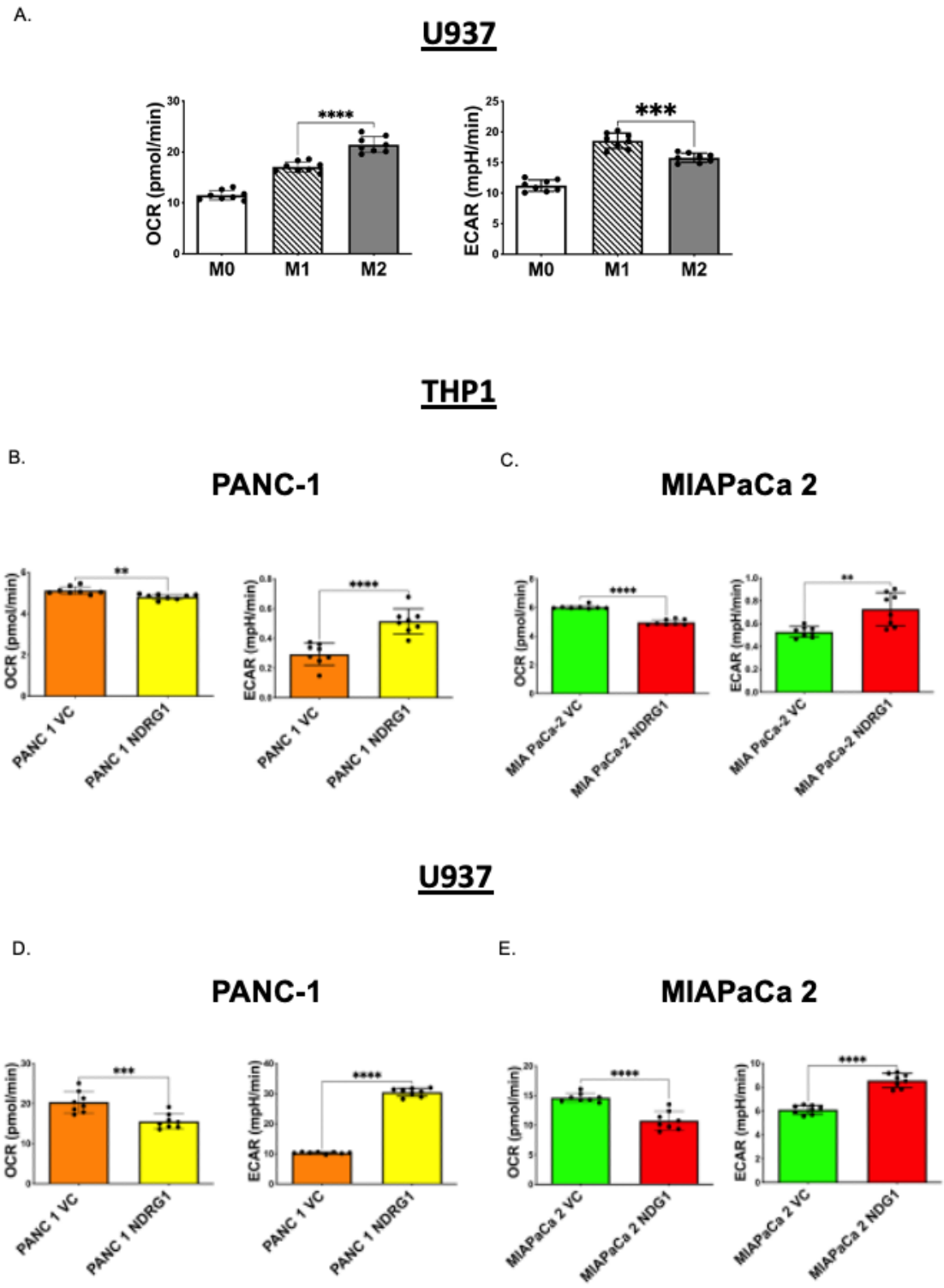

Figure 4.15: NDRG1 increased ECAR and decreased OCR in the macrophages exposed to PDAC CM. (A) The Seahorse analyser was used to measure the oxygen consumption rate (OCR) and extracellular acidification rate (ECAR) in U937 M0, M1 and M2 macrophages. The ECAR and OCR for THP1 macrophages exposed to PANC-1 **(B)** or MIAPaCa-2 (**C**) conditioned medium derived from VC or NDRG1 over-expressing cells. Results are mean ± SD (n = 3). *p<0.05, **p<0.01 ***p<0.001 ****p<0.0001 denote statistical significance comparing NDRG1 to the VC control or M1 to M2, as indicated.

4.3.8. Western blot analysis of metabolic enzymes in exposed macrophages

Following our findings above that NDRG1 in PDAC cells can influence the metabolism of exposed macrophages, we conducted further studies to examine the expression of key metabolic proteins in THP-1 and U937 macrophages exposed to PANC-1 or MIAPaCa-2 CM.

We collected CM from either VC, NDRG1 or ΔCAP-NDRG1 PANC-1 or MIAPaCa-2 cells which were cultured for 24 hours under normoxia or hypoxia. This CM was then incubated with THP-1 and U937 M0 macrophages for 24 hours under normoxia, followed by protein extraction from the macrophages to look for key metabolic enzymes (**Figure 4.16A**). Specifically, we analyzed the expression of metabolic enzymes found to be associated with glycolysis, namely Hexokinase II (HK 2) and glucose transporter 1 (GLUT1), as well as the M2 macrophage marker Arg-1. M1 macrophages were found to have increased expression of glucose transporters (GLUTs) to facilitate the uptake of carbohydrates and perform aerobic glycolysis [309, 311]. The first step in glucose metabolism is regulated by HK 2, which converts glucose to glucose-6-phosphate (G6P) [309, 312]. On the other hand, M2 macrophages can metabolize arginine *via* the expression of Arg-1 [309, 313] and display an increased level of oxidative phosphorylation (OXPHOS), fatty acid synthesis (FAS), and glutamine metabolism [309].

Examining the THP-1 macrophages exposed to PANC-1 CM, our results indicate that the expression of HK 2 in THP-1 cells was significantly increased when these macrophages were exposed to NDRG1 and ΔCAP-NDRG1 CM relative to VC CM from PANC-1 cells cultured under normoxia (**Figure 4.16B**). However, the opposite result was observed using CM from PANC-1 cells cultured under hypoxia with HK 2 levels being slightly reduced by NDRG1 CM, and significantly reduced by ΔCAP-NDRG1 CM when compared to VC CM (**Figure 4.16B**).

GLUT1 levels were also significantly increased in response to NDRG1 and ΔCAP-NDRG1 CM from normoxic PANC-1 cells, while no significant difference was observed when using CM from hypoxic PANC1 cells (**Figure 4.16B**). The M2 marker Arg-1 was significantly decreased by the normoxic CM from NDRG1 and Δ CAP-NDRG1 cells when compared to VC CM. However, the opposite effect was observed when using CM from hypoxic conditions with NDRG1 CM increasing Arg-1 in THP-1 macrophages compared to VC CM (**Figure 4.16B**).

Similar results were also observed when THP-1 macrophages were exposed to MIAPaCa-2 CM, with the glycolysis proteins HK 2 and GLUT1 both being increased by NDRG1 and ΔCAP-NDRG1 CM from normoxic cells, while Arg-1 was reduced under these conditions (**Figure 4.16C**). It is important to mention that VC CM from both PANC-1 and MIAPaCa-2 cells also had a differential effect on the THP-1 macrophages when it was generated under hypoxia *vs.* normoxia. Consistently, the hypoxic VC CM potently increased HK 2 and GLUT1, while reducing Arg-1 in these cells. These findings were further validated in the U937 M0 macrophages exposed to CM derived from both PANC-1 and MIAPaCa-2 cells. As found with the THP-1 cells, NDRG1 and ΔCAP-NDRG1 CM generated under normoxia increased HK 2 and GLUT1, while reducing Arg-1, whereas the opposite effect was observed for HK 2 and Arg-1 using CM generated under hypoxia (**Figure 4.16D and E**).

These results suggest that NDRG1 expression in PDAC cells significantly alters key metabolic pathways in macrophages, leading to a metabolic profile that is more typical of M1 macrophages under normoxia, supporting our earlier evidence that NDRG1 promotes the polarization of macrophages into the M1 phenotype. Unexpectedly, this effect appears to have been somewhat reversed under hypoxic conditions, where a more M2-like phenotype may be promoted by the NDRG1-expressing PDAC cells.

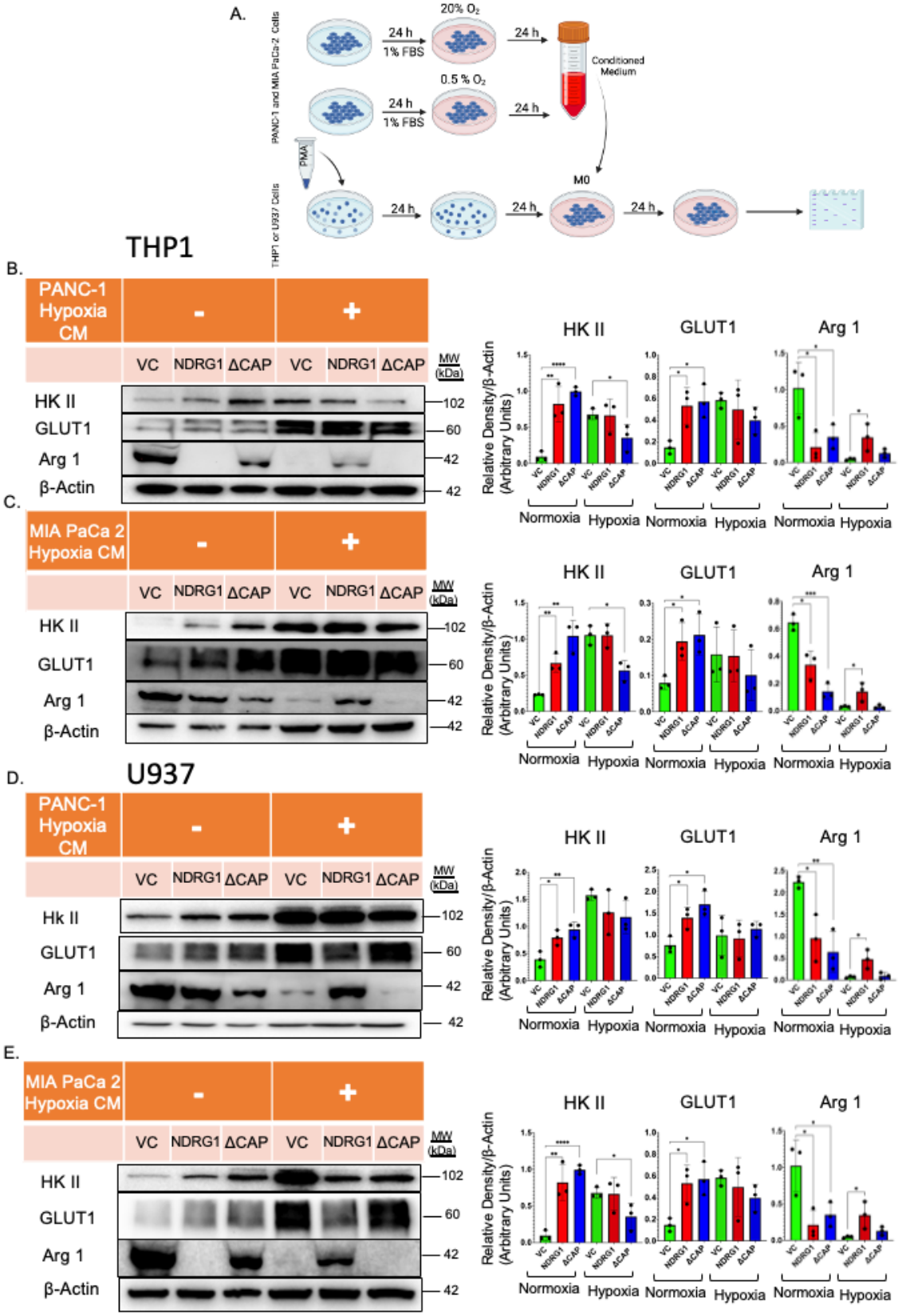
A.
PANC-1 and MIA PaCa-2 Cells
THP1 or U937 Cells
24 h
1% FBS
20% O2
0.5 % O2
24 h
Conditioned Medium
PMA
M0
THP1
B.
PANC-1 Hypoxia CM
C.
MIA PaCa 2 Hypoxia CM
D.
U937
E.
MIA PaCa 2 Hypoxia CM
VC
NDRG1
ΔCAP
MW (kDa)
HK II
GLUT1
Arg 1
β-Actin
102
60
42
Relative Density/β-Actin (Arbitrary Units)
Normoxia
Hypoxia

Figure 4.16: NDRG1 impacts the metabolism of macrophages exposed to PDAC conditioned media. (A) Schematic diagram of the experimental procedure to collect PDAC conditioned medium (CM), which was collected after 24 hours of incubation in normoxia or hypoxia and added to macrophages for 24 hours. Western blot analysis of HK II, GLUT1 and Arg1 in THP-1 cells exposed to either PANC-1 (**B**) or MIAPaCa-2 (**C**) CM derived from VC, NDRG1 or ΔCAP-NDRG1 (ΔCAP) under normoxia or hypoxia. Western blot analysis of HK II, GLUT1 and Arg1 in U937 cells exposed to either PANC-1 (**D**) or MIAPaCa-2 (**E**) CM derived from VC, NDRG1 or ΔCAP-NDRG1 (ΔCAP) under normoxia or hypoxia. Results are mean ± SD (n = 3). *p<0.05, **p<0.01 ***p<0.001 ****p<0.0001 denote statistical significance comparing each condition to the relevant VC control.

4.3.9. NDRG1 expression in PDAC cells influences macrophage metabolism.

To further explore the metabolism of macrophages exposed to PDAC, we conducted a Mitoplate S-1 assay, which measures mitochondrial function by quantifying the rates of electron flow through the electron transport chain following exposure to different metabolic substrates. U937 cells were differentiated into M0 macrophages as described above **(*Section 4.2.5*)**. The cells were then exposed to CM from either VC or NDRG1-expressing PANC-1 cells for 72 hours, followed by seeding into the MitoPlate S-1 and incubation of 6 hours at 37°C. Substrate metabolism was assessed by monitoring a colorimetric change, and the optical density was recorded at 590 nm at an interval of 30 minutes for 12 cycles using a kinetic plate reader (**Figure 4.17A**).

The results indicated that pre-incubation with PANC1 NDRG1 CM increased the macrophage metabolism of α-D-Glucose, D-Glucose-6-PO4 and cis-aconitic acid (**Figure 4.17B, C and D**). In contrast, pre-incubation with PANC1 NDRG1 CM reduced the ability of macrophages to metabolise L-glutamic acid, L-glutamine and L-ornithine (**Figure 4.17E, F and G**). This assay also demonstrated that PANC1 NDRG1 CM decreased the metabolism of TCA cycle metabolism substrates such as Citric Acid, D, L-Isocitric Acid and D, L-β-Hydroxy-Butyric acid (**Figure 4.17H**).

Further, macrophages pre-exposed to VC CM were found to metabolise L-Lactic acid more over time than those pre-exposed to NDRG1 CM, suggesting their increased activity of the TCA cycle (OXPHOS), which is consistent with an M2-like phenotype (**Figure 4.17H**). Overall, the results in Figures 4.15, 4.16 and 4.17 demonstrate that NDRG1 expression in PDAC cancer cells can significantly alter the metabolism of exposed macrophages, leading to an M1-like metabolic state under normoxic conditions.

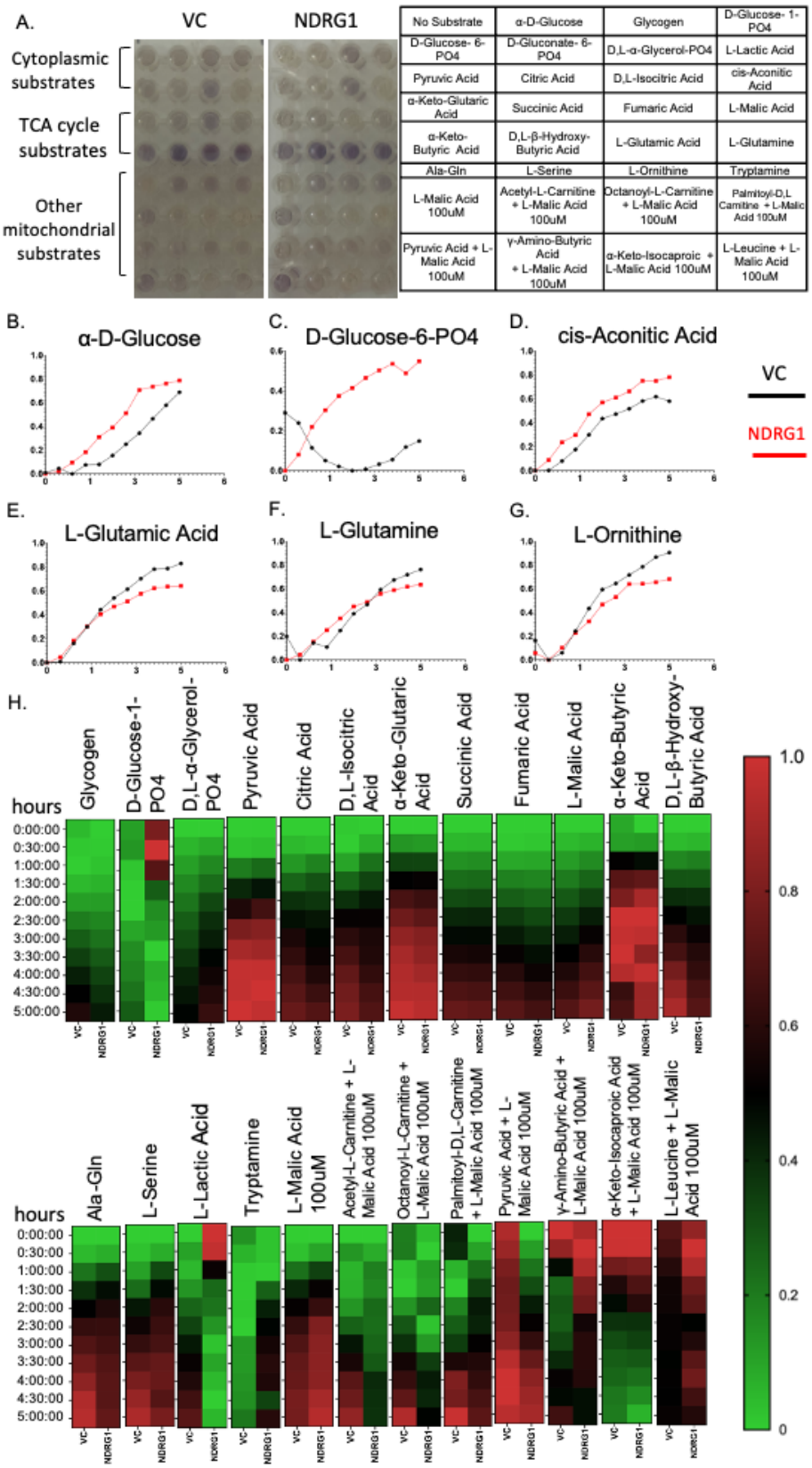
A.
VC
NDRG1
Cytoplasmic substrates
TCA cycle substrates
Other mitochondrial substrates
No Substrate
α-D-Glucose
Glycogen
D-Glucose- 1-PO4
D-Glucose- 6-PO4
D-Gluconate- 6-PO4
D,L-α-Glycerol-PO4
L-Lactic Acid
Pyruvic Acid
Citric Acid
D,L-Isocitric Acid
cis-Aconitic Acid
α-Keto-Glutaric Acid
Succinic Acid
Fumaric Acid
L-Malic Acid
α-Keto-Butyric Acid
D,L-β-Hydroxy-Butyric Acid
L-Glutamic Acid
L-Glutamine
Ala-Gln
L-Serine
L-Ornithine
Tryptamine
L-Malic Acid 100uM
Acetyl-L-Carnitine + L-Malic Acid 100uM
Octanoyl-L-Carnitine + L-Malic Acid 100uM
Palmitoyl-D,L Carnitine + L-Malic Acid 100uM
Pyruvic Acid + L-Malic Acid 100uM
γ-Amino-Butyric Acid + L-Malic Acid 100uM
α-Keto-Isocaproic + L-Malic Acid 100uM
L-Leucine + L-Malic Acid 100uM
B.
α-D-Glucose
C.
D-Glucose-6-PO4
D.
cis-Aconitic Acid
VC
NDRG1
E.
L-Glutamic Acid
F.
L-Glutamine
G.
L-Ornithine
H.
hours
Glycogen
D-Glucose-1-PO4
D,L-α-Glycerol-PO4
Pyruvic Acid
Citric Acid
D,L-Isocitric Acid
α-Keto-Glutaric Acid
Succinic Acid
Fumaric Acid
L-Malic Acid
α-Keto-Butyric Acid
D,L-β-Hydroxy-Butyric Acid
0:00:00
0:30:00
1:00:00
1:30:00
2:00:00
2:30:00
3:00:00
3:30:00
4:00:00
4:30:00
5:00:00
VC
NDRG1
hours
Ala-Gln
L-Serine
L-Lactic Acid
Tryptamine
L-Malic Acid 100uM
Acetyl-L-Carnitine + L-Malic Acid 100uM
Octanoyl-L-Carnitine + L-Malic Acid 100uM
Palmitoyl-D,L-Carnitine + L-Malic Acid 100uM
Pyruvic Acid + L-Malic Acid 100uM
γ-Amino-Butyric Acid + L-Malic Acid 100uM
α-Keto-Isocaproic Acid + L-Malic Acid 100uM
L-Leucine + L-Malic Acid 100uM
1.0
0.8
0.6
0.4
0.2
0

Figure 4.17: NDRG1 influences the mitochondrial metabolism of exposed U937 macrophages to PDAC CM. U937 macrophage were incubated with PANC-1 CM for 72h and then seeded into Mitoplate S-1 to be assessed by monitoring a colorimetric change at 590 nm at an interval of 30 minutes for 10 cycles using a kinetic plate reader. **(A)** Image of the plate layout after dye reduction, indicated by the purple colour formation in U937 macrophage cells. Kinetic graphs of D-Glucose **(B)**, D-Glucose-6-PO4 **(C)**, cis-Aconitic Acid **(D)**, L-Glutamic Acid **(E)**, L-Glutamine **(F)**, and L-Ornithine **(G)** comparing U937 macrophages exposed to VC or NDRG1 CM for 72 h prior to assay. **(H)** Heat maps for all remaining Mitoplate S-1 substrates comparing the U937 macrophages exposed to VC to NDRG1 CM. The substrates were normalized to the no-substrate control or L-malic acid 100uM. The data presented is a representative analysis of the average of three independent experiments.

4.3.10. Profile of extracellular vesicles (EVs) secretion from MIA PaCa-2 cells.

As demonstrated in the studies above, NDRG1 expression in PDAC cells has profound impacts on macrophages that are exposed to the CM of these cells. To further understand the mechanisms by which this is occurring, we investigated the secretome of PDAC cells and how this is altered in response to NDRG1 over-expression. It is important to note that the secretome of cancer cells contains numerous cytokines and chemokines as well as extracellular vesicles (EVs) which can transport a plethora of proteins, mRNAs and metabolites to neighbouring TME cells.

Recent studies have found that EVs in particular have the ability to control macrophage polarization through intercellular signal transduction, ultimately impacting disease progression [314]. EVs that are derived from PDAC and enriched in ICAM-1 and arachidonic acid (AA) can stimulate macrophages to transform into an M2 phenotype, leading to the secretion of pro-tumorigenic factors like VEGF, MCP-1, IL-1β, and MMP-9 [315].

Hence, we first characterized the small EVs (also known as exosomes) being secreted by MIAPaCa-2 VC and NDRG1 over-expressing cells. Conditioned medium was collected from these cells and consequent centrifugation steps were applied to isolate out the oncosomes, large EVs and finally the small EVs (**Figure 4.18A**). Proteomic analysis was then performed on the small EVs to assess whether NDRG1 expression in the MIAPaCa-2 cells influenced small EV cargo.

The analysis of Gene Ontology (GO) **(Table 4.2)** revealed that the expression of NDRG1 impacted the expression of exosome proteins involved in various biological processes (BP) related to the immune TME, including response to interleukin-7, response to oxidative stress, macroautophagy, intrinsic apoptotic signaling pathway, cellular response to type II interferon, cell redox homeostasis, response to reactive oxygen species, complement activation, activation of immune response, leukocyte migration, regulation of innate immune response, leukocyte-mediated immunity, lymphocyte-mediated immunity, and leukocyte-mediated cytotoxicity (**Figure 4.18B**).

Table 4.2. The analysis of Gene Ontology (GO)

Category	ID	Description	q value	geneID
GO BP	GO:0098760	response to interleukin-7	9.05E-09	PDIA3/HSPD1/ATP5F1B/RAD23B/STIP1/P4HB/CRKL/HDGF/GIPC1/YBX1/ATIC
GO BP	GO:0098761	cellular response to interleukin-7	9.05E-09	PDIA3/HSPD1/ATP5F1B/RAD23B/STIP1/P4HB/CRKL/HDGF/GIPC1/YBX1/ATIC
GO BP	GO:0006979	response to oxidative stress	2.32E-07	BANF1/APP/RACK1/PARK7/TRAP1/ADAM9/MACROH2A1/UBQLN1/PARP1/PRDX5/PRDX4/GSS/DHCR24/CYB5B/EIF2S1/STK26/RPS3/PCNA/ANXA1/HSPB1/PRKCD/APOE/PRDX6/PPIA/HBB/SOD1/CAT/IDH1/CRK/PSMB5/CDK1/EGFR/G6PD/TP53/PRDX3/PRNP/SFPQ/NONO/NQO1/HBA2/STAT1/P4HB/PRDX2/LONP1/OXSR1/GSR/S100A7/STAU1/PRDX1/TXN/CAPN2/MAPK1/COL1A1/VNN1/SRC/ARG1/HP/ATP2A2/GSTP1/DHFR/KRT1/STX4
GO BP	GO:0016236	macroautophagy	4.17E-07	SPTLC1/GAA/VTA1/VCP/CHMP1A/CHMP5/STX12/VPS4B/HGS/UBQLN1/CHMP2A/VPS4A/ARL8B/ATP6V0D1/LAMP2/CHMP4B/SQSTM1/QSOX1/SLC25A5/RALB/CALR/ATP6V1G1/VPS28/RAB23/SNX5/PHB2/RAB1B/VPS37B/LGALS8/TSG101/TP53/NSFL1C/GAPDH/CTSD/RAB7A/ATP6V1B2/CHMP1B/CAPN1/MVB12A/RAB1A/CDC37/ATP6V1E1/PAFAH1B2/VPS35/RHEB/GNAI3/VPS26A/SRC/ATP2A2/ATP6V1A
GO BP	GO:0097193	intrinsic apoptotic signaling pathway	1.79E-06	TNFRSF10B/DNAJA1/CAV1/RACK1/PARK7/TRAP1/DNM1L/HINT1/CLU/UBQLN1/EPHA2/DDX5/PARP1/VDAC2/RPL11/PTTG1IP/DDX3X/CYCS/RPS3/S100A8/HSPB1/HRAS/PRKCD/CCAR2/PPIA/RPS7/SOD1/TPT1/PRKDC/RPL26/ERP29/MIF/HNRNPK/HYOU1/TP53/SFPQ/NONO/ENO1/CD44/P4HB/BAG6/TMEM109/S100A9/HDAC1/VNN1/SRC
GO BP	GO:0071346	cellular response to type II interferon	8.07E-06	MYO1C/VIM/EPRS1/FLNB/VAMP3/SYNCRIP/ZYX/JAK1/RPL13A/STXBP1/TP53/GAPDH/GSN/ACTR3/STAT1/CDC37/CDC42/HPX/STXBP3/ACTR2/KIF5B/ASS1/ARG1/STX4
GO BP	GO:0045454	cell redox homeostasis	1.58E-05	PRDX5/PRDX4/GLRX3/TXNRD1/PRDX6/BOLA2B/PRDX3/ERP44/NQO1/PRDX2/GSR/PRDX1/TXN

GO BP	GO:0000302	response to reactive oxygen species	2.44E-05	RACK1/PARK7/TRAP1/ADAM9/PRDX5/STK26/RPS3/PCNA/ANXA1/PRKCD/APOE/HBB/SOD1/CAT/CRK/CDK1/EGFR/PRDX3/NQO1/HBA2/STAT1/PRDX2/S100A7/PRDX1/TXN/CAPN2/MAPK1/COL1A1/SRC/ARG1/HP/GSTP1/DHFR
GO BP	GO:2001234	negative regulation of apoptotic signaling pathway	0.00011811	DNAJA1/PARK7/TRAP1/CLU/CSNK2A1/ITGA6/VDAC2/PSME3/PTTG1IP/DDX3X/HSPB1/CCAR2/GNAI2/SLC25A5/PPIA/TPT1/MIF/HYOU1/SLC25A6/CSNK2A2/NONO/LMNA/THBS1/ENO1/CD44/LGALS3/PRDX2/ITGAV/HDAC1/PSMD10/GNAI3/SRC/SERPINE1/GSTP1
GO BP	GO:0034341	response to type II interferon	0.00013799	MYO1C/VIM/EPRS1/FLNB/VAMP3/SYNCRIP/ZYX/JAK1/RPL13A/STXBP1/TP53/GAPDH/GSN/ACTR3/STAT1/CDC37/CDC42/HPX/STXBP3/ACTR2/KIF5B/ASS1/ARG1/STX4
GO BP	GO:0006956	complement activation	0.00018757	CD46/CLU/CD59/C1QBP/A2M/FCN2/C9/C7/C5/CFI/CFB/C3/C4A/KRT1
GO BP	GO:0008631	intrinsic apoptotic signaling pathway in response to oxidative stress	0.00024074	PARK7/TRAP1/UBQLN1/PARP1/HSPB1/PRKCD/PPIA/SOD1/SFPQ/NONO/P4HB/VNN1
GO BP	GO:0002253	activation of immune response	0.00025633	EZR/CD46/PAK2/SLC39A10/CAV1/ITCH/CD81/NECTIN2/LYN/HSP90AA1/CLU/UBQLN1/CD59/WNK1/C1QBP/A2M/GRB2/XRCC6/HSPD1/DDX3X/RPS3/IGHA1/XRCC5/HRAS/PRKCD/HLA-A/PHB2/PRKDC/FCN2/PRNP/SFPQ/NONO/YES1/KHDRBS1/LGALS3/ZDHHC5/C9/IGHG1/CRKL/BAG6/MATR3/HMGB1/UFD1/C7/C5/RTN4/CFI/LTF/MAPK1/BTN2A1/CFB/SRC/C3/UBE2N/FLOT1/C4A/KRT1
GO BP	GO:0006959	humoral immune response	0.00040142	CD46/NOTCH1/NOTCH2/CD81/CLU/CD59/C1QBP/A2M/KRT6A/IGHA1/HLA-A/LYZ/FCN2/F2/PRSS3/RPS19/JCHAIN/GAPDH/DMBT1/C9/GPI/S100A9/C7/C5/S100A7/HPX/RPL30/CFI/TF/LTF/CFB/C3/C4A/KRT1
GO BP	GO:0050900	leukocyte migration	0.00084681	MSN/JAM3/APP/CD81/RAC2/DNM1L/LYN/PLEC/ADAM10/ITGA6/MYH9/ITGA3/WNK1/C1QBP/WDR1/BSG/ANXA1/S100A8/PPIA/RAC1/CALR/RHOA/CRK/MIF/RPL13A/THBS4/RPS19/THBS1/YES1/ITGB1/LGALS3/CRKL/HMGB1/PAFAH1B1/PPIB/OXSR1/S100A9/CDC42/AIMP1/C5/S100A7/CD9/MAPK1/SRC/SERPINE1/CD99

GO BP	GO:0045088	regulation of innate immune response	0.00097306	PAK2/BANF1/CAV1/ITCH/NECTIN2/LYN/HSP90AA1/UBQLN1/C1QBP/PARP1/LAMP1/A2M/XRCC6/HSPD1/DDX3X/PVR/CASP8/XRCC5/APOE/HLA-B/HLA-A/PHB2/GRN/PRKDC/CRK/FCN2/DHX9/RPS19/SFPQ/NONO/ZDHHC5/SERPINB9/CDC37/MATR3/HMGB1/UFD1/HPX/RTN4/LTF/PTPN11/SRC/ARG1/TTLL12/FLOT1
GO BP	GO:0002455	humoral immune response mediated by circulating immunoglobulin	0.00119227	CD46/CD81/CLU/C1QBP/C9/C7/C5/HPX/CFI/C3/C4A
GO BP	GO:0006958	complement activation, classical pathway	0.00154348	CD46/CLU/C1QBP/C9/C7/C5/CFI/C3/C4A
GO BP	GO:0002443	leukocyte mediated immunity	0.0022096	CD46/NDFIP1/TFRC/CD81/RAC2/NECTIN2/DDX21/LYN/CLU/C1QBP/LAMP1/ARL8B/HSPD1/WDR1/PVR/HLA-C/PRKCD/HLA-B/HLA-A/CYRIB/CRK/F2/TUBB4B/STXBP1/TUBB/C9/IGHG1/SNAP23/SERPINB9/HMGB1/HPRT1/C7/C5/HPX/STXBP3/PRDX1/CFI/KIF5B/B2M/DDX1/ARG1/C3/C4A/STX4/CTSC
GO BP	GO:0002449	lymphocyte mediated immunity	0.00438676	CD46/NDFIP1/TFRC/CD81/NECTIN2/CLU/C1QBP/LAMP1/ARL8B/HSPD1/PVR/HLA-C/PRKCD/HLA-B/HLA-A/CYRIB/CRK/TUBB4B/TUBB/C9/IGHG1/SERPINB9/HMGB1/HPRT1/C7/C5/HPX/PRDX1/CFI/KIF5B/B2M/ARG1/C3/C4A/CTSC
GO BP	GO:0001909	leukocyte mediated cytotoxicity	0.00473302	NECTIN2/LAMP1/ARL8B/PVR/HLA-C/HLA-B/HLA-A/CYRIB/CRK/F2/TUBB4B/TUBB/IGHG1/SERPINB9/HPRT1/PRDX1/KIF5B/B2M/ARG1/CTSC
GO CC	GO:0001772	immunological synapse	0.00194901	EZR/CD81/ARHGDIA/MYH9/PRKAR1A/NPTN/PDCD6IP/LGALS3/SCRIB
GO MF	GO:0023026	MHC class II protein complex binding	0.00208679	CD81/ANXA11/HSP90AA1/PKM/HSPA8/YWHAE/B2M/HSP90AB1
GO MF	GO:0023023	MHC protein complex binding	0.00322052	CD81/ANXA11/HSP90AA1/PKM/HSPA8/CYRIB/YWHAE/B2M/HSP90AB1

Regarding the GO cellular components (CC), NDRG1 was found to affect the expression of exosome proteins associated with the immunological synapse. This is an area of contact between lymphocytes and their target cells, which facilitates lymphocyte activation [316]. Examining the molecular function (MF) by GO, which analyses the biochemical activity of gene products [317], exosomes derived from NDRG1 expressing cells were found to contain proteins associated with MHC class II protein complex binding (**Figure 4.18B**).

These results demonstrate that NDRG1 expression in PDAC cells can influence their exosome cargo to potentially impact the function of immune cells in the PDAC TME. Notably, these results hint at NDRG1 potentially affecting a wide spectrum of immune cells in the PDAC TME, including lymphocytes.

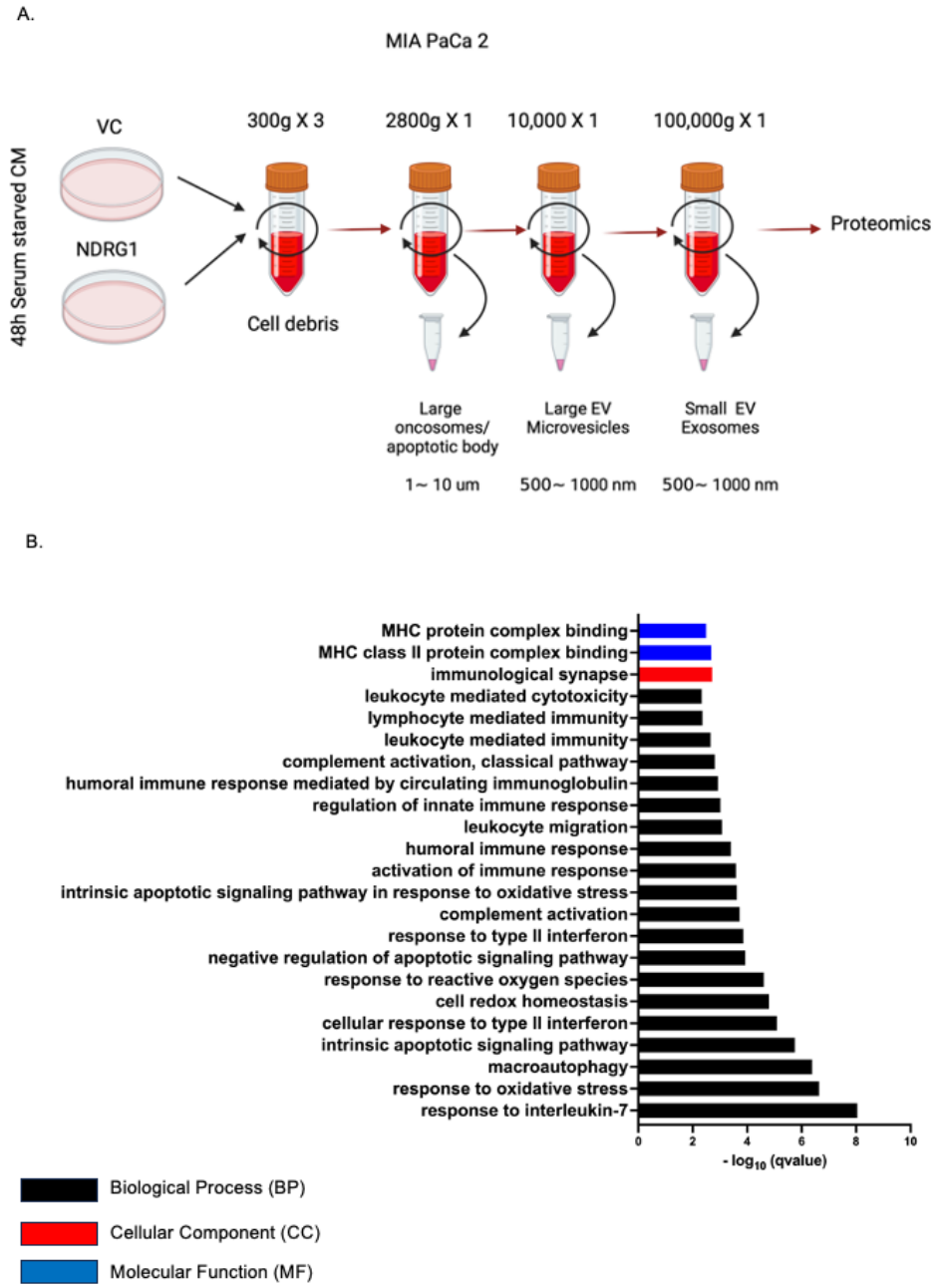

Figure 4.18: NDRG1 expression influences the protein cargo of small extracellular vesicles secreted from MIAPaCa-2 cells. (A) Schematic diagram of the isolation procedure to enrich for small extracellular vesicles (EVs) from MIAPaCa-2 conditioned medium. **(B)** Gene Ontology (GO) term enrichment analysis performed following an unbiased proteomic analysis of the small EC's collected from VC and NDRG1 expressing MIAPaCa-2 cells. The GO terms that were significantly enriched were selected based on a q value less than < 0.05. GO terms include the categories of Biological Processes (Black), Cellular Components (Red), and Molecular Functions (Blue).

4.3.11. Profile of cytokine secretion from MIAPaCa-2 cells.

Considering our focus on how NDRG1 expression in PDAC cells influences macrophage polarization, metabolism and function, we sought to directly investigate the cytokines involved in this cross-talk by performing a cytokine/chemokine array on the CM of MIAPaCa-2 VC and NDRG1 cells.

Hypoxia also plays a crucial role in the immune microenvironment of PDAC and is involved in its pathogenesis [318]. To determine the mechanism by which NDRG1 influenced macrophage polarization, we examined the cytokines secreted by the MIAPaCa-2 VC and NDRG1 cells under both normoxic and hypoxic conditions **(Figure 4.19)**. This was particularly pertinent considering the contrasting effects that hypoxic CM had on macrophage metabolism proteins HK 2, GLUT-1 and Arg-1 when compared to normoxic CM (as shown in ***Figure 4.16***). The MIAPaCa-2 VC and NDRG1 cells were incubated under normoxia (1% FBS and 20% O2) or hypoxia (1% FBS and 0.5% O_2) for 24 hours followed by collection of their CM. A human cytokine antibody array was then used to assess the expression of 80 human cytokines in the CM generated from the VC and NDRG1 cells (**Figure 4.19A-D**).

Densitometric analysis of the cytokine array dot blots revealed that under normoxia, the over-expression of NDRG1 in MIAPaCa-2 cells decreased the production of IFN-γ, MCP-1, FGF-9, IL-16, and IP-10 while increasing the production of TNF-α, IGF-I, Angiogenin, BDNF, MIF, TGFβ-3, TIMP-1, and TIMP-2 when compared to VC cells **(Figure 4.19E)**.

When comparing the MIAPaCa-2 VC cells exposed to hypoxia to their normoxia counterparts, we observed a general increase in most of the cytokines examined, with a very marked increase in the secretion of IL-8, IL-10, MCSF, MIP-1b, RANTES, TNF-α, EGF, IGF-1, Angiogenin,

Eotaxin, MIF, TGF-β3, TIMP-1 and TIMP-2 (**Figure 4.19E**). Notably, the over-expression of NDRG1 in these cells potently inhibited the hypoxia-induced levels of IL-8, IL-10, RANTES, TNF-α, EGF and Eotaxin **(Figure 4.19E)**, suggesting that NDRG1 influences how MIAPaCa-2 cells respond to hypoxia.

A.

MIAPaCa 2 VC (Normoxia) CM

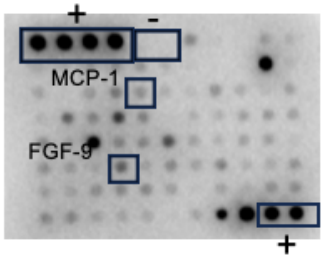

B.

MIAPaCa 2 NDRG1 (Normoxia) CM

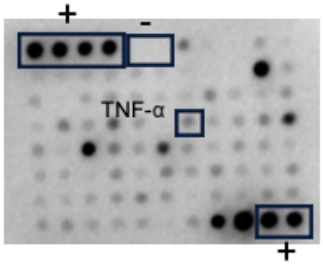

	A	B	C	D	E	F	G	H	I	J	K
1	Pos	Pos	Pos	Pos	Neg	Neg	ENA-78	GCSF	GM-CSF	GRO	GRO-α
2	I-309	IL-1α	IL-1β	IL-2	IL-3	IL-4	IL-5	IL-6	IL-7	IL-8	IL-10
3	IL-12 p40/p70	IL-13	IL-15	IFN-γ	MCP-1	MCP-2	MCP-3	MCSF	MDC	MIG	MIP-1b
4	MIP-1δ	RANTES	SCF	SDF-1	TARC	TGF-β1	TNF-α	TNF-β	EGF	IGF-I	Angiogenin
5	Oncostatin M	Thrombopoietin	VEGF	PDGF-BB	Leptin	BDNF	BLC	Ck β 8-1	Eotaxin	Eotaxin-2	Eotaxin-3
6	FGF-4	FGF-6	FGF-7	FGF-9	Flt-3 Ligand	Fractalkine	GCP-2	GDNF	HGF	IGFBP-1	IGFBP-2
7	IGFBP-3	IGFBP-4	IL-16	IP-10	LIF	LIGHT	MCP-4	MIF	MIP-3α	NAP-2	NT-3
8	NT-4	Osteopontin	Osteoprotegerin	PARC	PIGF	TGF-β2	TGF-β3	TIMP-1	TIMP-2	Pos	Pos

C.

MIAPaCa 2 VC (Hypoxia) CM

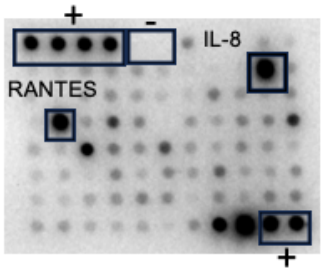

D.

MIAPaCa 2 NDRG1 (Hypoxia) CM

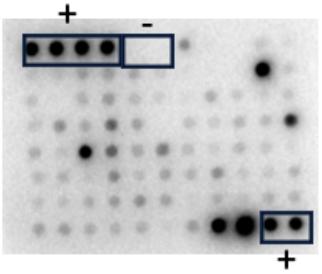

E.

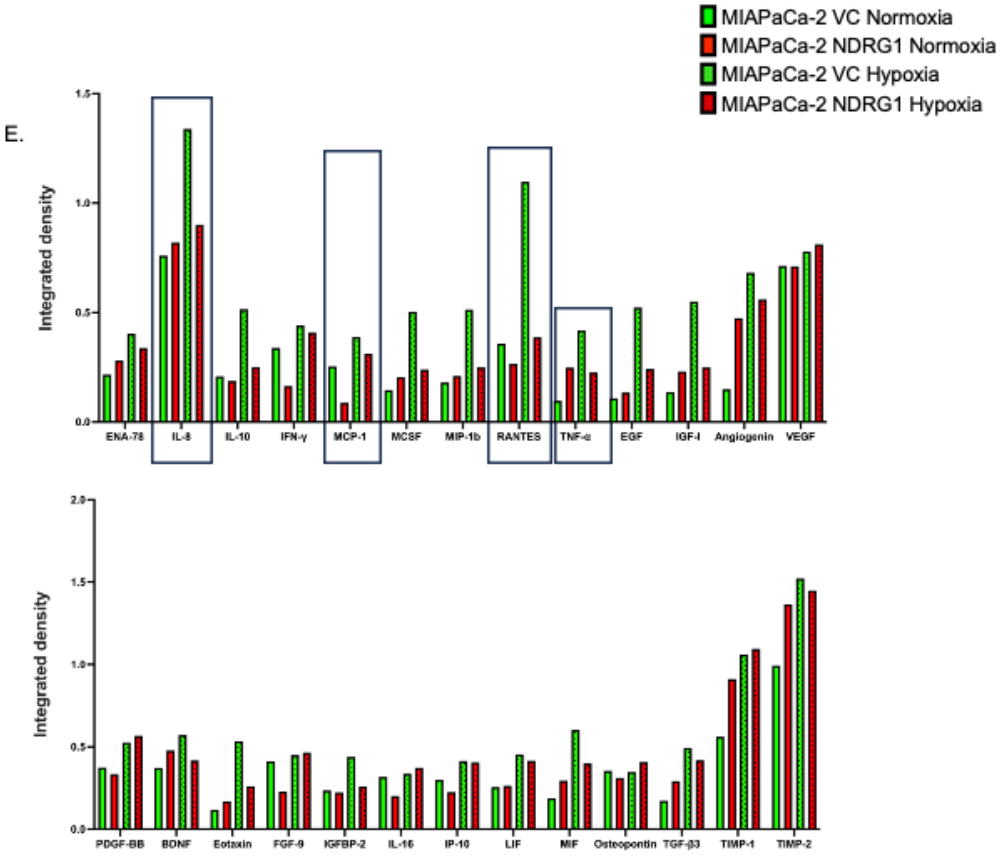

Figure 4.19: NDRG1 expression in MIAPaCa-2 cells influences the secretion of numerous chemokines and cytokines under normoxic and hypoxic conditions.
MIAPaCa-2 VC (**A, C**) and NDRG1 (**B, D**) cells were incubated in either normoxia (**A, B**) or hypoxia (**C, D**) for 24 h, and then the overlaying media was incubated with human cytokine antibody array Dot Blot membranes (Abcam). **(A)** The cytokines/chemokines and their position on the dot blot membrane are shown on the right. The membranes were analysed and quantified *via* the Fiji-ImageJ software and densitometric analysis was performed (n=1) (**E**).

To further validate these findings, we performed ELISA assays to confirm the effect of NDRG1 expression on the secretion of TNF-α, MCP-1, RANTES and IL-8 cytokines, as these cytokines were found to have the most robust differences between the VC and NDRG1 cells and are also known for their effects on the immune TME.

Studies have shown that TNF-α triggers macrophages to differentiate into the M1 phenotype and infiltrate the necrotic zone [319]. In agreement with the cytokine array, we also observed a significant rise in the level of TNF-α in the cell culture supernatants of PANC-1 NDRG1 compared to PANC-1 VC under normoxia (**Figure 4.20A**). Notably, under hypoxia this effect was lost, with no significant difference between NDRG1 and VC (**Figure 4.20A**). Similar results were obtained in MIAPaCa-2 cells, where TNF-α was slightly but significantly elevated in normoxic cells over-expressing NDRG1 compared to VC (**Figure 4.20B**).

Elevated expression levels of MCP-1 has been shown to drive the polarization of M0 macrophages towards an M2-like phenotype [320]. Examining the effect of NDRG1 on MCP-1 secretion by the PANC-1 cells, our results demonstrate that the level of MCP-1 was significantly lower in PANC1 NDRG1 when compared to PANC1 VC (**Figure 4.20C**). This effect was consistent under both normoxia and hypoxia (**Figure 4.20C**). Similarly, NDRG1 over-expression also decreased the level of MCP-1 in MIAPaCa-2 cells when compared to the VC, although this effect was only significant under normoxia (**Figure 4.20D**).

Several studies indicated that RANTES (also known as CCL5) polarizes macrophages toward an M2-like phenotype [321, 322]. As shown in our cytokine array, the levels of RANTES were potently elevated in the VC cell culture supernatants exposed to hypoxia when compared to VC cells under normoxia (**Figure 4.20E**). Notably, while NDRG1 increased RANTES

secretion under normoxia in the PANC-1 cells, it was able to significantly reduce the secretion of this cytokine under hypoxia when compared to VC, essentially inhibiting the hypoxia-induced increase in RANTES (**Figure 4.20E**). Similarly, increased levels of RANTES were also observed in the cell culture supernatants of MIAPaCa-2 VC cells under hypoxia when compared to VC cells under normoxia, with NDRG1 over-expression significantly reducing the levels of this cytokine under both conditions (**Figure 4.20F**).

IL-8 is another cytokine that has been shown to promote the M2 polarization of TAMs [323]. As found in our cytokine array, we observed a significant increase in the levels of IL-8 in the cell culture supernatants of PANC 1 VC cultured under hypoxia when compared to these cells under normoxia (**Figure 4.20G**). While NDRG1 did not affect the secretion of IL-8 under normoxia, it significantly reduced IL-8 secretion under hypoxia when compared to the VC (**Figure 4.20G**). We also observed a slight but significant increase in the levels of IL-8 in cell culture supernatants of MIAPaCa-2 VC cells under hypoxia when compared to these cells under normoxia, with NDRG1 expression significantly reducing IL-8 secretion under both conditions (**Figure 4.20H**).

These results demonstrate that NDRG1 affects the secretion of key cytokines that influence the tumour microenvironment and macrophage polarization. This may explain the ability of PDAC cells expressing NDRG1 to alter the polarization of neighbouring macrophages. It is also important to note that NDRG1 altered the response of both PANC-1 and MIAPaCa-2 cells to hypoxia, reducing the hypoxia-mediated increase in cytokines such as RANTES and IL-8.

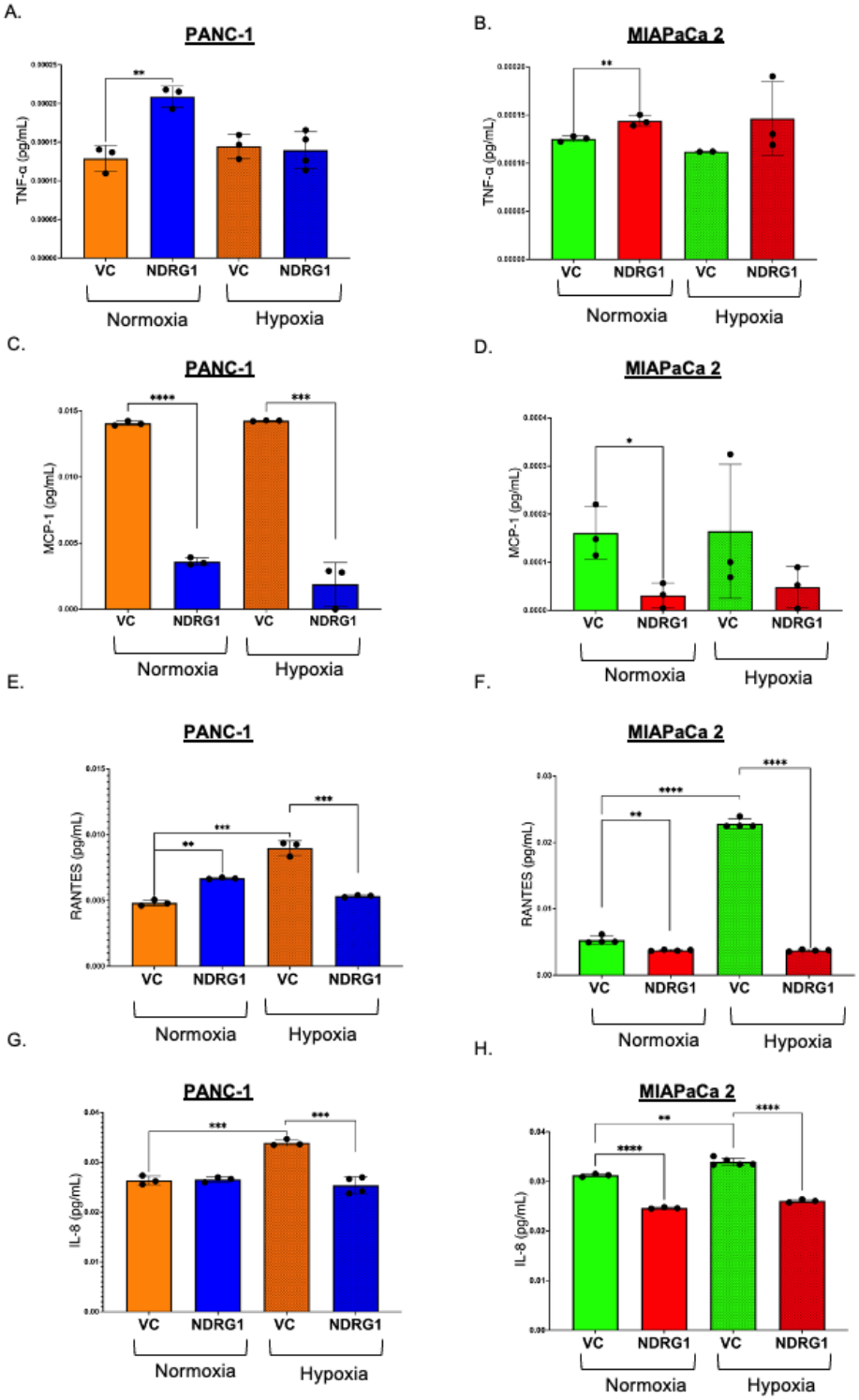

Figure 4.20: ELISA assays reveal that NDRG1 affects the secretion of TNF-α, MCP-1, RANTES and IL-8 by PDAC cells. The overlaying media from PANC-1 and MIAPaCa-2 cells was collected after a 24 h incubation under normoxic or hypoxic conditions commercial ELISA kits for TNF-α (**A, B**), MCP-1 (**C, D**), RANTES (**E, F**) and IL-8 (**G, H**). Results are mean ± SD (n = 3). *p<0.05, **p<0.01 ***p<0.001 ****p<0.0001 denote statistical significance comparing NDRG1 to the VC control, or normoxia to hypoxia, as indicated.

4.3.12. NDRG1 expression in PDAC cells altered the NF-κB pathway of exposed macrophages.

Considering that our cytokine and ELISA assays above demonstrate that NDRG1 expression in PDAC cells can significantly increase the secretion of TNF-α, we conducted further studies to assess the effect of NDRG1 on a key target of TNF-α signalling in macrophages, namely the NF-κB pathway. Activation of the NF-κB pathway by TNF-α positively regulates M1 polarization and promotes M1-mediated production of pro-inflammatory cytokines such as IL-12 [324]. To investigate the effect of PDAC NDRG1 on the NF-κB pathway in exposed macrophages, we conducted an experiment where THP-1 and U937 M0 macrophage cells were exposed to VC, NDRG1 or ΔCAP-NDRG1 CM from either PANC-1 or MIAPaCa-2 cells for 72 hours. We then analyzed the expression of IκBα, p-NF-κB p65 (Ser536) and total NF-κB p65 using Western Blot.

Examining the effect of PANC-1 CM on the THP-1 cells, we observed that VC CM potently increased the inhibitor of NF-κB, namely IκBα, in these cells when compared to the M0 control macrophages that were not exposed to the PANC-1 CM (**Figure 4.21A**). Importantly, NDRG1 and ΔCAP-NDRG1 were able to significantly inhibit this effect, reducing the levels of IκBα to a level comparable to the untreated M0 macrophages **(Figure 4.21A)**. This would suggest that NDRG1 promotes activation of the NF-κB pathway in macrophages. However, when examining the NF-κB p65 transcription factor total levels and its activating phosphorylation at Ser536, we observed that both NDRG1 and ΔCAP-NDRG1 CM reduced the levels of these proteins when compared to the VC CM **(Figure 4.21A)**. This unexpected result contradicts the increased observed with IκBα and suggests a more complex regulation of NF-κB signalling.

Similar results were observed in the THP-1 cells treated with CM from MIAPaCa 2 cells expressing NDRG1 and ΔCAP-NDRG1 compared to VC-treated cells **(Figure 4.21B)**. We also exposed U937 M0 macrophage cells to CM derived from PANC-1 and MIA PaCa-2 cells to further validate these findings. The results obtained again showed a significant degradation in IκBα, as well as a decrease in the expression of p-NF-κB p65 (Ser536) and NF-κB p65 in U937 cells incubated with CM from either PANC-1 or MIAPaCa-2 cells expressing NDRG1 and ΔCAP-NDRG1 compared to VC CM **(Figure 4.21C, D)**.

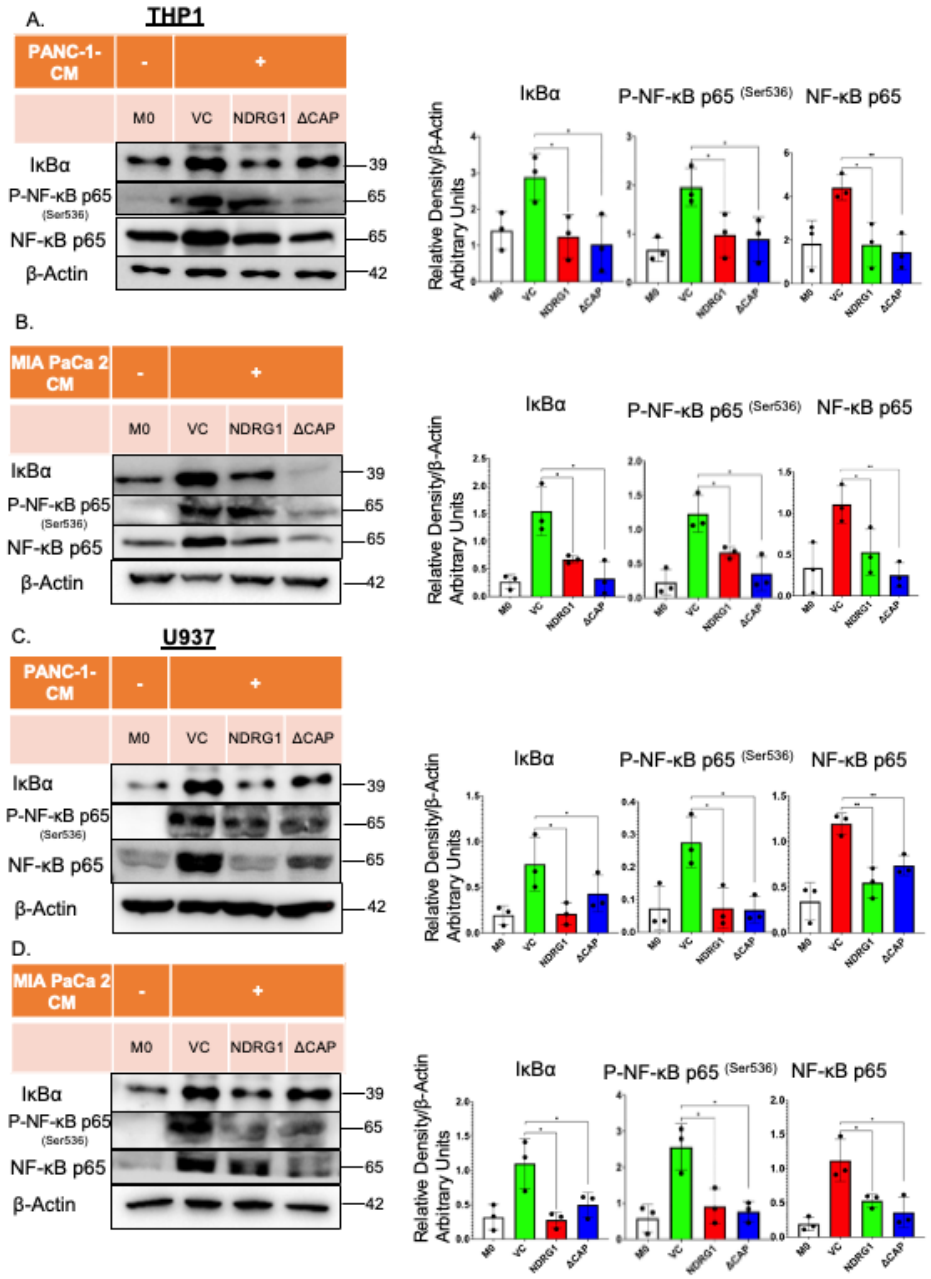

Figure 4.21: NDRG1 activated the NF-κB signalling pathway in macrophages. THP1 cells treated with CM from PANC-1 (**A**) and MIAPaCa-2 (**B**) VC, NDRG1 and ΔCAP-NDRG1 cells were assessed for IκBα, P-NF-κB p65 $^{(Ser536)}$ and NF-κB p65 *via* Western blot. U937 cells treated with CM from PANC-1 (**C**) and MIAPaCa-2 (**D**) VC, NDRG1 and ΔCAP-NDRG1 cells were assessed for IκBα, P-NF-κB p65 $^{(Ser536)}$ and NF-κB p65 *via* Western blot. **(**β-actin was used as a loading control. Results are mean ± SD (n = 3). *p<0.05, **p<0.01 denote statistical significance comparing each condition to the VC control.

As activation of NF-κB p65 can occur rapidly and results in the translocation of NF-κB p65 to the nucleus, we next examined how PDAC CM influenced NF-κB p65 localization after a shorter incubation of 24 hrs (*vs.* the 72-hr incubation period above). We conducted an experiment where THP-1 and U937 M0 macrophage cells were exposed to VC, NDRG1 or ΔCAP-NDRG1 CM from either PANC-1 or MIAPaCa-2 cells for 24 hours. We then analyzed the expression of NF-κB p65 using IF. The results showed an increase in the translocation of NF-κB p65 to the nucleus in M0 macrophages exposed to PANC-1 NDRG1 and PANC-1 ΔCAP-NDRG1 CM when compared to PANC-1 VC CM **(Figure 4.22A)**. Similar results were observed in the THP-1 cells treated with CM from MIAPaCa-2 cells expressing NDRG1 and ΔCAP-NDRG1 compared to VC-treated cells **(Figure 4.22B)**.

We also exposed U937 M0 macrophage cells to CM derived from PANC-1 and MIAPaCa-2 cells to further validate these findings. The results obtained again showed an increase in the nuclear translocation of NF-κB p65 in U937 M0 macrophages incubated with CM from either PANC-1 or MIAPaCa-2 cells expressing NDRG1 and ΔCAP-NDRG1 compared to VC CM **(Figure 4.23A and B)**.

These findings indicate that NDRG1 expression in PDAC cells activates the NF-κB pathway in THP1 and U937-derived macrophages after a 24-hr incubation period, further confirming that NDRG1 promotes a pro-inflammatory macrophage phenotype.

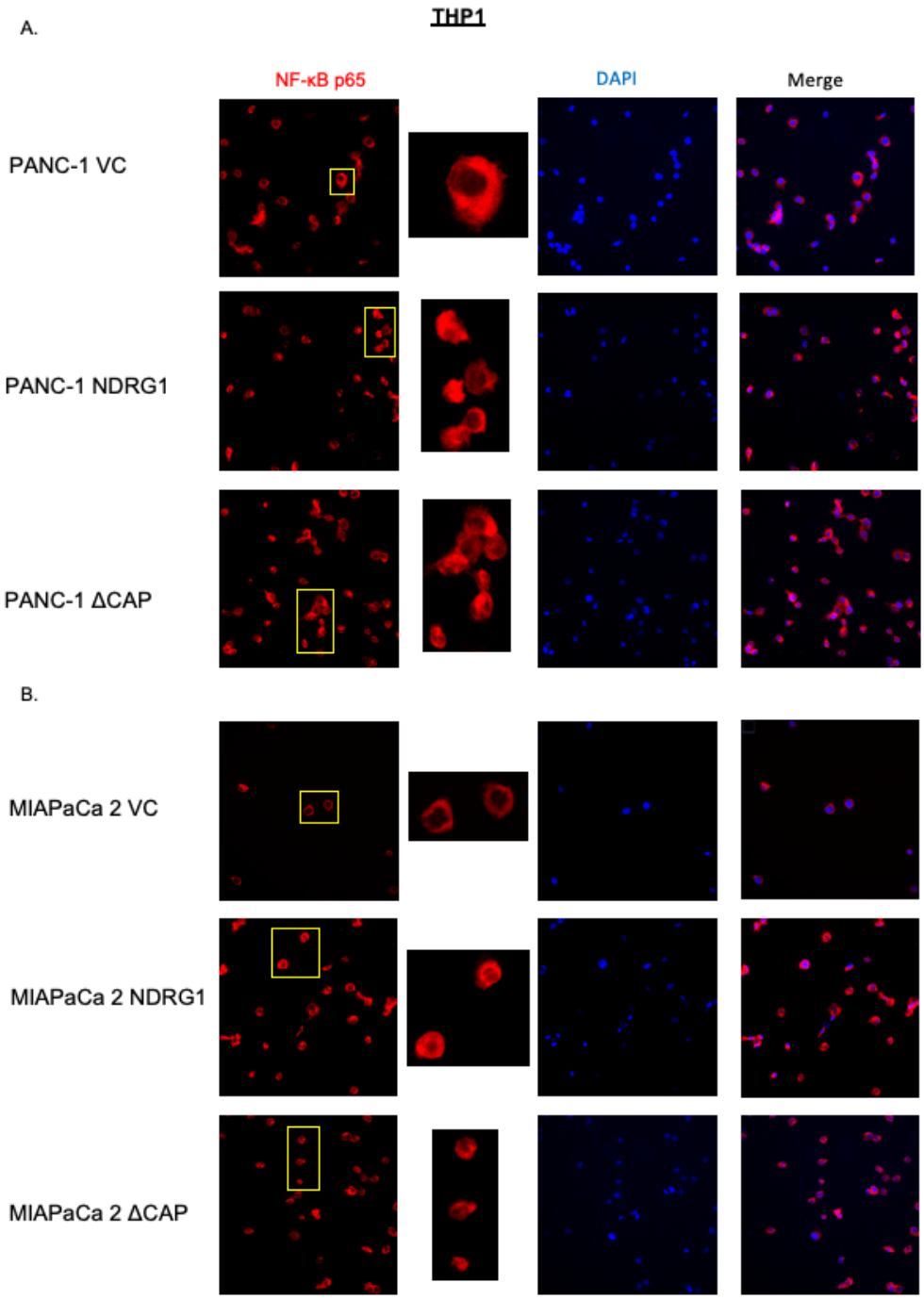

Figure 4.22: NDRG1 induced the NF-κB nuclear translocation in THP1 macrophages. The THP-1 macrophages were exposed to PANC-1 (**A**) or MIAPaCa-2 (**B**) VC, NDRG1 or ΔCAP-NDRG1 CM for 24 h, followed by immunofluorescence to stain for NF-κB p65 (red) and DAPI (blue). Cells were imaged using a 3i Marianas LightSheet™ microscope.

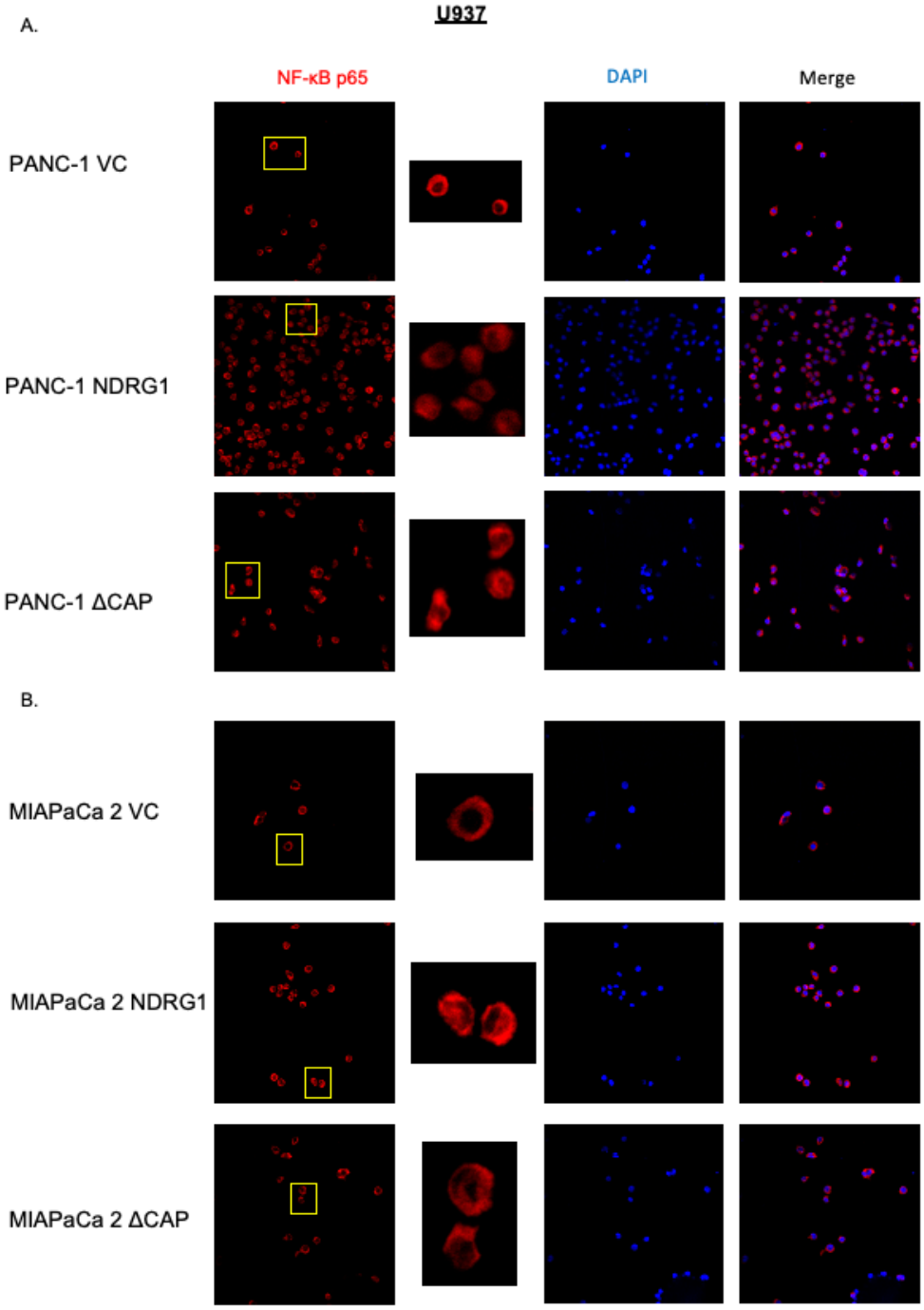

Figure 4.23: NDRG1 induced the NF-κB nuclear translocation in U937 macrophages. The U937 macrophages were exposed to PANC-1 (**A**) or MIAPaCa-2 (**B**) VC, NDRG1 or ΔCAP-NDRG1 CM for 24 h, followed by immunofluorescence to stain for NF-κB p65 (red) and DAPI (blue). Cells were imaged using a 3i Marianas LightSheet™ microscope.

Overall, the data presented herein demonstrates that when the levels of NDRG1 are increased in PDAC cells, it inhibits the activation of macrophages towards the M2 phenotype and enhances the activation of the M1 phenotype. Additionally, the results demonstrate that NDRG1 affects macrophage metabolism by promoting glycolysis and impairing the TCA cycle. Increased secretion of TNF-α from PDAC cells expressing NDRG1 might play a key role in this effect, leading to activation of the NF-κB signalling pathway in macrophages, which is known to promote a pro-inflammatory macrophage phenotype [325].

4.4. Discussion

Monocytes are circulating cells in peripheral blood that can differentiate into tumour-associated macrophages (TAM) after migrating into tumour tissue. These macrophages usually take on the M2 phenotype, have immunosuppressive properties and play a crucial role in tumour progression [295, 326]. Cancer cells release various cytokines or exosomes to directly polarize macrophages into M2 TAMs and indirectly manipulate them by altering their metabolism or creating a hypoxic environment [327]. Further, polarized TAMs express programmed cell death protein 1 (PD-L1), signal regulatory protein alpha (SIRPα), or sialic acid binding Ig like lectin 10 (Siglec-10) to suppress the anti-tumour activities of other immune cells in the TME [327]. Earlier studies have shown that NDRG1 functions as a metastasis suppressor in PDAC and was recently found to inhibit multiple oncogenic signalling pathways in PDAC cells and their crosstalk with PSCs [288, 328-330]. As the effect of NDRG1 on immune cells in the TME has never been examined, our study focussed on how this metastasis suppressor influences macrophage polarization in the TME.

To determine how the secretome of PDAC cells influences monocyte polarization into macrophages, we utilized PDAC conditioned media (CM) from either the VC NDRG1 or ΔCAP-NDRG1 cells. Several studies have demonstrated that tumour CM can induce human monocytes to differentiate into suppressive M2-like macrophages *in vitro*. For instance, a study found that the CM of colon cancer cells led to an increase in the expression of CD206 and CD163 in THP-1 cells [295]. The CM of the Lewis lung carcinoma cell line LL-2 induced migration, proliferation, and M2-like polarization of mouse primary bone marrow-derived macrophages (BMDMs) while inhibiting M1-like polarization [331]. The CM of pancreatic ductal adenocarcinoma cells PANC-1 and BxPC-3 increased M2 macrophage markers CD163 and CD204 in THP-1 monocytes [332]. Our findings agree with these earlier observations in

that using the CM from both PANC-1 and MIAPaCa-2 PDAC VC cells did indeed increase the M2 macrophage phenotype of both THP-1 and U937 monocytes, leading to increased expression of the M2 markers, CD206 and CD163. Furthermore, we demonstrate the over-expression of NDRG1 in these pancreatic cancer cell lines significantly altered the differentiation of THP-1 and U937 monocytes, leading to reduced M2 polarization and instead promoting an M1-like macrophage phenotype.

Earlier studies identified this region as crucial for protein-protein interactions or ligand binding [291, 292]. The CAP region, located within the α/β hydrolase fold of NDRG1, has been deleted to create ΔCAP-NDRG1 [212]. The results show that deletion of the CAP region affects the NDRG1-mediated effect in various experiments, such as macrophage polarization, ROS, and IL-12. However, the differences observed between the effects of NDRG1 and ΔCAP NDRG1 may simply be due to the different expression levels of these proteins. In fact, ΔCAP NDRG1 was expressed at a much higher level in PANC cells while being lower in MIAPaCa-2 cells compared to full-length NDRG1. Further studies are required to elucidate if the CAP region is important for the effects of NDRG1 on PDAC-mediated macrophage polarization

The role of CAFs in macrophage polarization

The progression of a tumour is associated with the infiltration of immune cells into the primary tumour. M1 macrophages produce reactive oxygen species (ROS) and cytokines such as IL-6, IL-12, IL-23, and TNF-α, which are associated with pro-inflammatory activities [333-335]. However, M2 macrophages promote tumour growth by releasing adrenomedullin and vascular endothelial growth factors (VEGFs) to support angiogenesis. Additionally, they express immunosuppressive molecules like IL10, programmed death-ligand 1 (PD-L1), and TGFβ, which further facilitate tumour growth [336]. In PDAC, which is characterized by extensive

desmoplasia and contains a high density of CAFs, these immunosuppressive effects are further amplified. In fact, 3D co-cultures of pancreatic cancer cells and CAFs with monocytes was found to promote M2-like macrophage polarization by stimulating the production of immunosuppressive cytokines [275]. In PDAC, CAFs present in the TME have been found to upregulate signalling molecules like IL-17, which play a role in recruiting monocytes and myeloid-derived suppressor cells (MDSCs) [337]. CAFs also secrete elevated amounts of IL-33, which plays a role in recruiting TAMs and promoting the polarization of M2 macrophages *via* its Suppression of Tumorigenicity 2 **(**ST2) receptor [338].

Recent studies by our group have demonstrated that NDRG1 can inhibit the cross-talk between PDAC cells and PSCs, inhibiting their conversion into CAFs and reducing the production of cytokines and growth factors from both PDAC and CAFs [205, 206]. In the current study, we further show that in co-cultures of PDAC cells combined with CAFs, NDRG1 expression in PDAC cells also decreases the polarization of macrophages into the M2 phenotype while increasing their polarization into the M1 phenotype. This suggests that the ability of NDRG1 to alter cross-talk between PDAC cells and CAFs could also contribute to altering the polarization of macrophages in the TME, inhibiting their immunosuppressive phenotype and instead promoting M1 macrophage polarization. This was evident by the significantly increased cytotoxicity observed in the PDAC-CAF-Monocyte co-cultures when NDRG1 was over-expressed. However, it is important to note that in the current study, we also demonstrated that NDRG1 expression in PDAC cells co-cultured alone with the monocytes was enough to alter their polarization, and thus these effects are not dependent on the presence of CAFs.

Cell cycle regulation in macrophages

In the present study, we also examined the effect of NDRG1 on the macrophage cell cycle, as a recent landmark study has demonstrated that the cell cycle influences macrophage plasticity during polarization [297]. This latter study demonstrated that the M1 macrophage polarization program is primarily limited to the G1 phase of the cell cycle [297]. In contrast, a significant portion of M2 macrophage polarization occurs during the S-G2/M phase [297, 298, 339]. Our research suggests that the expression of NDRG1 in PDAC cells can influence the cell cycle of exposed macrophages. In response to NDRG1 CM from PDAC cells, the proportion of exposed macrophages in the G0/G1 phase was consistently increased, while the number of macrophages in the S-phase was significantly reduced when compared to control CM. These effects are consistent with increased polarization of exposed macrophages into the M1 phenotype.

The potential mechanisms by which NDRG1 expression in PDAC cells can influence the macrophage cell cycle could be mediated by the altered secretome of PDAC cells. For instance, we demonstrate that NDRG1 significantly increased the production of TNF-α, while reducing the production of MCP-1 by PDAC cells. Notably, TNF-α has been shown to regulate the expression of cell cycle genes in macrophages leading to cell cycle arrest [340]. Further, MCP-1 binding to macrophages induces activation of the PI3K/AKT signalling pathway [341], which can influence the expression of multiple cell cycle proteins including p21, p27, cyclin D and cdk2 to promote the G1/S transition [342]. While we did not examine the expression of these cell cycle proteins in the macrophages, earlier studies have shown that NDRG1 expression can up-regulate $p21^{wafl}$ expression in PDAC cell [343]. Overall, these findings indicate a potential role for NDRG1 in regulating the cell cycle machinery of macrophages, which may contribute to the altered macrophage polarization observed.

Macrophage metabolism

Another factor that influences macrophage polarization is the metabolic cross-talk within the TME, which can cause metabolic reprogramming of macrophages [344]. M1 macrophages primarily rely on glycolytic metabolism, and the increase of GLUT1 is essential for glycolytic activity as it assists in rapid glucose uptake [311, 345]. M2 macrophages express the arginase enzyme (Arg-1), which breaks arginine down into ornithine and urea. Furthermore, ornithine can fuel downstream pathways like polyamine and proline syntheses, which are critical for cellular growth and tissue repair [346]. High levels of Arg-1 in macrophages also restricts the availability of arginine for the iNOS-mediated synthesis of NO, which is required for the cytotoxic effects of macrophages [346].

In the current study we demonstrate that NDRG1 expression in PDAC cells led to increased glycolysis in exposed macrophages (as evidenced by higher expression of GLUT1 and glycolysis enzyme HK 2), leading to higher ECAR rates by these macrophages. This is consistent with an M1-macrophage metabolic phenotype. Further, this was accompanied by significantly reduced Arg-1 protein levels and increased iNOS levels, which suggests that arginine metabolism was shuttled more towards generation of NO rather than ornithine in the macrophages exposed to NDRG1 CM. This was further validated by the mitoplate assay, which demonstrated that NDRG1 CM exposed macrophages had increased metabolism of α-D-Glucose, D-Glucose-6-PO4 and cis-Aconitic Acid, which reflect increased glycolysis. This same assay also revealed the reduced ability of NDRG1 CM exposed macrophages to metabolize ornithine, which is likely a consequence of the reduced Arg-1 protein levels in these cells.

Importantly, the above effects were observed under normoxia. It is important to note that when the PDAC CM was generated under hypoxic conditions and then incubated with the macrophages, we observed significant differences in the metabolic profiles of the macrophages. For instance, HK 2 levels were being reduced in the hypoxic NDRG1 CM exposed macrophages while Arg-1 levels were increased when compared to the hypoxic VC CM. This suggests that the secretome of the PDAC cells is altered under hypoxia and was potentially promoting a more M2-like metabolic phenotype under this condition. This was further validated by the cytokine array assay, which revealed that NDRG1 significantly altered the secretome of PDAC cells under hypoxia, with cytokines such as IFN-γ, MCP-1, FGF-9 and IL-16 being increased under hypoxia in these cells.

Hypoxia-inducible factor (HIF1α) 1α is a metabolic regulator that plays a role in the M1 polarization of macrophages. When HIF1α is overexpressed, it increases glycolysis and the production of pentose phosphate pathway intermediates [347]. Due to time limitations, we did not assess the expression levels of HIF-1 in the macrophages exposed to PDAC CM, and this is something that requires further investigation. However, it is important to note that the induction of NDRG1 under hypoxic conditions primarily relies on the HIF-1 transcription factor [348]. Overall, these findings suggest a potential role for NDRG1 in impacting the metabolism of macrophages in normoxia and hypoxia.

Cytokine-mediated signalling in macrophages

In this study, we sought to investigate the NDRG1 mechanisms involved in the effect of macrophage polarization. We investigated the cytokines involved in this communication by conducting a cytokine/chemokine array on the CM of MIAPaCa-2 VC and NDRG1 cells. Elevated expression levels of Human Monocyte Chemoattractant Protein-1 (MCP-1/CCL2)

have been found to trigger the upregulation of Monocyte Chemotactic Protein-Induced Protein 1 (MCPIP1) in macrophage *via* the STAT3 pathway. This, in turn, leads to the polarization of Mφs towards an M2-like phenotype [320]. Blocking the CCL2-CCR2 axis effectively suppresses tumor development in esophageal squamous cell carcinoma (ESCC) by inhibiting monocyte infiltration and TAMs accumulation in the tumor microenvironment [349]. In osteonecrosis, TNF-a triggers macrophages to differentiate into the M1 phenotype and infiltrate the necrotic zone. A significant number of M1 macrophages are then present in the region. However, when TNF-a expression decreases, the necrotic zone sees a larger population of M2 macrophages[319]. Blocking TNF-α inhibits M1 polarization through pathways independent of STAT1 and IRF-1 [350]. We observed that NDRG1 reduced the secretion of MCP-1 from PDAC cells and increased the level of TNF-α, which is evidence that NDRG1 likely affects macrophage polarization through cytokine/chemokine secretion from PDAC cells (**Figure 4.24**).

The activity of NF-κB regulates the transcription of multiple pro-inflammatory cytokines such as TNF-α, IL-1β, IL-6, and IL-12 in macrophages [351-353]. We hypothesized that the increased TNF-α production by NDRG1 over-expressing PDAC cells would enhance the activation of NF-κB signalling and contribute to a robust inflammatory response by the macrophages. This hypothesis was supported by our observation that NDRG1 CM reduced the expression of IκBα in the exposed macrophages. As IκBα sequesters NF-κB in the cytosol, essentially preventing its activation, we expected to observe increased NF-κB phosphorylation at Ser 536, which leads to its activation [354, 355].

However, our western blot analysis showed the opposite effect, suggesting that after a 72-h incubation the effect on NF-κB activation may have already happened. Examining NF-κB

localization at an earlier time-point of 24 h did show a slight increase in nuclear NF-κB levels, suggesting that the activation of this pathway in macrophages occurred shortly after exposure to the PDAC NDRG1 CM. As NF-κB signalling directly enhances IL-12 production by macrophages, we concluded that NDRG1 is likely regulating IL-12 production by macrophages *via* its effects on NF-κB activity (**Figure 4.24**). However, further studies are required to elucidate the timeline and dynamics of the NF-κB activation following exposure to the PDAC cells. In particular, the NF-κB transcriptional activation in the exposed macrophages will need to be confirmed.

In conclusion, in pancreatic cancer cells, the upregulation of NDRG1 inhibits the activation of macrophages to the M2 phenotype and increases activation of the M1 phenotype. This is achieved by activating the NF-κB signalling may be through the increased secretion of TNF-α.

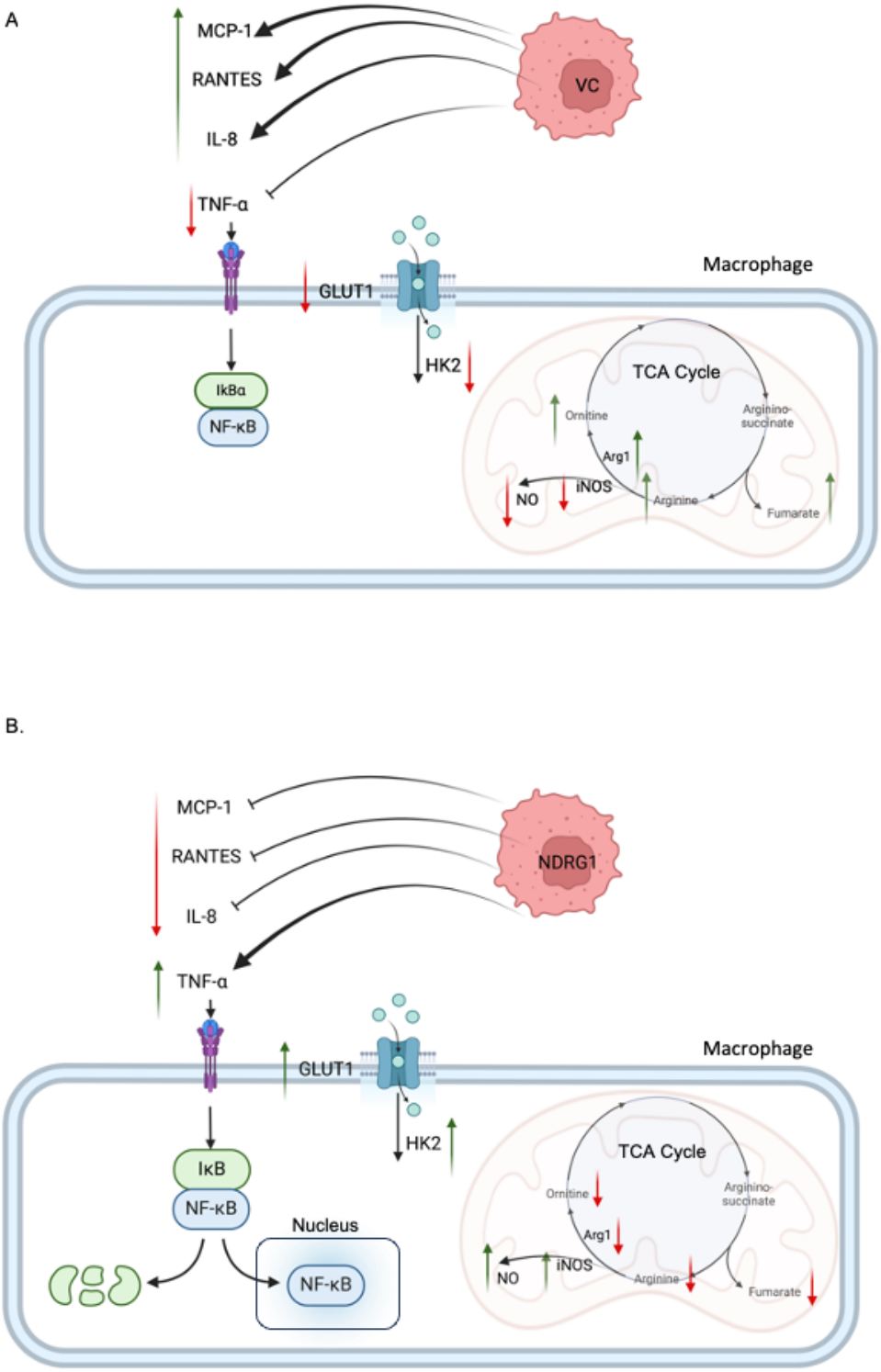

Figure 4.24: Schematic diagram demonstrating how NDRG1 effects on macrophage metabolism influences their phenotype and polarization. (A) effect of PDAC VC on macrophages in NF-κB signalling and metabolism pathways. **(B)** effect of PDAC NDRG1 on macrophages in NF-κB signalling and metabolism pathways.

Chapter 5: Effect of NDRG1 on metabolic cross-talk between PDAC cells and CAFs

5.1 Introduction

Pancreatic cancer has the lowest 5-year survival rate at around 11 % compared to other types of cancer, making it the deadliest type. Currently, surgery is the most effective treatment option, but only a small percentage of pancreatic cancer cases, about 10–20%, are operable at the time of diagnosis [170, 207]. Pancreatic ductal adenocarcinoma (PDAC) is an extremely aggressive and often fatal malignancy characterized by late diagnosis and poor response to available treatments [208]. PDAC is the most common form of pancreatic neoplasm, predominantly found in the exocrine component of the pancreas and represents over 90% of pancreatic cancer cases [208].

Extensive desmoplasia is a notable characteristic of the microenvironment in PDAC. Earlier research indicated that desmoplasia encourages the proliferation, invasion, and chemoresistance of PDAC cells [356]. Desmoplasia, a prominent feature of PDAC, involves the proliferation of dense fibrotic tissue surrounding tumour cells [357]. Desmoplasia consists of extracellular matrix (ECM) proteins, pancreatic stellate cells (PSCs) with myofibroblastic characteristics, and immune cells related to numerous cytokines, growth factors, and enzymes responsible for metabolizing ECM [358].

In PDAC, pancreatic stellate cells (PSCs) become activated (aPSCs) from their quiescent state (qPSCs). These activated cells are a major source of cancer-associated fibroblasts (CAFs) in PDAC. PSC-derived CAFs play a crucial role in the desmoplastic reaction by synthesizing ECM proteins and producing growth factors and cytokines that stimulate cancer cell proliferation and migration [359, 360].

CAFs, which are the main type of stromal cells, can be activated by nearby cancer cells to undergo aerobic glycolysis. This results in the release of high-energy metabolites such as pyruvate and lactate. The neighbouring cancer cells, particularly in normoxia, absorb and use these metabolites in oxidative phosphorylation (OXPHOS) [213, 361].

BCAA aminotransferase (BCAT) is responsible for converting Branched-chain amino acids (BCAAs) to branched-chain α-keto acids (BCKAs). The cells contain two primary forms of BCAT: BCAT1, located in the cytoplasm, and BCAT2, located in the mitochondrion. These proteins facilitate the transfer of amino groups [362]. Overexpression of BCAT2 enhanced cell proliferation and survival of PDAC cells [363]. High levels of BCAT1 protein in CAFsled to an increase in the secretion of BCKA, which in turn fuelled the growth of PDAC cells [364]. The activity of stromal-BCAT1 is upregulated in stromal cells through SMAD5 activation by transforming growth factor-β (TGF-β) secreted by PDAC cells [364].

N-myc downstream-regulated gene-1 (NDRG1) was shown to function as a metastasis suppressor in PDAC, with its anti-cancer effects being partly mediated by its ability to inhibit oncogenic signalling pathways in PDAC cells including PI3K/AKT, EGFR/MAPK and NF-κB [329, 365]. Notably, NDRG1 also inhibited the production of TGF-β by PDAC cells, which led to reduced activation of PSCs into CAFs [205]. Considering its effects on PDAC cell metabolism (as demonstrated in ***Chapter 3***) and its ability to alter the secretome of PDAC cells (as shown in ***Chapter 4***), we next sought to investigate whether NDRG1 expression in PDAC cells could alter the metabolic cross-talk with PSCs.

In this study, we performed co-culture experiments on PDAC cells and PSCs to gain a more comprehensive insight into the effect of NDRG1 on cell metabolism in both cells when they

are cultured together. Our findings indicate that NDRG1 reduced the metabolic flux, including both glycolysis and oxidative phosphorylation (OXPHOS) in co-culture spheroids consisting of PDAC cells and PSCs. Furthermore, NDRG1 reduced the expression of BCAT1 and BCAT2 in PDAC cells co-cultured with PSCs, demonstrating a novel role for NDRG1 in regulating the exchange of BCAA's in the PDAC tumour microenvironment.

5.2. MATERIALS & METHODS

5.2.1. Cell Culture

The human pancreatic cancer cells PANC-1,MIAPaCa-2 and Human Pancreatic Stellate Cells (HPaSteC) were cultured as described above ***(Section 2.1)***.

5.2.2 Stable transfection

PANC-1 and MIAPaCa-2 cell lines were transfected as described above ***(Section 2.2)***.

5.2.3. Protein Extraction

The protein extraction for whole cells was extracted as described above ***(Section .2.5)***.

5.2.4. Western Blot Analysis

Western blot was performed *via* standard methods as described above ***(Section 2.6)*** using antibodies listed in **Table 5.1**.

Table 5.1: The list of primary and secondary antibodies used for western blot studies.

No	Name of antibody	Catalogue #	Company	Dilution
1	Fumarase	4567	Cell Signalling	1:1000
2	PFKP	8164	Cell Signalling	1:1000
3	IDH1	3997	Cell Signalling	1:1000
4	ACO2	6571	Cell Signalling	1:1000
5	Hexokinase II	2867	Cell Signalling	1:1000
6	α-Smooth Muscle Actin	19245	Cell Signalling	1:1000
7	BCAT1	88785	Cell Signalling	1:1000

8	BCAT2	79764	Cell Signalling	1:1000
9	BCKDH-E1α	90198	Cell Signalling	1:1000
10	Phospho-BCKDH-E1α (Ser293)	40368	Cell Signalling	1:1000
11	SMAD5	12534	Cell Signalling	1:1000
12	NDRG1	9485	Cell Signalling	1:1000
13	β-Actin	A5316	Sigma-Aldrich	1:10,000
14	Mouse IgG secondary	A4416	Sigma-Aldrich	1:10,000
15	Rabbit IgG secondary	A6154	Sigma-Aldrich	1:10,000

5.2.5. Preparation of Conditioned media (CM)

The Conditioned media (CM) were collected as described above ***(Section 2.10)***.

5.2.6. XFe96 seahorse assay

3D spheroid co-cultures containing PDAC cells and PSCs were generated using Corning® 96-well Clear Round Bottom Ultra-Low Attachment Microplates (Corning Costar, #7007). 10% methylcellulose (Sigma) medium was used to enhance spheroid formation [290]. Specifically, 2500 cells of PANC-1 or MIAPaCa-2 for monoculture and 1000 PANC-1 or MIAPaCa-2 cells mixed with 1500 PSCs for co-culture were seeded into each well and incubated at 37°C with 5% CO_2 with media being replaced every 3-4 days. The spheroids were seeded on day 5 in a Seahorse XF 96-well plate from Agilent Seahorse XFe96/XF Pro Extracellular Flux Assay Kits (Agilent Technologies, Santa Clara, CA). The Baseline Oxygen Consumption Rate (OCR) and Extracellular Acidification Rate (ECAR) were measured as described above ***(Section 2.7)***.

5.2.7. MitoPlate S-1

The mitochondrial metabolic activity of PSC cells was analyzed using MitoPlate S-1 (Biolog Cat. #14105, Hayward, CA, U.S.A.) according to the manufacturer's instructions. 3D spheroid PSCs were generated using Corning® 96-well Clear Round Bottom Ultra-Low Attachment Microplates (Corning Costar, #7007). 10% methylcellulose (Sigma) medium was used to enhance spheroid formation [290]. Specifically, 2500 PSC cells were seeded into each well and incubated at 37°C with 5% CO2 with MIAPaCa-2 CM from VC and NDRG1 for 72h. Spheroids were digested, and then the cell solution was passed through a 75-micron filter [366]. The mitochondrial metabolic activity was analyzed using MitoPlate S-1 as described above ***(Section 2.9)***.

5.2.8. Indirect co-culture

PANC-1, MIAPaCa-2, and PSCs cells were used for indirect co-culture in a Transwell 6-well plate (Corning). In one condition, PANC-1 or MIAPaCa-2 cells were seeded at 2 X 10^5 in a 6-well plate, and PSCs cells at a density of 1.6 X 10^5 in a Transwell insert in a second 6-well plate. In the second condition, the PSCs were seeded in the 6-well plate, and PANC-1 and MIAPaCa-2 cells were placed in the Transwell insert. All plates were then incubated overnight at 37^o in the incubator. The following day, the inserts were transferred into the corresponding wells in the 6-well plate.

5.2.9. Statistics and densitometry

The experimental data were compared using a student t-test and presented as mean ± standard deviation (SD). All experiments were conducted in triplicate, and statistical significance was considered when the p-value was < 0.05. The results are shown as mean ± SD ($n = 3$). Statistical significance levels are denoted as follows: *$p<0.05$, **$p<0.01$, ***$p<0.001$, ****$p<0.0001$. The densitometry data was analyzed using GraphPad Prism 10 (GraphPad, U.S.A.) and Microsoft Excel (Microsoft, U.S.A.).

5.3. Results

5.3.1 Upregulation of NDRG1 in PANC-1 and MIAPaCa-2 cells impacts the cellular oxygen consumption rate (OCR) and extracellular acidification rate (ECAR) in PDAC monoculture and PDAC-PSCs co-culture spheroids.

To investigate the impact of NDRG1 expression on the metabolism of PDAC cells, we initially established stable transfections of PANC-1 and MIAPaCa-2 cells. These cells expressed either the vector control (VC) or wild-type NDRG1 (NDRG1). As expected, the Western blot results indicated that PANC-1 and MIAPaCa-2 cells overexpressing NDRG1 exhibited significantly higher NDRG1 expression than the VC cells (**Figures 5.1A and 1B**).

The primary metabolic change in pancreatic cancer is the modification of glycolysis. This altered glycolytic process is carefully regulated in cancer cells to fulfil their rapid growth requirements and to generate essential components for synthesizing compounds [231]. An earlier study demonstrated that incubating PDAC cells with PSC conditioned media didn't change glycolysis, but significantly increased oxygen consumption by 20-40% [163]. In the current study, the PDAC cells were directly co-cultured with PSCs as 3D spheroids to more accurately reflect the *in vivo* structure. The effect of NDRG1 expression in the PDAC cells on the oxygen consumption rate (OCR) and the extracellular acidification rate (ECAR) was then measured using the Seahorse Analyzer in both PDAC monoculture and PDAC + PSC co-culture spheroids.

In this study we used 2 PDAC cell lines, namely PANC-1 and MIAPaCa-2 (transfected with either VC or NDRG1) to establish both monoculture spheroids, as well as co-culture spheroids with PSC cells **(Figure 5.1C and D)**.

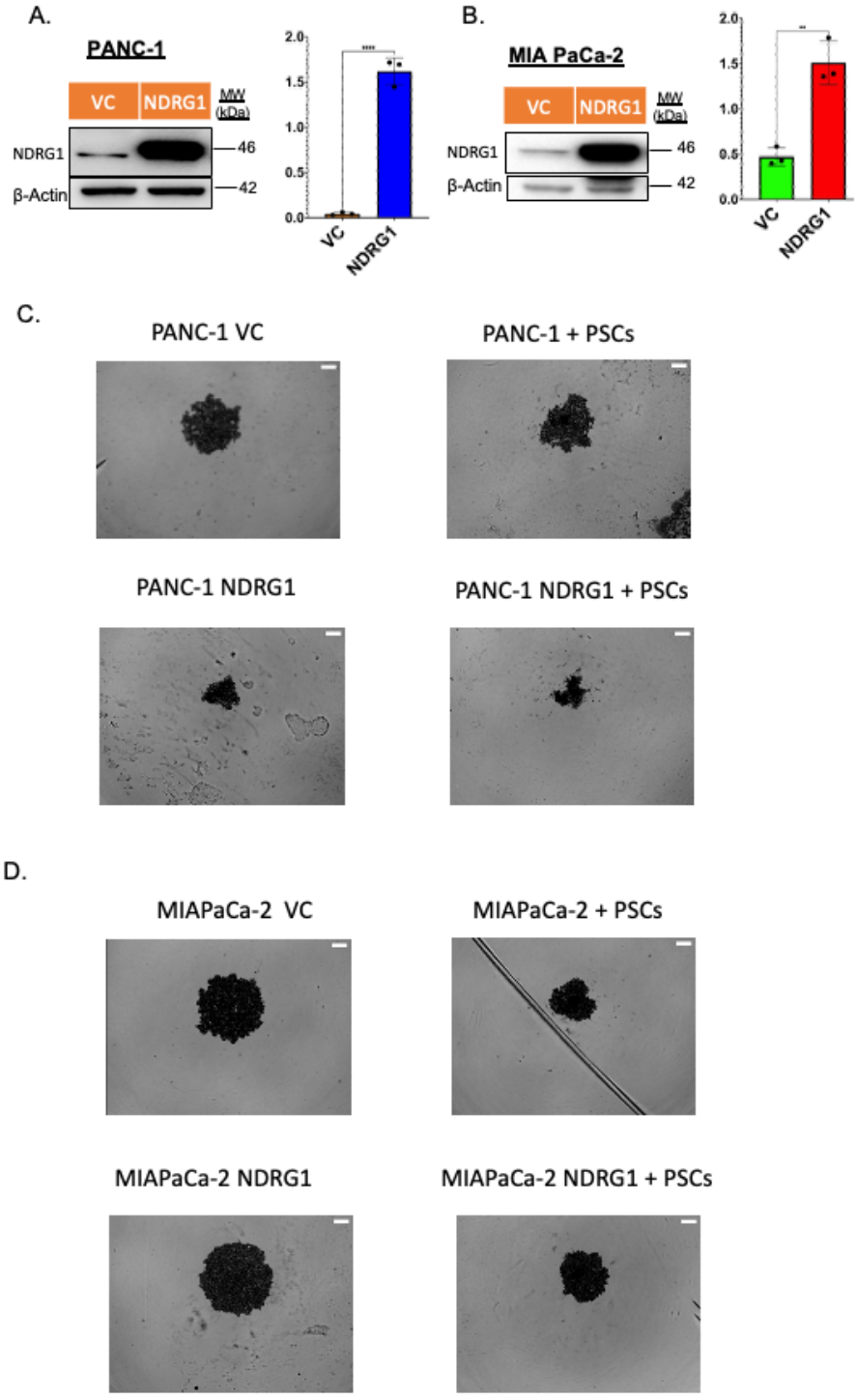

Figure 5.1: NDRG1 impact the PDAC-PSCs co-culture.
(**A**) PANC-1 and (**B**) MIAPaCa-2 cells stably transfected with VC and NDRG1. β-actin was used as a loading control. PDAC cells were mixed with PSCs fibroblasts for 5 days, and Brightfield images (from InCucyte SX5) at day 5 showing the VC or NDRG1 cells monocultured (2500 cells) or co-cultured with PSCs (1000 PDAC cells + 1500 PSCs) in **(C)** PANC-1 and **(D)** MIAPaCa-2. Results are mean ± SD (n = 3). **p<0.01 ****p<0.0001 denote statistical significance comparing each condition to the relevant VC control.

The results indicated that NDRG1 significantly reduced the ECAR while significantly increasing the OCR in PANC-1 NDRG1 monoculture spheroids compared to PANC-1 VC monoculture spheroids **(Figure 5.2A)**. Notably, the addition of PSCs into the PANC-1 VC spheroids led to a significant increase in OCR when compared to the PANC-1 monoculture spheroids, suggesting extensive metabolic cross-talk was occurring between these two cell types. However, NDRG1 significantly decreased this effect, leading to a potent reduction in both the ECAR and the OCR when compared to VC co-culture spheroids **(Figure 5.2A)**.

Similar results were observed in MIAPaCa-2 cells, where NDRG1 again significantly reduced the ECAR while increasing the OCR in the monoculture spheroids **(Figure 5.2B)**, while significantly decreasing both the ECAR and the OCR in co-culture spheroids when compared to the VC co-culture spheroids **(Figure 5.2B)**.

These findings suggest that NDRG1 decreased both glycolysis and oxidative phosphorylation (OXPHOS) in PANC-1 and MIAPaCa-2 spheroids that were co-cultured with PSCs, indicating that NDRG1 inhibits the metabolic cross-talk between these two cell types.

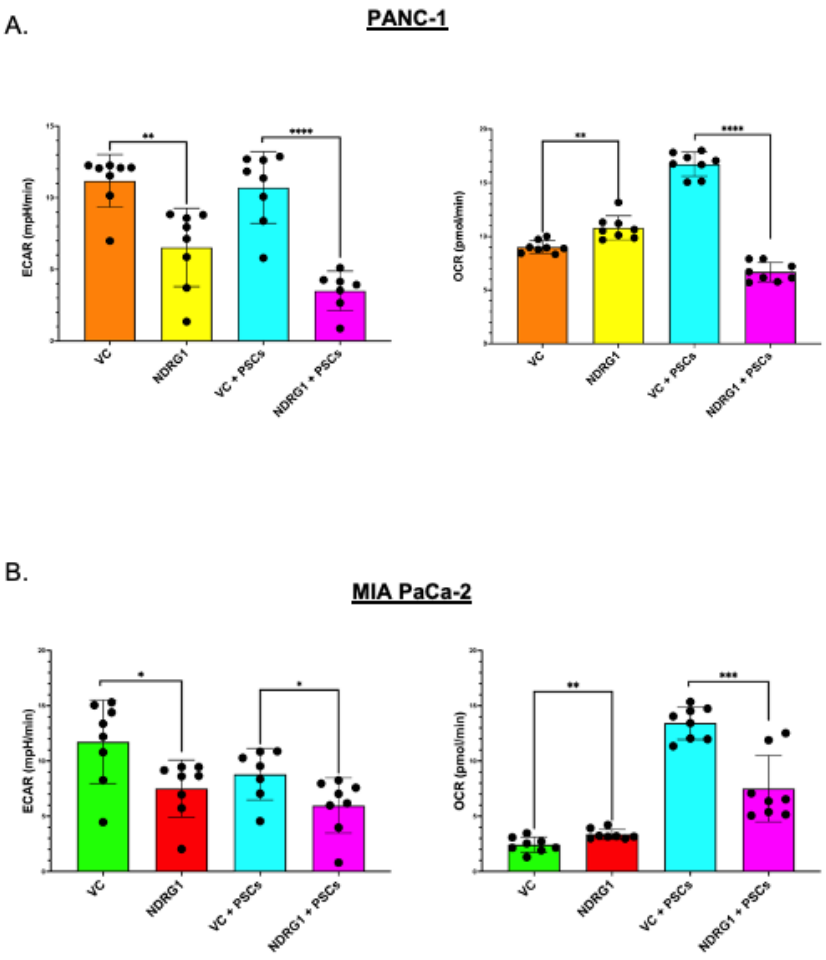

Figure 5.2: NDRG1 decreased ECAR and increased OCR in the PDAC-PSCs co-culture spheroids.

The Seahorse analyser was used to measure the oxygen consumption rate (OCR) and extracellular acidification rate (ECAR) in PDAC monoculture and PDAC-PSCs co-culture. The ECAR and OCR for PANC-1 **(A)** or MIAPaCa-2 **(B)**. Results are mean ± SD (n = 3). *p<0.05, **p<0.01 ***p<0.001 ****p<0.0001 denote statistical significance comparing each condition to the relevant VC control.

5.3.2. Western blot analysis of metabolic enzymes in indirect co-cultures of PDAC and PSC cells.

Following our findings above that NDRG1 can impact the metabolism in PDAC-PSCs co-culture spheroids, we conducted further studies to examine the expression of essential metabolic enzymes in PANC-1, MIAPaCa-2 and PSCs following 72 h of co-culture using a transwell set up, as illustrated in **Figure 5.3**.

Activated PSCs show increased levels of α-smooth muscle actin (α-SMA), produce excessive ECM, and secrete growth factors that promote the metastatic progression of PDAC [213, 367]. The PSC activation marker α-SMA levels were reduced in PSC cells after exposure to CM from NDRG1-overexpressing PDAC cells when compared to those exposed to VC CM (**Figure 5.4**), which was in agreement with our previous work [205] and suggests that NDRG1 is reducing PSC activation into CAFs.

We next examined metabolic enzyme involved in both glycolysis (HK2, PFKP) and the TCA cycle (IDH1, Fumerase and ACO2). HK2, which had higher expression in the PANC-1 cells compared to the PSCs, was significantly reduced by NDRG1 in PANC-1 cells, with no marked effect in the PSCs. This suggests that NDRG1 is reducing glycolysis in the PANC-1 cells but not the PSCs. Notably, PFKP was not significantly affected by NDRG1 in either the PANC-1 or PSC cells. The TCA cycle enzymes, NDRG1 significantly reduced fumarase expression in the co-cultured PSCs cells, while NDRG1 significantly reduced ACO2 in the co-cultured PANC-1 cells and the PSCs, suggesting suppression of the TCA cycle in both cell types. Interestingly, IDH1 was reduced by NDRG1 in the PANC-1 cells, while being significantly increased in the PSCs co-cultured with PANC-1 NDRG1 cells **(Figure 5.4)**.

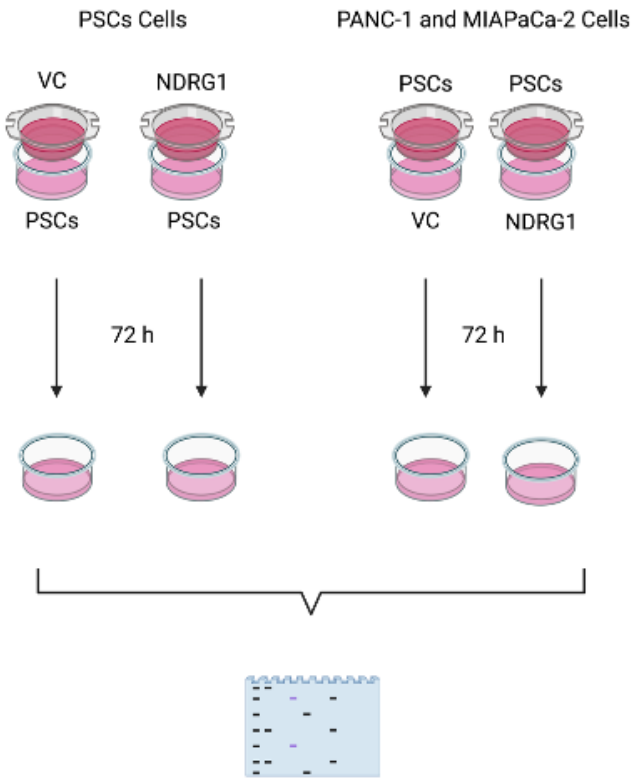

Figure 5.3: Schematic diagram of the experimental procedure for indirect co-culture of PDAC and PSCs.
PANC-1 or MIAPaCa-2 cells were seeded at 2 X 10^5 into 6-well plates, while PSCs were seeded into Transwell inserts at a density of 1.6 X 10^5 in a second 6-well plate. Following attachment, the PSC-containing transwell inserts were placed into the 6-well plates containing the PDAC cells and co-cultured for 72 h, followed by protein extraction of the PDAC cells and Western blot analysis. To assess the effect on PSCs, the opposite set up was established, with PDAC cells in the Transwell inserts and PSC's in the 6-well plates.

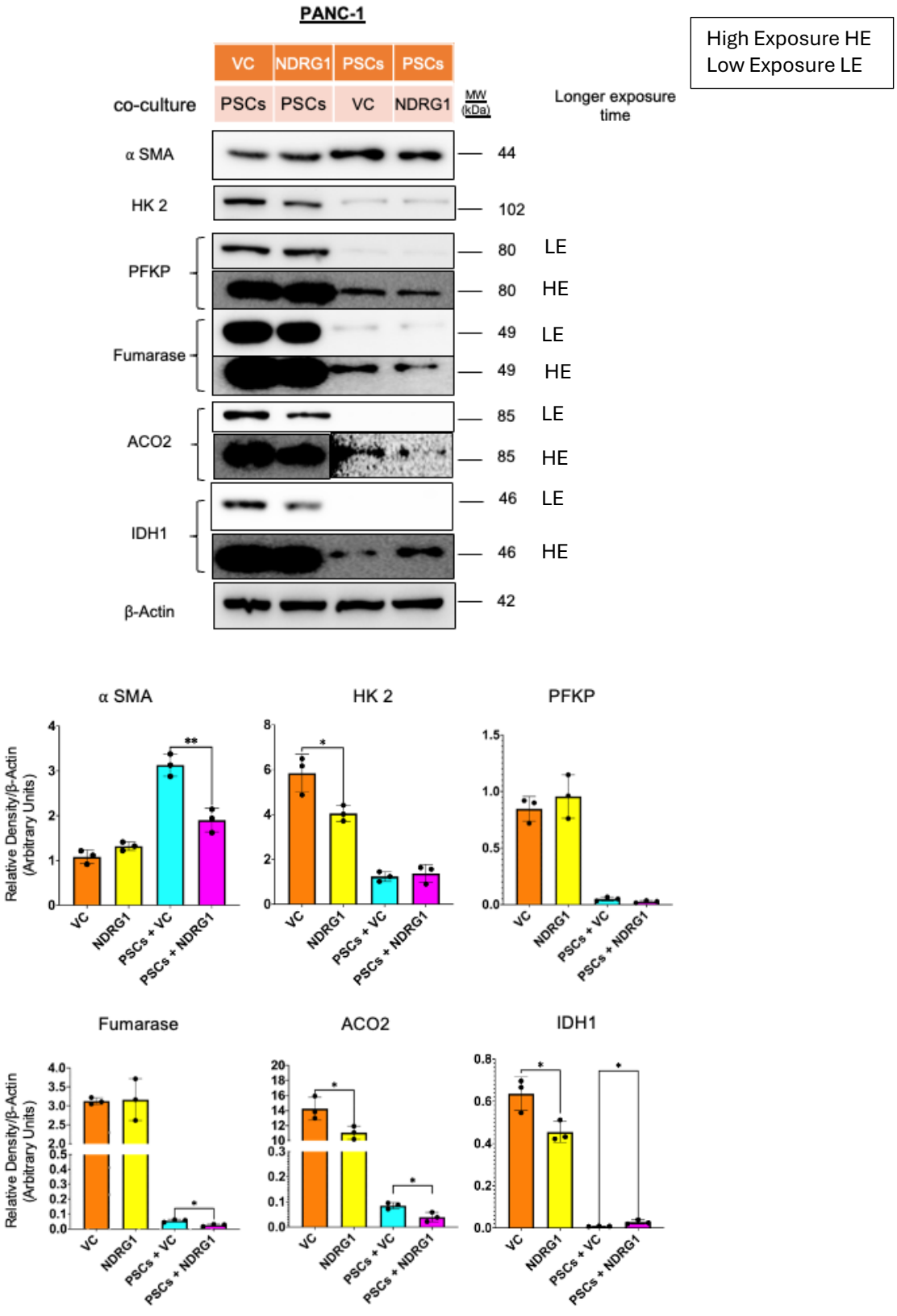

Figure 5.4: NDRG1 impacts the metabolism of PANC-1 and PSCs co-culture.
Western blots and densitometric analysis of α SMA, HK2, PFKP, fumarase, ACO2 and IDH1 in PANC-1 and PSCs co-cultures. β-actin was used as a loading control. Results are mean ± SD (n = 3). *p<0.05, **p<0.01 denote statistical significance comparing each condition to the relevant VC control.

Overall, this data demonstrates that NDRG1 influences multiple metabolic enzymes not only in PDAC cells, but also in PSCs that are exposed to these PDAC cells.

We observed similar results in MIAPaCa-2 cells, where the expression of HK2, IDH1, Fumarase, and ACO2 were significantly reduced in the MIAPaCa-2 NDRG1 cells compared to the relevant VC cells in co-culture with PSCs **(Figure 5.5)**.

Examining the PSC cells co-cultured with MIAPaCa-2 cells, NDRG1 again decreased the expression of αSMA suggesting reduced activation of these cells **(Figure 5.5)**. Furthermore, PSCs co-cultured with MIAPaCa-2 NDRG1 cells also expressed increased HK2 and IDH1 levels, while having lower ACO2 expression compared to PSCs co-cultured with MIAPaCa-2 VC cells **(Figure 5.5)**.

The findings indicate that NDRG1 potentially reduces glycolysis in PDAC cells and demonstrate that NDRG1 expression can influence different enzymes in the TCA cycle in both PDAC cells and PSCs.

High Exposure HE
Low Exposure LE

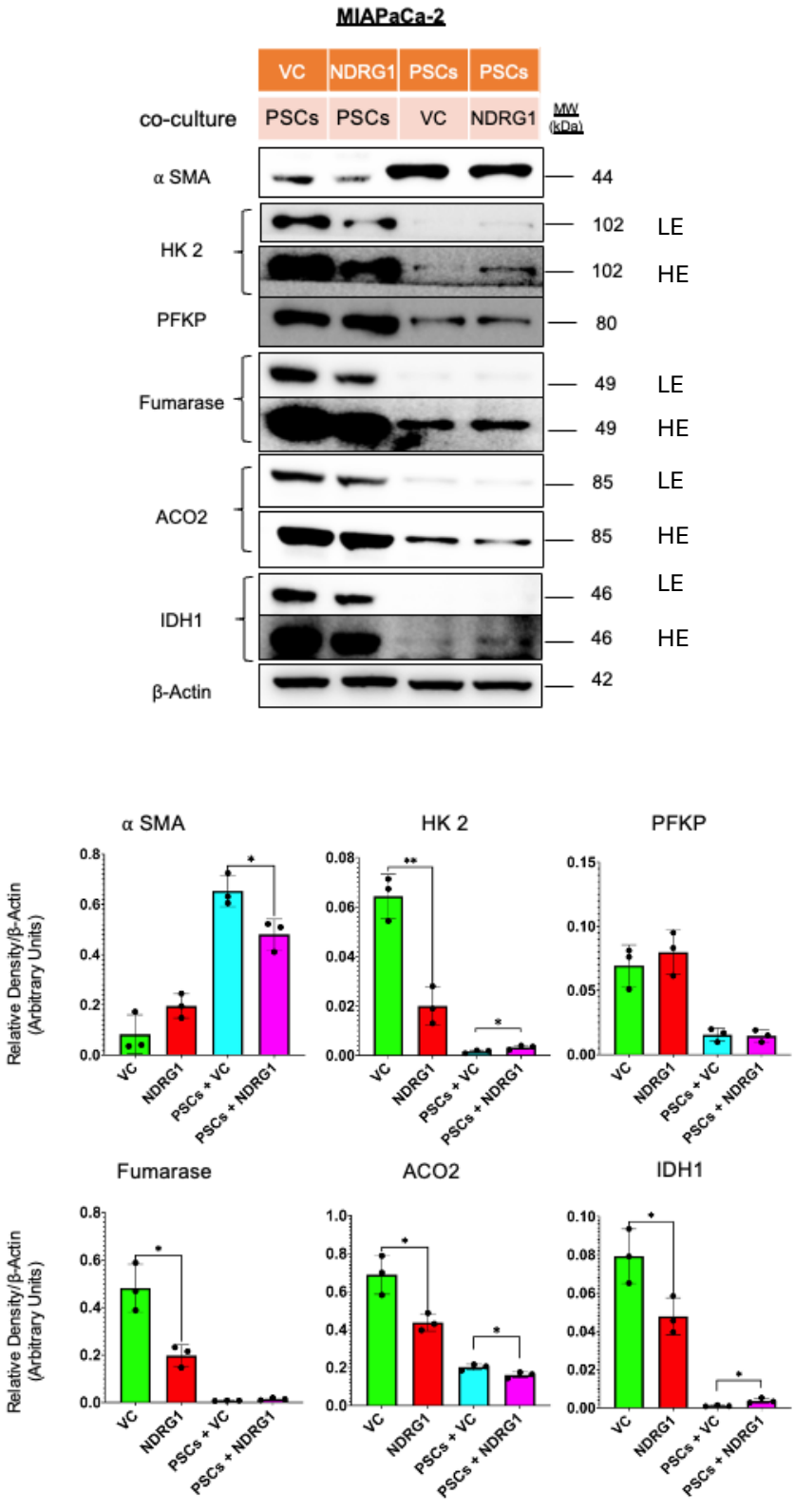

Figure 5.5: NDRG1 impacts the metabolism of MIAPaCa-2 and PSCs co-culture. Western blots and densitometric analysis of α SMA, HK2, PFKP, Fumarase, ACO2 and IDH1 in MIAPaCa-2 and PSCs co-culture. β-actin was used as a loading control. Results are mean ± SD (n = 3). *p<0.05, **p<0.01 denote statistical significance comparing each condition to the relevant VC control.

5.3.3 The expression of NDRG1 in PDAC cells impacts the PSCs' mitochondrial metabolism.

To further investigate how NDRG1 expression in PDAC cells influences the metabolism of PSCs, we conducted a Mitoplate S-1 assay. This assay evaluates mitochondrial function by measuring the rate of electron flow through the electron transport chain following exposure to 31 metabolic substrates. It utilizes 96-well plates that are pre-loaded with tests specifically created to assess the impact of a wide range of substrates on mitochondrial function.

The PSCs were exposed to either MIAPaCa-2 VC and NDRG1 cells CM for 72 hours. Subsequently, the PSCs were incubated at 37°C for 7 hours, and the absorbance at 590 nm was measured at 30-minute intervals **(Figure 5.6A)**.

The findings showed that NDRG1 decreased the metabolism of several substrates, including α-D-Glucose, D-Glucose-1-PO4, and L-lactic acid **(Figure 5.6B, C and D)**. Regarding TCA cycle substrates, the results indicated reduced fumaric, succinic acid and cis-aconitic acid metabolism **(Figure 5.6E and G)**. Additionally, NDRG1 reduced the metabolism of D, L-Isocitric Acid **(Figure 5.6H)**, L-Glutamic Acid **(Figure 5.6I),** and L-Glutamine **(Figure 5.6J)** in PSC cells**.**

The results show that NDRG1 overexpression in PDAC cells affects the glycolysis and TCA cycle activity of PSC cells **(Figure 5.7)**.

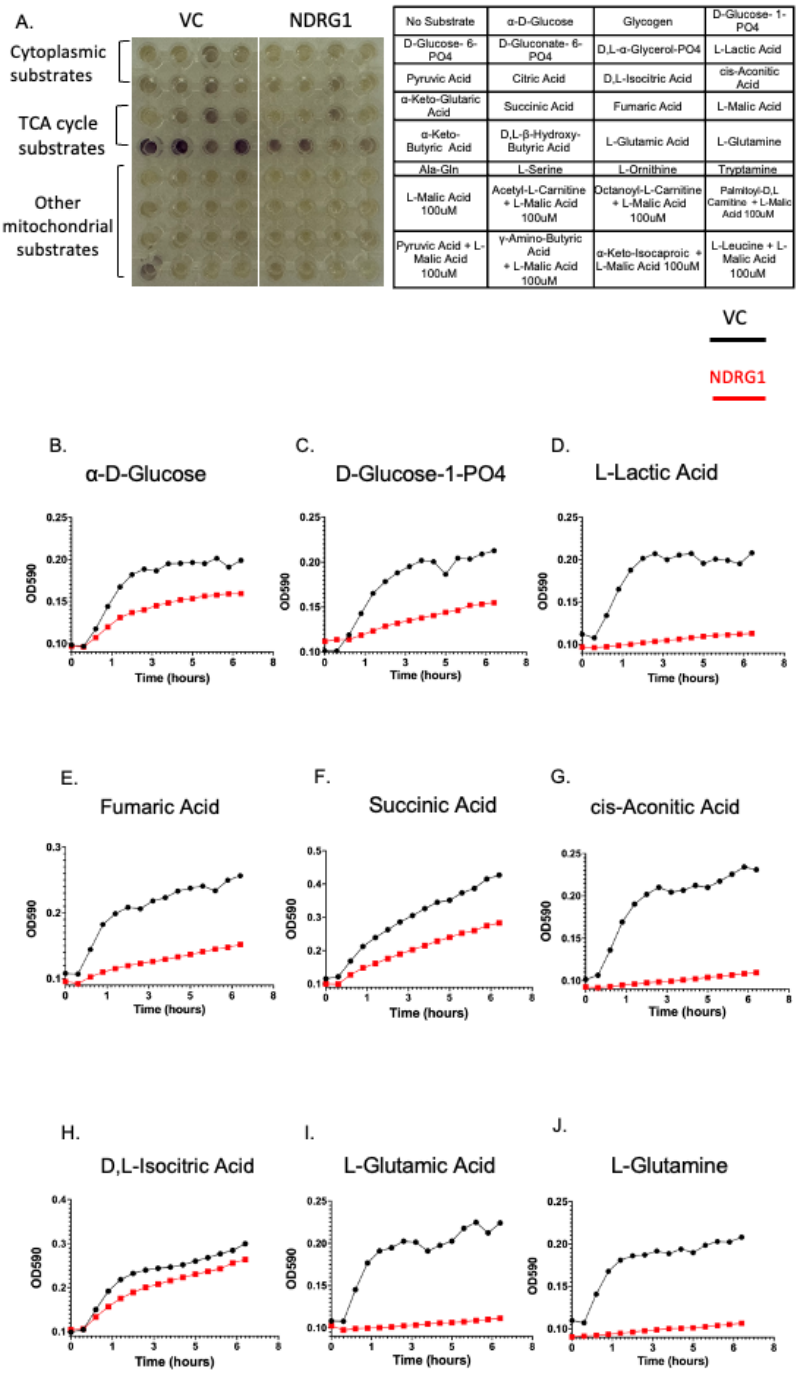

Figure 5.6: NDRG1 influences the mitochondrial metabolism of exposed PSCs to MIAPaCa-2 CM. PSCs spheroids were incubated with MIAPaCa-2 CM for 72h and then seeded into Mitoplate S-1 to be assessed by monitoring a colorimetric change at 590 nm at an interval of 30 minutes for 12 cycles using a kinetic plate reader. **(A)** Image of the plate layout after dye reduction, indicated by the purple colour formation in U937 macrophage cells. Kinetic graphs of D-Glucose **(B)**, D-Glucose-1-PO4 **(C)**, L-Lactic Acid **(D)**, Fumaric Acid **(E)**, Succinic Acid **(F)**, cis-Aconitic Acid **(G),** D, L-Isocitric Acid **(H),** L-Glutamic Acid **(I),** L-Glutamine **(J),** comparing PSCs cells exposed to MIAPaCa-2 VC (black) or NDRG1 (red) CM for 72 h prior to assay. The substrates were normalized to the no-substrate control or L-malic acid 100uM. The data presented is a representative analysis of the average of three independent experiments.

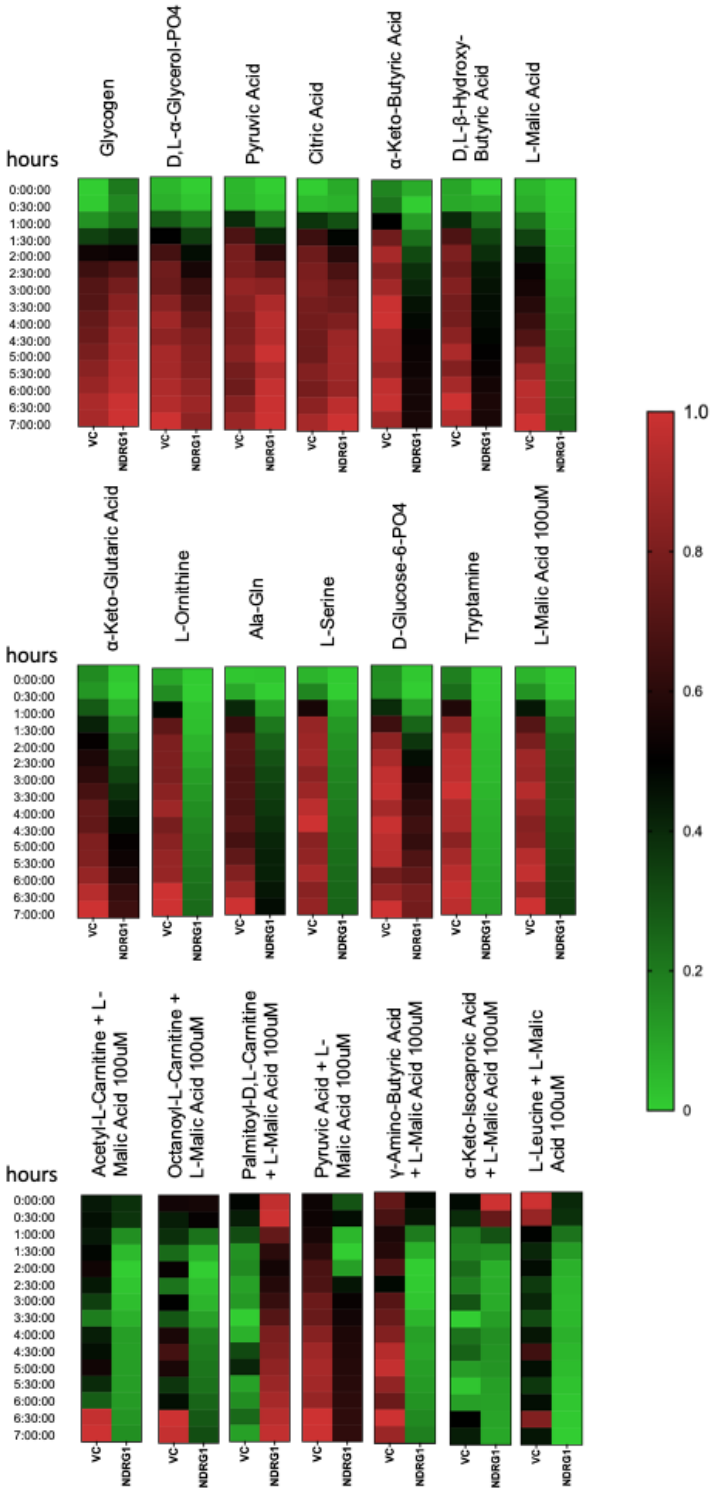

Figure 5.7: NDRG1 influences the mitochondrial metabolism of exposed PSCs to MIAPaCa-2 CM. PSCs spheroids were incubated with MIAPaCa-2 CM for 72h and then seeded into Mitoplate S-1 to be assessed by monitoring a colorimetric change at 590 nm at an interval of 30 minutes for 12 cycles using a kinetic plate reader. Heat maps for all remaining Mitoplate S-1 substrates comparing PSCs cells exposed to MIAPaCa-2 VC or NDRG1 CM for 72 h prior to assay. The substrates were normalized to the no-substrate control or L-malic acid 100uM. The data presented is a representative analysis of the average of three independent experiments.

5.3.4. NDRG1 impacts cross-talk between PDAC cells and PSCs/CAFs.

The results above demonstrate that NDRG1 can significantly influence the expression of various metabolic enzymes and influence the processing of numerous metabolic substrates. Knocking down branched-chain amino acid transaminase 2 (BCAT2) had a significant impact on impairing the proliferation of PDAC cells. Additionally, the proliferation of PDAC cells was greatly inhibited when branched-chain α-keto acid dehydrogenase A (BCKDHA) was knocked down [223]. PDAC cells secrete TGF-β, which activates SMAD5 in CAFs. This upregulates BCAT1 activity, leading to increased secretion of BCKAs, which are then provided to PDAC cells for BCAA synthesis [364]. To determine if NDRG1 influences the BCAA-mediated cross-talk between PDAC cells and PSCs, we conducted additional studies to analyze the expression of the BACC metabolism proteins, namely Smad5, BCAT1, BCAT2, BCKDH-E1α and P-BCKDH-E1α (Ser293) in a co-cultures of PANC-1 or MIAPaCa-2 cells with PSCs.

The results indicate that while Smad5 levels were unaffected, the expression of BCAT1 in the PANC-1 NDRG1 co-cultured with PSCs significantly decreased compared to the relevant PANC-1 VC cells. At the same time, the BCAT2, BCKDH-E1α and P-BCKDH-E1α (Ser293) were not significantly affected **(Figure 5.8)**. This suggests that NDRG1 reduced BCAT1 in PDAC cells.

Examining the PSCs co-cultured with PANC-1 NDRG1, the expression BCAT1 was increased compared to PSCs co-cultured with PANC-1 VC cells, while the other proteins in this pathway were not significantly affected **(Figure 5.8)**. This suggests that exposure to NDRG1-expressing PDAC cells may increase BCAA deamination in PSCs.

High Exposure HE
Low Exposure LE

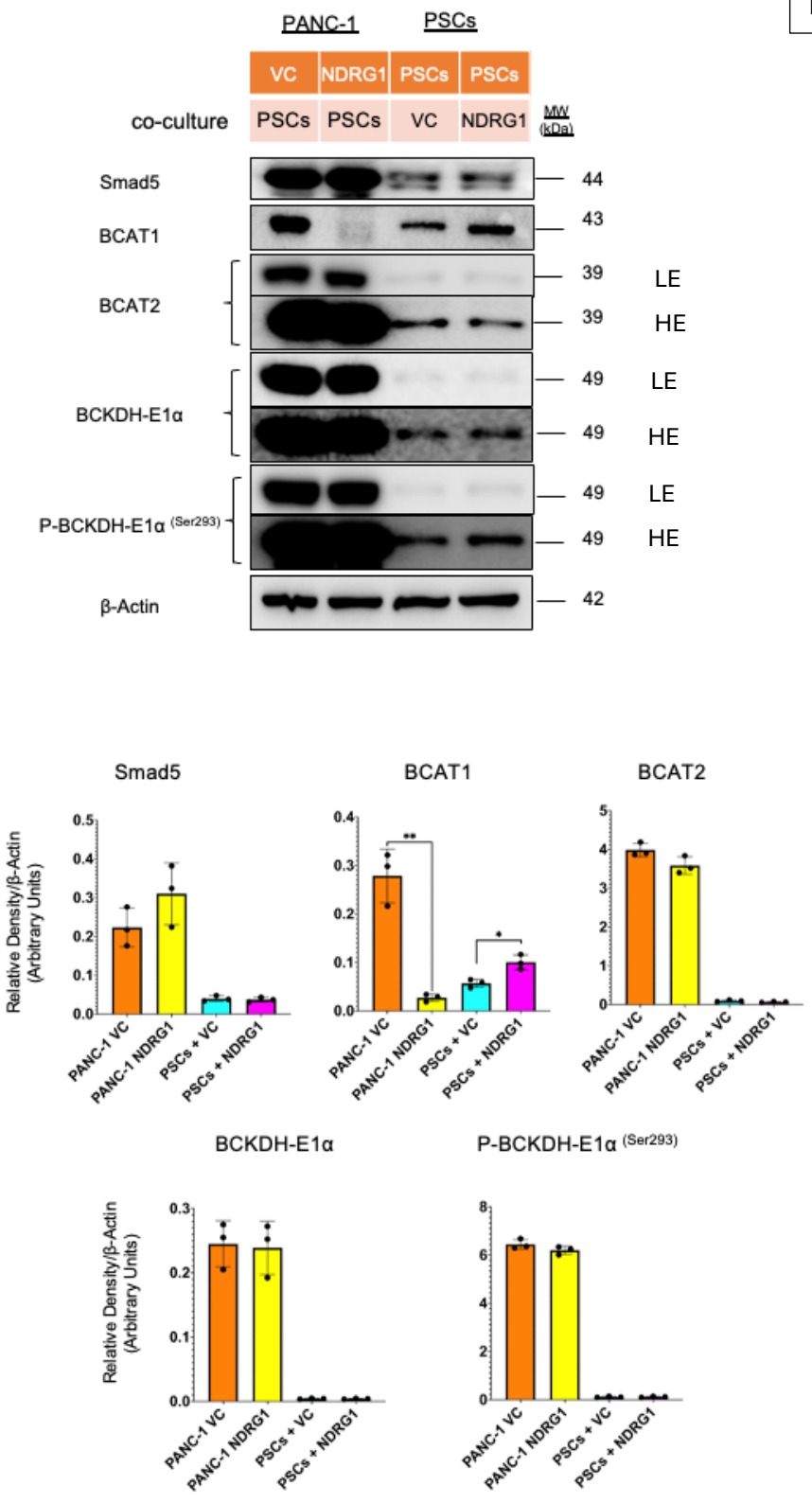

Figure 5.8: NDRG1 impacts the branched-chain amino acid metabolism of PANC-1 and PSCs co-culture. Western blots and densitometric analysis of Smad5, BCAT1, BCAT2, BCKDH-E1α and P-BCKDH-E1α (Ser293) in PANC-1 and PSCs co-culture. β-actin was used as a loading control. Results are mean ± SD (n = 3). Results are mean ± SD (n = 3). *p<0.05, **p<0.01 denote statistical significance comparing each condition to the VC control.

We observed similar results in MIAPaCa-2 cells. The findings indicate that the expression of BCAT1, BCAT2, BCKDH-E1α, and P-BCKDH-E1α (Ser293) in the MIAPaCa-2 NDRG1 cells co-cultured with PSCs were significantly reduced compared to the relevant MIAPaCa-2 VC cells **(Figure 5.9)**. Examining the PSC cells, we again observed that in PSCs co-cultured with MIAPaCa-2 NDRG1 cells, the expression of BCAT1 increased compared to PSCs co-cultured with MIAPaCa-2 VC cells **(Figure 5.9)**.

Overall, our findings suggest that NDRG1 reduces the expression of BCAT1 in PANC-1 and MIAPaCa-2 cells when co-cultured with PSCs, while it increases the expression of BCAT1 in PSCs cells. This suggests that NDRG1 might be influencing the BCAA-mediated cross-talk between PDAC cells and PSCs.

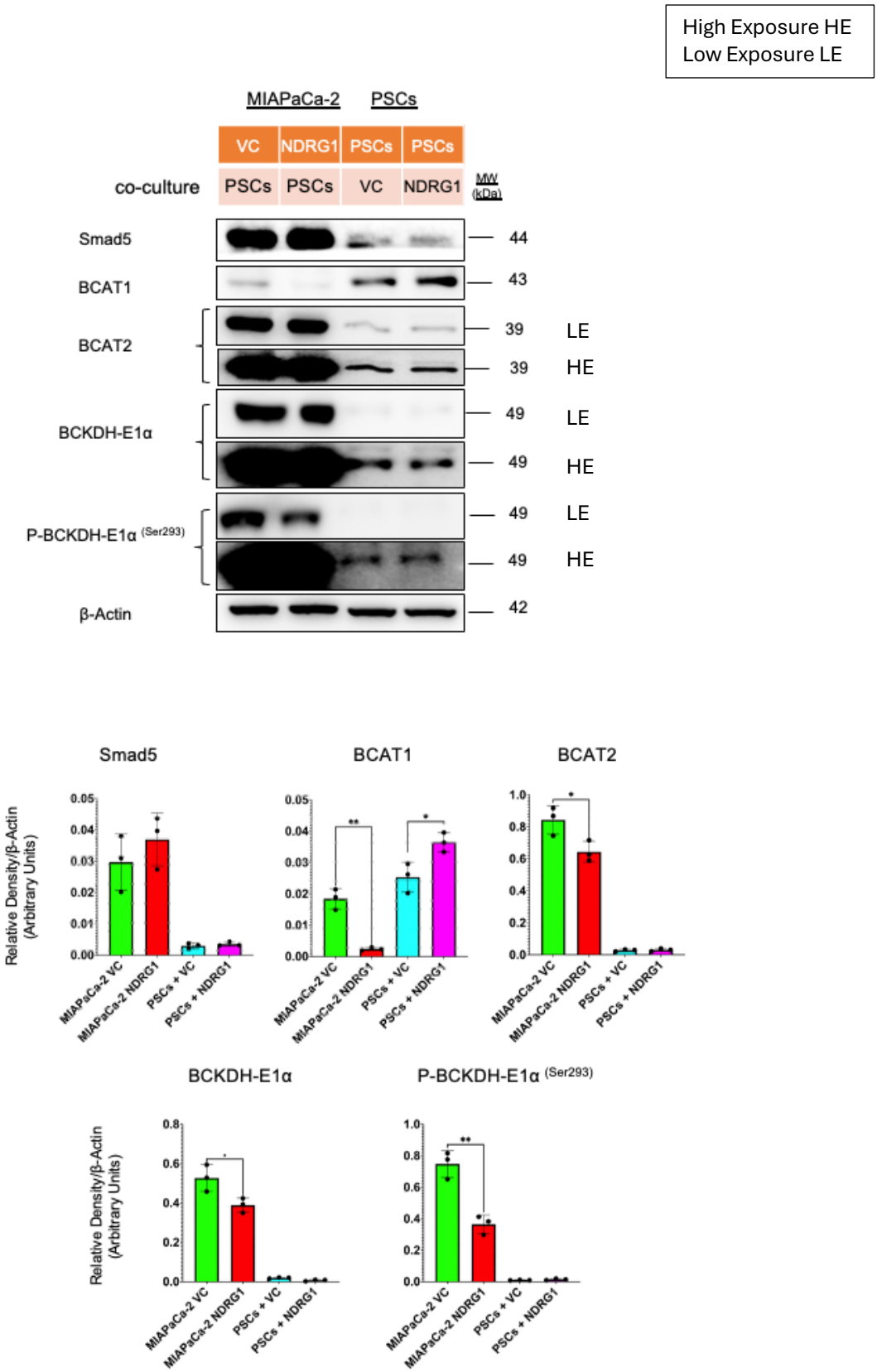

Figure 5.9: NDRG1 impacts the branched-chain amino acid metabolism of MIAPaCa-2 and PSCs co-culture. Western blots and densitometric analysis of smad5, BCAT1, BCAT2, BCKDH-E1α and P-BCKDH-E1α (Ser293) in MIAPaCa-2 and PSCs co-culture. β-actin was used as a loading control. Results are mean ± SD (n = 3). Results are mean ± SD (n = 3). *p<0.05, **p<0.01 denote statistical significance comparing each condition to the VC control.

5.4. Discussion

The reverse Warburg effect explains that CAFs can carry out glycolysis to generate pyruvate and lactate, which they can then provide to cancer cells for use in the mitochondrial tricarboxylic acid (TCA) cycle [210]. CAFs primarily rely on glycolysis as their main metabolic pathway due to the increased expression of Hypoxia-inducible factor 1-alpha (HIF-1α) and monocarboxylate transporter (MCT 4). On the other hand, they preferentially use glutamine for the TCA cycle. Unlike PDAC cells, CAFs can withstand glucose deprivation but are vulnerable to glutamine depletion [368]. Considering NDRG1's impact on PDAC cell metabolism (***Chapter 3)***, our research focused on examining its effect on metabolic cross-talk between PDAC cells and PSCs/CAFs.

PSCs play a vital role in the metabolism and progression of PDAC [369]. Higher levels of glutamine synthetase in both the tumour and stroma were individually predictive of a worse prognosis in PDAC patients. The glutamine that PSCs secrete boosted the basal OCR in PDAC cells. When glutamine synthetase was depleted in PSCs, PDAC proliferation significantly decreased [369]. Our study indicated that NDRG1 reduced the OCR and ECAR rates in PDAC-PSC co-culture spheroids, indicating reduced metabolic cross-talk between these cells. This was accompanied by the reduced ability of PSCs to metabolize a number of metabolic substrates after exposure to PDAC cells over-expressing NDRG1. Notably, glutamine and glutamic acid were among the metabolic substrates whose metabolism was dramatically reduced in PSCs following exposure to NDRG1 expressing PDAC cells *vs.* their VC counterparts. PSCs exposed to NDRG1 expressing PDAC cells also had a reduced ability to metabolise substrates involved in the glycolysis pathway (α-D-Glucose and D-Glucose-1-PO4), TCA cycle (fumaric, succinic acid and cis-aconitic acid) polyamine metabolism (L-ornithine), amino acids (e.g. tryptophan, serine, alanine) and fatty acid metabolism (acetyl-L-

carnitine, octanoyl-L-carnitine , and palmitoyl-D, L-carnitine) – suggesting that the ability of PSCs to act as metabolite-generating powerhouses was significantly impaired by NDRG1 expression. This is further evidence that NDRG1 functions to "break" the metabolic cross-talk between PDAC cells and PSCs and may reduce the ability of PDAC cells to re-program the PSC metabolism, thereby inhibiting the "reverse Warburg effect".

CAFs support the TCA cycle by supplying cancer cells with organic compounds such as lactate and pyruvate and amino acids such as alanine and glutamine, increasing mitochondrial activity [370]. In return, cancer cells trigger mitochondrial dysfunction in CAFs, along with mitophagy and ROS production, strengthening their reciprocal interaction [370].

Another key metabolic cross-talk pathway between PDAC cells and CAFs is the exchange of pyruvate and lactate. CAFs are often induced to undergo enhanced glycolysis to produce pyruvate and lactate, which they can then supply to cancer cells for use in the mitochondrial TCA cycle [210] . Our results indicated that NDRG1 disrupted this cross-talk, as evidenced by: ***(1)*** reduced ECAR in the NDRG1 PDAC-PSC co-culture spheroids demonstrating reduced glycolysis and lactic acid production; ***(2)*** reduced expression of TCA cycle enzymes in PDAC cells, suggesting that the utilization of PSC-derived metabolites would be impaired; ***(3)*** reduced OCR in the PDAC-PSC co-cultures further suggesting inhibition of the TCA cycle, and; ***(4)*** generally reduced potential of PSCs to metabolise numerous metabolic substrates following exposure to NDRG1-expressing PDAC cells, as shown by the mitoplate assay. The primary subclassification of cancer-associated fibroblasts (CAFs) in pancreatic ductal adenocarcinoma (PDAC) includes myCAFs (α-SMA+), iCAFs (α-SMA−, secreting IL-6), and apCAFs (MHC-II+) [371]. Therefore, future studies should evaluate the differences in effects between these phenotypes.

The uptake of BCAAs by cancer cells constitutes another pathway by which these cells can fuel their TCA cycle by scavenging leucine, isoleucine and valine from the TME. These BCAA's are subsequently transported into the mitochondria and deaminated by BCAT1, enabling their use in the TCA cycle and for the generation of nucleotides and lipids [372, 373]. The TGF-β/SMAD5 axis has a direct impact on BCAT1 in CAFs. It influences the uptake of the extracellular matrix from the tumour microenvironment, which provides amino acid precursors for the secretion of branched-chain ketoacids (BCKAs) by CAFs [364]. These BCKAs are then taken up by PDAC cells and oxidised by BCKDH to produce succinyl-CoA and acetyl-CoA that are used in the TCA cycle [364].

Our results indicate that NDRG1 reduced the expression of BCAT1 and BCAT2 in PDAC cells when co-cultured with PSCs, suggesting that the ability of these cancer cells to scavenge and metabolize BCAA's has been impaired. Conversely, NDRG1 increased the expression of BCAT1 in PSCs. This suggests that NDRG1-expressing cells are potentially enhancing the ability of PSCs to metabolise BCAAs, although the fate of these remains to be investigated. It is possible that these BCAAs are converted to BCKAs by the PSC cells and then secreted out into the TME – although our evidence suggests that they are not able to be utilized by the PDAC cells over-expressing NDRG1. It could be speculated that the increased BCKAs secreted by the PSCs could influence other cells in the PDAC TME, such as macrophages [374], although this requires further investigation.

In conclusion, following our observations that NDRG1 influenced PDAC cell metabolism and secretome (***Chapters 3 and 4***, respectively), we further demonstrate that this influences the

metabolic cross-talk with PSCs/CAFs, potentially reducing their ability to participate in the "reverse Warburg effect" and provide metabolic sustenance and support to PDAC cells.

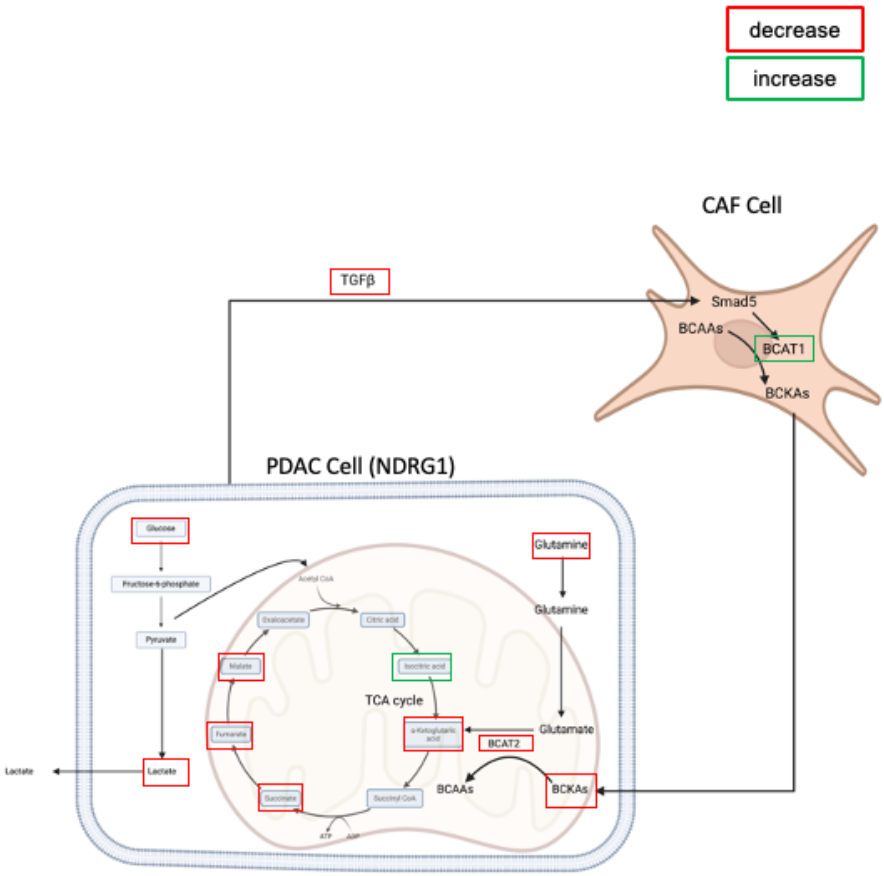

Figure 5.10: Schematic diagram demonstrating the impact of NDRG1 on the PDAC-PSCs metabolic cross-talk. Metabolites and metabolic enzymes in red are inhibited by NDRG1, while those in green as up-regulated/enhance by NDRG1 expression.

Chapter 6: General Discussion and Future Directions

6.1. Prelude

Several studies have shown that NDRG1 acts as a metastasis suppressor in pancreatic and other cancers [229, 375-377]. NDRG1 in PDAC inhibits oncogenic pathways associated with TGF-β and Wnt, which affect metastatic progression and the TME [184]. The novel anti-cancer agent DpC, which has undergone clinical trials, successfully enhanced NDRG1 levels, leading to a significant reduction in the growth and spread of PDAC in vivo. Additionally, it decreased the activation of PSCs and suppressed the production of ECM [205, 206]. Research indicates that the expression of NDRG1 can notably decrease the growth of PDAC in an in vivo orthotopic model. This implies that NDRG1 functions as a tumour suppressor by promoting apoptosis instead of directly affecting cell proliferation, showing no impact on cell cycle distribution [378]. A study has shown that Cap43 also referred to as NDRG1, plays a significant role in survival rates after radical surgery. The findings indicate that patients who do not express Cap43 tend to have worse prognoses compared to those with Cap43 expression [379]. Research suggests that NDRG1 may be a valuable diagnostic tool for evaluating the severity of pancreatic cancers, while enhanced protein characterization could help in determining the appropriate intensity for adjuvant therapy planning [380].The PDAC TME is known for its extensive fibrosis and hypo-vascularization, leading to significant intratumoral hypoxia. These factors contribute to its aggressiveness, resistance to therapy, and high mortality rate [381]. PDAC cells have been shown to alter metabolic processes, including those related to glucose, amino acids, and lipid metabolism. They rely on constant nourishment from the TME for their survival, growth, and invasion [217].

This project aimed to investigate the impact of NDRG1 on PDAC cell metabolism, its effect on the TME, and the metabolic cross-talk between PDAC cells and CAFs. Moreover, it examined how NDRG1 expression in PDAC cells influences macrophage polarization. The

research described in this thesis includes some fundamental and exciting discoveries, revealing that NDRG1 can markedly alter the metabolism of PDAC cells, as well the metabolic cross-talk with PSCs and macrophages that are exposed to these PDAC cells.

6.2 NDRG1 mediates the metabolic cross-talk between PDAC cells and PSCs

Given the extensive evidence demonstrating that NDRG1 significantly alters PDAC metabolism (as shown in ***Chapter 3***), it was imperative to investigate whether this would in turn interrupt the metabolic cross talk between PDAC cells and PSCs. Indeed, previous studies from our lab have shown that NDRG1 expression in PDAC cells can inhibit PSC activation, reducing the ability of exposed PSCs to produce ECM components such as collagen and tenascin C [205, 206].

The first crucial evidence that NDRG1 is also able to inhibit metabolic cross-talk between PDAC cells and PSC's came from ***Chapter 5***, where Seahorse analysis of co-cultured PDAC and PSC spheroids demonstrated that NDRG1 potently reduced both ECAR and OCR rates and significantly reduced the growth of these spheroids. Further investigation revealed that NDRG1 expression in PDAC cells was also able to alter the expression of metabolic enzymes in PSCs co-cultured with these PDAC cells. Specifically, the TCA cycle enzymes Fumerase, ACO2 and IDH1 were impacted. This was further validated by mitoplate analysis, which revealed that PSCs that had been exposed to NDRG1-expressing PDAC cells subsequently had significantly lower abilities to metabolize substrates such as glucose, TCA metabolites, amino acids and even fatty acids.

Investigating amino acid metabolism by PDAC cells revealed that over-expression of NDRG1 reduced the uptake of multiple amino acids, including BCAAs into PDAC cells by downregulating the expression of membrane transporters LAT1 and ASCT2. The uptake of essential amino acids *via* LAT1 plays a crucial role in tumour growth and proliferation by activating multiple signalling pathways, including the mTOR pathway [382, 383]. Interestingly, we found that NDRG1 could significantly inhibit the expression of ASCT2 and LAT1, leading to decreased BCAA uptake and inhibiting the mTORC1 pathway in PDAC cells.

Examining the effect of NDRG1 on BCAA metabolism when PDAC cells were co-cultured with PSCs revealed that NDRG1 reduces the expression of BCAT1 and BCAT2 in PDAC cells, while it increases the expression of BCAT1 in PSCs. These results suggest that NDRG1 potentially inhibits the exchange of BCAA's and its metabolites between PDAC cells and PSCs. Notably, the expression of ASCT2 and LAT1 in PDAC cells and PSCs when co-cultured were not examined and should be investigated in the future to gain a better insight into the exchange of BCAA and their metabolites between these cells. The increased BCAT1 in PSCs following exposure to NDRG1 expressing PDAC cells was an unexpected result that also requires further investigation. It is important to note that despite causing the PSCs to express more BCAT1, NDRG1 has generally a suppressive effect on both PSC and PDAC metabolism. This begs the question: what is the functional effect of increased BCAT1 in the PSCs and does this lead to more BCAA metabolites, such as BCKA, being secreted into the TME? This will be an important topic for future investigations, particularly as BCKAs in the TME could potentially also influence immune cells such as macrophages [374].

Another important mechanism of metabolic cross-talk between PDAC cells and PSC/CAFs is *via* the reverse Warburg effect, which leads to altered glycolysis. Glycolysis is crucial in enabling cancer cells to sustain their vigorous production of biological compounds and energy needs, potentially supporting the initiation of tumours, invasion, angiogenesis, and metastasis even in nutrient and oxygen deplete environments [153]. Immunohistochemical analysis of human PDAC specimens revealed that increased NDRG1 levels were associated with decreased HIF1α, indicating that NDRG1 functions as a suppressor of HIF1α in PDAC [198] .Therefore, our research focused on examining the effect of NDRG1 on the metabolism of PDAC cells under both normoxic and hypoxic conditions. In ***Chapter 3*** we show that the expression of NDRG1 in PDAC cells resulted in decreased expression of glycolysis enzymes GLUT1, HK2, and down-stream production of lactic acid, leading to lower ECAR rates in PDAC cells. Additionally, this was associated with a significant reduction in the number of TCA cycle enzymes, which suggests that the ability of PDAC cells to adapt to nutrient deprivation by scavenging metabolites such as glutamine and other amino acids and use them to replenish the TCA cycle is also impaired in response to NDRG1 over-expression. This suggests that NDRG1 makes PDAC cells less adaptable to conditions such as nutrient deprivation or hypoxic stress.

This was further evident when examining how PDAC cells responded to hypoxia. In ***Chapter 3*** it was also shown that in response to hypoxia, PDAC cells potently up-regulated metabolic enzymes involved in glycolysis and the TCA cycle including HK2, Fumerase and DLST. However, NDRG1 significantly inhibited this effect. In addition, the secretome analysis of PDAC cells in ***Chapter 4*** found that the secretion of a number of cytokines that were up-regulated in response to hypoxia in VC cells, were reduced by NDRG1 over-expression. These

included RANTES (CCL5) and IL-8, both of which are involved in driving metastasis and creating an immune suppressive TME [113, 384].

Overall, this thesis sheds new light on PDAC metabolic pathways and metabolic cross-talk with PSCs. It reveals previously unknown effects of NDRG1 on multiple metabolic pathways in PDAC cells and underscores its anti-cancer effects in this disease context.

6.3 NDRG1 expression in PDAC cells and its effect on macrophage metabolism and polarization

Tumour associated macrophages (TAMs) comprise 11% of the cellular components in the PDAC TME, being the main immune cell component, and are often polarized into the immune-suppressive M2 phenotype which supports angiogenesis and metastasis [73]. Another key discovery in this thesis is the ability of NDRG1 expression in PDAC cells to potently influence the polarization of TAMs. One previous study has suggested that NDRG1 expression is required for differentiation of bone marrow-derived macrophages into osteoclasts to support bone remodelling [385]. This latter study also found that NDRG1 enhanced differentiation of TAMs, although the mechanisms underlying these effects remained to be established.

In this thesis, we examined the effect of NDRG1 on macrophage polarization. We found that overexpressing NDRG1 in PDAC cells significantly changed monocyte differentiation, resulting in decreased M2 polarization and promoting an M1-like macrophage phenotype. This effect was found to be linked to macrophage metabolism, which was significantly impacted in response to NDRG1 expressing PDAC cells. Our findings in **Chapter 4** indicate that NDRG1 increased glycolysis in macrophages, which is consistent with an M1-macrophage metabolic phenotype [308]. On the other hand, OXPHOS, a feature of M2 macrophages, was reduced in

macrophages exposed to NDRG1 expressing PDAC cells. Our analysis into macrophage metabolism further revealed that macrophages exposed to NDRG1 expressing PDAC cells had reduced expression of Arg-1, while increasing iNOS. This suggests that NDRG1 changes how macrophages metabolise L-arginine, as this amino acid can either be converted to nitric oxide by iNOS to induce a cytotoxic effect (as occurs in M1 macrophages), or it can be converted into L-ornithine by Arg-1 to be used for polyamine metabolism and cell proliferation (as is common in M2 macrophages which over-express Arg-1; [308]).

These NDRG1-mediated effects on macrophage metabolism can be linked back to the altered metabolism of PDAC cells, as demonstrated in **Chapter 3**. For instance, NDRG1 was found to reduce glycolysis and ECAR in PDAC cultures, suggesting reduced lactate secretion into the TME. We also found that NDRG1 expression in PDAC cells reduced the secretion of succinate into the media. Both lactate and succinate have been reported to drive M2 polarization in TAMs [386]. Hence, this could be one mechanism by which NDRG1 expression in PDAC cells can alter the metabolism and polarization of exposed macrophages.

Another potential mechanism may involve the uptake of amino acids. In ***Chapter 3*** we demonstrate that NDRG1 significantly reduced the uptake of BCAAs and glutamine from the extracellular media. This was due to the reduced LAT1 and ASCT2 levels in the PDAC cells. Notably, glutamine and BCAAs are also required for macrophage activation into the cytotoxic M1 phenotype [387, 388]. When these amino acids are scarce, as they often are in the PDAC TME due to the enhanced cancer cell uptake, the M0 macrophages are converted into the M2 phenotype [387, 388]. Hence, by reducing the uptake of these crucial amino acids by PDAC cells, NDRG1 expression leads to more amino acids in the TME, which are then able to be used by macrophages to polarize into the M1 phenotype, as was demonstrated in ***Chapter 4***.

Besides the metabolic cross-talk, we also investigated the potential cytokines involved in the altered macrophage polarization by NDRG1. These results demonstrated that NDRG1 decreased the expression of MCP-1 and CCL2, while increasing the expression of TNF-α. TNF-α activates the NF-κB pathway, which is responsible for promoting M1 polarization and facilitating the production of pro-inflammatory cytokines like IL-12 [324]. These findings suggest the mechanism by which the expression of NDRG1 affects the polarization of macrophages towards the M1 phenotype also involved the altered secretion of key cytokines.

Finally, the polarization of macrophages has also recently been linked to CAFs, with CAF-derived cytokines inducing immunosuppression in PDAC [275, 371]. Considering our observations that NDRG1 inhibits the activation of PSCs into CAFs (***Chapter 5***), it is plausible that the effects on macrophage polarization are also in part mediated by the reduced CAF activation. Indeed, our co-culture spheroids consisting of PDAC cells, PSCs and monocytes demonstrated potent inhibition of M2 macrophage polarization. However, further studies are required to establish this experimentally, particularly under physiologically relevant conditions such as hypoxia.

6.4. Future Directions

6.4.1. Effect of NDRG1 on PDAC-PSCs cell cross-talk and macrophage polarization *in vivo*

The thesis demonstrates that NDRG1 expression in PDAC cells reduces monocyte polarization into the M2 macrophage phenotype and promotes the M1 phenotype. Additionally, NDRG1 expression affects the metabolism of PDAC and macrophage cells under both normoxia and hypoxia conditions, as well as the metabolic cross-talk between PDAC cells and PSCs. While

this study utilized 2 well-characterized commercial monocyte cell lines, namely THP-1 and U937, further studies are needed to validate these effects using fresh human blood-derived monocytes. This is particularly important as the THP-1 and U937 cells were derived from patients with leukaemia and lymphoma, respectively, and may not accurately represent the physiology of monocytes from healthy blood donors.

Further studies are needed to investigate the infiltration and polarization of monocytes in co-culture spheroids consisting of PDAC and CAF. This will involve using CD45 or CD68 as markers for immune cells and EpCAM as a marker for epithelial cells. The goal is to determine whether the macrophages that have been polarized to M1 or M2 types have infiltrated the spheroid or are merely surrounding it. However, the study did not assess whether NDRG1 can affect the PDAC-PSC cross-talk using *in vivo* models. Hence, further studies using immunocompetent *in vivo* models will be important to perform. This could be achieved using the murine PDAC cells derived from the KPC transgenic mouse model. These cells can be stably transfected to over-express NDRG1, or have NDRG1 silenced, and then used to establish orthotopic xenografts in the pancreas using methodology previously employed by our lab [205, 206]. The resulting tumours could then be analyzed not only for growth and metastasis, but also for the presence of different CAF subtypes and immune cells. Further research an in vivo experiment will be conducted using a syngeneic mouse model, where (mouse cells +/— NDRG1) will be implanted orthotopically into the pancreas. Following this, the mice will be treated with immunotherapy to determine whether the expression of NDRG1 in cancer cells influences the treatment response and affects immune cell infiltration into the tumour. Further research is required to explore how NDRG1 affects the expression of Cytotoxic T-lymphocyte antigen 4 (CTLA-4) and programmed cell death protein 1 (PD-1), as both are inhibitory immune checkpoints.

6.4.2. Further study of the effect of NDRG1 in hypoxia

The findings in this thesis showed that NDRG1 significantly changed the secretome of PDAC cells under hypoxia. This led to increased cytokines such as IFN-γ, MCP-1, FGF-9, and IL-16 in these cells. Additionally, NDRG1 resulted in a decrease in the expression of HIF-1α in PDAC cells under hypoxia. The study also explored the metabolic effect of NDRG1 in PDAC, the metabolic interaction between PDAC cells and CAFs, and macrophage metabolism in hypoxia compared to normoxia. As a result, further research is needed to understand the effect of NDRG1 in hypoxia, including co-culture spheroids under hypoxia, then performing metabolic analysis *via* Seahorse under hypoxic conditions, and performing direct and indirect co-culture under hypoxia, as hypoxia is an essential factor in the TME that contributes to the pathogenesis of PDAC [318].

6.4.3. Further study of the effect of NDRG1 on the LAT1 expression in PDAC-CAFs cross-talk

The findings of the thesis indicate that NDRG1 reduces the uptake of glutamine and BCAAs by PDAC cells through the suppression of both LAT1 and ASCT2 amino acid transporters. Additionally, the results demonstrate that NDRG1 decreases the expression of BCAT1 and BCAT2 in PDAC cells when they are co-cultured with PSCs. As a result, it is important to conduct further studies on the expression of LAT1 in CAF and PDAC in the future. Further studies are needed to examine the expression of these transporters in the PSCs and macrophages co-cultured with PDAC cells. This will help us understand whether BCAAs are transferred from one cell type to another. Additionally, the downstream mTOR signalling pathways in PSC and macrophages exposed to PDAC cells should also be investigated.

PDAC remains a largely incurable disease, with rapid development of resistance to standard therapies. A key factor driving this resistance is the extensive metabolic re-wiring of the PDAC TME, which supports tumour growth and metastasis while suppressing the immune response. This thesis demonstrates that NDRG1 expression in PDAC cells reduces monocyte polarization into the M2 macrophage phenotype and promotes the M1 phenotype. Furthermore, NDRG1 expression affects the metabolism of PDAC and macrophage cells under both normoxia and hypoxia conditions, as well as the metabolic cross-talk between PDAC cells and PSCs. However, further studies are needed to validate these effects using in vivo models.

Chapter 7: References

1. Standring, S., *Gray's Anatomy : The Anatomical Basis of Clinical Practice*. 41 ed. Gray's Anatomy. 2016: Elsevier Health Sciences.
2. Beger, H.G., et al., *The Pancreas : An Integrated Textbook of Basic Science, Medicine, and Surgery*. 2018, Newark, UNITED KINGDOM: John Wiley & Sons, Incorporated.
3. Kleeff, J., et al., *Pancreatic cancer*. Nature Reviews Disease Primers, 2016. **2**(1): p. 16022.
4. Kallis, Y.N. and D. Westaby, *Physiology and function of the pancreas*. 2014, John Wiley & Sons, Ltd: Oxford. p. 33-35.
5. Hu, J.-X., et al., *Pancreatic cancer: A review of epidemiology, trend, and risk factors*. World journal of gastroenterology, 2021. **27**(27): p. 4298-4321.
6. Klein, A.P., *Pancreatic cancer epidemiology: understanding the role of lifestyle and inherited risk factors*. Nature Reviews Gastroenterology & Hepatology, 2021: p. 1-10.
7. Ren, B., et al., *Tumor microenvironment participates in metastasis of pancreatic cancer*. Molecular cancer, 2018. **17**(1): p. 108-108.
8. Jin, C. and L. Bai, *Pancreatic Cancer–Current Situation and Challenges*. Gastroenterol Hepatol Lett, 2020. **2**(1): p. 1-3.
9. Ghaneh, P., E. Costello, and J.P. Neoptolemos, *Biology and management of pancreatic cancer*. Gut, 2007. **56**(8): p. 1134-52.
10. Pourshams, A., et al., *The global, regional, and national burden of pancreatic cancer and its attributable risk factors in 195 countries and territories, 1990–2017: a systematic analysis for the Global Burden of Disease Study 2017*. The Lancet Gastroenterology & Hepatology, 2019. **4**(12): p. 934-947.
11. Bosetti, C., et al., *Cigarette smoking and pancreatic cancer: an analysis from the International Pancreatic Cancer Case-Control Consortium (Panc4)*. Annals of Oncology, 2012. **23**(7): p. 1880-1888.
12. Xu, M., et al., *Obesity and Pancreatic Cancer: Overview of Epidemiology and Potential Prevention by Weight Loss*. Pancreas, 2018. **47**(2): p. 158-162.
13. Arslan, A.A., et al., *Anthropometric measures, body mass index, and pancreatic cancer: a pooled analysis from the Pancreatic Cancer Cohort Consortium (PanScan)*. Archives of internal medicine, 2010. **170**(9): p. 791-802.
14. Huang, B.Z., et al., *New-Onset Diabetes, Longitudinal Trends in Metabolic Markers, and Risk of Pancreatic Cancer in a Heterogeneous Population*. Clinical gastroenterology and hepatology, 2020. **18**(8): p. 1812-1821.e7.
15. Li, D., et al., *Diabetes and risk of pancreatic cancer: a pooled analysis of three large case-control studies*. Cancer causes & control : CCC, 2011. **22**(2): p. 189-197.
16. Ohmoto, A., S. Yachida, and C. Morizane, *Genomic features and clinical management of patients with hereditary pancreatic cancer syndromes and familial pancreatic cancer*. International journal of molecular sciences, 2019. **20**(3): p. 561.
17. Kirkegård, J., et al., *Acute Pancreatitis and Pancreatic Cancer Risk: A Nationwide Matched-Cohort Study in Denmark*. Gastroenterology (New York, N.Y. 1943), 2018. **154**(6): p. 1729-1736.

18. Rijkers, A.P., et al., *Risk of Pancreatic Cancer After a Primary Episode of Acute Pancreatitis*. Pancreas, 2017. **46**(8): p. 1018-1022.
19. DePinho, R.A. and N. Bardeesy, *Pancreatic cancer biology and genetics*. Nature reviews. Cancer, 2002. **2**(12): p. 897-909.
20. Ungkulpasvich, U., et al., *Pancreatic Cancer and Detection Methods*. Biomedicines, 2023. **11**(9).
21. Borazanci, E., et al., *Adenosquamous carcinoma of the pancreas: Molecular characterization of 23 patients along with a literature review*. World J Gastrointest Oncol, 2015. **7**(9): p. 132-40.
22. Su, G.H., *Pancreatic Cancer Methods and Protocols*. 3rd ed. 2019. ed. Methods in Molecular Biology, 1882. 2019, New York, NY: Springer New York.
23. Neoptolemos, J.P., et al., *Pancreatic Cancer*. 2010, New York, NY: Springer New York.
24. Vincent, A., et al., *Pancreatic cancer*. Lancet (London, England), 2011. **378**(9791): p. 607-620.
25. Bazzichetto, C., et al., *From Genetic Alterations to Tumor Microenvironment: The Ariadne's String in Pancreatic Cancer*. Cells, 2020. **9**(2): p. 309.
26. Murphy, S.J., et al., *Genetic alterations associated with progression from pancreatic intraepithelial neoplasia to invasive pancreatic tumor*. Gastroenterology, 2013. **145**(5): p. 1098-1109.e1.
27. Hong, S.-M., et al., *Genome-wide somatic copy number alterations in low-grade PanINs and IPMNs from individuals with a family history of pancreatic cancer*. Clinical cancer research : an official journal of the American Association for Cancer Research, 2012. **18**(16): p. 4303-4312.
28. Bailey, P., et al., *Genomic analyses identify molecular subtypes of pancreatic cancer*. Nature, 2016. **531**(7592): p. 47-52.
29. Yachida, S., et al., *Clinical significance of the genetic landscape of pancreatic cancer and implications for identification of potential long-term survivors*. Clin Cancer Res, 2012. **18**(22): p. 6339-47.
30. Bannoura, S.F., et al., *Targeting KRAS in pancreatic cancer: new drugs on the horizon*. Cancer and Metastasis Reviews, 2021: p. 1-17.
31. Prior, I.A., P.D. Lewis, and C. Mattos, *A comprehensive survey of Ras mutations in cancer*. Cancer research, 2012. **72**(10): p. 2457-2467.
32. Pylayeva-Gupta, Y., E. Grabocka, and D. Bar-Sagi, *RAS oncogenes: weaving a tumorigenic web*. Nature reviews. Cancer, 2011. **11**(11): p. 761-774.
33. Hong, D.S., et al., *KRAS(G12C) Inhibition with Sotorasib in Advanced Solid Tumors*. N Engl J Med, 2020. **383**(13): p. 1207-1217.
34. Hallin, J., et al., *The KRAS(G12C) Inhibitor MRTX849 Provides Insight toward Therapeutic Susceptibility of KRAS-Mutant Cancers in Mouse Models and Patients*. Cancer Discov, 2020. **10**(1): p. 54-71.
35. Luo, J., *KRAS mutation in pancreatic cancer*. Seminars in oncology, 2021.
36. Chan, S.H., J. Chiang, and J. Ngeow, *CDKN2A germline alterations and the relevance of genotype-phenotype associations in cancer predisposition*. Hereditary Cancer in Clinical Practice, 2021. **19**(1): p. 21.
37. Stefanoudakis, D., et al., *Significance of TP53, CDKN2A, SMAD4 and KRAS in Pancreatic Cancer*. Current Issues in Molecular Biology, 2024. **46**(4): p. 2827-2844.

38. Kimura, H., et al., *The Role of Inherited Pathogenic CDKN2A Variants in Susceptibility to Pancreatic Cancer*. Pancreas, 2021. **50**(8): p. 1123-1130.
39. Bruce, J.L., et al., *Requirements for Cell Cycle Arrest by p16INK4a*. Molecular Cell, 2000. **6**(3): p. 737-742.
40. Schutte, M., et al., *Abrogation of the Rb/p16 tumor-suppressive pathway in virtually all pancreatic carcinomas*. Cancer research, 1997. **57**(15): p. 3126-3130.
41. Maitra, A., S.E. Kern, and R.H. Hruban, *Molecular pathogenesis of pancreatic cancer*. Best Practice & Research Clinical Gastroenterology, 2006. **20**(2): p. 211-226.
42. Bertoli, C., J.M. Skotheim, and R.A.M. de Bruin, *Control of cell cycle transcription during G1 and S phases*. Nature reviews. Molecular cell biology, 2013. **14**(8): p. 518-528.
43. Ozenne, P., et al., *The ARF tumor suppressor: Structure, functions and status in cancer*. International Journal of Cancer, 2010. **127**(10): p. 2239-2247.
44. Ko, A., S.Y. Han, and J. Song, *Dynamics of ARF regulation that control senescence and cancer*. BMB Rep, 2016. **49**(11): p. 598-606.
45. Yachida, S. and C. Iacobuzio-Donahue, *Evolution and dynamics of pancreatic cancer progression*. Oncogene, 2013. **32**(45): p. 5253-5260.
46. Bieging, K.T., S.S. Mello, and L.D. Attardi, *Unravelling mechanisms of p53-mediated tumour suppression*. Nature reviews. Cancer, 2014. **14**(5): p. 359-370.
47. Latres, E., et al., *Chromosome 17 abnormalities and TP53 mutations in adult soft tissue sarcomas*. The American journal of pathology, 1994. **145**(2): p. 345-355.
48. Redston, M.S., et al., *p53 mutations in pancreatic carcinoma and evidence of common involvement of homocopolymer tracts in DNA microdeletions*. Cancer research, 1994. **54**(11): p. 3025-3033.
49. Pellegata, N., et al., *K-ras and p53 gene mutations in pancreatic cancer: ductal and nonductal tumors progress through different genetic lesions*. Cancer research, 1994. **54**(6): p. 1556-1560.
50. Yang, Y., et al., *Small molecule inhibitors of HDM2 ubiquitin ligase activity stabilize and activate p53 in cells*. Cancer Cell, 2005. **7**(6): p. 547-559.
51. de Snoo, F.A. and N.K. Hayward, *Cutaneous melanoma susceptibility and progression genes*. Cancer Letters, 2005. **230**(2): p. 153-186.
52. Hruban, R.H., et al., *Tumor-suppressor genes in pancreatic cancer*. Journal of hepato-biliary-pancreatic surgery, 1998. **5**(4): p. 383-391.
53. Tascilar, M., et al., *The SMAD4 protein and prognosis of pancreatic ductal adenocarcinoma*. Clinical Cancer Research, 2001. **7**(12): p. 4115-4121.
54. Visani, M., et al., *Molecular alterations in pancreatic tumors*. World journal of gastroenterology, 2021. **27**(21): p. 2710-2726.
55. Siegel, P.M. and J. Massagué, *Cytostatic and apoptotic actions of TGF-β in homeostasis and cancer*. Nature Reviews Cancer, 2003. **3**(11): p. 807-820.
56. Ahmed, S., et al., *The TGF-β/Smad4 Signaling Pathway in Pancreatic Carcinogenesis and Its Clinical Significance*. Journal of clinical medicine, 2017. **6**(1): p. 5.
57. Qian, Y., et al., *Molecular alterations and targeted therapy in pancreatic ductal adenocarcinoma*. Journal of hematology & oncology, 2020. **13**(1): p. 130-130.

58. Dai, C., et al., *SMAD4 represses FOSL1 expression and pancreatic cancer metastatic colonization*. Cell Reports, 2021. **36**(4): p. 109443.
59. Dougan, S.K., *The pancreatic cancer microenvironment*. The Cancer Journal, 2017. **23**(6): p. 321-325.
60. Murakami, T., et al., *Role of the tumor microenvironment in pancreatic cancer*. Annals of gastroenterological surgery, 2019. **3**(2): p. 130-137.
61. Xue, R., et al., *A Rising Star in Pancreatic Diseases: Pancreatic Stellate Cells*. Frontiers in physiology, 2018. **9**: p. 754-754.
62. Apte, M.V., et al., *Periacinar stellate shaped cells in rat pancreas: identification, isolation, and culture*. Gut, 1998. **43**(1): p. 128-133.
63. Apte, M.V., R.C. Pirola, and J.S. Wilson, *Pancreatic stellate cells: a starring role in normal and diseased pancreas*. Frontiers in physiology, 2012. **3**: p. 344-344.
64. Masamune, A., et al., *Roles of pancreatic stellate cells in pancreatic inflammation and fibrosis*. Clinical Gastroenterology and Hepatology, 2009. **7**(11): p. S48-S54.
65. McCarroll, J.A., et al., *Vitamin A inhibits pancreatic stellate cell activation: implications for treatment of pancreatic fibrosis*. Gut, 2006. **55**(1): p. 79-89.
66. Ene-Obong, A., et al., *Activated pancreatic stellate cells sequester CD8+ T cells to reduce their infiltration of the juxtatumoral compartment of pancreatic ductal adenocarcinoma*. Gastroenterology, 2013. **145**(5): p. 1121-32.
67. Lunardi, S., et al., *IP-10/CXCL10 induction in human pancreatic cancer stroma influences lymphocytes recruitment and correlates with poor survival*. Oncotarget, 2014. **5**(22): p. 11064-80.
68. Sun, Q., et al., *The impact of cancer-associated fibroblasts on major hallmarks of pancreatic cancer*. Theranostics, 2018. **8**(18): p. 5072-5087.
69. Sperb, N., M. Tsesmelis, and T. Wirth, *Crosstalk between Tumor and Stromal Cells in Pancreatic Ductal Adenocarcinoma*. International journal of molecular sciences, 2020. **21**(15): p. 5486.
70. Guo, T. and J. Xu, *Cancer-associated fibroblasts: a versatile mediator in tumor progression, metastasis, and targeted therapy*. Cancer and Metastasis Reviews, 2024.
71. Biffi, G., et al., *IL1-Induced JAK/STAT Signaling Is Antagonized by TGFβ to Shape CAF Heterogeneity in Pancreatic Ductal Adenocarcinoma*. Cancer discovery, 2019. **9**(2): p. 282-301.
72. Huang, H., et al., *Mesothelial cell-derived antigen-presenting cancer-associated fibroblasts induce expansion of regulatory T cells in pancreatic cancer*. Cancer Cell, 2022. **40**(6): p. 656-673.e7.
73. Peng, J., et al., *Single-cell RNA-seq highlights intra-tumoral heterogeneity and malignant progression in pancreatic ductal adenocarcinoma*. Cell Res, 2019. **29**(9): p. 725-738.
74. Choi, J.-I., et al., *Cancer-initiating cells in human pancreatic cancer organoids are maintained by interactions with endothelial cells*. Cancer Letters, 2021. **498**: p. 42-53.
75. Katsuta, E., et al., *Pancreatic adenocarcinomas with mature blood vessels have better overall survival*. Scientific reports, 2019. **9**(1): p. 1-11.
76. Gordon, S., *Alternative activation of macrophages*. Nature reviews immunology, 2003. **3**(1): p. 23-35.

77. Barros, M.H.M., et al., *Macrophage Polarisation: an Immunohistochemical Approach for Identifying M1 and M2 Macrophages*. PLOS ONE, 2013. **8**(11): p. e80908.
78. Yu, M., et al., *Prognostic value of tumor-associated macrophages in pancreatic cancer: a meta-analysis*. Cancer management and research, 2019. **11**: p. 4041-4058.
79. Yang, S., Q. Liu, and Q. Liao, *Tumor-Associated Macrophages in Pancreatic Ductal Adenocarcinoma: Origin, Polarization, Function, and Reprogramming*. Front Cell Dev Biol, 2020. **8**: p. 607209.
80. Glazer, E.S., et al., *Effect of macrophages on pancreatic cancer*. Journal of clinical oncology, 2018. **36**(4_suppl): p. 324-324.
81. Xiong, C., et al., *Tumor-associated macrophages promote pancreatic ductal adenocarcinoma progression by inducing epithelial-to-mesenchymal transition*. Aging (Albany NY), 2021. **13**(3): p. 3386-3404.
82. Boltjes, A. and F. van Wijk, *Human dendritic cell functional specialization in steady-state and inflammation*. Frontiers in immunology, 2014. **5**: p. 131-131.
83. Deicher, A., et al., *Targeting dendritic cells in pancreatic ductal adenocarcinoma*. Cancer cell international, 2018. **18**: p. 85-85.
84. Palucka, K. and J. Banchereau, *Cancer immunotherapy via dendritic cells*. Nature reviews. Cancer, 2012. **12**(4): p. 265-277.
85. Caligiuri, M.A., *Human natural killer cells*. Blood, 2008. **112**(3): p. 461-469.
86. Cooper, M.A., T.A. Fehniger, and M.A. Caligiuri, *The biology of human natural killer-cell subsets*. Trends in immunology, 2001. **22**(11): p. 633-640.
87. Kumar, S., *Natural killer cell cytotoxicity and its regulation by inhibitory receptors*. Immunology, 2018. **154**(3): p. 383-393.
88. Marcon, F., et al., *NK cells in pancreatic cancer demonstrate impaired cytotoxicity and a regulatory IL-10 phenotype*. Oncoimmunology, 2020. **9**(1): p. 1845424-1845424.
89. Lee, H.S., et al., *Peripheral natural killer cell activity is associated with poor clinical outcomes in pancreatic ductal adenocarcinoma*. Journal of Gastroenterology and Hepatology, 2021. **36**(2): p. 516-522.
90. Bergenfelz, C., et al., *Systemic Monocytic-MDSCs Are Generated from Monocytes and Correlate with Disease Progression in Breast Cancer Patients*. PLOS ONE, 2015. **10**(5): p. e0127028.
91. Zhang, B., et al., *Circulating and Tumor-Infiltrating Myeloid-Derived Suppressor Cells in Patients with Colorectal Carcinoma*. PLOS ONE, 2013. **8**(2): p. e57114.
92. Gabrilovich, D.I. and S. Nagaraj, *Myeloid-derived suppressor cells as regulators of the immune system*. Nature reviews. Immunology, 2009. **9**(3): p. 162-174.
93. Youn, J.-I., et al., *Subsets of myeloid-derived suppressor cells in tumor-bearing mice*. Journal of immunology (Baltimore, Md. : 1950), 2008. **181**(8): p. 5791-5802.
94. Pergamo, M. and G. Miller, *Myeloid-derived suppressor cells and their role in pancreatic cancer*. Cancer gene therapy, 2017. **24**(3): p. 100-105.
95. Johnson, B.A., 3rd, et al., *Strategies for Increasing Pancreatic Tumor Immunogenicity*. Clinical cancer research : an official journal of the American Association for Cancer Research, 2017. **23**(7): p. 1656-1669.

96. Chang, J.H., Y. Jiang, and V.G. Pillarisetty, *Role of immune cells in pancreatic cancer from bench to clinical application: An updated review*. Medicine, 2016. **95**(49): p. e5541-e5541.
97. Wang, R.-F., *The role of MHC class II-restricted tumor antigens and CD4+ T cells in antitumor immunity*. Trends in Immunology, 2001. **22**(5): p. 269-276.
98. Mosmann, T.R., et al., *Two types of murine helper T cell clone. I. Definition according to profiles of lymphokine activities and secreted proteins*. The Journal of Immunology, 1986. **136**(7): p. 2348.
99. Suzuki, D., et al., *Effects of perioperative immunonutrition on cell-mediated immunity, T helper type 1 (Th1)/Th2 differentiation, and Th17 response after pancreaticoduodenectomy*. Surgery, 2010. **148**(3): p. 573-581.
100. De Monte, L., et al., *Intratumor T helper type 2 cell infiltrate correlates with cancer-associated fibroblast thymic stromal lymphopoietin production and reduced survival in pancreatic cancer*. The Journal of experimental medicine, 2011. **208**(3): p. 469-478.
101. Fogar, P., et al., *Pancreatic cancer alters human CD4+ T lymphocyte function: a piece in the immune evasion puzzle*. Pancreas, 2011. **40**(7): p. 1131-1137.
102. Wörmann, S., et al., *The immune network in pancreatic cancer development and progression*. Oncogene, 2014. **33**(23): p. 2956-2967.
103. McLane, L.M., M.S. Abdel-Hakeem, and E.J. Wherry, *CD8 T cell exhaustion during chronic viral infection and cancer*. Annual review of immunology, 2019. **37**: p. 457-495.
104. Hiraoka, N., et al., *Prevalence of FOXP3+ regulatory T cells increases during the progression of pancreatic ductal adenocarcinoma and its premalignant lesions*. Clinical Cancer Research, 2006. **12**(18): p. 5423-5434.
105. Dong, H., et al., *Tumor-associated B7-H1 promotes T-cell apoptosis: a potential mechanism of immune evasion*. Nature medicine, 2002. **8**(8): p. 793-800.
106. Soares, K.C., et al., *PD-1/PD-L1 blockade together with vaccine therapy facilitates effector T-cell infiltration into pancreatic tumors*. Journal of immunotherapy (Hagerstown, Md. : 1997), 2015. **38**(1): p. 1-11.
107. Ryschich, E., et al., *Control of T-cell–mediated immune response by HLA class I in human pancreatic carcinoma*. Clinical cancer research, 2005. **11**(2): p. 498-504.
108. Thomas, D.A. and J. Massagué, *TGF-β directly targets cytotoxic T cell functions during tumor evasion of immune surveillance*. Cancer cell, 2005. **8**(5): p. 369-380.
109. Carstens, J.L., et al., *Spatial computation of intratumoral T cells correlates with survival of patients with pancreatic cancer*. Nature communications, 2017. **8**: p. 15095-15095.
110. Fukunaga, A., et al., *CD8+ tumor-infiltrating lymphocytes together with CD4+ tumor-infiltrating lymphocytes and dendritic cells improve the prognosis of patients with pancreatic adenocarcinoma*. Pancreas, 2004. **28**(1): p. e26-e31.
111. Curiel, T.J., et al., *Specific recruitment of regulatory T cells in ovarian carcinoma fosters immune privilege and predicts reduced survival*. Nature medicine, 2004. **10**(9): p. 942-949.

112. Liyanage, U.K., et al., *Prevalence of regulatory T cells is increased in peripheral blood and tumor microenvironment of patients with pancreas or breast adenocarcinoma*. The Journal of Immunology, 2002. **169**(5): p. 2756-2761.
113. Tan, M.C.B., et al., *Disruption of CCR5-dependent homing of regulatory T cells inhibits tumor growth in a murine model of pancreatic cancer*. Journal of immunology (Baltimore, Md. : 1950), 2009. **182**(3): p. 1746-1755.
114. Tewari, N., et al., *The presence of tumour-associated lymphocytes confers a good prognosis in pancreatic ductal adenocarcinoma: an immunohistochemical study of tissue microarrays*. BMC cancer, 2013. **13**: p. 436-436.
115. Koizumi, M., et al., *Increased B cell-activating factor promotes tumor invasion and metastasis in human pancreatic cancer*. PloS one, 2013. **8**(8): p. e71367-e71367.
116. Pylayeva-Gupta, Y., et al., *IL35-Producing B Cells Promote the Development of Pancreatic Neoplasia*. Cancer discovery, 2016. **6**(3): p. 247-255.
117. Truong, L.-H. and S. Pauklin, *Pancreatic Cancer Microenvironment and Cellular Composition: Current Understandings and Therapeutic Approaches*. Cancers, 2021. **13**(19): p. 5028.
118. Lu, P., V.M. Weaver, and Z. Werb, *The extracellular matrix: a dynamic niche in cancer progression*. The Journal of cell biology, 2012. **196**(4): p. 395-406.
119. Perez, V.M., J.F. Kearney, and J.J. Yeh, *The PDAC Extracellular Matrix: A Review of the ECM Protein Composition, Tumor Cell Interaction, and Therapeutic Strategies*. Frontiers in oncology, 2021. **11**: p. 751311-751311.
120. Wang, D., et al., *The Extracellular Matrix: A Key Accomplice of Cancer Stem Cell Migration, Metastasis Formation, and Drug Resistance in PDAC*. Cancers (Basel), 2022. **14**(16).
121. Ferrara, B., et al., *The Extracellular Matrix in Pancreatic Cancer: Description of a Complex Network and Promising Therapeutic Options*. Cancers, 2021. **13**(17): p. 4442.
122. Holle, A.W., J.L. Young, and J.P. Spatz, *In vitro cancer cell–ECM interactions inform in vivo cancer treatment*. Advanced Drug Delivery Reviews, 2016. **97**: p. 270-279.
123. Lu, P., et al., *Extracellular matrix degradation and remodeling in development and disease*. Cold Spring Harb Perspect Biol, 2011. **3**(12).
124. Daley, W.P., S.B. Peters, and M. Larsen, *Extracellular matrix dynamics in development and regenerative medicine*. Journal of Cell Science, 2008. **121**(3): p. 255-264.
125. Franchi, M., et al., *Extracellular matrix biomechanical roles and adaptation in health and disease*. The FEBS Journal, 2024. **291**(3): p. 430-440.
126. Geiger, B. and K.M. Yamada, *Molecular architecture and function of matrix adhesions*. Cold Spring Harb Perspect Biol, 2011. **3**(5).
127. Wolfenson, H., I. Lavelin, and B. Geiger, *Dynamic regulation of the structure and functions of integrin adhesions*. Dev Cell, 2013. **24**(5): p. 447-58.
128. Liang, D., et al., *Targeting extracellular matrix through phytochemicals: a promising approach of multi-step actions on the treatment and prevention of cancer*. Front Pharmacol, 2023. **14**: p. 1186712.
129. Barker, H.E., T.R. Cox, and J.T. Erler, *The rationale for targeting the LOX family in cancer*. Nature Reviews Cancer, 2012. **12**(8): p. 540-552.

130. Levental, K.R., et al., *Matrix crosslinking forces tumor progression by enhancing integrin signaling.* Cell, 2009. **139**(5): p. 891-906.
131. Phillips, P.A., et al., *Rat pancreatic stellate cells secrete matrix metalloproteinases: implications for extracellular matrix turnover.* Gut, 2003. **52**(2): p. 275-282.
132. Bulle, A. and K.-H. Lim, *Beyond just a tight fortress: contribution of stroma to epithelial-mesenchymal transition in pancreatic cancer.* Signal Transduction and Targeted Therapy, 2020. **5**(1): p. 249.
133. Shields, M.A., et al., *Pancreatic cancer cells respond to type I collagen by inducing snail expression to promote membrane type 1 matrix metalloproteinase-dependent collagen invasion.* The Journal of biological chemistry, 2011. **286**(12): p. 10495-10504.
134. van der Zee, J.A., et al., *Tumour basement membrane laminin expression predicts outcome following curative resection of pancreatic head cancer.* British journal of cancer, 2012. **107**(7): p. 1153-1158.
135. Topalovski, M. and R.A. Brekken, *Matrix control of pancreatic cancer: New insights into fibronectin signaling.* Cancer letters, 2016. **381**(1): p. 252-258.
136. Placencio-Hickok, V.R., et al., *Hyaluronan heterogeneity in pancreatic ductal adenocarcinoma: Primary tumors compared to sites of metastasis.* Pancreatology, 2021.
137. Lu, C., et al., *WDR5-H3K4me3 epigenetic axis regulates OPN expression to compensate PD-L1 function to promote pancreatic cancer immune escape.* Journal for immunotherapy of cancer, 2021. **9**(7): p. e002624.
138. McElroy, M.K., et al., *Upregulation of thrombospondin-1 and angiogenesis in an aggressive human pancreatic cancer cell line selected for high metastasis.* Molecular cancer therapeutics, 2009. **8**(7): p. 1779-1786.
139. Li, Y., et al., *The Interplay Between Inflammation and Stromal Components in Pancreatic Cancer.* Front Immunol, 2022. **13**: p. 850093.
140. Bhatia, R., et al., *Cytokines chattering in pancreatic ductal adenocarcinoma tumor microenvironment.* Seminars in Cancer Biology, 2022.
141. Błogowski, W., et al., *Selected Cytokines in Patients with Pancreatic Cancer: A Preliminary Report.* PLOS ONE, 2014. **9**(5): p. e97613.
142. Das, S., et al., *Tumor Cell-Derived IL1β Promotes Desmoplasia and Immune Suppression in Pancreatic Cancer.* Cancer research, 2020. **80**(5): p. 1088-1101.
143. Wu, Y.S., et al., *Paracrine IL-6 signaling mediates the effects of pancreatic stellate cells on epithelial-mesenchymal transition via Stat3/Nrf2 pathway in pancreatic cancer cells.* Biochimica et Biophysica Acta (BBA) - General Subjects, 2017. **1861**(2): p. 296-306.
144. Holmer, R., et al., *Interleukin-6: a villain in the drama of pancreatic cancer development and progression.* Hepatobiliary & Pancreatic Diseases International, 2014. **13**(4): p. 371-380.
145. Li, M., et al., *Interleukin-8 increases vascular endothelial growth factor and neuropilin expression and stimulates ERK activation in human pancreatic cancer.* Cancer science, 2008. **99**(4): p. 733-737.
146. Funamizu, N., et al., *Macrophage migration inhibitory factor induces epithelial to mesenchymal transition, enhances tumor aggressiveness and predicts clinical*

outcome in resected pancreatic ductal adenocarcinoma. International journal of cancer, 2013. **132**(4): p. 785-794.
147. Shen, W., et al., *TGF-β in pancreatic cancer initiation and progression: two sides of the same coin*. Cell & bioscience, 2017. **7**: p. 39-39.
148. Egberts, J.-H., et al., *Anti–Tumor Necrosis Factor Therapy Inhibits Pancreatic Tumor Growth and Metastasis*. Cancer Research, 2008. **68**(5): p. 1443.
149. Ali, A., et al., *Metabolic Pathways as a Novel Landscape in Pancreatic Ductal Adenocarcinoma*. Cancers (Basel), 2022. **14**(15).
150. Islam, M.M., et al., *Exploring the metabolic landscape of pancreatic ductal adenocarcinoma cells using genome-scale metabolic modeling*. iScience, 2022. **25**(6): p. 104483.
151. Ying, H., et al., *Oncogenic Kras maintains pancreatic tumors through regulation of anabolic glucose metabolism*. Cell, 2012. **149**(3): p. 656-70.
152. Yun, J., et al., *Glucose deprivation contributes to the development of KRAS pathway mutations in tumor cells*. Science, 2009. **325**(5947): p. 1555-9.
153. Chang, X., et al., *Glycolysis in the progression of pancreatic cancer*. Am J Cancer Res, 2022. **12**(2): p. 861-872.
154. Cao, L., et al., *Glycometabolic rearrangements--aerobic glycolysis in pancreatic cancer: causes, characteristics and clinical applications*. Journal of Experimental & Clinical Cancer Research, 2020. **39**(1): p. 267.
155. Lu, J., M. Tan, and Q. Cai, *The Warburg effect in tumor progression: mitochondrial oxidative metabolism as an anti-metastasis mechanism*. Cancer letters, 2015. **356**(2 Pt A): p. 156-164.
156. Liberti, M.V. and J.W. Locasale, *The Warburg Effect: How Does it Benefit Cancer Cells?* Trends Biochem Sci, 2016. **41**(3): p. 211-218.
157. Bose, S. and A. Le, *Glucose Metabolism in Cancer*, in *The Heterogeneity of Cancer Metabolism*, A. Le, Editor. 2018, Springer International Publishing: Cham. p. 3-12.
158. Semenza, G.L., *HIF-1 mediates metabolic responses to intratumoral hypoxia and oncogenic mutations*. J Clin Invest, 2013. **123**(9): p. 3664-71.
159. Marín-Hernández, A., et al., *HIF-1alpha modulates energy metabolism in cancer cells by inducing over-expression of specific glycolytic isoforms*. Mini Rev Med Chem, 2009. **9**(9): p. 1084-101.
160. Reyes-Castellanos, G., R. Masoud, and A. Carrier, *Mitochondrial Metabolism in PDAC: From Better Knowledge to New Targeting Strategies*. Biomedicines, 2020. **8**(8): p. 270.
161. Kamphorst, J.J., et al., *Human pancreatic cancer tumors are nutrient poor and tumor cells actively scavenge extracellular protein*. Cancer Res, 2015. **75**(3): p. 544-53.
162. Fu, Y., et al., *The reverse Warburg effect is likely to be an Achilles' heel of cancer that can be exploited for cancer therapy*. Oncotarget, 2017. **8**(34): p. 57813-57825.
163. Sousa, C.M., et al., *Pancreatic stellate cells support tumour metabolism through autophagic alanine secretion*. Nature, 2016. **536**(7617): p. 479-483.
164. Tan, Z., et al., *Hypoxia: a barricade to conquer the pancreatic cancer*. Cell Mol Life Sci, 2020. **77**(16): p. 3077-3083.

165. McDonald, P.C., et al., *Regulation of pH by Carbonic Anhydrase 9 Mediates Survival of Pancreatic Cancer Cells With Activated KRAS in Response to Hypoxia*. Gastroenterology, 2019. **157**(3): p. 823-837.
166. Tao, J., et al., *Targeting hypoxic tumor microenvironment in pancreatic cancer*. Journal of Hematology & Oncology, 2021. **14**(1): p. 14.
167. Hu, Q., et al., *UHRF1 promotes aerobic glycolysis and proliferation via suppression of SIRT4 in pancreatic cancer*. Cancer Letters, 2019. **452**: p. 226-236.
168. Erkan, M., et al., *The role of stroma in pancreatic cancer: diagnostic and therapeutic implications*. Nature Reviews Gastroenterology & Hepatology, 2012. **9**(8): p. 454-467.
169. Guillaumond, F., et al., *Strengthened glycolysis under hypoxia supports tumor symbiosis and hexosamine biosynthesis in pancreatic adenocarcinoma*. Proc Natl Acad Sci U S A, 2013. **110**(10): p. 3919-24.
170. Siegel, R.L., et al., *Cancer statistics, 2022*. CA: A Cancer Journal for Clinicians, 2022. **72**(1): p. 7-33.
171. Sally, Á., et al., *Current and Future Therapies for Pancreatic Ductal Adenocarcinoma*. Cancers (Basel), 2022. **14**(10).
172. Conroy, T., et al., *Current standards and new innovative approaches for treatment of pancreatic cancer*. Eur J Cancer, 2016. **57**: p. 10-22.
173. Ryan, D.P., T.S. Hong, and N. Bardeesy, *Pancreatic Adenocarcinoma*. New England Journal of Medicine, 2014. **371**(11): p. 1039-1049.
174. *National Comprehensive Cancer Network : Practice guidelines in oncology for pancreatic adenocarcinoma. Version 2*. 2015.
175. Sardar, M., et al., *Pharmacotherapeutic options for pancreatic ductal adenocarcinoma*. Expert Opinion on Pharmacotherapy, 2022. **23**(18): p. 2079-2089.
176. Mizrahi, J.D., et al., *Pancreatic cancer*. The Lancet, 2020. **395**(10242): p. 2008-2020.
177. Manji, G.A., et al., *Current and Emerging Therapies in Metastatic Pancreatic Cancer*. Clinical Cancer Research, 2017. **23**(7): p. 1670-1678.
178. Hamed, S.S., R.M. Straubinger, and W.J. Jusko, *Pharmacodynamic modeling of cell cycle and apoptotic effects of gemcitabine on pancreatic adenocarcinoma cells*. Cancer Chemother Pharmacol, 2013. **72**(3): p. 553-63.
179. Ahmed, A.A., et al., *A G-quadruplex-binding compound shows potent activity in human gemcitabine-resistant pancreatic cancer cells*. Sci Rep, 2020. **10**(1): p. 12192.
180. Thota, R., J.M. Pauff, and J.D. Berlin, *Treatment of metastatic pancreatic adenocarcinoma: a review*. Oncology (Williston Park), 2014. **28**(1): p. 70-4.
181. Jiang, S., et al., *A comprehensive review of pancreatic cancer and its therapeutic challenges*. Aging (Albany NY), 2022. **14**(18): p. 7635-7649.
182. Zheng, R., et al., *Frontiers and future of immunotherapy for pancreatic cancer: from molecular mechanisms to clinical application*. Frontiers in Immunology, 2024. **15**.
183. Qu, X., et al., *Characterization and expression of three novel differentiation-related genes belong to the human NDRG gene family*. Mol Cell Biochem, 2002. **229**(1-2): p. 35-44.

184. Joshi, V., S.R. Lakhani, and A.E. McCart Reed, *NDRG1 in Cancer: A Suppressor, Promoter, or Both?* Cancers, 2022. **14**(23): p. 5739.
185. Shaw, E., et al., *Identification of a novel class in the α/β hydrolase fold superfamily: The N-myc differentiation-related proteins.* Proteins: Structure, Function, and Bioinformatics, 2002. **47**(2): p. 163-168.
186. Park, K.C., et al., *Identification of differential phosphorylation and sub-cellular localization of the metastasis suppressor, NDRG1.* Biochimica et Biophysica Acta (BBA) - Molecular Basis of Disease, 2018. **1864**(8): p. 2644-2663.
187. Zhou, R.-H., et al., *Characterization of the Human NDRG Gene Family: A Newly Identified Member, NDRG4, Is Specifically Expressed in Brain and Heart.* Genomics, 2001. **73**(1): p. 86-97.
188. Kim-Fuchs, C., et al., *The silencing of N-myc downstream-regulated gene-1 in an orthotopic pancreatic cancer model leads to more aggressive tumor growth and metastases.* Dig Surg, 2014. **31**(2): p. 135-42.
189. Bandyopadhyay, S., et al., *Role of the putative tumor metastasis suppressor gene Drg-1 in breast cancer progression.* Oncogene, 2004. **23**(33): p. 5675-5681.
190. Guan, R.J., et al., *Drg-1 as a differentiation-related, putative metastatic suppressor gene in human colon cancer.* Cancer Res, 2000. **60**(3): p. 749-55.
191. Bandyopadhyay, S., et al., *The Drg-1 gene suppresses tumor metastasis in prostate cancer.* Cancer Res, 2003. **63**(8): p. 1731-6.
192. Dang, C., et al., *Identification of dysregulated genes in cutaneous squamous cell carcinoma.* Oncol Rep, 2006. **16**(3): p. 513-9.
193. Nishio, S., et al., *Cap43/NDRG1/Drg-1 is a molecular target for angiogenesis and a prognostic indicator in cervical adenocarcinoma.* Cancer letters, 2008. **264**(1): p. 36-43.
194. Cheng, J., et al., *NDRG1 as a biomarker for metastasis, recurrence and of poor prognosis in hepatocellular carcinoma.* Cancer Lett, 2011. **310**(1): p. 35-45.
195. Azuma, K., et al., *NDRG1/Cap43/Drg-1 may predict tumor angiogenesis and poor outcome in patients with lung cancer.* Journal of Thoracic Oncology, 2012. **7**(5): p. 779-789.
196. Murakami, Y., et al., *N-myc downstream-regulated gene 1 promotes tumor inflammatory angiogenesis through JNK activation and autocrine loop of interleukin-1α by human gastric cancer cells.* J Biol Chem, 2013. **288**(35): p. 25025-25037.
197. Kovacevic, Z., et al., *Novel Thiosemicarbazone Iron Chelators Induce Up-Regulation and Phosphorylation of the Metastasis Suppressor N-myc Down-Stream Regulated Gene 1: A New Strategy for the Treatment of Pancreatic Cancer.* Molecular Pharmacology, 2011. **80**(4): p. 598.
198. Liu, W., et al., *A new facet of NDRG1 in pancreatic ductal adenocarcinoma: Suppression of glycolytic metabolism.* Int J Oncol, 2017. **50**(5): p. 1792-1800.
199. Ghafouri-Fard, S., et al., *A review on the role of NDRG1 in different cancers.* Molecular Biology Reports, 2023. **50**(7): p. 6251-6264.
200. Deer, E.L., et al., *Phenotype and genotype of pancreatic cancer cell lines.* Pancreas, 2010. **39**(4): p. 425-35.
201. Yunis, A.A., G.K. Arimura, and D.J. Russin, *Human pancreatic carcinoma (MIA PaCa-2) in continuous culture: sensitivity to asparaginase.* Int J Cancer, 1977. **19**(1): p. 128-35.

202. Lieber, M., et al., *Establishment of a continuous tumor-cell line (panc-1) from a human carcinoma of the exocrine pancreas*. Int J Cancer, 1975. **15**(5): p. 741-7.
203. Gradiz, R., et al., *MIA PaCa-2 and PANC-1 - pancreas ductal adenocarcinoma cell lines with neuroendocrine differentiation and somatostatin receptors*. Sci Rep, 2016. **6**: p. 21648.
204. Moore, P.S., et al., *Genetic profile of 22 pancreatic carcinoma cell lines*. Virchows Archiv, 2001. **439**(6): p. 798-802.
205. Geleta, B., et al., *Targeting Wnt/tenascin C-mediated cross talk between pancreatic cancer cells and stellate cells via activation of the metastasis suppressor NDRG1*. J Biol Chem, 2022. **298**(3): p. 101608.
206. Geleta, B., et al., *Breaking the cycle: Targeting of NDRG1 to inhibit bi-directional oncogenic cross-talk between pancreatic cancer and stroma*. The FASEB Journal, 2021. **35**(2): p. e21347.
207. Bestari, M.B., I.R. Joewono, and A.F. Syam, *A Quest for Survival: A Review of the Early Biomarkers of Pancreatic Cancer and the Most Effective Approaches at Present*. Biomolecules, 2024. **14**(3): p. 364.
208. Sarantis, P., et al., *Pancreatic ductal adenocarcinoma: Treatment hurdles, tumor microenvironment and immunotherapy*. World J Gastrointest Oncol, 2020. **12**(2): p. 173-181.
209. Pereira-Nunes, A., et al., *Lactate and Lactate Transporters as Key Players in the Maintenance of the Warburg Effect*, in *Tumor Microenvironment : The Main Driver of Metabolic Adaptation*, J. Serpa, Editor. 2020, Springer International Publishing: Cham. p. 51-74.
210. Pavlides, S., et al., *The reverse Warburg effect: Aerobic glycolysis in cancer associated fibroblasts and the tumor stroma*. Cell Cycle, 2009. **8**(23): p. 3984-4001.
211. Biffi, G. and D.A. Tuveson, *A FATal Combination: Fibroblast-Derived Lipids and Cancer-Derived Autotaxin Promote Pancreatic Cancer Growth*. Cancer Discovery, 2019. **9**(5): p. 578-580.
212. Shi, X.H., et al., *The expression and localization of N-myc downstream-regulated gene 1 in human trophoblasts*. PLoS One, 2013. **8**(9): p. e75473.
213. Chang, J., et al., *Re-Shaping the Pancreatic Cancer Tumor Microenvironment: A New Role for the Metastasis Suppressor NDRG1*. Cancers, 2023. **15**(10): p. 2779.
214. Han, H. and D.D. Von Hoff, *SnapShot: pancreatic cancer*. Cancer Cell, 2013. **23**(3): p. 424-424.e1.
215. Feig, C., et al., *The pancreas cancer microenvironment*. Clin Cancer Res, 2012. **18**(16): p. 4266-76.
216. Pavlova, N.N. and C.B. Thompson, *The Emerging Hallmarks of Cancer Metabolism*. Cell Metab, 2016. **23**(1): p. 27-47.
217. Dong, S., et al., *Glucose metabolism and tumour microenvironment in pancreatic cancer: A key link in cancer progression*. Front Immunol, 2022. **13**: p. 1038650.
218. Cantor, J.R. and D.M. Sabatini, *Cancer cell metabolism: one hallmark, many faces*. Cancer Discov, 2012. **2**(10): p. 881-98.
219. Vulturar, R., et al., *One Molecule for Mental Nourishment and More: Glucose Transporter Type 1-Biology and Deficiency Syndrome*. Biomedicines, 2022. **10**(6).

220. Yu, M., et al., *Metabolic phenotypes in pancreatic cancer*. PLoS One, 2015. **10**(2): p. e0115153.
221. Sharen, G., et al., *Prognostic value of GLUT-1 expression in pancreatic cancer: results from 538 patients*. Oncotarget, 2017. **8**(12): p. 19760-19767.
222. Kurahara, H., et al., *Significance of Glucose Transporter Type 1 (GLUT-1) Expression in the Therapeutic Strategy for Pancreatic Ductal Adenocarcinoma*. Ann Surg Oncol, 2018. **25**(5): p. 1432-1439.
223. Lee, J.H., et al., *Branched-chain amino acids sustain pancreatic cancer growth by regulating lipid metabolism*. Exp Mol Med, 2019. **51**(11): p. 1-11.
224. Hattori, A., et al., *Cancer progression by reprogrammed BCAA metabolism in myeloid leukaemia*. Nature, 2017. **545**(7655): p. 500-504.
225. Fuchs, B.C. and B.P. Bode, *Amino acid transporters ASCT2 and LAT1 in cancer: Partners in crime?* Seminars in Cancer Biology, 2005. **15**(4): p. 254-266.
226. Mayers, J.R., et al., *Elevation of circulating branched-chain amino acids is an early event in human pancreatic adenocarcinoma development*. Nat Med, 2014. **20**(10): p. 1193-1198.
227. Yanagisawa, N., et al., *High expression of L-type amino acid transporter 1 (LAT1) predicts poor prognosis in pancreatic ductal adenocarcinomas*. Journal of Clinical Pathology, 2012. **65**(11): p. 1019.
228. Altan, B., et al., *Relationship between LAT1 expression and resistance to chemotherapy in pancreatic ductal adenocarcinoma*. Cancer Chemotherapy and Pharmacology, 2018. **81**(1): p. 141-153.
229. Wangpu, X., et al., *The metastasis suppressor, NDRG1, inhibits "stemness" of colorectal cancer v ia down-regulation of nuclear β-catenin and CD44*. Oncotarget, 2015. **6**(32).
230. Spivak-Kroizman, T.R., et al., *Hypoxia Triggers Hedgehog-Mediated Tumor–Stromal Interactions in Pancreatic Cancer*. Cancer Research, 2013. **73**(11): p. 3235-3247.
231. Yan, L., et al., *Glucose Metabolism in Pancreatic Cancer*. Cancers (Basel), 2019. **11**(10).
232. Han, J., et al., *Glucose promotes cell proliferation, glucose uptake and invasion in endometrial cancer cells via AMPK/mTOR/S6 and MAPK signaling*. Gynecol Oncol, 2015. **138**(3): p. 668-75.
233. Roberts, D.J. and S. Miyamoto, *Hexokinase II integrates energy metabolism and cellular protection: Akting on mitochondria and TORCing to autophagy*. Cell Death Differ, 2015. **22**(2): p. 248-57.
234. Koivunen, P., et al., *Inhibition of Hypoxia-inducible Factor (HIF) Hydroxylases by Citric Acid Cycle Intermediates: POSSIBLE LINKS BETWEEN CELL METABOLISM AND STABILIZATION OF HIF **. Journal of Biological Chemistry, 2007. **282**(7): p. 4524-4532.
235. Isaacs, J.S., et al., *HIF overexpression correlates with biallelic loss of fumarate hydratase in renal cancer: novel role of fumarate in regulation of HIF stability*. Cancer Cell, 2005. **8**(2): p. 143-53.
236. Pollard, P.J., et al., *Accumulation of Krebs cycle intermediates and over-expression of HIF1alpha in tumours which result from germline FH and SDH mutations*. Hum Mol Genet, 2005. **14**(15): p. 2231-9.

237. Shen, N., et al., *DLST-dependence dictates metabolic heterogeneity in TCA-cycle usage among triple-negative breast cancer.* Commun Biol, 2021. **4**(1): p. 1289.
238. Reitman, Z.J. and H. Yan, *Isocitrate dehydrogenase 1 and 2 mutations in cancer: alterations at a crossroads of cellular metabolism.* J Natl Cancer Inst, 2010. **102**(13): p. 932-41.
239. Belisario, D.C., et al., *Hypoxia Dictates Metabolic Rewiring of Tumors: Implications for Chemoresistance.* Cells, 2020. **9**(12).
240. Radogna, F., et al., *Assessment of Mitochondrial Cell MetabolismMetabolism by Respiratory Chain Electron FlowRespiratory chain electron flow Assays*, in *Mitochondrial Medicine : Volume 2: Assessing Mitochondria*, V. Weissig and M. Edeas, Editors. 2021, Springer US: New York, NY. p. 129-141.
241. Carillo, M.R., et al., *L-Carnitine in Drosophila: A Review.* Antioxidants (Basel), 2020. **9**(12).
242. Zhou, X., et al., *The role of serine metabolism in lung cancer: From oncogenesis to tumor treatment.* Front Genet, 2022. **13**: p. 1084609.
243. Oliveira, L.B., et al., *Metabolomic Profiling of Plasma Reveals Differential Disease Severity Markers in COVID-19 Patients.* Frontiers in Microbiology, 2022. **13**.
244. Booth, S.C., A.M. Weljie, and R.J. Turner, *COMPUTATIONAL TOOLS FOR THE SECONDARY ANALYSIS OF METABOLOMICS EXPERIMENTS.* Computational and Structural Biotechnology Journal, 2013. **4**(5): p. e201301003.
245. Moreira, J.D., et al., *The Redox Status of Cancer Cells Supports Mechanisms behind the Warburg Effect.* Metabolites, 2016. **6**(4).
246. Hodson, N., et al., *Characterisation of L-Type Amino Acid Transporter 1 (LAT1) Expression in Human Skeletal Muscle by Immunofluorescent Microscopy.* Nutrients, 2017. **10**(1).
247. Baird, F.E., et al., *Tertiary active transport of amino acids reconstituted by coexpression of System A and L transporters in Xenopus oocytes.* Am J Physiol Endocrinol Metab, 2009. **297**(3): p. E822-9.
248. Nicklin, P., et al., *Bidirectional transport of amino acids regulates mTOR and autophagy.* Cell, 2009. **136**(3): p. 521-34.
249. Dodd, K.M. and A.R. Tee, *Leucine and mTORC1: a complex relationship.* American Journal of Physiology-Endocrinology and Metabolism, 2012. **302**(11): p. E1329-E1342.
250. Kim, D.-H., et al., *mTOR Interacts with Raptor to Form a Nutrient-Sensitive Complex that Signals to the Cell Growth Machinery.* Cell, 2002. **110**(2): p. 163-175.
251. Chen, Y., E.M. Li, and L.Y. Xu, *Guide to Metabolomics Analysis: A Bioinformatics Workflow.* Metabolites, 2022. **12**(4).
252. Sevinsky, C.J., et al., *NDRG1 regulates neutral lipid metabolism in breast cancer cells.* Breast Cancer Res, 2018. **20**(1): p. 55.
253. McKeown, S.R., *Defining normoxia, physoxia and hypoxia in tumours-implications for treatment response.* Br J Radiol, 2014. **87**(1035): p. 20130676.
254. Koong, A.C., et al., *Pancreatic tumors show high levels of hypoxia.* Int J Radiat Oncol Biol Phys, 2000. **48**(4): p. 919-22.

255. Anderson, M., et al., *Hexokinase 2 promotes tumor growth and metastasis by regulating lactate production in pancreatic cancer.* Oncotarget, 2017. **8**(34): p. 56081-56094.
256. Yin, X., et al., *Lipid metabolism in pancreatic cancer: emerging roles and potential targets.* Cancer Communications, 2022. **42**(12): p. 1234-1256.
257. Lim, G.B., *Inhibiting fatty acid oxidation promotes cardiomyocyte proliferation.* Nature Reviews Cardiology, 2020. **17**(5): p. 266-267.
258. Qu, Q., et al., *Fatty acid oxidation and carnitine palmitoyltransferase I: emerging therapeutic targets in cancer.* Cell Death & Disease, 2016. **7**(5): p. e2226-e2226.
259. Ni, Y., et al., *The roles of IDH1 in tumor metabolism and immunity.* Future Oncol, 2022. **18**(35): p. 3941-3953.
260. Itsumi, M., et al., *Idh1 protects murine hepatocytes from endotoxin-induced oxidative stress by regulating the intracellular NADP(+)/NADPH ratio.* Cell Death Differ, 2015. **22**(11): p. 1837-45.
261. Liu, S., T. Cadoux-Hudson, and C.J. Schofield, *Isocitrate dehydrogenase variants in cancer — Cellular consequences and therapeutic opportunities.* Current Opinion in Chemical Biology, 2020. **57**: p. 122-134.
262. Merlot, A.M., et al., *The metastasis suppressor, NDRG1, differentially modulates the endoplasmic reticulum stress response.* Biochim Biophys Acta Mol Basis Dis, 2019. **1865**(9): p. 2094-2110.
263. Newstead, S., *Insights into L-type heteromeric amino acid transporters.* Nature Structural & Molecular Biology, 2019. **26**(6): p. 395-396.
264. Conciatori, F., et al., *Role of mTOR Signaling in Tumor Microenvironment: An Overview.* Int J Mol Sci, 2018. **19**(8).
265. Iriana, S., et al., *Targeting mTOR in Pancreatic Ductal Adenocarcinoma.* Front Oncol, 2016. **6**: p. 99.
266. Jin, J., et al., *Targeting glutamine metabolism as a therapeutic strategy for cancer.* Experimental & Molecular Medicine, 2023. **55**(4): p. 706-715.
267. Bott, A.J., et al., *Glutamine Anabolism Plays a Critical Role in Pancreatic Cancer by Coupling Carbon and Nitrogen Metabolism.* Cell Rep, 2019. **29**(5): p. 1287-1298.e6.
268. Hidalgo, M., et al., *Addressing the challenges of pancreatic cancer: Future directions for improving outcomes.* Pancreatology, 2015. **15**(1): p. 8-18.
269. Zhao, L., et al., *Survival Benefit of Pembrolizumab for Patients With Pancreatic Adenocarcinoma: A Case Series.* J Med Cases, 2022. **13**(5): p. 240-243.
270. Park, W., A. Chawla, and E.M. O'Reilly, *Pancreatic Cancer: A Review.* Jama, 2021. **326**(9): p. 851-862.
271. Pratt, H.G., et al., *Macrophage and Neutrophil Interactions in the Pancreatic Tumor Microenvironment Drive the Pathogenesis of Pancreatic Cancer.* Cancers (Basel), 2021. **14**(1).
272. Kota, J., et al., *Pancreatic cancer: Stroma and its current and emerging targeted therapies.* Cancer Letters, 2017. **391**: p. 38-49.
273. Vaish, U., et al., *Cancer-Associated Fibroblasts in Pancreatic Ductal Adenocarcinoma: An Update on Heterogeneity and Therapeutic Targeting.* Int J Mol Sci, 2021. **22**(24).

274. Mao, X., et al., *Crosstalk between cancer-associated fibroblasts and immune cells in the tumor microenvironment: new findings and future perspectives*. Mol Cancer, 2021. **20**(1): p. 131.
275. Kuen, J., et al., *Pancreatic cancer cell/fibroblast co-culture induces M2 like macrophages that influence therapeutic response in a 3D model*. PLOS ONE, 2017. **12**(7): p. e0182039.
276. Goehrig, D., et al., *Stromal protein βig-h3 reprogrammes tumour microenvironment in pancreatic cancer*. Gut, 2019. **68**(4): p. 693-707.
277. Zhu, Y., et al., *Tissue-Resident Macrophages in Pancreatic Ductal Adenocarcinoma Originate from Embryonic Hematopoiesis and Promote Tumor Progression*. Immunity, 2017. **47**(2): p. 323-338.e6.
278. Cui, R., et al., *Targeting tumor-associated macrophages to combat pancreatic cancer*. Oncotarget, 2016. **7**(31): p. 50735-50754.
279. Yang, S., Q. Liu, and Q. Liao, *Tumor-Associated Macrophages in Pancreatic Ductal Adenocarcinoma: Origin, Polarization, Function, and Reprogramming*. Frontiers in cell and developmental biology, 2021. **8**: p. 607209-607209.
280. Habtezion, A., M. Edderkaoui, and S.J. Pandol, *Macrophages and pancreatic ductal adenocarcinoma*. Cancer Lett, 2016. **381**(1): p. 211-6.
281. Garcia Garcia, C.J., et al., *Stromal HIF2 Regulates Immune Suppression in the Pancreatic Cancer Microenvironment*. Gastroenterology, 2022. **162**(7): p. 2018-2031.
282. Kurahara, H., et al., *Significance of M2-Polarized Tumor-Associated Macrophage in Pancreatic Cancer*. Journal of Surgical Research, 2011. **167**(2): p. e211-e219.
283. Hao, N.B., et al., *Macrophages in tumor microenvironments and the progression of tumors*. Clin Dev Immunol, 2012. **2012**: p. 948098.
284. Liu, Y., et al., *LncRNA-PACERR induces pro-tumour macrophages via interacting with miR-671-3p and m6A-reader IGF2BP2 in pancreatic ductal adenocarcinoma*. J Hematol Oncol, 2022. **15**(1): p. 52.
285. Sharma, A., et al., *The prostate metastasis suppressor gene NDRG1 differentially regulates cell motility and invasion*. Molecular Oncology, 2017. **11**(6): p. 655-669.
286. Li, Q. and H. Chen, *Transcriptional silencing of N-Myc downstream-regulated gene 1 (NDRG1) in metastatic colon cancer cell line SW620*. Clinical & Experimental Metastasis, 2011. **28**(2): p. 127-135.
287. Liu, W., et al., *N-myc downstream regulated gene 1 modulates Wnt-β-catenin signalling and pleiotropically suppresses metastasis*. EMBO Mol Med, 2012. **4**(2): p. 93-108.
288. Menezes, S.V., et al., *The metastasis suppressor, NDRG1, attenuates oncogenic TGF-β and NF-κB signaling to enhance membrane E-cadherin expression in pancreatic cancer cells*. Carcinogenesis, 2018. **40**(6): p. 805-818.
289. Lane, D.J.R., et al., *Expanding horizons in iron chelation and the treatment of cancer: Role of iron in the regulation of ER stress and the epithelial–mesenchymal transition*. Biochimica et Biophysica Acta (BBA) - Reviews on Cancer, 2014. **1845**(2): p. 166-181.
290. Rustamov, V., et al., *Long-term 3D culture of the SCC4 cell line using three different culture methods and initial seeding densities*. Journal of Cellular Biotechnology, 2017. **3**: p. 41-50.

291. Lim, S.C., et al., *The metastasis suppressor NDRG1 directly regulates androgen receptor signaling in prostate cancer*. J Biol Chem, 2021. **297**(6): p. 101414.
292. Mustonen, V., et al., *Crystal and solution structure of NDRG1, a membrane-binding protein linked to myelination and tumour suppression*. The FEBS Journal, 2021. **288**(11): p. 3507-3529.
293. Genin, M., et al., *M1 and M2 macrophages derived from THP-1 cells differentially modulate the response of cancer cells to etoposide*. BMC Cancer, 2015. **15**(1): p. 577.
294. Yang, M., et al., *Macrophage phenotypic subtypes diametrically regulate epithelial-mesenchymal plasticity in breast cancer cells*. BMC Cancer, 2016. **16**(1): p. 419.
295. Sawa-Wejksza, K., et al., *Colon cancer–derived conditioned medium induces differentiation of THP-1 monocytes into a mixed population of M1/M2 cells*. Tumor Biology, 2018. **40**(9): p. 1010428318797880.
296. Jayasingam, S.D., et al., *Evaluating the Polarization of Tumor-Associated Macrophages Into M1 and M2 Phenotypes in Human Cancer Tissue: Technicalities and Challenges in Routine Clinical Practice*. Frontiers in Oncology, 2020. **9**.
297. Daniel, B., et al., *Macrophage inflammatory and regenerative response periodicity is programmed by cell cycle and chromatin state*. Molecular Cell, 2023. **83**(1): p. 121-138.e7.
298. Liu, L., et al., *BCG immunotherapy inhibits cancer progression by promoting the M1 macrophage differentiation of THP-1 cells via the Rb/E2F1 pathway in cervical carcinoma*. Oncol Rep, 2021. **46**(5): p. 245.
299. Madsen, N.H., et al., *Monocyte Infiltration and Differentiation in 3D Multicellular Spheroid Cancer Models*. Pathogens, 2021. **10**(8).
300. Leary, E., et al., *Quantitative Live-Cell Confocal Imaging of 3D Spheroids in a High-Throughput Format*. SLAS Technol, 2018. **23**(3): p. 231-242.
301. Chen, Y., et al., *Tumor-associated macrophages: an accomplice in solid tumor progression*. Journal of Biomedical Science, 2019. **26**(1): p. 78.
302. Verreck, F.A., et al., *Human IL-23-producing type 1 macrophages promote but IL-10-producing type 2 macrophages subvert immunity to (myco)bacteria*. Proc Natl Acad Sci U S A, 2004. **101**(13): p. 4560-5.
303. Mirlekar, B. and Y. Pylayeva-Gupta, *IL-12 Family Cytokines in Cancer and Immunotherapy*. Cancers (Basel), 2021. **13**(2).
304. Tan, H.Y., et al., *The Reactive Oxygen Species in Macrophage Polarization: Reflecting Its Dual Role in Progression and Treatment of Human Diseases*. Oxid Med Cell Longev, 2016. **2016**: p. 2795090.
305. Aminin, D. and Y.-M. Wang, *Macrophages as a "weapon" in anticancer cellular immunotherapy*. The Kaohsiung Journal of Medical Sciences, 2021. **37**(9): p. 749-758.
306. Pan, Y., et al., *Tumor-Associated Macrophages in Tumor Immunity*. Frontiers in Immunology, 2020. **11**.
307. Štampar, M., et al., *Characterization of In Vitro 3D Cell Model Developed from Human Hepatocellular Carcinoma (HepG2) Cell Line*. Cells, 2020. **9**(12): p. 2557.

308. Viola, A., et al., *The Metabolic Signature of Macrophage Responses*. Frontiers in Immunology, 2019. **10**.
309. Liu, Y., et al., *Metabolic reprogramming in macrophage responses*. Biomarker Research, 2021. **9**(1): p. 1.
310. Yang, Z. and X.F. Ming, *Functions of arginase isoforms in macrophage inflammatory responses: impact on cardiovascular diseases and metabolic disorders*. Front Immunol, 2014. **5**: p. 533.
311. Freemerman, A.J., et al., *Metabolic reprogramming of macrophages: glucose transporter 1 (GLUT1)-mediated glucose metabolism drives a proinflammatory phenotype*. J Biol Chem, 2014. **289**(11): p. 7884-96.
312. Wilson, J.E., *Isozymes of mammalian hexokinase: structure, subcellular localization and metabolic function*. Journal of Experimental Biology, 2003. **206**(12): p. 2049-2057.
313. Mills, C.D., et al., *M-1/M-2 Macrophages and the Th1/Th2 Paradigm1*. The Journal of Immunology, 2000. **164**(12): p. 6166-6173.
314. Tang, D., et al., *Extracellular Vesicle/Macrophage Axis: Potential Targets for Inflammatory Disease Intervention*. Front Immunol, 2022. **13**: p. 705472.
315. Linton, S.S., et al., *Tumor-promoting effects of pancreatic cancer cell exosomes on THP-1-derived macrophages*. PLoS One, 2018. **13**(11): p. e0206759.
316. Cassioli, C. and C.T. Baldari, *Lymphocyte Polarization During Immune Synapse Assembly: Centrosomal Actin Joins the Game*. Frontiers in Immunology, 2022. **13**.
317. Thomas, P.D., *The Gene Ontology and the Meaning of Biological Function*. Methods Mol Biol, 2017. **1446**: p. 15-24.
318. Abou Khouzam, R., et al., *Hypoxia, a Targetable Culprit to Counter Pancreatic Cancer Resistance to Therapy*. Cancers (Basel), 2023. **15**(4).
319. Wu, X., et al., *TNF-a mediated inflammatory macrophage polarization contributes to the pathogenesis of steroid-induced osteonecrosis in mice*. International Journal of Immunopathology and Pharmacology, 2015. **28**(3): p. 351-361.
320. Xu, R., et al., *CCL2 promotes macrophages-associated chemoresistance via MCPIP1 dual catalytic activities in multiple myeloma*. Cell Death & Disease, 2019. **10**(10): p. 781.
321. Zhuang, Y., et al., *Blocking the CCL5-CCR5 Axis Using Maraviroc Promotes M1 Polarization of Macrophages Cocultured with Irradiated Hepatoma Cells*. J Hepatocell Carcinoma, 2021. **8**: p. 599-611.
322. Zhu, Y.-y., et al., *CCL5 secreted by luminal B breast cancer cells induces polarization of M2 macrophages through activation of MEK/STAT3 signaling pathway via CCR5*. Gene, 2022. **812**: p. 146100.
323. Xiao, P., et al., *Neurotensin/IL-8 pathway orchestrates local inflammatory response and tumor invasion by inducing M2 polarization of Tumor-Associated macrophages and epithelial-mesenchymal transition of hepatocellular carcinoma cells*. Oncoimmunology, 2018. **7**(7): p. e1440166.
324. Kratochvill, F., et al., *TNF Counterbalances the Emergence of M2 Tumor Macrophages*. Cell Rep, 2015. **12**(11): p. 1902-14.

325. Hoover, A.A., et al., *Increased canonical NF-kappaB signaling specifically in macrophages is sufficient to limit tumor progression in syngeneic murine models of ovarian cancer.* BMC Cancer, 2020. **20**(1): p. 970.
326. Patysheva, M., et al., *Monocyte programming by cancer therapy.* Front Immunol, 2022. **13**: p. 994319.
327. Wang, H., et al., *The Impact of the Tumor Microenvironment on Macrophage Polarization in Cancer Metastatic Progression.* Int J Mol Sci, 2021. **22**(12).
328. Kovacevic, Z., et al., *The Metastasis Suppressor, N-MYC Downstream-regulated Gene-1 (NDRG1), Down-regulates the ErbB Family of Receptors to Inhibit Downstream Oncogenic Signaling Pathways.* J Biol Chem, 2016. **291**(3): p. 1029-52.
329. Dixon, K.M., et al., *Dp44mT targets the AKT, TGF-β and ERK pathways via the metastasis suppressor NDRG1 in normal prostate epithelial cells and prostate cancer cells.* Br J Cancer, 2013. **108**(2): p. 409-19.
330. Jin, R., et al., *The metastasis suppressor NDRG1 modulates the phosphorylation and nuclear translocation of β-catenin through mechanisms involving FRAT1 and PAK4.* Journal of Cell Science, 2014. **127**(14): p. 3116-3130.
331. Zhang, Y., et al., *Tumor cell-derived conditioned medium induced pro-tumoral phenotypes in macrophages through calcium-nuclear factor κB interaction.* BMC Cancer, 2022. **22**(1): p. 1327.
332. Chen, S.-j., et al., *Tumor-driven like macrophages induced by conditioned media from pancreatic ductal adenocarcinoma promote tumor metastasis via secreting IL-8.* Cancer Medicine, 2018. **7**(11): p. 5679-5690.
333. Zheng, X., et al., *Redirecting tumor-associated macrophages to become tumoricidal effectors as a novel strategy for cancer therapy.* Oncotarget, 2017. **8**(29): p. 48436-48452.
334. Stout, R.D., et al., *Macrophages Sequentially Change Their Functional Phenotype in Response to Changes in Microenvironmental Influences1*. The Journal of Immunology, 2005. **175**(1): p. 342-349.
335. Biswas, S.K. and A. Mantovani, *Macrophage plasticity and interaction with lymphocyte subsets: cancer as a paradigm.* Nature Immunology, 2010. **11**(10): p. 889-896.
336. van Dalen, F.J., et al., *Molecular Repolarisation of Tumour-Associated Macrophages.* Molecules, 2018. **24**(1).
337. Mucciolo, G., et al., *IL17A critically shapes the transcriptional program of fibroblasts in pancreatic cancer and switches on their protumorigenic functions*. Proceedings of the National Academy of Sciences, 2021. **118**(6): p. e2020395118.
338. Andersson, P., et al., *Molecular mechanisms of IL-33-mediated stromal interactions in cancer metastasis*. JCI Insight, 2018. **3**(20).
339. Xaus, J., et al., *Interferon gamma induces the expression of p21waf-1 and arrests macrophage cell cycle, preventing induction of apoptosis*. Immunity, 1999. **11**(1): p. 103-13.
340. Jacobson, E.C., et al., *TNF-α Differentially Regulates Cell Cycle Genes in Promyelocytic and Granulocytic HL-60/S4 Cells*. G3 (Bethesda), 2019. **9**(8): p. 2775-2786.

341. Fei, L., et al., *Targeting the CCL2/CCR2 Axis in Cancer Immunotherapy: One Stone, Three Birds?* Front Immunol, 2021. **12**: p. 771210.
342. Xu, N., et al., *Akt: a double-edged sword in cell proliferation and genome stability.* J Oncol, 2012. **2012**: p. 951724.
343. Moussa, R.S., Z. Kovacevic, and D.R. Richardson, *Differential targeting of the cyclin-dependent kinase inhibitor, p21CIP1/WAF1, by chelators with anti-proliferative activity in a range of tumor cell-types.* Oncotarget, 2015. **6**(30): p. 29694-711.
344. Wang, S., et al., *Metabolic Reprogramming Induces Macrophage Polarization in the Tumor Microenvironment.* Front Immunol, 2022. **13**: p. 840029.
345. Kaur, K.K., G. Allahbadia, and M. Singh, *Targeting macrophage polarization for therapy of diabesity–the feasibility of early improvement of insulin sensitivity and insulin resistance-a comprehensive systematic review.* J Diab Metab Disorder Control, 2021. **8**(1): p. 6-25.
346. Rath, M., et al., *Metabolism via Arginase or Nitric Oxide Synthase: Two Competing Arginine Pathways in Macrophages.* Front Immunol, 2014. **5**: p. 532.
347. Wang, T., et al., *HIF1α-Induced Glycolysis Metabolism Is Essential to the Activation of Inflammatory Macrophages.* Mediators Inflamm, 2017. **2017**: p. 9029327.
348. Cangul, H., *Hypoxia upregulates the expression of the NDRG1 gene leading to its overexpression in various human cancers.* BMC Genet, 2004. **5**: p. 27.
349. Yang, H., et al., *CCL2-CCR2 axis recruits tumor associated macrophages to induce immune evasion through PD-1 signaling in esophageal carcinogenesis.* Molecular Cancer, 2020. **19**(1): p. 41.
350. Lin, S.H., et al., *Treatment with TNF-α inhibitor rectifies M1 macrophage polarization from blood CD14+ monocytes in patients with psoriasis independent of STAT1 and IRF-1 activation.* J Dermatol Sci, 2018. **91**(3): p. 276-284.
351. Liu, T., et al., *NF-κB signaling in inflammation.* Signal Transduction and Targeted Therapy, 2017. **2**(1): p. 17023.
352. Wang, N., H. Liang, and K. Zen, *Molecular mechanisms that influence the macrophage m1-m2 polarization balance.* Front Immunol, 2014. **5**: p. 614.
353. Sica, A. and A. Mantovani, *Macrophage plasticity and polarization: in vivo veritas.* J Clin Invest, 2012. **122**(3): p. 787-95.
354. Christian, F., E.L. Smith, and R.J. Carmody, *The Regulation of NF-κB Subunits by Phosphorylation.* Cells, 2016. **5**(1).
355. Nelson, D.E., et al., *Oscillations in NF-κB Signaling Control the Dynamics of Gene Expression.* Science, 2004. **306**(5696): p. 704-708.
356. Cannon, A., et al., *Desmoplasia in pancreatic ductal adenocarcinoma: insight into pathological function and therapeutic potential.* Genes Cancer, 2018. **9**(3-4): p. 78-86.
357. Ebelt, N.D., V. Zamloot, and E.R. Manuel, *Targeting desmoplasia in pancreatic cancer as an essential first step to effective therapy.* Oncotarget, 2020. **11**(38).
358. Pandol, S., et al., *Desmoplasia of Pancreatic Ductal Adenocarcinoma.* Clinical Gastroenterology and Hepatology, 2009. **7**(11, Supplement): p. S44-S47.

359. Nielsen, M.F., M.B. Mortensen, and S. Detlefsen, *Key players in pancreatic cancer-stroma interaction: Cancer-associated fibroblasts, endothelial and inflammatory cells*. World J Gastroenterol, 2016. **22**(9): p. 2678-700.
360. Erkan, M., et al., *StellaTUM: current consensus and discussion on pancreatic stellate cell research*. Gut, 2012. **61**(2): p. 172-8.
361. Qin, C., et al., *Metabolism of pancreatic cancer: paving the way to better anticancer strategies*. Molecular Cancer, 2020. **19**(1): p. 50.
362. Ericksen, R.E. and W. Han, *Give and take: competition for BCAAs in the tumour microenvironment*. Nature Metabolism, 2020. **2**(8): p. 657-658.
363. Li, J.-T., et al., *BCAT2-mediated BCAA catabolism is critical for development of pancreatic ductal adenocarcinoma*. Nature Cell Biology, 2020. **22**(2): p. 167-174.
364. Zhu, Z., et al., *Tumour-reprogrammed stromal BCAT1 fuels branched-chain ketoacid dependency in stromal-rich PDAC tumours*. Nature Metabolism, 2020. **2**(8): p. 775-792.
365. Kovacevic, Z., et al., *The iron-regulated metastasis suppressor NDRG1 targets NEDD4L, PTEN, and SMAD4 and inhibits the PI3K and Ras signaling pathways*. Antioxid Redox Signal, 2013. **18**(8): p. 874-87.
366. Compton, S.L.E., et al., *Metabolic Reprogramming of Ovarian Cancer Spheroids during Adhesion*. Cancers (Basel), 2022. **14**(6).
367. Hessmann, E., et al., *Fibroblast drug scavenging increases intratumoural gemcitabine accumulation in murine pancreas cancer*. Gut, 2018. **67**(3): p. 497-507.
368. Knudsen, E.S., et al., *Unique metabolic features of pancreatic cancer stroma: relevance to the tumor compartment, prognosis, and invasive potential*. Oncotarget, 2016. **7**(48).
369. Liu, H., et al., *Pancreatic stellate cells exploit Wnt/β-catenin/TCF7-mediated glutamine metabolism to promote pancreatic cancer cells growth*. Cancer Letters, 2023. **555**: p. 216040.
370. Nocquet, L., P.P. Juin, and F. Souazé, *Mitochondria at Center of Exchanges between Cancer Cells and Cancer-Associated Fibroblasts during Tumor Progression*. Cancers, 2020. **12**(10): p. 3017.
371. Stouten, I., N. van Montfoort, and L. Hawinkels, *The Tango between Cancer-Associated Fibroblasts (CAFs) and Immune Cells in Affecting Immunotherapy Efficacy in Pancreatic Cancer*. Int J Mol Sci, 2023. **24**(10).
372. Salcedo, C., et al., *Functional Metabolic Mapping Reveals Highly Active Branched-Chain Amino Acid Metabolism in Human Astrocytes, Which Is Impaired in iPSC-Derived Astrocytes in Alzheimer's Disease*. Frontiers in Aging Neuroscience, 2021. **13**.
373. Mann, G., et al., *Branched-chain Amino Acids: Catabolism in Skeletal Muscle and Implications for Muscle and Whole-body Metabolism*. Front Physiol, 2021. **12**: p. 702826.
374. Cai, Z., et al., *Branched-chain ketoacids derived from cancer cells modulate macrophage polarization and metabolic reprogramming*. Frontiers in Immunology, 2022. **13**.

375. Ellen, T.P., et al., *NDRG1, a growth and cancer related gene: regulation of gene expression and function in normal and disease states*. Carcinogenesis, 2007. **29**(1): p. 2-8.
376. Strzelczyk, B., et al., *Identification of High-Risk Stage II Colorectal Tumors by Combined Analysis of the NDRG1 Gene Expression and the Depth of Tumor Invasion*. Annals of Surgical Oncology, 2009. **16**(5): p. 1287-1294.
377. Ando, T., et al., *Decreased expression of Ndrg1 is correlated with tumor progression and poor prognosis in patients with esophageal squamous cell carcinoma*. Diseases of the Esophagus, 2006. **19**(6): p. 454-458.
378. Angst, E., et al., *N-myc downstream regulated gene-1 expression correlates with reduced pancreatic cancer growth and increased apoptosis in vitro and in vivo*. Surgery, 2011. **149**(5): p. 614-624.
379. Maruyama, Y., et al., *Tumor Growth Suppression in Pancreatic Cancer by a Putative Metastasis Suppressor Gene Cap43/NDRG1/Drg-1 through Modulation of Angiogenesis*. Cancer Research, 2006. **66**(12): p. 6233-6242.
380. Angst, E., et al., *Cellular differentiation determines the expression of the hypoxia-inducible protein NDRG1 in pancreatic cancer*. Br J Cancer, 2006. **95**(3): p. 307-13.
381. Hollinshead, K.E.R., et al., *Respiratory Supercomplexes Promote Mitochondrial Efficiency and Growth in Severely Hypoxic Pancreatic Cancer*. Cell Rep, 2020. **33**(1): p. 108231.
382. Norrsell, R., et al., *L-type Amino Acid Transporter 1 as a Therapeutic Target in Pancreatic Cancer*. Cancer Control, 2024. **31**: p. 10732748241251583.
383. Hayashi, K., et al., *c-Myc is crucial for the expression of LAT1 in MIA Paca-2 human pancreatic cancer cells*. Oncol Rep, 2012. **28**(3): p. 862-866.
384. Shi, Q., et al., *Constitutive and inducible interleukin 8 expression by hypoxia and acidosis renders human pancreatic cancer cells more tumorigenic and metastatic*. Clin Cancer Res, 1999. **5**(11): p. 3711-21.
385. Watari, K., et al., *Impaired differentiation of macrophage lineage cells attenuates bone remodeling and inflammatory angiogenesis in Ndrg1 deficient mice*. Scientific reports, 2016. **6**: p. 19470-19470.
386. Kes, M.M.G., et al., *Oncometabolites lactate and succinate drive pro-angiogenic macrophage response in tumors*. Biochimica et Biophysica Acta (BBA) - Reviews on Cancer, 2020. **1874**(2): p. 188427.
387. Jiang, Q., et al., *Glutamine Is Required for M1-like Polarization of Macrophages in Response to Mycobacterium tuberculosis Infection*. mBio, 2022. **13**(4): p. e01274-22.
388. Dong, Y., et al., *Branched-chain amino acids promotes the repair of exercise-induced muscle damage via enhancing macrophage polarization*. Front Physiol, 2022. **13**: p. 1037090.